Practical Equation of State for Non-Spherical and Asymmetric Systems

by

Marlie du Rand

Dissertation presented for the Degree

of

DOCTOR OF PHILOSOPHY IN ENGINEERING
(Chemical Engineering)

in the Department of Chemical Engineering

at the University of Stellenbosch

Promoter

Prof. Izak Nieuwoudt

STELLENBOSCH

DATE: December 2004

DECLARATION

I, the undersigned, hereby declare that the work contained in this dissertation is my own original work and that I have not previously in its entirety or in parts, submitted it at any university for a degree.

Marlie du Rand

Date:13 August 2004

Summary

In this study an equation of state has been developed for the specific purpose of representing systems of simple non-polar spherical and chain-like components and their mixtures for practical applications. To be applied in engineering calculations, the model has to be accurate, be able to represent mixtures with large size asymmetry without the use large binary interaction parameters, and be mathematically simple enough to ensure rapid computations.

The model is developed through a sequential evaluation of the statistical mechanical theory of particles and the various approaches available to extend it to real fluid systems.

The equation of state developed in this work models the real fluid systems as interacting with a highly simplified two step potential model. The repulsive interactions are represented by a newly developed simplified form of the hard sphere equation of state, capable of representing the known hard sphere virial coefficients and phase behaviour to a high degree of accuracy. This equation has a realistic closest packed limiting density in between the idealised hard sphere fluid random and crystal structure limits. The attractive interactions between the particles are incorporated into the model through a perturbation expansion represented in the form of a double summation perturbation approximation. The perturbation matrix was optimised to have the lowest order in density necessary to still be able to accurately represent real fluid properties. In a novel approach to obtain simple mixing rules that result in the theoretically correct second virial coefficient composition dependence, the perturbation matrix is constrained in such a manner that only the first perturbation term has a term that is first order in density. From a detailed evaluation of the various methods available to represent chain-like non-spherical systems it was finally concluded that the Perturbed Hard Chain Theory provided an ideal compromise between model simplicity and accuracy, and this method is used to extend the equation to chain-like systems. Finally the model is extended to fluid mixtures by uniquely developed mixing rules resulting in the correct mixture composition dependence both at low and high system densities.

The newly developed equation of state is shown to be capable of representing the pure component systems to a comparable degree of accuracy as the generally applied equations of state for non-spherical systems found in the literature. The proposed equation is furthermore also shown equal or improve on the predictive ability of these models in the representation of

fluid mixtures consisting out of similar chainlike or size and energetic asymmetric components.

Finally, the computational time required to model the behaviour of large multi-component fluid mixtures using the new equation of state is significantly shorter that that of the other semi-empirical equations of state currently available in the literature.

Opsomming

Hierdie werkstuk behels die ontwikkeling van ‘n toestandsvergelyking wat spesifiek gerig is op toepassings in alledaagse, praktiese ingenieurstipe berekeninge en daartoe instaat is om sisteme bestaande uit nie-polêre spferiese- en ketting-tipe komponente en hulle mengsels te kan beskyf. Om aan hierdie vereistes te voldoen moet die toestandsvergelyking die relevante sisteme akkuraat kan modelleer, slegs klein interaksie parameters benodig om mengsels van komponente met groot verskille in molekulêre groottes akkuraat voor te stel en steeds wiskundig eenvoudig genoeg wees om vinnige berekeninge te verseker.

Die vergelyking is ontwikkel deur ‘n sistematiese evaluering van die statisitiese meganiese teorie van partikels en die verskillende metodes om hierdie teorië op werklike sisteme toe te pas.

Die toestandsvergelyking beskryf die intermolekulêre interaksie tussen die verskillende komponente met ‘n hoogs vereenvoudigde twee-stap interaksie potensiaal model. Die afstotende kragte tussen die komponente word in ag geneem deur ‘n nuwe vergelyking wat ontwikkel is om die gedrag van ‘n ideale harde spfeer sisteem te modelleer. Hierdie hardespfeermodel is daartoe instaat om die viriale koeffisiënte en die fase gedrag van teoretiese harde spfeer sisteme akkuraat te modelleer, en het ‘n maksimum digtheidslimiet wat tussen teoretiese waardes van ‘n perfek geordende en nie-geordende harde spheer sisteem lê.

Die aantrekkinskragte tussen die partikels word beskou as ‘n perturbasie van die harde-spheer vergelyking. ‘n Term bestaande uit ‘n dubbelle sommasiefunksie word gebruik om hierdie perturbasie uitbreiding voor te stel. Die sommasie term is geoptimiseer sodat die finale toestandsvergelyking die laagste digtheidsgraad het wat steeds tot ‘n akkurate voorstelling van die termodinamiese gedrag van werklike sisteme lei. Die sommasiefunksie is so gespesifiseer dat die eerste term van die perturbasie uitbreiding slegs ‘n eerste graadse orde in digtheid het in ‘n unieke benadering om te verseker dat die mengreëls van die toestandsvergelyking die teoreties korrekte samestellingafhanklikheid van die mengselvirialekoeffisiente tot gevolg het.

‘n Deeglike ondersoek van die verskillende metodes om die toepassing van die toestandsvergelyking uit te brei tot die moddellering van nie-spheriese ketting-tipe molekules is gedoen en daar is uiteindelik tot die gevolgtrekking gekom dat die Geperturbeerde Harde

Kettingteorie (PHCT) die mees geskikde metode is vir hierdie doel en is op die vergelyking toegepas.

As ‘n laaste stap in die toestandsvergelykingontwikkelling is daar mengreëls ontwikkel vir die vergelyking wat die korrekte samestellingsafhanklikheid toon vir beide die lae en hoë digtheidskondisies.

Die model wat in hierdie studie ontwikkel is, is met verskeie ander bekende toestandsvergelykings, wat daartoe instaat is om nie-spferiese sisteme te modelleer, vergelyk en daar is gevind dat die nuwe model daartoe instaat is om suiwer sisteme net so goed as die bestaande vergelykings te modelleer. Verder is daar ook gevind dat die nuwe vergelyking die modellering van verskeie mensels van kettingtipe komponente en komponente van uiteenlopende groottes of interaksie energieë kan ewenaar of verbeter.

Laastens is daar ook gevind dat die tyd nodig vir die modellering van die termodinamiese gedrag van mengsels van ‘n groot hoeveelheid komponente aansienlik korter is vir die nuwe model as die ander bekende semi-empiriese vergelykings.

Acknowlegements

There are many people, without whom this thesis would not have been possible.

I would firstly like to thank my supervisor Prof. I. Niewoudt, for all his help and guidance in the form of invaluable discussions, helpful suggestions, constructive criticisms, and for allowing me the opportunity to gain a lot of international exposure to the field; and his, wife, Traute, for providing continual moral support both at home, in Stellenbosch, and during time spent in Germany.

Then I would like to thank all the staff and colleagues at the Department of Process Engineering, for their general support and the pleasant working environment within which I could complete my studies.

I would also like to express my gratitude towards Prof. G. Brunner from the Department of Thermische Verfahrenstechnik at the Technical University of Hamburg-Harburg in Germany, for hosting me during two visits to his department in 2001 and 2002, and for allowing me the use their facilities and the opportunity to interact with the students there.

On the non-academic side I would like to thank all my friends and family in Stellenbosch, for their friendship and support, not only during the completion of my doctoral studies, but over my entire time at Stellenbosch.

Lastly, I would like to acknowledge my gratitude towards my parents, for their unwavering support and love over the entire course of this project without which this work would never have come to fruition.

The financial assistance off the National Research Foundation (NRF) towards this research is hereby acknowledged.

Table of Contents

Glossary

Name	Description	Pg.	Source
2D	Mixing rules using volume fractions and adhering to the second virial coefficient composition dependence boundary condition	222	---
BACK	Combination of SAFT EOS and models for hard convex bodies	159	[167]
BH	Barker and Henderson Perturbation Theory	33	[16]
BMCS	Boublík Mansouri Carnahan Starling mixing rule	199	[137]
CCOR	Cubic-Chain of Rotators Hard sphere equation	58	[43]
CK or Two Step Model	Intermolecular interaction energy	83	[42]
COR	Chain of Rotators	151	[43]
CP	Cotterman-Prausnitz mixing rule	221	[48]
CS	Carnahan Starling Hard sphere equation	56	[32]
CWA	Weeks-Chandler-Anderson Perturbation Theory	39	[288]
DDLC	Density dependant local composition mixing rules	209	[97]
G	Guggenheim Hard sphere equation	58	[87]
G^E-EOS	EOS using the excess Gibbs Energy mixing rules	204	[103]
GF	Generalized Flory EOS	154	[58]
GF-D	Generalized Flory – Dimer EOS	155	[95]
GFH	Generalized Flory-Huggins EOS	154	[58]
HCB	Hard Convex Body EOS	142	[28]
HS	Hard Sphere EOS		
HS1	Proposed simple hard sphere equation 1	67	---
HS2	Proposed simple hard sphere equation 2	67	---
HS3	Proposed simple hard sphere equation 3	67	---
HS3CK	Defined EOS – HS3 hard sphere term with a double summation perturbation approximation with a CK intermolecular energy	118	---
HS3CK-ltd	HS2CK EOS with a constrained perturbation approximation summation matrix	136	---

Name	Description	Pg.	Source
HS3LJ-mean	Defined EOS – HS3 hard sphere term with a double summation perturbation approximation with a LJ intermolecular energy with the mean interaction energy of the model equal to the component critical temperature for small atoms or molecules	118, 121	---
HS3LJ-real	Defined EOS – HS3 hard sphere term with a double summation perturbation approximation with a LJ intermolecular energy with a realistic intermolecular potential	118, 121	---
HS3LLS	Defined EOS – HS3 hard sphere term with a local composition perturbation term approximation	118	---
HS3SW	Defined EOS – HS3 hard sphere term with a double summation perturbation approximation with a SW intermolecular energy	118	---
HSC	Hard Sphere Chain EOS	---	---
K	Kolafa Hard sphere model	57	[28]
LJ	Lennard-Jones interaction energy	21	[170]
LLS	Local composition model for the perturbation term	108	[184]
MHV1 and MHV2	Modified Huron-Vidal mixing rules	205	[53,143]
Original-SAFT	SAFT EOS as developed by Huang and Radosz	158, 257	[100-101]
PC-SAFT	Perturbed-Chain-SAFT EOS	167	[85]
PHCT	Perturbed Hard Chain Theory	150	[20,60]
PHSC	Perturbed Hard Sphere Chain EOS	161	[44]
PY-C	Percus-Yevick Compressibility equation for hard spheres	55	[209]
PY-P	Percus-Yevick Pressure equation for hard spheres	55	[209]
RH	Ree and Hoover Padé Hard sphere approximation	57	[174]
S	Shah Hard sphere compressibility	58	[192]
SAFT	Statistical Associating fluid theory	157	[65,152]
SAFT-D	Extension of SAFT EOS that includes dimer behaviour	159	[81]
SAFT-LJ	SAFT EOS applied to Lennard-Jones segments	158	[117,151]
SAFT-SW	SAFT EOS applied to Square-Well segments	158	[5]
SAFT-VR	SAFT EOS applied to segments variable attractive well widths	159	[82]

Name	Description	Pg.	Source
Simple-PHCT	HS3CK with a 3x3 double summation perturbation matrix extended to chained systems using the perturbed hard chain theory	170	---
Simple-PHCT-ltd	Simple-PHCT EOS with constrained perturbation matrix	171	---
Simple-PHSC	HS3CK with a 3x3 double summation perturbation matrix extended to chained systems using the perturbed hard sphere chain approach	168	---
Simple-PHSC-ltd	Simple-PHSC EOS with constrained perturbation matrix	171	---
Simple-SAFT	HS3CK with a 3x3 double summation perturbation matrix extended to chained systems using the statistical association fluid theory	163	---
Simple-SAFT-ltd	Simple-SAFT EOS with constrained perturbation matrix	171	---
Soft-SAFT	Similar to SAFT-LJ EOS but extended to heteronuclear chains	159	[21]
SPHCT	Simplified perturbed hard chain theory	212	[111]
SRK	Soave-Redlich-Kwong EOS	253	[196]
SW	Square –Well potential energy	20	[170]
TPT	Thermodynamic Perturbation Theory	156	[231-235]
TPT-D	Extension of a TPT EOS that includes dimer behaviour	159	[36]
TPT-LJ	EOS based on TPT with Lennard-Jones segments	158	[13]
TPT-SW	EOS based on TPT with Square-Well segments	158	[14]
VDW	Van der Waals hard sphere model	52	[217]
VF	Volume fraction mixing rules	221	[101]
YK-1	Yelash-Kraska hard sphere approximation 1	60	[242]
YK-2	Yelash-Kraska hard sphere approximation 2	60	[242]
YKD-CS	Yelash-Kraska correction on the CS hard sphere equation	59	[273]
YKD-VDW	Yelash-Krasha correction on the VDW hard sphere term	59	[243]

List of Figures

Figure **Pg**

List of Tables

Chapter 1 ***Introduction***

In the chemical engineering field one of the most important requirements is the ability to be able to accurately represent and predict the physical behaviour of the various chemical systems in a quantifiable and accurate manner. The field of thermodynamics involve the study of the relation of the physical state of a pure chemical species or mixtures there to the physically measurable quantities of temperature, pressure and volume. An all encompassing model from which it is possible to infer the physical state of all systems from these quantities is however as yet unattainable. Instead there has to be relied on various models specifically geared to represent real systems under certain limiting conditions. Equations of state form part of this body of models, and can be used to relate the temperature, pressure and volume properties of specific fluid systems.

The first major step in the evolution of the equation of state from simply being a model representing an ideal gaseous phase is generally accepted as the conception of the Van der Waals equation of state [217] in 1873 - an intuitively developed model capable of representing vapour-liquid phase equilibria. Since the end of the 19^{th} century, there has been a vast variety of empirical models proposed in an attempt to improve the accuracy and general applicability of this equation of state. However, these empirical models invariably fail when asked to represent fluid systems that are far removed from the idealised state of spherical non-polar particles in the low or intermediate pressure range.

The second evolutionary leg of the equations of state lies in the development of a fluid model from first principals. This field of study has been gaining great impetus since the advent of the personal computer, which facilitates the evaluation of complex mathematical functions and the statistical mechanical simulations of theoretical systems. Using the theoretically based arguments researchers are attempting to develop models for systems removed from the idealised state. The current level of knowledge and understanding in the field and the degree of complexity of the real fluid systems are however severely constraining - the current theoretically based models are often limited to simplified theoretical systems, mathematically cumbersome and not generally applicable to real fluid systems and applications.

In an attempt to overcome the problem of representing real fluid systems that are more complex than the spherical non-polar systems, a third type of equation of state has developed

as a hybrid between the empirical and theoretically based equations. In these models the lessons learnt from the theoretical systems are adapted empirically in order to represent the real fluid behaviour. Until the theory and computational power of the personal computers have been developed to satisfactory levels, it is from this field that the majority of the modern equations of state are expected to evolve.

The impetus for this current study came from the desire to represent the phase equilibria of a mixture of chainlike non-polar n-alkanes with a supercritical solvent such as ethane, n-propane or carbon dioxide. The modelling of this fluid system is generally complicated by three factors:

1. The non-spherical chainlike structure of some of the solutes.
2. The size asymmetry between the solutes and solvents.
3. The relatively high pressure of the system (above the critical pressure of the solvent).

Attempts to model the system with the existing equations of state resulted in excessively long computational times using the semi-empirical models and the use of unrealistically large binary interaction parameters when using the Van der Waals type equation of state.

These findings point to a gap in the current body of knowledge regarding semi-empirical equations of state.

It is the aim of this study to partially address this problem, by developing an equation of state that will meet the following specific criteria:

1. The ability to accurately represent small spherical non-polar components in the saturated liquid, vapour and supercritical phases.
2. An accurate representation of the fluid properties of simple chain-like molecules such as n-alkanes.
3. The successful representation of mixtures of chained systems as well as systems with a large degree of size asymmetry up to pressures to within close proximity of the mixture critical point. (As it is generally known that simple equations of state fail in the exact representation of the mixture critical point, the performance of the model in this region will not be used as a criterion for the evaluation of the equation of state.)

4. Reduce computational times.

The sequential route in the development of a new equation of state that would meet the above mentioned criteria is outlined in the series of chapters in this work. Briefly summarised the various sections entail the following:

- *A review of the existing theoretical approaches*:

A review of the statistical mechanical theory underlying the theoretical models and the various approaches towards developing a theoretical equation of state is done.

- *Development of a Hard Sphere repulsive model*

In this section a new hard sphere equation of state is developed to represent the repulsive interactions between the various particles in the fluid mixture.

- *Development of a perturbation model for the attractive interactions*

In this step the attractive interactions of spherical particles are taken into account in the new model.

- *Extension of the model towards chain-like systems*

Three main theories regarding the representation of chain-like systems, the Statistical Associating Fluid Theory, the Perturbed Hard Sphere Chain Theory and the Perturbed Hard Chain Theory are evaluated by assessing their ability to extend the new equation from spherical systems to chain-like systems whilst maintaining accuracy and computational simplicity.

- *The development of suitable mixing rules for the application to fluid mixtures*

The final step in the model development involves the extension of the new equation of state to fluid mixtures by developing suitable mixing and combination rules for the model.

The new equation is evaluated against some of the most widely accepted cubic and semi-empirical equations of state found in the literature in order to determine whether the requirements set at the onset of the process, that of model accuracy and simplicity have indeed

been met. The various computational algorithms and regression techniques developed and used during this study are also reviewed.

The steps followed in the development of the equation of state in this study are summarised in Figure 1.1 below:

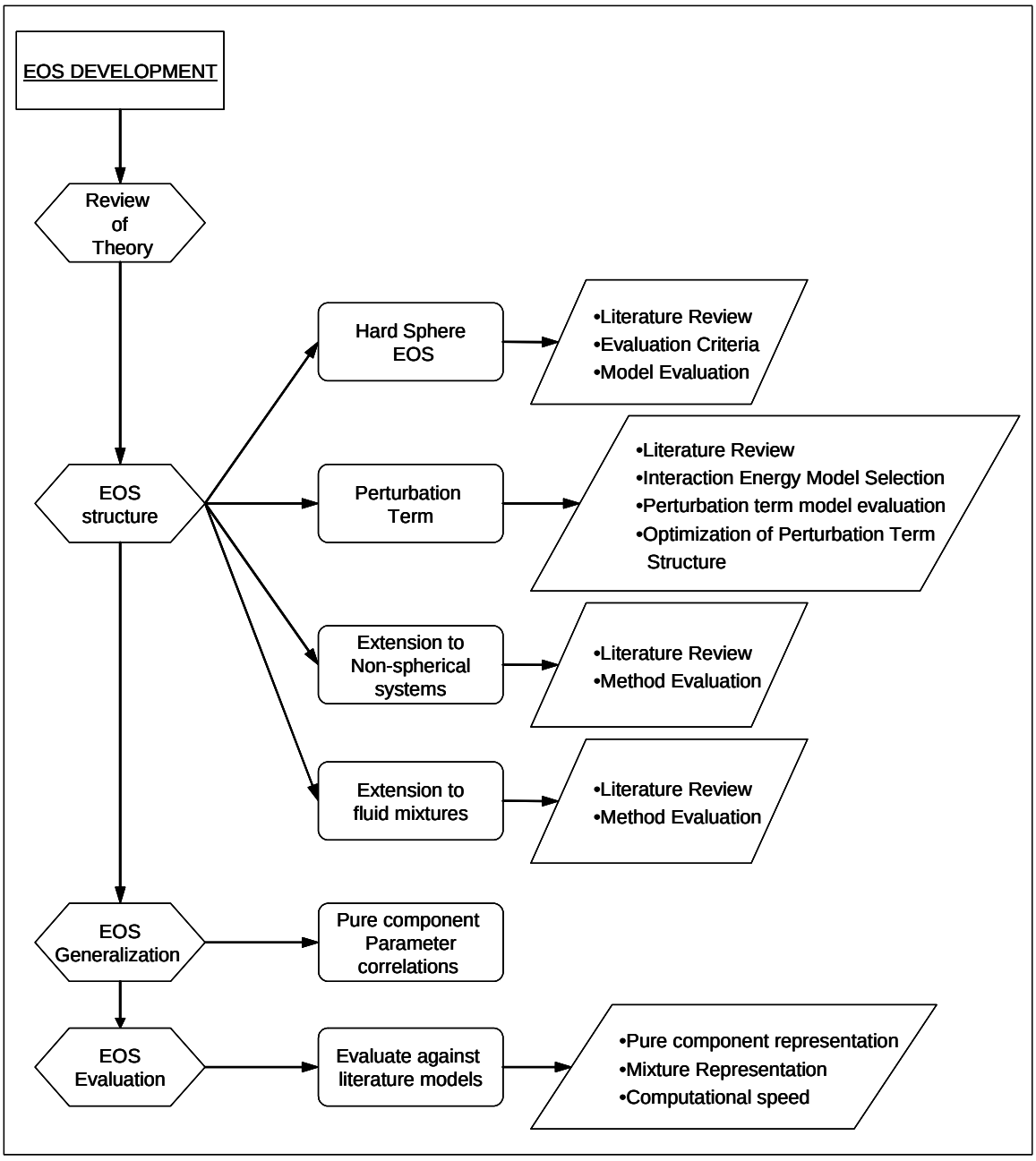

Figure 1.1 Flow diagram of logical progression in the development of the EOS in this study.

Chapter 2 ***Equations of State***

2.1 INTRODUCTION

In order to apply the thermodynamic laws to a real system it is necessary that that system be represented in some mathematical form. The search for an all-encompassing mathematical description of a real system can be seen as the Holy Grail of thermodynamic modelling. In the meantime models based on simplified systems, limited to specific thermodynamic bounds have to be used.

There are two approaches to representing a real system mathematically. The first, the *equation of state*, EOS, approach, aims to model the *P-v-T* behaviour of the system, be it a pure component or mixture. The second approach is the modelling of the excess Gibbs free energy of a liquid mixture, with an *activity coefficient model*. It is on the first of these approaches that this work will focus.

As stated above, the equation of state provides the functional relationship between the system pressure, temperature and volume, and may be found in either the pressure or volume explicit form:

$$P = f(T, v) \qquad 2.1$$

or

$$v = h(P, T) \qquad 2.2$$

The simplest equation of state can be derived from the laws of Boyle and Charles

$$\frac{Pv}{T} = R \qquad 2.3$$

Where R is known as the universal gas constant. Equation 2.3 is known as the ideal gas law, and is only strictly applicable to idealised systems with no molecular volume and intermolecular forces.

By using a compressibility term, z, equation 2.3 may be extended to real systems. The compressibility term contains the all effects of the molecular interactions on the *P-v-T* behaviour of a real system. The compressibility of an ideal system is equal to 1.

$$\frac{Pv}{RT} = z \qquad 2.4$$

It is the expression of this relationship (shown in equation 2.4) in terms of physical measurable properties that is the aim of the numerous equations of state that are in existence today. The equations of state can be regarded as the tool with which we can determine the effect that the behaviour of the individual molecules have on the macroscopic properties of the system, such as the system pressure or volume.

The field of statistical thermodynamics provides such a molecular theory or interpretation of macroscopic systems. Although many equations of state have been developed without an explicit statistical thermodynamic base, a basic understanding of the field does prove to be useful in improving and extending the applications of the equations.

2.2 OVERVIEW OF A STATISTICAL THERMODYNAMIC EQUATIONS

The study of statistical thermodynamics is of course a vast and complex field. This section aims to provide a brief overview of the necessary concepts required in the study of simple fluid behaviour where a simple fluid refers to a fluid consisting out of non-polar monatomic or small molecular particles, with no or negligible rotational and vibrational movement.

For a more detailed discussion the reader is referred to the many texts on the subject matter such as [93, 142].

2.2.1 The Partition Function

The concept that the bulk properties of a system is determined by the properties of the individual components making up that system serves as an entry point to the field of statistical thermodynamics. It can therefore be said the internal energy of a system is the sum of all the energies of the individual molecules within that system. In the *classical* statistical thermodynamical approach it was assumed that *all* energies values are available to a system or

molecule, however with the advent of *quantum* mechanics it is now known that energy is quantized and only certain energy values can be obtained (Figure 2.1).

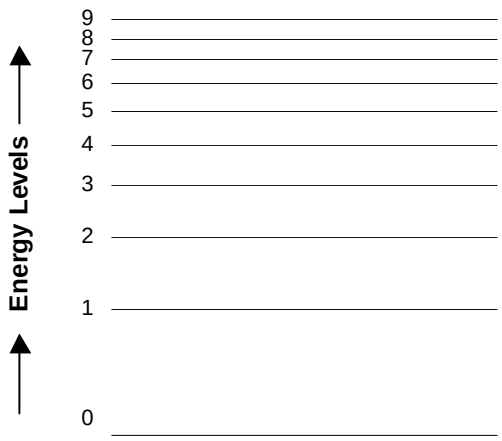

Figure 2.1 Representation of energy levels available to a molecule

Looking at any system, at a specific temperature or energy, at a specific moment in time, on a molecular scale, not all the molecules will occupy the same energy levels. However due to the vast number of molecules in such a system, only the most probable distribution between the levels will determine the overall state of the system.

The *Boltzmann distribution law* can be derived to determine the most probable number of molecules per energy level for a specific total energy:

$$N_j = p_j e^{\alpha} e^{-\beta \varepsilon_j} \qquad 2.5$$

Where j indicates the specific energy level, N_j the number of molecules in that level and ε_j the energy value of the specific level. p_j is known as the *degeneracy* of the energy level, and represents the number of energy *states* in the system which have the same value for ε. Equation 2.5 may also be written in terms of energy states, i.

$$N_i = e^{\alpha} e^{-\beta \varepsilon_i} \qquad 2.6$$

Where $\varepsilon_i = \varepsilon_j$ and

$$N_j = p_j * N_i \qquad 2.7$$

By assigning a value of zero to the lowest energy level that the molecules can occupy (j=0), α may be determined from equation 2.5 as $e^{\alpha} = p_0 N_0$, and represents the number of molecules in the lowest energy state. It can also be shown that $\beta = 1/kT$ [79], where k is the Boltzmann constant.

(Strictly speaking equation 2.12 and the use of the Boltzmann law is only correct when the number of energy states available to the system is much larger than N. The system temperature should therefore be high enough to enable the molecules to have access to the higher energy levels. This will generally be a valid assumption for most real systems, far removed from absolute zero.)

The total number of molecules in the system, N, equal the sum of all the molecules in the various energy levels:

$$N = \sum_i N_i = N_0 \sum_i \exp\left(\frac{-\varepsilon_i}{kT}\right) = N_0 \sum_j p_j \exp\left(\frac{-\varepsilon_j}{kT}\right) \qquad 2.8$$

Equation 2.5 may now be written as:

$$N_j = \frac{N p_j \exp\left(-\varepsilon_j / kT\right)}{\sum_j p_j \exp\left(-\varepsilon_j / kT\right)} \qquad 2.9$$

The denominator in this expression called the *molecular partition function*, and may be seen as containing information on how on average a molecule may be distributed between the energy levels or states [79]:

$$q = \sum_j p_j \exp\left(-\varepsilon_j / kT\right) = \sum_i \exp\left(-\varepsilon_i / kT\right) \qquad 2.10$$

In a closed isothermal system, with N, V and T given, the total partition function is known as the *canonical partition function* and is the product of all the individual molecular partition functions. For a system of individually identifiable molecules it may be written as:

$$Q = q^N \qquad 2.11$$

However for a system of indistinguishable molecules equation 2.11 has to be modified:

$$Q = \frac{1}{N!} q^N \qquad 2.12$$

The canonical partition function refers to the overall distribution of all the particles in the system over all the possible energy states.

Equation 2.12 may be further expanded on the assumption that the total energy of the molecule consists out of contributions of various energy types such as translational, rotational, vibrational, electronic, nuclear etc. Each of the energy types will contribute to the total partition function and may be considered individually:

$$\varepsilon = \varepsilon_{trans} + \varepsilon_{rot} + \varepsilon_{vib} + \varepsilon_{elec} + \varepsilon_{nucl} \ldots \qquad 2.13$$

$$Q = \frac{1}{N!} \left(\sum_i e^{-\beta \varepsilon_i} \right)^N$$

$$= \frac{1}{N!} \left(\sum_i e^{-\beta \left(\varepsilon_{trans} + \varepsilon_{rot} + \varepsilon_{vib} + \varepsilon_{elec} + \varepsilon_{nucl} \right)_i} \right)^N$$

$$= \frac{1}{N!} q_{trans}{}^N q_{rot}{}^N q_{vib}{}^N q_{elec}{}^N \qquad 2.14$$

There are many other partition functions describing other thermodynamic environments. Two of these are known as the *microcanonical* and *grand canonical* partition functions or ensembles. A microcanonical partition describes an *isolated* system, were *N, V* and *E* (the system energy) are known, and a grand canonical ensemble, an *open isothermal* system, where μ, the chemical potential, *V* and *T* are known.

In a grand canonical ensemble, as opposed to the canonical partition function, are not only the distribution of the particles allowed to vary over the energy states in the system, but also the number of particles within the system. It can be shown that the grand canonical partition function is represented by:

$$\Xi(V,T,\mu) = \sum_N^{\infty} Q(N,V,T) e^{N\mu/kT} \qquad 2.15$$

The classical thermodynamic properties can be expressed in terms of the various partition functions. Some of the thermodynamic properties expressed in terms of the canonical partition function are listed in Table 2.1. These functions provide the link between the molecular behaviour and the overall system properties.

Table 2.1 Some thermodynamic properties in terms of the Canonical Partition Function

$A = -kT \ln Q$	2.16	$E = kT^2 \left(\frac{\partial \ln Q}{\partial T} \right)_{N,V}$	2.17
$P = kT \left(\frac{\partial \ln Q}{\partial V} \right)_{N,T}$	2.18	$\mu = -kT \left(\frac{\partial \ln Q}{\partial N} \right)_{V,T}$	2.19

2.2.2 Canonical Distribution Function and the Configurational Integral

The development of a partition function of a fluid is first demonstrated for an ideal fluid, as the simplest case. An ideal fluid classified as a fluid consisting out of particles with no physical volume or intermolecular forces between them.

The translational partition function for an ideal particle can be shown to be the following [79]:

$$q_{trans} = \left(\frac{2\pi mkT}{h^2} \right)^{3/2} V \qquad 2.20$$

h is Planck's constant and m the mass of the particle. The term $(2\pi mkT/h^2)^{1/2}$ is known as the *De Broglie wavelength* and is traditionally denoted by Λ.

The canonical partition function of an ideal fluid is therefore:

$$Q = \frac{1}{N!} \frac{V^N}{\Lambda^{3N}} {q_{rot}}^N {q_{vib}}^N {q_{elec}}^N {q_{nucl}}^N \qquad 2.21$$

and may be simplified even further in the case of a monatomic ideal fluid without any rotational or vibrational motions. The only partition functions that will have an effect on the system properties will then be the translational, electronic and nuclear partition functions.

$$Q = \frac{1}{N!} \frac{V^N}{\Lambda^{3N}} {q_{elec}}^N {q_{nucl}}^N \qquad with \quad {q_{rot}}^N = {q_{vib}}^N = 1 \qquad 2.22$$

For the purpose of our investigation it is not necessary to focus on the actual partition functions of the electronic, nuclear energy distributions, save to note that the electronic and nuclear partition functions are solely dependent on the electronic and nuclear energy levels and their partition functions and not on the system volume or intermolecular interactions and hence will not influence the actual equation of state or system pressure. The reader is referred to the various texts on statistical mechanics [93, 142] for the partition functions for these energy distributions.

In the case of a real fluid, particles will occupy some of the system volume and also experience intermolecular forces. Both of these effects will influence the translational motion of the particle, and must be taken into account in the partition function. The solution of the rotational and vibrational partition functions is again equal to 1 for monatomic fluids and independent of the fluid volume for small molecular fluids. Equation 2.21 may be expressed as:

$$\begin{aligned} Q &= \frac{1}{N!}\frac{1}{\Lambda^{3N}} {q_{rot}}^N {q_{vib}}^N {q_{elec}}^N {q_{nucl}}^N Z_{config} \\ &= \frac{1}{N!}\frac{1}{\Lambda^{3N}} {q_{elec}}^N {q_{nucl}}^N Z_{config} \qquad \textit{with} \quad {q_{rot}}^N = {q_{vib}}^N = 1 \end{aligned} \tag{2.23}$$

where Z_{config} is known as the *classical configurational integral*. It is in this term that all the *real* properties of the fluid are taken into account. It is a function of the intermolecular energy $U(\mathbf{r}_1,\mathbf{r}_2,\ldots\mathbf{r}_N)$ which is dependent on the positions of all the particles in the system volume. (Hence the term *configurational* integral.) At system temperatures high enough to ensure large quantum numbers, Z_{config} may be evaluated in the classical (not quantum) statistical mechanic limit and integrated over the phase volume instead of taking summations as the energy differences between the higher quantum levels become very small. (As mentioned in section 2.2.1, temperatures of interest in this work are far removed from absolute zero, the classical statistical mechanical approach will therefore be valid). The configurational integral may therefore be evaluated as follows:

$$Z_{config} = \iint e^{-\beta U(\mathbf{r}_1,\mathbf{r}_2\ldots\mathbf{r}_N)} d\mathbf{r}_1 d\mathbf{r}_2 \ldots d\mathbf{r}_N \tag{2.24}$$

If equation 2.24 were to be evaluated for an ideal fluid where U=0, from the definition, the exponent term would be equal to 1 and $Z_{config} = V^N$, and equation 2.21 would be recovered.

2.2.3 The Radial Distribution and Probability Functions

With the information on the intermolecular energies over the system volume, it is now possible to derive some equations relating to the arrangement or distribution of the molecules or particles in a fluid.

The probability that molecule 1 is in $d\mathbf{r}_1$ at $\mathbf{r}_1$, molecule 2 in $d\mathbf{r}_2$ at $\mathbf{r}_2$… molecule N in $d\mathbf{r}_N$ at $\mathbf{r}_N$ can be shown to be:

$$P^{(N)}(\mathbf{r}_1,\mathbf{r}_2\ldots\mathbf{r}_N)d\mathbf{r}_1 d\mathbf{r}_2\ldots d\mathbf{r}_N = \frac{e^{-\beta U_N}}{Z_{config}} d\mathbf{r}_1 d\mathbf{r}_2\ldots d\mathbf{r}_N \qquad 2.25$$

From this, the probability that molecule 1 can be found in $d\mathbf{r}_1$ at $\mathbf{r}_1$, molecule 2 in $d\mathbf{r}_2$ at $\mathbf{r}_2$… molecule i in $d\mathbf{r}_i$ at $\mathbf{r}_i$ irrespective of the positions of molecules (i + 1) to N, may be calculated by integrating equation 2.25 over the coordinates of the molecules (i + 1) to N.

$$P^{(i)}(\mathbf{r}_1,\mathbf{r}_2\ldots\mathbf{r}_i) = \frac{\int\int e^{-\beta U_N} d\mathbf{r}_{i+1}\ldots d\mathbf{r}_N}{Z_{config}} \qquad 2.26$$

Equation 2.26 can be extended to a system of *indistinguishable* molecules, where the probability that *any* molecule can be found in $d\mathbf{r}_1$ at $\mathbf{r}_1$, *any* molecule in $d\mathbf{r}_2$ at $\mathbf{r}_2$… *any* molecule in $d\mathbf{r}_i$ at $\mathbf{r}_i$ irrespective of the positions of the rest of the molecules ($\mathbf{r}_i$ represents the vector coordinates of particle *i* in the phase space):

$$\rho^{(i)}(\mathbf{r}_1,\mathbf{r}_2\ldots\mathbf{r}_i) = \frac{N!}{(N-i)!} P^{(i)}(\mathbf{r}_1,\mathbf{r}_2\ldots\mathbf{r}_i) \qquad 2.27$$

In an indistinguishable system, such as a fluid, all the points or positions in the system volume are equivalent, and any molecule is just as likely to occupy one position as another. In other words $\rho^{(1)}$ is independent of $d\mathbf{r}_1$. The probability that any molecule may be found in $d\mathbf{r}_1$ at $\mathbf{r}_1$ irrespective of the rest of the system is equivalent to the probability of finding any molecule at any dV in V, which is equivalent to the average system density ρ. The following expression is therefore valid for all fluids:

$$\frac{1}{V}\int \rho^{(1)}(\mathbf{r}_1)d\mathbf{r}_1 = \rho^{(1)} = \frac{N}{V} = \rho \qquad 2.28$$

A distribution function, $g^{(i)}(\boldsymbol{r}_1,\boldsymbol{r}_2...\boldsymbol{r}_i)$, provides the degree of the correlation or interdependence of the molecules in their distribution in the system volume:

$$\rho^{(i)}(\mathbf{r}_1,\mathbf{r}_2\ldots\mathbf{r}_i)=\rho^i g^{(i)}(\mathbf{r}_1,\mathbf{r}_2\ldots\mathbf{r}_i) \qquad 2.29$$

or substituting equations 2.26 and 2.27 into 2.29:

$$g^{(i)}(\mathbf{r}_1,\mathbf{r}_2\ldots\mathbf{r}_i)=\left(\frac{V}{N}\right)^i\frac{N!}{(N-i)!}\frac{\iint e^{-\beta U_N}\,d\mathbf{r}_{i+1}\ldots d\mathbf{r}_N}{Z_{config}} \qquad 2.30$$

The function, $g^{(2)}(\boldsymbol{r}_1,\boldsymbol{r}_2)$, is called the *radial distribution function*, and is generally denoted as $g(r)$, where r refers to the distance between a central molecule and a second. It can be seen as the factor by which the *local density* deviates from the average system or *bulk density* about some central molecule. The term $\rho g(\boldsymbol{r})d\boldsymbol{r}$, or $\rho g(r)4\pi r^2 dr$ in spherical coordinates, represents the number of molecules between r and $r+dr$ about a central molecule:

$$\int_0^\infty \rho g(\mathbf{r})d\mathbf{r}=\int_0^\infty \rho g(r)4\pi r^2 dr = N-1\approx N \qquad 2.31$$

The radial distribution function, and the correlation functions in general, although not explicitly shown in the equations above, are dependent not only on $\boldsymbol{r}$, but also the system density, ρ, and temperature. It should also be noted that as $\boldsymbol{r}\to 0$, $g(\boldsymbol{r},\rho,T)\to 0$ and as $\boldsymbol{r}\to\infty$, $g(\boldsymbol{r},\rho,T)\to 1$.

2.2.4 Molecular Correlation Functions

The correlation functions are closely related to the distribution functions defined in the previous section. They are a measure of the departure of the distributions from their random values [179]. In this section only the pair correlation functions are described, as they will be required later on. Correlation functions can, however, also be determined for triplets or higher groups of molecules.

The notation used in the previous section will be continued here, where $\boldsymbol{r}_i$ represents the vector coordinates of particle i, whilst r and r_{12} refer to the distance between particles 1 and 2 and r_{ij} to the distance between particles i and j.

The first function to be defined is the *total correlation function, h*(*r*):

$$h(r) = g(r) - 1 \qquad 2.32$$

This function is in essence a *residual* distribution function, as in an ideal fluid the localised density is identical to the average or system density over the entire phase space, because of the absence of intermolecular interactions to give localised order. This leads to a $g^{ideal}(r)$ value equal to 1. $h(r_{12})$ represents the total influence that particle 1 has on particle 2 at a distance of r_{12}.

In 1914 Ornstein and Zernike [73, 93, 161] proposed the total correlation function could be separated into two components, a direct component $c(r_{12})$, representing the influence that particle 1 has on particle 2 directly, and an indirect component, representing the influence by particle 1 on particle 2 through the other particles in the system, such as through the direct influence of particle 1 on particle 3 , which then would influence particle 2 either directly or indirectly. Mathematically this behaviour is expressed as follows:

$$h(r_{12}) = c(r_{12}) + \rho \int c(r_{13}) h(r_{23}) d\mathbf{r}_3 \qquad 2.33$$

Equation 2.33 is known as the *Ornstein-Zernike* equation and is the defining equation of the direct correlation function.

Another function, known as the *Meyer f-function*, has also been introduced into the statistical mechanical theory in order to simplify the mathematical expression of a term that is commonly found in statistical mechanical expressions:

$$f_{ij} = f(r_{ij}) = e^{-u(r_{ij})} - 1 \qquad 2.34$$

Finally, in order to facilitate integration, a function is introduced that remains continuous over all values of *r* even when *u*(*r*) and *g*(*r*) are discontinuous (For example at $r=\sigma$ in the case of a hard sphere potential model, see section 2.2.6.a)

$$y(r) = g(r) e^{\beta u(r)} \qquad 2.35$$

2.2.5 The Thermodynamic functions in terms of the Radial Distribution function.

An important assumption that first has to be made before the radial distribution function can be applied in the thermodynamic equations is that the total intermolecular or potential energy is *pair-wise additive*.

$$U_N\left(\mathbf{r}_{1,},\mathbf{r}_{2,}\ldots\mathbf{r}_{N,}\right)=\sum_i\sum_j u\left(r_{ij}\right) \qquad 2.36$$

Equation 2.36 is the sum over all the *pairs* of molecules and r_{ij} is the distance between the two molecules.

If we substitute equation 2.23 into equation 2.17 we will get the following:

$$E=-3NkT^2\left(\frac{\partial\ln(\Lambda)}{\partial T}\right)_{N,V}+NkT^2\left(\frac{\partial\ln\left(q_{rot}q_{vib}q_{elec}q_{nucl}\right)}{\partial T}\right)_{N,V}+ kT^2\left(\frac{\partial\ln\left(Z_{config}\right)}{\partial T}\right)_{N,V} \qquad 2.37$$

The first term in equation 2.37 is the kinetic energy of the system and can easily be shown to be equal to *3/2NkT*. The second term represents the internal energy contribution by the rotational, vibrational, nuclear and electronic energies of the system. These energies are usually very small in comparison to the kinetic energy contribution. Since most of the calculations in this work involves residual properties the first two terms would disappear (as they are present in the ideal fluid as well), and it is therefore not necessary to study them further. The configurational integral term represents the *average* potential energy of the system, $\bar{U}$. It can be developed further as follows:

$$\overline{U}=\frac{\iint U\left(\mathbf{r}_1,\mathbf{r}_2\ldots\mathbf{r}_N\right)e^{-\beta U\left(\mathbf{r}_1,\mathbf{r}_2\ldots\mathbf{r}_N\right)}d\mathbf{r}_1d\mathbf{r}_2\ldots d\mathbf{r}_N}{\iint e^{-\beta U\left(\mathbf{r}_1,\mathbf{r}_2\ldots\mathbf{r}_N\right)}d\mathbf{r}_1d\mathbf{r}_2\ldots d\mathbf{r}_N} \qquad 2.38$$

The right hand part of equation 2.38 is the canonical ensemble average of the intermolecular energy and the equation is based on Gibbs's postulate that a mechanical thermodynamic property of a system is equal to the average of thermodynamic property taken giving all the energy states the same weight [142]. The denominator in this equation is equivalent to the configurational integral, equation 2.24. By applying the approximation of pair-wise additivity,

$U(\mathbf{r}_1,\mathbf{r}_2...\mathbf{r}_N)$ is the sum of N(N-1)/2 pair interactions, and equation 2.38 may be written as follows:

$$\overline{U} = \frac{N(N-1)}{2}\iint u(r_{12})\left\{\frac{\iint e^{-\beta U(\mathbf{r}_3\ldots\mathbf{r}_N)}d\mathbf{r}_3\ldots d\mathbf{r}_N}{Z_{config}}\right\}d\mathbf{r}_1 d\mathbf{r}_2 \qquad 2.39$$

Equation 2.26 can be identified in this expression. Substituting equations 2.27 and 2.28 into equation 2.39:

$$\overline{U} = \frac{N(N-1)}{2}\iint u(r_{12})P^{(2)}(\mathbf{r}_1,\mathbf{r}_2)d\mathbf{r}_1 d\mathbf{r}_2$$

$$= \frac{1}{2}\iint u(r_{12})\rho^{(2)}(\mathbf{r}_1,\mathbf{r}_2)d\mathbf{r}_1 d\mathbf{r}_2$$

$$= \frac{1}{2}\iint u(r_{12})\rho^2 g^{(2)}(\mathbf{r}_1,\mathbf{r}_2)d\mathbf{r}_1 d\mathbf{r}_2 \qquad 2.40$$

Changing the variables of integration to the spherical distance, *r*, between a central molecule a second molecule, leads to the final form of the average intermolecular potential energy of the system:

$$\overline{U} = \frac{N^2}{2V}\int u(r)g(r)4\pi r^2 dr \qquad 2.41$$

Since the configurational integral contains all the volume dependent properties of the system, the system pressure, calculated with equation 2.18, is purely a function of Z_{config}:

$$P = kT\left(\frac{\partial \ln Q}{\partial V}\right)_{N,T} = kT\left(\frac{\partial \ln Z_{config}}{\partial V}\right)_{N,T} \qquad 2.42$$

In order to solve this differential it is convenient to express equation 2.24 in its Cartesian coordinates,

$$Z_{config} = \iint e^{-\beta U(\mathbf{r}_1,\mathbf{r}_2\ldots\mathbf{r}_N)}dx_1 dy_1 dz_1 dx_2 dy_2 dz_2 \ldots dx_N dy_N dz_N \qquad 2.43$$

and then changing the variables of integration so that the limits become constants, and U an explicit function of V:

$$x_i = x_i' V^{1/3} \qquad y_i = y_i' V^{1/3} \qquad etc. \tag{2.44}$$

$$r_{ij} = \left[\left(x_i - x_j \right)^2 + \left(y_i - y_j \right)^2 + \left(z_i - z_j \right)^2 \right]^{1/2}$$

$$= V^{1/3} \left[\left(x_i' - x_j' \right)^2 + \left(y_i' - y_j' \right)^2 + \left(z_i' - z_j' \right)^2 \right]^{1/2} \tag{2.45}$$

and

$$Z_{config} = \int_0^1 \ldots \int_0^1 \iiint e^{-\beta U} \, dx_1' \ldots dz_N' \tag{2.46}$$

$$U = \sum_{1 \le i < j \le N} u\left(r_{ij} \right) \tag{2.47}$$

with

$$\left(\frac{\partial Z_{config}}{\partial V} \right)_{N,T} = NV^{N-1} \int_0^1 \ldots \int_0^1 \iiint e^{-\beta U} \, dx_1' \ldots dz_N' - \frac{NV^N}{kT} \int_0^1 \ldots \int_0^1 \iiint e^{-\beta U} \frac{\partial U}{\partial V} dx_1' \ldots dz_N' \tag{2.48}$$

and

$$\frac{\partial U}{\partial V} = \sum_{1 \le i < j \le N} \frac{r_{ij}}{3V} \frac{du\left(r_{ij} \right)}{dr_{ij}} = \sum_{1 \le i < j \le N} \frac{r_{ij}}{3V} u'\left(r_{ij} \right) \tag{2.49}$$

When equations 2.46 to 2.49 are substituted into 2.42 the *pressure equation* can be determined in terms of the statistical mechanical expressions:

$$P = \frac{NkT}{V} - \frac{N^2}{6V^2} \int_0^\infty r u'(r) g(r) 4\pi r^2 dr \tag{2.50}$$

For a detailed derivation of the following two equations the reader is referred to [142]. Both of the equations are derived from the *grand canonical partition function*, as defined in equation 2.15 :

The derivation of the chemical potential makes use of a coupling parameter, ξ, which varies between 0 and 1, and is used to add and remove one particle from the system, while all the others interact normally.

$$\frac{\mu}{kT} = \ln \rho\Lambda^3 + \ln\left(q_{rot} q_{vib} q_{elec} q_{nucl}\right) + \frac{\rho}{kT} \int_0^1 \int_0^\infty u(r) g(r,\xi) 4\pi r^2 dr d\xi \qquad 2.51$$

The *compressibility* equation is another equation, like the *pressure equation*, equation 2.46, that relates the system pressure, P, to the radial distribution function, but unlike the latter, can be derived without making the assumption of *pair-wise additivity* of the intermolecular energies.

$$kT\left(\frac{\partial \rho}{\partial P}\right) = 1 + \rho \int \left(g(r) - 1\right) d\mathbf{r} \qquad 2.52$$

From the 3 thermodynamic equations for energy, pressure and chemical potential, equations 2.37, 2.50 and 2.51 all the other thermodynamic values, enthalpy, entropy etc., can be determined, and when applied along with expressions for $u(r)$ and $g(r,\rho,T)$ the representation of the fluid will be complete.

2.2.6 Intermolecular energy

In a real fluid a particle is constantly subjected to various intermolecular forces or interactions due to the presence of other particles in the fluid. These forces give rise to the intermolecular or potential energy of the particles, and may be broadly classified under the following types [170]:

- *Electrostatic forces* present between ions and between permanent dipoles, quadrupoles and other higher multipoles.
- *Induced forces* between a permanent dipole or quadrupole and an induced dipole.

- *Specific forces* that result in effects such as association and the formation of hydrogen bonds.
- *Dispersion* (*London*) *forces* present in a system of nonpolar atoms or molecules.

The intermolecular energy is a balance between the various attractive and repulsive interactions in a system, with positive energies indicating an overall net repulsive force and a negative potential energy, a net attractive force.

As already stated in section 2.2 only the potential energies present in a system of nonpolar *atoms* or molecules that are *spherically symmetrical* will be considered in this discussion. The potential energy of non-symmetrical particles is a function of orientation of the particles relative to one another and brings an added degree of complexity to the models. The assumption of the *pair-wise additivity* of intermolecular energies is continued, and only two particle interactions need be considered.

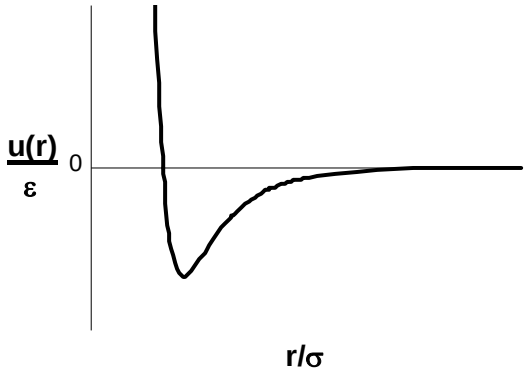

Figure 2.2 Typical potential energy of a nonpolar system

In a nonpolar system the potential energy results as a consequence of short-range repulsive forces due to the overlapping of electron clouds, and longer-range interactions as a result of *induced-dipole – induced-dipole* interactions. Figure 2.2 is a typical plot of the variation of the intermolecular energy, $u(r)$, with intermolecular distance, r.

The induced dipole forces, or *London forces*, were shown by London [134] to be inversely proportional to the relative distance between the particles raised to the 6^{th} power. An equation describing a non-polar spherically symmetrical system should therefore ideally have the following form:

$$u(r) = u_{repulsive}(r) - \frac{C}{r^6} \qquad 2.53$$

2.2.6.a Hard-Sphere Potential

This potential is the simplest model of a real fluid. It has no attractive contribution, and treats the particles as hard spheres. This implies that the only interaction between the particles is due to collisions, and that the smallest distance between any two particles will be equal to one particle diameter, σ.

$$u(r) = \begin{cases} \infty & r < \sigma \\ 0 & r > \sigma \end{cases} \qquad 2.54$$

2.2.6.b Square Well Potential

The *square well* model is an expansion of the hard sphere potential, and incorporates an attractive contribution in the form of a square well, in order to simulate a more realistic potential energy whilst still maintaining its simplicity.

$$u(r) = \begin{cases} \infty & r < \sigma \\ -\varepsilon & \sigma < r < \lambda\sigma \\ 0 & r > \lambda\sigma \end{cases} \qquad 2.55$$

ε represents the well depth in the model, and λ controls the width of the well. λ usually varies between 1.5 and 2 [142].

2.2.6.c Sutherland Potential

Combining the hard-sphere potential model with attractive *London force* contribution of equation 2.53, leads to the *Sutherland* model. *K* is a constant specific to the molecule.

$$u(r) = \begin{cases} \infty & r < \sigma \\ -\dfrac{K}{r^6} & r > \sigma \end{cases} \qquad 2.56$$

2.2.6.d Lennard-Jones 12-6 Potential

The Lennard-Jones potential gives a much more realistic approximation of the real molecular interaction energy compared to the models discussed above. (See Figure 2.3.)

It incorporates the correct attractive form of the intermolecular energy, as expressed in equation 2.53, and represents the repulsive contribution as an inverse function of intermolecular distance raised to the 12^{th} power. This enables the function to model the steep decline in the short-range repulsive forces with increased distance between the particles. The term ε, in equation 2.57, again indicates the maximum well depth and lowest intermolecular potential, and is found at the point where the intermolecular attractive and repulsive forces are in balance.

$$u(r) = 4\varepsilon\left(\left(\frac{\sigma}{r}\right)^{12} - \left(\frac{\sigma}{r}\right)^{6}\right) \qquad 2.57$$

In this equation σ is the collision diameter, or the intermolecular distance, and indicates the distance at which the potential function is equal to zero.

It is important to note that the Lennard-Jones potential model does not approximate the particles as hard spheres and allows the particles to be in closer proximity than what the hard sphere type models would dictate at sufficiently high system energies. This simulates the phenomena of overlapping outer electron orbitals at high energy levels. The Lennard-Jones model allows particles, providing they have enough energy, to interpenetrate completely, in effect treating a particle as consisting out of a point centre surrounded by a completely soft or penetrable cloud.

2.2.6.e The Kihara Potential

The Kihara potential is an extension of the Lennard-Jones potential model, approximating the particles as consisting out of a hard impenetrable core, surrounded by penetrable electron cloud. The Kihara potential model has been developed for wide variety of core geometries of which only the simplest form of a spherical core is presented here:

$$u(r)=\begin{cases}\infty & r<2a \\ 4\varepsilon\left(\left(\frac{\sigma-2a}{r-2a}\right)^{12}-\left(\frac{\sigma-2a}{r-2a}\right)^{6}\right) & r>2a\end{cases} \qquad 2.58$$

In this equation the parameter *a* represents the hard core radius, and σ the collision diameter.

2.2.6.f The Exp-6 or Modified Buckingham potential

Theoretical calculations have suggested that the repulsive potential contributions should be an exponential function in *r*, rather than the inverse power function used in the Lennard-Jones model [170]. The *exp-6* or *modified Buckingham potential model* follows this approach alongside equation 2.53:

$$u(r)=\begin{cases}\infty & r<s \\ \frac{\varepsilon}{1-(6/\gamma)}\left(\frac{6}{\gamma}\exp\left(1-\frac{r}{r_{\min}}\right)-\left(\frac{r_{\min}}{r}\right)^{6}\right) & r>s\end{cases} \qquad 2.59$$

The function goes through a theoretically incorrect maximum at very small values of *r* and necessitates the lower hard-sphere boundary condition for $r<s$, where *s* is the location of the maximum. $-\varepsilon$ is the minimum intermolecular potential at distance r_{min} and γ is a measure of the steepness of the repulsive wall. The collision diameter σ and the distance *s* are dependent on the values assigned to γ and r_{min} model constants.

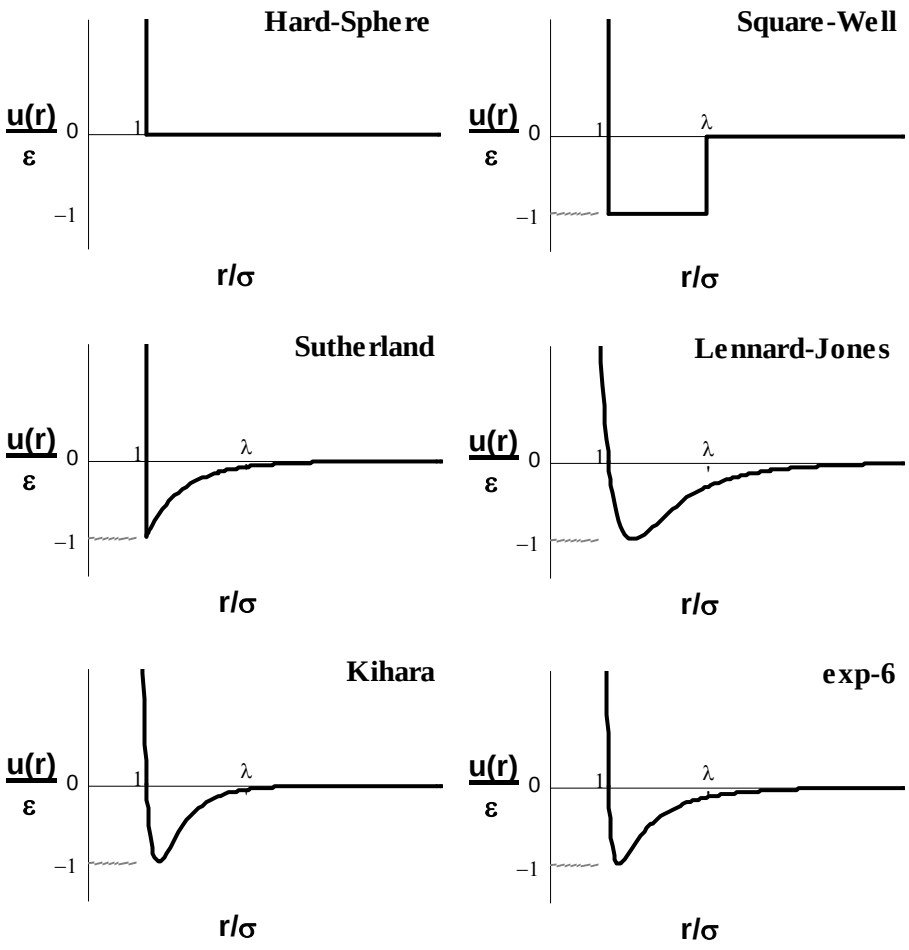

Figure 2.3 Intermolecular potential models for spherical particles

Figure 2.3 is a scaled representation of the various intermolecular potential functions. It should be noted that when the potential models are fitted to a real molecule, such as argon, each function will have its own, and possibly widely differing, values for σ and ε. (For the sake of the representation here a value of 1.5 had been assigned to λ in the hard-sphere model, 0.25σ to a in the Kihara model and 50 to the γ parameter in the exp-16 model.)

2.3 STATISTICAL MECHANICAL EQUATIONS OF STATE

2.3.1 Virial Equation of State

The virial equation of state is a well known and broadly applied equation of state, used to successfully represent may gaseous systems. It was first proposed by Thiesen in 1885 as a MacLauren expansion about zero density or ideal gas state [190, 210]. (Any gas approaches ideal gas behaviour as the system density, ρ, approaches zero, or the system volume tends

towards infinity.) The volume function coefficients, B_2, B_3 and B_4 etc. are known as the *virial coefficients*, and serve as corrections on the deviation from the ideal behaviour as the system density increases.

$$\frac{P}{\rho kT} = 1 + B_2'\rho + B_3'\rho^2 + B_4'\rho^3 + \ldots \qquad 2.60$$

The equation's strength however lies not only in its performance in representing the gaseous phase, but also in the fact that it is not merely an empirical equation, but has a rigorous theoretical foundation [190]. The virial equation of state can be directly derived from the statistical mechanical equations, providing relations between the coefficients and the interactions between clusters of particles, with the virial coefficient B_2 representing two body interactions, coefficient B'_3, 3 body interactions, etc.

The virial equation of state is derived, from theoretical basis, from the grand canonical partition function as defined in section 2.2.2 [142] and the virial coefficients have the following statistical mechanical meaning:

$$B_1' = 1 \qquad 2.61$$

$$B_2' = -\frac{1}{2!V}\left(Z_2 - Z_1^{\,2}\right) \qquad 2.62$$

$$B_3' = -\frac{1}{3V^2}\left[V\left(Z_3 - 3Z_2Z_1 + 2Z_1^{\,3}\right) - 3\left(Z_2 - Z_1^{\,2}\right)^2\right] \qquad 2.63$$

and

$$Z_1 = \int d\mathbf{r}_1 = V \qquad 2.64$$

$$Z_2 = \iint e^{-\beta U_2}\, d\mathbf{r}_1 d\mathbf{r}_2 \qquad 2.65$$

$$Z_3 = \iiint e^{-\beta U_3}\, d\mathbf{r}_1 d\mathbf{r}_2 d\mathbf{r}_3 \qquad 2.66$$

etc.

where Z_i refers to the configurational integral and U_i the intermolecular energy of a system with i particles. From equations 2.63 and 2.65 it is clear that the second virial coefficient is

dependent on the interaction between 2 particles, and from equations 2.64 and 2.66 that the third viral coefficient on the interactions between a maximum of 3 particles.

In order to determine the intermolecular energy of a 3-particle system as needed in equation 2.66, the simplifying assumption of pair-wise additivity (Equation 2.36) should again be made.

Using the *Meyer f-function*, equation 2.34, to simplify the expression, and with some algebraic manipulation the virial coefficients may now be expressed in their final form:

$$B_2'(T) = -\frac{1}{2V}\iint f_{12}\,d\mathrm{r}_1 d\mathrm{r}_2 \qquad 2.67$$

$$B_3'(T) = -\frac{1}{3V}\iiint f_{12} f_{13}\,d\mathrm{r}_1 d\mathrm{r}_2 d\mathrm{r}_3 \qquad 2.68$$

From the fourth virial coefficient the expressions become very long and unmanageable and need to be expressed with the aid of cluster diagrams and graph theory, and entails the sums of integrals over the coordinates of *i* particles, where *i* is the virial coefficient number B_i. (Graph theory and the applications there of are beyond the scope of this discussion.)

By substituting an intermolecular potential function (such as discussed in section 2.2.6) into the virial coefficient equations the actual values of the coefficients may be calculated. Unfortunately substituting any realistic potential function, such as the Lennard-Jones potential, will result in an integral that can only be solved numerically. The hard-sphere model (section 2.2.6.a) gives the following result for B'_2:

$$B_2'(T) = -\frac{1}{2V}\int_0^{\infty}\left(e^{-\beta u_{12}} - 1\right)d\mathrm{r}_1 d\mathrm{r}_2 = -\frac{1}{2}\int_o^{\sigma} -4\pi r^2 dr_{12} = \frac{2\pi\sigma^3}{3} = 4b_0' \qquad 2.69$$

The second virial coefficient of a hard sphere is equal to four times the volume of a hard sphere (generally denoted by b'_0).

B'_2 calculated using the square well model gives the following result:

$$B_2' = b_0'\left(1 - \left(\lambda^3 - 1\right)\left(e^{\beta\varepsilon} - 1\right)\right) \qquad 2.70$$

Using the two square well parameters λ and ε as well as the hard sphere diameter σ (in the b'_0 term) as the adjustable parameters this very basic model can be made to fit the virial coefficient data of real systems exceptionally well [142].

It unfortunately becomes increasingly complicated even when using a simple model such as the hard sphere potential to calculate the higher virial coefficients. (See section 3.4.1.b.)

It is of course generally known that the virial equation is unable to represent the vapour-liquid transition and that irrespective of how many coefficients are applied the equation is not suitable for the application to the high-density liquid phase. Even after corrections have been made for the non-additivity of the interaction energies, it seems that the approach of treating the interactions as a series of two-, three-, four-body interactions etc. is not sufficient at high densities. Another approach has to be used to represent the liquid phase behaviour.

2.3.2 Liquid phase equation of state

As mentioned at the end of section 2.2.5 the thermodynamic behaviour of a fluid system is completely described by the energy, pressure and chemical potential equations, equations 2.37, 2.50 and 2.51. All that is required is an intermolecular potential model, already discussed in section 2.2.6, and an expression for the radial distribution function.

The radial distribution function, unfortunately, is not a simple function to determine, but rather a complex relation between intermolecular distance, temperature and system density, and cannot be determined without making simplifying assumptions.

Once a solution for the radial distribution function has been found it may be linked to the thermodynamic functions, by the *energy, pressure* or *compressibility* equations (equations .2.41, 2.50 and 2.52 respectively).

There are essentially three different methods of determining $g(r)$:

- *Experimental* techniques
- *Integro-differential* methods, using the *superposition approximation*.
- *Integral* methods based on the *direct correlation function*.

Each of these will be discussed in brief in the following sections.

2.3.2.a *Experimental Techniques*

The radial distribution function can be determined experimentally in two ways, either by physical experiments on a real system or by the computer simulation of a theoretical system.

The degree of order in the arrangement of the molecules in a real system can be determined experimentally by studying the X-ray diffraction pattern of that system. A solid will give a sharp pattern, since the molecules are arranged in a regular repeating order, and a fluid will have a more diffuse pattern, as the molecules are now able to move around freely, but with some local short range order. As the system density is decreased, all traces of order will disappear, and $g(r)$ will tend towards 1, the value of an ideal gas.

Experimental values for the radial distribution functions of theoretical systems, on the other hand, can be determined through computer simulation. By performing either *Monte Carlo* or *molecular dynamic* simulations on a system with particles interacting according to a specific theoretical fluid model, such as the hard-sphere or Lennard-Jones potential models, the validity of various assumptions and theories about fluid behaviour may be investigated.

Although the actual values of the radial distribution functions can be obtained by experiment, these values provide no information on the how $g(r)$ is related to the fluid properties.

2.3.2.b *Integro-Differential functions*

One of the first equations for $g(r)$ derived from first principals is known as the *Kirkwood* equation [179]. It uses the potential function, equation 2.27, with an introduced a coupling parameter, ξ, as a starting point in its derivation. The potential function is *differentiated* with respect to ξ, which leads to the following expression [93]:

$$-kT\ln g^{(2)}(r_{12},\xi)=\xi u(r_{12})+\rho\int_0^{\xi}\int_V u(r_{13})\left[g^{(3)}(\mathbf{r}_1,\mathbf{r}_2,\mathbf{r}_3,\xi)-g^{(2)}(r_{13},\xi)\right]d\mathbf{r}_3 d\xi \qquad 2.71$$

Equation 2.71 gives $g^{(2)}$ in terms of $g^{(3)}$ or, in general, $g^{(n)}$ in terms of $g^{(n+1)}$. This type of coupled equation is called a hierarchy. This expression of the radial distribution function is exact with no simplifying assumptions, unfortunately, however, there is no exact way to break the hierarchy in order to express $g^{(2)}$ in a closed from.

Kirkwood made the following assumption [122], known as the *superposition assumption*, in order to solve the integral in equation 2.71:

$$g^{(3)}(\mathbf{r}_1,\mathbf{r}_2,\mathbf{r}_3) \approx g^{(2)}(\mathbf{r}_1,\mathbf{r}_2)g^{(2)}(\mathbf{r}_2,\mathbf{r}_3)g^{(2)}(\mathbf{r}_1,\mathbf{r}_3) \qquad 2.72$$

which leads to the final form of the *Kirkwood* equation:

$$-kT\ln g(r_{12},\xi) = \xi u(r_{12}) + \rho\int_0^{\xi}\int_V u(r_{13})g(r_{13},\xi)[g(r_{23})-1]d\mathbf{r}_3 d\xi \qquad 2.73$$

A different approach in deriving the distribution function is to, instead of differentiating equation 2.27 with respect to the coupling parameter, take the differential with respect to coordinates of a particle. As in the case of the Kirkwood equation, this approach also results in a coupled hierarchy, and must be uncoupled by means of the superposition approximation. The equation derived in this manner is known as the *Born-Green-Yvon* equation:

$$-\frac{\partial}{\partial r}[kT\ln g(r,\xi)+\xi u(r)] = \pi\xi\rho\int_0^{\infty}u'(s)g(s,\xi)ds\int_{|r-s|}^{|r+s|}\frac{s^2+r^2-R^2}{r^2}Rg(R)dR \qquad 2.74$$

Where *s* and *R* are dummy variables. A detailed derivation can be found in [92].

Unfortunately , even for simple models such as the hard-sphere fluid, both of these equations require numerical solutions of the integral [179].

2.3.2.c Direct correlation functions

Direct correlation functions, as the name suggests, are derived using the *Ornstein-Zernike* equation, equation 2.33, as starting point instead of the probability function as in the derivation of the integro-differential functions in the previous section.

Equation 2.33 provides a functional relationship between the *total* and *direct correlation functions*, $h(r)$ and $c(r)$. If another independent function between the two correlation functions could be found, equation 2.33 could be written in a closed form, and the radial distribution function determined. This is done through the use of graph theory, where the difference between the two functions is expressed in terms of a finite sum of graphs ordered by density. (From the definition of equation 2.33, direct correlation function graphs are a subset of the

total correlation graphs). Only the final equation will be presented here [190], for a more detailed derivation the reader is referred to a discussion on the graph theory involved in [179]:

$$h(r_{12}) - c(r_{12}) = \ln[h(r_{12}) + 1] + \frac{u(r_{12})}{kT} - B(r_{12}) \qquad 2.75$$

$B(r_{ij})$ contains all the unknown functions or graphs.

Choosing $B(r_{ij})=0$ (called the *hypernetted chain approximation*), and substituting the equation into equation 2.33 leads to the *hypernetted chain integral equation*. It is expressed in terms of $y(r_{12})$ (defined in equation 2.35):

$$\ln(y(r_{12})) = \rho \int \left[h(r_{13}) - \ln g(r_{13}) - \frac{u(r_{13})}{kT} \right] [g(r_{23}) - 1] d\mathbf{r}_3 \qquad 2.76$$

A second integral equation, known as the *Percus-Yevick integral equation* can be derived writing equation 2.71 in terms of $g(r_{12})$ and expanding the coefficient [190]:

$$g(r_{12}) \approx \exp\left[-\frac{u(r_{12})}{kT} + B(r_{12}) \right] [g(r_{12}) - c(r_{12}) + \ldots] \qquad 2.77$$

Setting $B(r_{ij})=0$ and ignoring the higher order terms of the expansion, yields the *Percus-Yevick approximation* [190]:

$$g(r_{12}) = \exp\left[-\frac{u(r_{12})}{kT} \right] [g(r_{12}) - c(r_{12})] \qquad 2.78$$

This approximation, combined with equation 2.43, gives a very simple expression for the radial distribution function in terms of $y(r_{12})$:

$$y(r_{12}) = 1 + \rho \int f(r_{13}) y(r_{13}) h(r_{23}) d\mathbf{r}_3 \qquad 2.79$$

The integral equations are generally combined with the pressure and compressibility equations, (equations 2.50 and 2.52) in order to describe the thermodynamic systems, however, only the Percus-Yevick equation applied to a hard sphere model results in an analytically solvable equation of state. Two different equations are obtained depending on whether the pressure or compressibility equations were used to link the radial distribution function to the

thermodynamic expressions. Had the Percus-Yevick equation been exact, and not required simplifying assumptions, the two approaches would have yielded identical equations of state.

Sengers et al. [190] contains a detailed discussion on recent developments and advances in the integral equation approach, which does not fall within the scope of this discussion.

2.3.3 The perturbation theory

An interesting result of the rigorous study of the radial distribution functions is that it has been found that the radial distribution function of a simple hard-sphere fluid model is surprisingly similar to the results of X-ray diffraction experiments on real systems and those calculated using more realistic fluid models (Lennard-Jones) [142, 220]. This lead to the speculation that the structural behaviour of a (single phase) fluid is strongly governed by the short-range repulsive forces, of which the hard sphere model is a fair approximation, and that the long range attractive forces contributes to a uniform attractive potential acts over the entire fluid system. Zwanzig made a similar observation in 1954, when he noted that at high temperatures, the equation of state of gases is determined largely by forces of repulsion between its components, and that at lower temperatures it should be possible to obtain the equation of state by considering forces of attraction as perturbations on the forces of repulsion [251]. This approach has been proven to be highly successful even at low temperatures and liquid densities [15, 16].

Zwanzig performed a perturbation expansion on the configurational integral of the canonical partition function, equation 2.24, by first assuming that the intermolecular energy of a system, U_N, can be separated into an unperturbed, $U_N^{(0)}$, and a perturbed part, $U_N^{(1)}$:

$$U_N = U_N^{(0)} + U_N^{(1)} \qquad 2.80$$

Equation 2.24 may then be written as follows:

$$Z_{config} = \iint e^{-\beta\left(U_N^{(0)} + U_N^{(1)}\right)} d\mathbf{r}_1 d\mathbf{r}_2 \ldots d\mathbf{r}_N$$

$$= \iint e^{-\beta\left(U_N^{(0)} + U_N^{(1)}\right)} d\mathbf{r}_1 d\mathbf{r}_2 \ldots d\mathbf{r}_N * \frac{\iint e^{-\beta U_N^{(0)}} d\mathbf{r}_1 d\mathbf{r}_2 \ldots d\mathbf{r}_N}{\iint e^{-\beta U_N^{(0)}} d\mathbf{r}_1 d\mathbf{r}_2 \ldots d\mathbf{r}_N}$$

$$= \iint e^{-\beta U_N{}^{(0)}} d\mathbf{r}_1 d\mathbf{r}_2 \ldots d\mathbf{r}_N * \frac{\iint e^{-\beta U_N{}^{(0)}} e^{-\beta U_N{}^{(1)}} d\mathbf{r}_1 d\mathbf{r}_2 \ldots d\mathbf{r}_N}{\iint e^{-\beta U_N{}^{(0)}} d\mathbf{r}_1 d\mathbf{r}_2 \ldots d\mathbf{r}_N} \qquad 2.81$$

The first term in equation 2.81 is the configurational integral of an unperturbed system, and the second term can be recognised as the canonical ensemble average of $exp(-\beta U_N{}^{(1)})$ in the unperturbed system. The configurational integral may therefore be expressed as:

$$Z_{config} = Z_{config}{}^{(0)} \left\langle \exp(-\beta U_N{}^{(1)} \right\rangle_0 \qquad 2.82$$

The exponential expression can now be expanded in a MacLauren series, which results in a power series in β:

$$\left\langle \exp\left(-\beta U_N{}^{(1)}\right) \right\rangle_0 = 1 - \beta \left\langle U_N{}^{(1)} \right\rangle + \frac{\beta^2}{2!} \left\langle \left(U_N{}^{(1)}\right)^2 \right\rangle - \frac{\beta^3}{3!} \left\langle \left(U_N{}^{(1)}\right)^3 \right\rangle + \ldots$$

$$= \sum_{k=0}^{\infty} \frac{(-\beta)^k}{k!} \left\langle \left(U_N{}^{(1)}\right)^k \right\rangle \qquad 2.83$$

The residual Helmholtz free energy (the *configurational Helmholtz free energy*), equation 2.16, of this system may then be expressed as:

$$A^{Resid} = \left(-kT \ln Q_N\right) - \left(-kT \ln Q_N{}^{ideal}\right)$$

$$= -\frac{1}{\beta} \ln Z_{config}$$

$$= -\frac{1}{\beta} \ln Z_{config}{}^{(0)} - \frac{1}{\beta} \ln \left\langle \exp\left(-\beta U_N{}^{(1)}\right) \right\rangle_0$$

$$= A^{(0)} + A^{(1)} \qquad 2.84$$

Where the first term of equation 2.84 is the Helmholtz free energy of the unperturbed system, and the second term the perturbation free energy:

$$-\beta A^{(1)} = \ln \left\langle \exp\left(-\beta U_N{}^{(1)}\right) \right\rangle_0 \qquad 2.85$$

Zwanzig expressed the perturbation free energy as a power series in β using the following function. w_i at this stage is some unknown function.

$$A^{(1)} = \sum_{i=1}^{\infty} \frac{w_i}{i!} (-\beta)^{i-1} \qquad 2.86$$

From equations 2.85, 2.86 and 2.83:

$$\exp\left(-\beta A^{(1)}\right) = \left\langle \exp\left(-\beta U_N{}^{(1)}\right) \right\rangle_0 = \exp\left(\sum_{i=1}^{\infty} \frac{w_i}{i!} (-\beta)^i \right) = \sum_{k=0}^{\infty} \frac{(-\beta)^k}{k!} \left\langle \left(U_N{}^{(1)}\right)^k \right\rangle \qquad 2.87$$

This w_i to be expressed in terms of $\langle U_N{}^{(1)} \rangle$. Zwanzig derived a general formula for w_i, but only the expressions of the first three w terms will be presented here:

$$w_1 = \left\langle U_N{}^{(1)} \right\rangle_0$$

$$w_2 = \left\langle \left(U_N{}^{(1)}\right)^2 \right\rangle_0 - \left\langle U_N{}^{(1)} \right\rangle_0{}^2$$

$$w_3 = \left\langle \left(U_N{}^{(1)}\right)^3 \right\rangle_0 - 3\left\langle \left(U_N{}^{(1)}\right)^2 \right\rangle_0 \left\langle U_N{}^{(1)} \right\rangle_0 + 2\left\langle U_N{}^{(1)} \right\rangle_0{}^2 \qquad 2.88$$

The residual Helmholtz free energy of the system is therefore equal to:

$$A^{Resid} = A^{(0)} + w_1 - \frac{\beta}{2} w_2 + O\left(\beta^2\right) \qquad 2.89$$

If the assumption of *pair-wise additivity* of the perturbation energy is made the w_1 may be determined as follows:

$$w_1 = \left\langle \sum_{i<j} u_{ij}{}^{(1)}\left(r_{ij}\right) \right\rangle_0 = \frac{N(N-1)}{2} \left\langle u^{(1)}\left(r_{12}\right) \right\rangle_0$$

$$= \frac{N(N-1)}{2} \frac{1}{Z_{config}{}^{(0)}} \iint e^{-\beta U_N{}^{(0)}} u^{(1)}\left(r_{12}\right) d\mathbf{r}_1 d\mathbf{r}_2 \ldots d\mathbf{r}_N$$

$$= \frac{N(N-1)}{2} \iint u^{(1)}(r_{12}) \frac{\iint e^{-\beta U_N{}^{(0)}} d\mathbf{r}_3 \ldots d\mathbf{r}_N}{Z_{config}{}^{(0)}} d\mathbf{r}_1 d\mathbf{r}_2 \qquad 2.90$$

substituting equation 2.27, the probability function, ρ_0, of the unperturbed system

$$w_1 = \frac{1}{2} \iint u^{(1)}(r_{12}) \rho_0{}^{(2)}(r_{12}) d\mathbf{r}_1 d\mathbf{r}_2 \qquad 2.91$$

and equation 2.29, the unperturbed system radial distribution function, $g_0(r_{12})$:

$$w_1 = \frac{\rho^2}{2} \iint u^{(1)}(r_{12}) g_0(r_{12}) d\mathbf{r}_1 d\mathbf{r}_2 = \frac{\rho^2 V}{2} \int_0^\infty u^{(1)}(r_{12}) g_0(r_{12}) 4\pi r^2 dr \qquad 2.92$$

The higher order w_i terms require expressions for the terms, $\langle \quad (U_N{}^{(1)})^i) \rangle_{(0)}$ where $i > 1$. These expressions require higher order probability or distribution functions of the unperturbed system, which are normally not known.

$$\begin{aligned} w_2 = & \frac{1}{4} \iint \rho_0{}^{(4)}(\mathbf{r}_1, \mathbf{r}_2, \mathbf{r}_3, \mathbf{r}_4) u^{(1)}(\mathbf{r}_1, \mathbf{r}_2) u^{(1)}(\mathbf{r}_3, \mathbf{r}_4) d\mathbf{r}_1 d\mathbf{r}_2 d\mathbf{r}_3 d\mathbf{r}_4 + \\ & \iint \rho_0{}^{(3)}(\mathbf{r}_1, \mathbf{r}_2, \mathbf{r}_3) u^{(1)}(\mathbf{r}_1, \mathbf{r}_2) u^{(1)}(\mathbf{r}_2, \mathbf{r}_3) d\mathbf{r}_1 d\mathbf{r}_2 d\mathbf{r}_3 + \\ & \frac{1}{2} \iint \rho_0{}^{(2)}(\mathbf{r}_1, \mathbf{r}_2) \left(u^{(1)}(\mathbf{r}_1, \mathbf{r}_2)\right)^2 d\mathbf{r}_1 d\mathbf{r}_2 \end{aligned} \qquad 2.93$$

By choosing a well defined reference term, where $g_0(r)$, $\rho_0(r)$ and $Z_{config}{}^{(0)}$ (and therefore $A^{(0)}$) are known, the Helmholtz free energy of the system can therefore be calculated up to the first perturbation. When the real system is not far removed from the reference unperturbed system, equation 2.89 is rapidly convergent, and only this first perturbation term is required, however if this is not the case the calculation of the second and higher perturbation terms are problematic. Two approaches have been suggested to overcome the problem of the poorly described multi-body distribution functions, and will be discussed in the following sections.

2.3.3.a The Barker and Henderson Theory

The Barker and Henderson [16] approach in approximating w_2 (equation 2.93) starts with dividing the intermolecular distances into discrete intervals (r_0,r_1),(r_1,r_2), $\ldots(r_j,r_{j+1})\ldots$ (r_k,r_{k+1}) As the interval width tends towards zero the original continuous description of the system can

be recovered. By dividing the intermolecular distances into intervals, the system has in effect been transformed into a grand canonical ensemble, with an average radial distribution function of g_0.

A probability function, equation 2.94, can then be defined to describe the probability that there would be N_i particles in the interval (r_i,r_{i+1}) for $i = 0,1\ldots$ in an *unperturbed* system:

$$\rho^{(k)}\left(N_0, N_1 \ldots N_j \ldots\right) \equiv \rho\left(\{N_j\}\right) \qquad 2.94$$

By choosing the interval, (r_j,r_{j+1}), small enough, the perturbing intermolecular potential $U^{(1)}(r_j,r_{j+1})$ can be considered as having a constant value $u_j^{(1)}$ over the entire interval. Equation 2.82 can then be written as:

$$Z_{config} = Z_{config}^{(0)} \left\langle \exp(-\beta \sum_j N_j u_j^{(1)} \right\rangle_0$$

$$= Z_{config}^{(0)} \sum_{N_0,N_2,\ldots} p\left(N_0, N_2, \ldots\right) \exp(-\beta \sum_j N_j u_j^{(1)}) \qquad 2.95$$

By expanding equation 2.95:

$$Z_{config} = Z_{config}^{(0)} \left[\sum_{\{N_j\}} \rho\left(\{N_j\}\right) - \beta \sum_j u_j^{(1)} \sum_{\{N_j\}} \rho\left(\{N_j\}\right) N_j + \right.$$

$$\left. \frac{\beta^2}{2} \sum_i \sum_j u_j^{(1)} u_j^{(1)} \sum_{\{N_j\}} \rho\left(\{N_j\}\right) N_i N_j \right]$$

$$Z_{config} = Z_{config}^{(0)} \left[1 - \beta \sum_j u_j^{(1)} \left\langle N_j \right\rangle + \frac{\beta^2}{2} \sum_i \sum_j u_j^{(1)} u_j^{(1)} \left\langle N_i N_j \right\rangle + \ldots \right] \qquad 2.96$$

and taking the logarithm:

$$A^{Resid} = A^{(0)} + \sum_j \left\langle N_j \right\rangle u_j^{(1)} - \frac{\beta}{2} \sum_i \sum_j \left(\left\langle N_i N_j \right\rangle - \left\langle N_i \right\rangle \left\langle N_j \right\rangle \right) u_j^{(1)} u_j^{(1)} + O\left(\beta^2\right) \qquad 2.97$$

The statistics involving a grand canonical ensemble or partition function have not been discussed in this work, and can be found in most texts on statistical thermodynamics [93],

[142]. From the grand canonical ensemble statistics it can be shown that the first and second moments of the N_j are all that is required to determine w_2, and that the first moment, $\langle N_j \rangle$, can be directly related to the average radial distribution function:

$$\left\langle N_j \right\rangle = 2\pi N\rho \int_{r_j}^{r_{j+1}} r^2 g_0(r)dr$$

$$= 2\pi r_i^{\,2} N\rho g_0\left(r_j\right)\left(r_j - r_{j-1}\right) \qquad 2.98$$

(Equation 2.98 is only valid if the interval width is sufficiently small.)

The second-moment term has to be evaluated approximately, and Barker and Henderson followed two approaches.

The first approach is called the *macroscopic compressibility* approach. If N_j is number of molecules in spherical cells surrounding a central molecule and the cells are treated as having macroscopic volumes, the number of molecules in different cells would be uncorrelated:

$$\left\langle N_i N_j \right\rangle - \left\langle N_i \right\rangle \left\langle N_j \right\rangle = 0 \qquad i \neq j \qquad 2.99$$

The fluctuation of the number of molecules in a specific shell would then be given by the variance in the number of particles in a grand canonical ensemble:

$$\left\langle N_i^{\,2} \right\rangle - \left\langle N_i \right\rangle^2 = \left\langle N_i \right\rangle kT\left(\frac{\partial\rho}{\partial P}\right)_0 = \left\langle N_i \right\rangle \frac{1}{\beta}\left(\frac{\partial\rho}{\partial P}\right)_0 \qquad 2.100$$

By substituting equations 2.98, 2.99 and 2.100 into equation 2.97 and taking the interval width to the continuum limit the following expression for the Helmholtz free energy can be obtained:

$$A^{Resid} = A^{(0)} + \frac{\rho^2 V}{2}\int_0^\infty u^{(1)}(r_{12})g_0(r_{12})4\pi r^2 dr$$

$$-\frac{\rho^2 V\beta}{4}\int_0^\infty \left[u^{(1)}(r_{12})\right]^2 \frac{1}{\beta}\left(\frac{\partial\rho}{\partial P}\right)_0 g_0(r_{12})4\pi r^2 dr + O\left(\beta^2\right) \qquad 2.101$$

The second approach is the more satisfactory approximation is that of using the *local* compressibility in the third term of equation 2.101. In instead of taking the pressure derivative of the average system density, the derivative is taken of the local density, $\rho g_0(r)$, effectively including the radial distribution in the differential. This *local compressibility approximation* results in the following expression for the Helmholtz free energy:

$$A^{Resid} = A^{(0)} + \frac{\rho^2 V}{2}\int_0^\infty u^{(1)}(r_{12})g_0(r_{12})4\pi r^2 dr - \frac{\rho^2 V\beta}{4}\int_0^\infty \left[u^{(1)}(r_{12})\right]^2 \frac{1}{\beta}\left(\frac{\partial}{\partial P}(\rho g_0(r_{12}))\right)_0 4\pi r^2 dr + O(\beta^2) \qquad 2.102$$

Up to this point in the derivation, no assumptions have been made on the type intermolecular potential model or the division of these models into an unperturbed and perturbation contribution. Barker and Henderson initially applied this approach to a square well fluid, taking the hard sphere repulsive potential as the unperturbed potential, and the attractive square well as the perturbation, using the results obtained from the *Percus-Yevick integral equation* for a hard sphere model to determine the values for $g_0(r)$ and $(\partial/\partial P)[\rho g_0(r)]_0$. They achieved excellent agreement with Monte Carlo and molecular dynamic simulations of a square well fluid. They also extended their work, to take into account the fact that the repulsive potential of real systems is not infinitely steep [15].

In their approach to model a Lennard-Jones fluid through the perturbation theory, they defined an intermolecular potential function $v(d,\sigma,r,\alpha,\gamma)$ that is not only dependent on the hard sphere diameter, σ, and intermolecular distance, r, but also incorporates an *inverse-steepness parameter*, α, and a *well depth parameter*, γ, to account for the finite steepness of the repulsive and the well depth of the attractive potential respectively. The function can be expressed as follows:

$$v(d,\sigma,\alpha,\gamma) = \begin{cases} u\left(d+(r-d)/\alpha\right) & d+(r-d)/\alpha < \sigma \\ 0 & \sigma < d+(r-d)/\alpha < d+(\sigma-d)/\alpha \\ \gamma u(r) & \sigma < r \end{cases} \qquad 2.103$$

The parameter α varies the steepness of the modified function in the repulsive region and parameter γ the depth of the potential in the attractive region. The d parameter is a distance parameter that will be defined later. For $\alpha=\gamma=0$ the equation 2.103 becomes a hard sphere

potential of parameter d, and for $\alpha=\gamma=1$ function is reduced to the original potential function $u(r)$.

The residual Helmholtz energy of the system can be expanded as a double Taylor series expansion about $\alpha=\gamma=0$, which leads to the following:

$$A^{Resid} = A^{(0)} + \alpha\left(\frac{\partial A}{\partial \alpha}\right)_{\substack{\alpha=0\\ \gamma=0}} + \gamma\left(\frac{\partial A}{\partial \gamma}\right)_{\substack{\alpha=0\\ \gamma=0}} + \frac{\alpha^2}{2}\left(\frac{\partial^2 A}{\partial \alpha^2}\right)_{\substack{\alpha=0\\ \gamma=0}} + \frac{\gamma^2}{2}\left(\frac{\partial^2 A}{\partial \gamma^2}\right)_{\substack{\alpha=0\\ \gamma=0}} + \ldots \qquad 2.104$$

It should be noted that the coefficients of $\alpha,\gamma,\alpha^2,\gamma^2$ etc. are all evaluated at conditions where $\alpha = \gamma = 0$, and that they are in fact hard-sphere quantities.

The original article by Barker and Henderson [15] contains the lengthy algebra involved in differentiating equation 2.104, of which only the final result will be presented here:

$$\begin{aligned} A^{Resid} = A^{(0)} &- \alpha 2\pi N\rho d^2 \frac{g_0(d)}{\beta}\left(d - \int_0^\sigma f(z)dz\right) + \gamma 2\pi\rho N\int_\sigma^\infty u(r)g_0(r)r^2 dr \\ &-\gamma^2\pi\rho N\left(\frac{\partial\rho}{\partial P}\right)_0 \frac{\partial}{\partial\rho}\left[\rho\int_\sigma^\infty u^2(r)g_0(r)r^2 dr\right] + O(\alpha^2) + O(\alpha\gamma) \end{aligned} \qquad 2.105$$

The first order terms of α and γ are exact, but the γ^2 term has been evaluated in terms of the *local compressibility approximation* as discussed above. (The $f(z)$ function is the Meyer function as defined in equation 2.34.)

Up to this point the distance parameter d has had no value assigned to it. By defining it as shown in equation 2.106, the second term in equation 2.105 will be equal to zero for all temperatures and densities.

$$d = \int_0^\sigma f(z)dz \qquad 2.106$$

The integral is a function of temperature but independent of the system density. The parameter d is therefore in effect a well defined temperature dependent hard sphere diameter.

By setting $\alpha = \gamma = 1$ in equation 2.105, the original potential function is recovered, and A^{Resid} becomes the residual Helmholtz energy of a system interacting with a potential function $u(r)$.

Barker and Henderson propose that by defining d in terms of equation 2.106, the values of the terms in α^2, $\alpha\gamma$ and other higher order combinations are considerably smaller than the γ^2 term, and may be ignored [15]. This residual Helmholtz energy equation may therefore be expressed as:

$$A^{Resid} = A^{(0)} + 2\pi\rho N\int_{\sigma}^{\infty} u(r)g_0(r)r^2dr - \pi\rho N\left(\frac{\partial\rho}{\partial P}\right)_0 \frac{\partial}{\partial\rho}\left[\rho\int_{\sigma}^{\infty} u^2(r)g_0(r)r^2dr\right] \qquad 2.107$$

When comparing equations 2.102 and 2.107, the expressions appear very similar. It should however be noted that, in equation 2.107, A_0, g_0 and $(\partial\rho/\partial P)_0$ are the Helmholtz free energy, radial distribution function and compressibility of a system of hard spheres of *diameter d*, and $u(r)$ the potential function of choice. The integrals in equation 2.107 are also evaluated over the *entire* potential function with the collision diameter, σ, as the lower boundary, as opposed to equation 2.102 where the integrals are taken over the perturbation potential $u^{(1)}(r)$, and evaluated between the bounds 0 and ∞.

It should also be noted that Barker and Henderson observed that the local and macroscopic approximations are unreliable at high densities [17]. These approximations are however still commonly applied in perturbation approximations because of the closed analytical expression of the second perturbation term that is obtained [35, 82, 85]. Smith et al. [195] proposed an alternative approximate evaluation of the second order perturbation term. Instead of the *macroscopic* or *local density approximations* they used equation 2.93 together with equation 2.29 and the s*uperposition approximation* for the radial distribution function, equation 2.72, to derive a series of integrals that has to be evaluated through graph theory. The superposition approximation is exact at low densities but inaccurate at high densities. A second alternative to the density approximations was recently proposed by Zhang [248]. In his work he aimed to provide a correction on the assumption, used in the macroscopic density approximation, that the number of molecules in neighbouring cells were uncorrelated. His approach resulted in the following expression for the second perturbation term:

$$A^{(2)} = -\frac{\rho^2 V\beta}{4}\left(1+2K\eta^2\right)\int_0^{\infty}\left[u^{(1)}(r_{12})\right]^2\frac{1}{\beta}\left(\frac{\partial\rho}{\partial P}\right)_0 g_0(r_{12})4\pi r^2dr \qquad 2.108$$

Where K is a proportion coefficient and $\eta = \pi\rho\sigma^3/6$, the reduced density. $K \approx (1/\eta_f)^2$ where η_f is the hard sphere freezing density and equal to 0.493 (See section 3.4.1.a.)

2.3.3.b The Chandler-Weeks-Andersen, CWA, Theory

Weeks, Chandler and Andersen [228] followed a different approach to Barker and Henderson in developing a perturbation equation applicable to real fluids. Instead of extending the perturbation to the second and higher terms, they used an alternative approach in selecting the unperturbed potential function which resulted in a rapid convergence of the expansion and hence requiring only the first perturbation term.

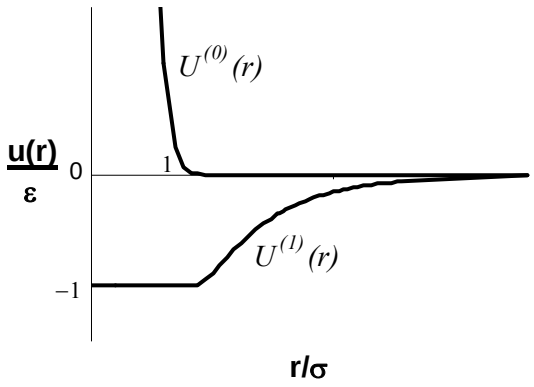

Figure 2.4 Chandler-Weeks-Anderson separation of Lennard-Jones potential into unperturbed and perturbation contributions.

Chandler et al. argued that the regions where the repulsive and attractive *forces* dominate, and not merely the separation of positive and negative intermolecular *potentials*, should govern the separation of the intermolecular energy into an unperturbed state and a perturbation contribution. According to the *CWA* theory the Lennard-Jones potential would therefore be separated as such:

$$u^{(0)}(r) = \begin{cases} u(r) + \varepsilon & r < 2^{1/6}\sigma \\ 0 & r \geq 2^{1/6}\sigma \end{cases} \qquad 2.109$$

$$u^{(1)}(r) = \begin{cases} -\varepsilon & r < 2^{1/6}\sigma \\ u(r) & r \geq 2^{1/6}\sigma \end{cases} \qquad 2.110$$

where ε represents the well depth of the original Lennard-Jones potential (equation 2.57). This separation is depicted in Figure 2.4.

The authors have shown that for a Lennard-Jones system, only using the first perturbation term, w_1, (equation 2.92), this approach has an accuracy of about 10% at low system densities at low and high temperatures, but that the accuracy is greatly improved at high system densities.

This approach, however, has the disadvantage that the properties of reference system, as defined in equation 2.109, is not as well defined as when using a hard-sphere potential model as the unperturbed state. To overcome this problem, Chandler et al. approximated $y_0(r)$ (equation 2.35) of the reference system as equivalent to $y_d(r)$ for a hard-sphere system with a hard-sphere diameter d. The radial distribution function of the reference system can then be calculated in terms of the hard-sphere system:

$$g_0(r) \approx y_d(r)\exp\left(-\beta u^{(0)}(r)\right) \qquad 2.111$$

The diameter d is determined by requiring that the thermodynamic properties of the reference system be equal to that of the hard-sphere system through the compressibility function, equation 2.52. This leads to the following relation ($u^{(d)}$ refers to the hard-sphere potential model):

$$\int\left(y_d e^{-\beta u^{(0)}(r)} - 1\right)d\mathbf{r} = \int\left(y_d e^{-\beta u^{(d)}(r)} - 1\right)d\mathbf{r} \qquad 2.112$$

d is therefore a function of temperature and density. Once the value of d has been determined at a given set of conditions, the Helmholtz free energy of the reference system, $A^{(0)}$, is taken to be that of the hard-sphere system with diameter d at the same density, and $g_0(r)$ determined through equation 2.111, thus providing all the information required to evaluate the total residual Helmholtz free energy expression:

$$A^{Resid} = A^{(0)} + \frac{\rho^2 V}{2}\int_0^\infty u^{(1)}(r_{12})g_0(r_{12})4\pi r^2 dr \qquad 2.113$$

2.4 EMPIRICAL EQUATIONS OF STATE AND STATISTICAL MECHANICS

In the previous section a brief overview was given of how the classical thermodynamic properties of a fluid, internal energy, Helmholtz free energy, pressure and entropy, can be determined from a statistical mechanical description a fluid.

However, many equations of state have been developed without a direct consideration of the fluid statistical mechanical properties. The question now arises of whether these equations are truly empirical in nature, or if they have some theoretical justification.

2.4.1 Virial Equation of State and Derivative functions

The theoretical derivation of the virial equation has already been discussed in some detail in section 2.3.1, where it has been shown how the MacLauren series expansion about ρ=0, has a definite statistical mechanical validation.

The virial equation of state when applied to the low-pressure region well away from the liquid-vapour phase transition is very reliable, even when truncated after the third or even second coefficient. [185, 190], but unfortunately as already have been discussed the equation is very slow to converge at high densities, and many virial coefficients are required before reasonably accurate results can be achieved. These higher order coefficients are generally not known, with only the second and to a smaller extent the third virial coefficients having been determined experimentally. [64]

Truncated forms of the virial equation state have been used by many authors as starting points in the development of empirical equations. Kamerlingh Onnes, in 1901, [108, 185] was the first to utilise the power series form of the virial equation of state to fit *P*-*v*-*T* data. He truncated the virial expansion after the 8th term, and dropped all the odd powers, except for the second term:

$$PV = A + \frac{B}{V} + \frac{C}{V^2} + \frac{D}{V^3} + \frac{E}{V^6} + \frac{F}{V^8} \qquad 2.114$$

These coefficients in this case have of course lost all their theoretical significance.

Another example an equation of state based on the virial coefficient expansion is the well known *Benedict-Webb-Rubin* equation with its many variations. It was first published in 1940 and used to model the *P-v-T* data of methane, ethane, propane and n-butane, and since then there have been many useful adaptations [10, 185]. The coefficients of these models are fitted to experimental pure component data, and again have no connotation to the original underlying theory.

Although empirical equations of this type are very accurate in their representation of pure component systems, the mixing rules, required to extend them to mixtures, remain largely unknown due to the vast number of component specific parameters required.

2.4.2 Van der Waals Type Equations of State

The original Van der Waals equation of state is probably one of the most influential equations that have ever been developed. This equation, proposed by Van der Waals in 1873, was the first capable of representing both the liquid and vapour phases with reasonable accuracy and could predict the liquid-vapour phase transition.

Van der Waals provided a correction for the volume occupied by the molecules themselves, which reduced the actual volume available for molecular motion, and took the attractive forces between the molecules into account. These attractive forces resulted in a reduction in the actual system pressure, and could be assumed to be proportional to the number of particles per unit volume, and inversely proportional to the system volume. Van der Waals postulated that the corrected system pressure and volume should obey the ideal gas law [190, 217]:

$$\left(P-\frac{a}{v^2}\right)(v-b)=RT \qquad 2.115$$

This expression can be written in the more generally known form:

$$P=\frac{RT}{v-b}-\frac{a}{v^2} \qquad 2.116$$

Parameter *b* represents the volume occupied by the molecules, and parameter *a* is characteristic of the intermolecular attractions. These parameters are characteristic of each fluid, and may either be obtained by fitting the EOS to pure component data over a range of temperatures and pressures or by enforcing the critical point conditions:

$$\left.\frac{\partial P}{\partial v}\right|_{P_c,T_c} = \left.\frac{\partial^2 P}{\partial v^2}\right|_{P_c,T_c} = 0 \qquad 2.117$$

Although Van der Waals derived this equation intuitively, it is also possible to derive it from of a statistical mechanical perspective, by making certain simplifying assumptions. This approach will be illustrated in the following sections, by firstly defining the *generalized Van der Waals partition function* and then making certain simplifying assumptions. It will also be shown how the other Van der Waals type or cubic equations of state are simply modifications of these assumptions.

2.4.2.a The Generalized Van der Waals Partition Function

When deriving a pressure equation only the configurational integral of the fluid needs to be considered. The configurational integral of an ideal fluid is equal to V^N. (Section 2.2.2)

$$Z_{config} = \int_0^V \int \exp(-\beta 0) d\mathbf{r}_1 \ldots d\mathbf{r}_N = \int_0^V \int d\mathbf{r}_1 \ldots d\mathbf{r}_N = V^N \qquad 2.118$$

For a hard-sphere fluid, the integral is identical to equation 2.118 except that the lower integration boundary is now the hard sphere diameter:

$$Z^{HS}{}_{config} = \int_0^V \int \exp(-\beta U_N) d\mathbf{r}_1 \ldots d\mathbf{r}_N = \int_0^\sigma \int \exp(-\infty) d\mathbf{r}_1 \ldots d\mathbf{r}_N + \int_\sigma^V \int d\mathbf{r}_1 \ldots d\mathbf{r}_N$$

$$= (V - V_\sigma)^N$$

$$= V_f{}^N \qquad 2.119$$

V_σ represents the *excluded volume*, the volume occupied by the actual hard sphere molecules and V_f, the *free volume* of the system, is the volume available to the molecules as they move about in the volume V.

By applying the perturbation theory to a fluid system, using a hard-sphere fluid as the reference, and assuming that the perturbation, containing all the attractive interactions between the molecules, is rapidly convergent so that only the first perturbation term is needed, equation 2.82 may be written as:

$$Z_{config} = {V_f}^N \exp\left(-\beta \left\langle {U_N}^{(1)} \right\rangle_0 \right) \tag{2.120}$$

and by substituting equation 2.92:

$$Z_{config} = {V_f}^N \exp\left[-\beta \frac{\rho^2 V}{2} \int_0^\infty u^{(1)}(r_{12}) g_0(r_{12}) 4\pi r^2 dr \right] \tag{2.121}$$

By defining the *mean potential energy*, φ, as the sum of all the binary interactions between a central molecule and the remaining molecules surrounding it, so that $\frac{1}{2}N\varphi$ represents the intermolecular potential of the entire system, equation 2.121 can be simplified even further: This leads to the following expression:

$$Z_{config} = {V_f}^N \exp\left[-\beta \frac{N\varphi}{2} \right] \tag{2.122}$$

Where the mean potential energy is given by:

$$\varphi = \frac{N}{V} \int_0^\infty u^{(1)}(r_{12}) g_0(r_{12}) 4\pi r^2 dr \tag{2.123}$$

The *generalized Van der Waals fluid partition function* can now be expressed as follows:

$$Q = \frac{1}{N!} \frac{1}{\Lambda^{3N}} (q_{rot} q_{vib} q_{elec} q_{nucl})^N {V_f}^N \left[\exp - \frac{N\varphi}{2kT} \right] \tag{2.124}$$

Finally, the pressure equation of this partition function, determined through equation 2.20, can be treated as consisting out of two contributions:

$$P = P^{(0)} + P^{(1)} \tag{2.125}$$

$P^{(0)}$ represents the hard-sphere pressure contribution, and is a function of the system free volume,

$$P^{(0)} = NkT \left(\frac{\partial \ln V_f}{\partial V} \right)_{N,T} \tag{2.126}$$

and the perturbation contribution, $P^{(1)}$, that is determined by:

$$P^{(1)} = -\frac{N}{2}\left(\frac{\partial \varphi}{\partial V}\right)_{N,T} \qquad 2.127$$

2.4.2.b Deriving the Van der Waals Equation

The original Van der Waals equation of state can be recovered from equations 2.125 through 2.127, by firstly noting that the excluded volume of a system of *two* molecules as equal to $4\pi\sigma^3/3$, where σ is the diameter one molecule, and by approximating the total excluded volume as $N/2$ times that value. The system free volume is then expressed as:

$$V_f = V - \frac{N}{2}\left(\frac{4\pi\sigma^3}{3}\right) = V - \frac{2\pi N}{3}\sigma^3 \qquad 2.128$$

Van der Waals used the following notation:

$$V_f = V - \frac{N}{N_A}b \qquad 2.129$$

Where $b=4b_0$, and b_0 is the volume of one mole of hard-sphere molecules. ($b_0=N_A\, b'_0 = N_A\pi\sigma^3/6$). Substituting equation 2.129 into the hard sphere pressure equation, equation 2.126, would lead to the first term of equation 2.116.

When evaluating the integral in equation 2.123 it is only necessary to integrate from the hard sphere diameter, σ, since the radial distribution function is equal to zero between $r=0$ and $r=\sigma$. In the derivation of his equation, Van der Waals assumed a uniform density over the system free volume [217] with a temperature independent attractive contribution. This essentially means that the radial distribution function of a Van der Waals fluid is equal to 1 over the entire volume, and independent of the system temperature and density. The result of the integral will therefore be equal to a constant value, which when expressed as $-a/N_A^2$ gives the perturbation pressure contribution as expressed by Van der Waals in equation 2.116, and the following mean potential function:

$$\varphi = -\frac{2aN}{N_A{}^2V} \qquad 2.130$$

2.4.2.c Modifications of the Van der Waals Equation

Following a similar approach to Vera and Prausnitz [219] the well known cubic, or Van der Waals type equations of state, can be shown to be modifications, or corrections to the simplifying assumption of a density and temperature independent radial distribution function.

Equation 2.123 can be expressed as a more general function of the mean potential energy:

$$\varphi = -\frac{4\pi N\sigma^3}{V} I = -6\frac{b}{N_A}\frac{N}{V} I \qquad 2.131$$

where b is the Van der Waals volume parameter (see 2.4.2.b) and

$$I = -\int_1^\infty u^{(1)}_{12}(x) g^{(0)}(x) dx \qquad 2.132$$

The integration parameter, x, is a dimensionless distance parameter $x=r/\sigma$.

The integral I can also be represented as consisting out of a dimensionless temperature and volume dependent part:

$$I = C \cdot G(V) \cdot J(T) \qquad 2.133$$

The C is a constant characteristic of the fluid. Van der Waals equation represents the limiting case where $G(V)=J(T)=1$.

The Soave-Redlich-Kwong equation [196], probably the most widely applied equation of state in practice, can be shown to have more complicated functional forms for $G(T)$ and $J(T)$:

$$G(V) = \frac{V}{N}\left(\frac{b}{N_A}\right)^{-1} \ln\left(1+\left(\frac{V}{N}\right)^{-1}\left(\frac{b}{N_A}\right)\right) \qquad 2.134$$

and

$$J(T) = \alpha(T) = \left(1 + mT_r^{0.5}\right)^2 \qquad 2.135$$

In equation 2.135 m is a quadratic function in the component acentric factor. The constant C, in equation 2.133, in this case is equal to $1/3(1/N^2)(a_c/N_A)/(b/N_A)$.

Another well known equation the Peng-Robinson EOS [163], has a similar $J(T)$, but a different volume functionality:

$$G(V)=\frac{V}{N}\frac{1}{2\sqrt{2}}\left(\frac{b}{N_A}\right)^{-1}\ln\left(\frac{V-\left(1-\sqrt{2}\right)\left(b/N_A\right)}{V-\left(1+\sqrt{2}\right)\left(b/N_A\right)}\right) \qquad 2.136$$

And in the case of a three parameter the Patel Teja EOS [162], $G(T)$ has the following form :

$$G(V)=\frac{V}{N}\frac{1}{R_1-R_2}\ln\left(\frac{V-R_1}{V-R_2}\right) \qquad 2.137$$

where

$$R_1=\frac{1}{2}\left(-\left(b/N_A\right)-\left(c/N_A\right)+\sqrt{\left(b/N_A\right)^2+6\left(b/N_A\right)\left(c/N_A\right)+\left(b/N_A\right)^2}\ \right) \qquad 2.138$$

$$R_1=\frac{1}{2}\left(-\left(b/N_A\right)-\left(c/N_A\right)-\sqrt{\left(b/N_A\right)^2+6\left(b/N_A\right)\left(c/N_A\right)+\left(b/N_A\right)^2}\ \right) \qquad 2.139$$

Over the years a vast variety of different approaches have been developed to correct the attractive term temperature dependence and the overall volumetric behaviour of the Van der Waals type equations of state by developing different formulations for $\alpha(T)$ and the Van der Waals repulsive term [10]. All of these approaches are in effect different attempts to account for the temperature and density dependence of the reference radial distribution function with different functions for $G(V)$ and $J(T)$.

In a further approach to improve the Van der Waals equation is to use more accurate expression of the system free volume in the place of equation 2.129 [10, 219, 229]. The *Carnahan-Starling* equation [32] is a well known equation, and widely applied as an alternative to the Van der Waals repulsive term. (This term and others will be discussed in detail in Chapter 3.)

Vast numbers of equations of state have been developed by combining these various approaches to the repulsive and attractive terms [10, 219, 229], with some of the models being more successful than others in representing different systems or conditions. However, all these proposed models adhere to the same basic assumptions of free volume and first perturbation integral approximations.

2.5 DEVELOPMENT OF A PRACTICAL EQUATION OF STATE

In everyday practical thermodynamic computations many repetitive calculations are made, mainly to determine system fugacities. The repetitive nature of these computations requires an algebraic equation of state that is simple enough to facilitate rapid calculations to avoid long computational times.

From the discussions in section 2.3, it is clear that the perturbation approach is more suited for the development of such a practical equation of state. The integro-differential and direct correlation approaches to determine radial distribution functions require simplifying assumptions before any results can be obtained, and even after simplification do not generally result in analytic equations of state. The highly idealised Percus-Yevick hard sphere fluid is the only exception to this, and even with this method two possible equations are obtained, depending on the approach followed in the model derivation. The perturbation approach on the other hand can use any simple well described reference system, and with minimal simplifying assumptions is able to describe a more complex fluid system. The simplifying assumptions in the case of the perturbation theories mainly involve the second and higher perturbation terms, which at realistic system densities should already have a relatively small influence on the system behaviour. As shown in section 2.4.2, many of the equations of state commonly used today actually stem from the generalised Van der Waals perturbation theory.

Within the perturbation theory a choice must be made between two approaches, the *Barker and Henderson* and the *WCA* theories. Both these approaches use a hard sphere fluid as reference term and require the evaluation of perturbation integrals over the hard sphere radial distribution function. They differ however in the nature of the reference hard sphere diameter, which could either be temperature or temperature and density dependent, the form of the perturbation energy potential and the definition of the reference radial distribution function.

The discussion up to this point only covered the development of an equation of state for spherically symmetric pure systems. In order to develop a successful equation of state for real fluids, the models also need to be able to represent non-spherical systems and mixtures.

The development of a suitable equation of state will therefore be divided into four stages:

- The development of a suitable hard sphere fluid model.
- The representation of the perturbation contribution.

- The extension of the model to non-spherical systems.
- The development of suitable mixing rules.

2.6 SUMMARY AND CONCLUSIONS

In this chapter it has been shown that how, from a microscopic view of a fluid system, equations of state can be derived which are able to describe the overall average macroscopic behaviour of a fluid system.

But although the development of an equation of state directly from first principals, by determining the radial distribution function of the fluid of interest, has merit when studying theoretical systems, the quality of the representation of a real system is dependent on the simplifying assumptions used in deriving the distribution function, thermodynamic relations (the assumption of *pair-wise additivity*) and the accuracy of the intermolecular potential function. It is clear then that this approach is unsuitable for development of an equation of state for a real fluid system, since although the Percus-Yevick integral equation can be solved analytically for a hard-sphere model, neither the integro-differential of direct correlation approaches result in an analytical equation of state when a realistic potential model is used.

The alternate approach, that of representing the fluid system as a perturbation expansion of a hard sphere reference system, appears to be mathematically more manageable, and it has been shown that the highly successful cubic equations of state can be derived through this approach.

The development of a practical equation of state through the perturbation theory will be approached in four stages:

- The development of a hard sphere reference term.
- The representation of the perturbation contribution.
- The correction for non-spherical molecules.
- The extension of the equation of state to mixtures.

These approaches will be investigated in detail in the subsequent chapters.

Chapter 3 ***Hard Sphere Reference Term***

3.1 INTRODUCTION

As discussed in the previous chapter, the perturbation approach will be used to develop an equation of state able to describe the phase behaviour of fluid consisting of simple, spherical non-polar molecules or individual atoms. The perturbation approach uses a hard sphere fluid with a temperature dependent hard sphere diameter as a reference fluid to represent the repulsive behaviour of the fluid particles and treats the attractive interactions as perturbations on this behaviour. The pressure of a simple fluid system can therefore seen as consisting out of two contributions, the hard sphere, $P^{(0)}$, and perturbation, $P^{(1)}$, pressures:

$$P = P^{(0)} + P^{(1)} \qquad 3.1$$

This chapter is concerned with determining an accurate description of the hard sphere contribution.

Because of their simplicity, hard sphere fluids have been extensively studied in order to gain insight into the behaviour of more complex systems. An overview of some of these existing hard sphere equations of state will be given and the development of a new, mathematically simple description will be investigated. (The fluid specific hard sphere diameters, and their temperature dependence will only be defined in Chapter 4.)

3.2 HARD SPHERE FLUID PROPERTIES

A hard sphere fluid as defined in 2.2.6.a consists out of hard (impenetrable) spherical particles with no intermolecular attraction. The potential function describing the system is expressed as follows (equation 2.54 in section 2.2.6.a):

$$u(r) = \begin{cases} \infty & r < \sigma \\ 0 & r > \sigma \end{cases} \qquad 3.2$$

As shown previously, pressure is a function of the configurational integral of the system:

$$P^{HS} = kT\frac{\partial}{\partial V}\left(\ln Z_{config}\right)_{N,T} \qquad 3.3$$

and for a hard sphere system, because of the lack of intermolecular interactions this Z_{config} is purely a function of the system free volume (equation 2.24):

$$Z_{config} = {V_f}^N \qquad 3.4$$

Alternatively, the system pressure of a hard sphere fluid can also be determined by directly evaluating the radial distribution function at the hard sphere diameter, σ. The expression exp(-$u(r)/kT$) is a step function for a hard sphere fluid, the derivative of which is a *Dirac delta function,* $\delta(r-\sigma)$, of the form:

$$\frac{\partial}{\partial r}\left(\exp\left(\frac{-u(r)}{kT}\right)\right) = -\frac{1}{kT}\exp\left(\frac{-u(r)}{kT}\right)u'(r) \qquad 3.5$$

Substituting equation 3.5 into the *pressure equation*, equation 2.50, leads to the following:

$$\begin{aligned}\frac{P}{\rho kT} &= 1-\frac{1}{6}\rho\int_0^\infty ru'(r)g(r)4\pi r^2 dr \\ &= 1+\frac{1}{6}\rho\int_0^\infty \frac{\partial}{\partial r}\left(\exp\left(\frac{-u(r)}{kT}\right)\right)g(r)\exp\left(\frac{u(r)}{kT}\right)4\pi r^3 dr \\ &= 1+\frac{4\pi\sigma^3}{6}\rho g(\sigma+) \end{aligned} \qquad 3.6$$

Finally by using the same definition for b as specified in section 2.4.2.b, with $b = 4b_0 = 4N_A b'_0 = N_A b$, the hard sphere compressibility may be expressed as follows:

$$z = 1 + b'\rho g(\sigma+) = 1 + b\rho_{mol} g(\sigma+) \qquad 3.7$$

Where ρ_{mol} is the molar density, i.e. the number of moles per unit volume.

From the expressions above, and the discussions in the previous chapter, it is clear that there are many routes through which a hard sphere equation of state can be derived. The various methods can be broadly classified as follows:

- The development of *free volume* expressions, taking account of the volume occupied by the molecules themselves and thus reducing the volume available for free motion.
- The solution of the radial distribution functions through the *integro-differential* and *integral* methods discussed in section 2.3.2.b.
- Performing *molecular simulations* to determine the radial distribution function at contact, $g(\sigma)$, or the system pressure as a function of density.
- Expressing the hard sphere pressure as a *virial equation of state* and determining the *virial coefficients* through the statistical mechanical expressions as discussed in section 2.3.1.

3.3 EXISTING HARD SPHERE EQUATIONS OF STATE

Over the years a vast variety of hard sphere equations of state have been proposed each with varying degrees of accuracy, complexity and range of application. Several of these models have been reviewed in the literature [19, 135, 150, 227, 229, 240], and their performance in representing the system pressure, compressibility, radial distribution function and virial coefficients compared to molecular simulation results.

Some of these models will now be discussed. As it has been found that there is no direct correlation between the model accuracy and its degree of complexity [150], the aim of this section is not to provide an exhaustive listing of *all* the hard sphere models in existence, but rather to provide an overview of the models that are in general use, are illustrative of the methods discussed above and are simple enough to facilitate their use in a practical equation of state,

3.3.1 Van der Waals hard sphere model

The Van der Waals hard sphere model, *VDW*, is a highly simplified representation of a hard sphere fluid, and is commonly applied in *cubic equations of state* such as the *SRK*[196] and *PR* equations[163].

Van der Waals [217] proposed an equation accounting for the physically excluded volume of the hard spherical molecules. In a system with two molecules the total volume unavailable for free motion is equal to $4/3\pi\sigma^3$, i.e. equal to a volume of a sphere with a radius equal to the hard sphere diameter. Van der Waals postulated that for a system of N molecules this excluded

volume would be equal to $(N/2)(4/3\pi\sigma^3)$, which leads to the following free volume expression:

$$V_f = V - \frac{N}{2}\left(\frac{4\pi\sigma^3}{3}\right) = V - \frac{N}{N_A}b = V - nb \qquad 3.8$$

This expression is strictly speaking only valid in one dimension, and it neglects the possible overlap of excluded volumes in systems with more than two molecules. Only at low densities, where the molecules are far apart, would this be a reasonable assumption. (This is illustrated in Figure 3.7, where it is shown that the *VDW* model is only able to represent the molecular simulation data at low densities.)

The Van der Waals free volume expression, equation 3.8, leads to the following hard sphere equation of state

$$P^{(0)} = \frac{NkT}{V - nb} \qquad 3.9$$

and hard sphere compressibility relation:

$$z = \frac{1}{1 - 4\eta} \qquad 3.10$$

η is the reduced density and is equal to $(N\pi\sigma^3/6)/V$ or the total volume of the hard sphere particles divided by the total system volume.

The equation of state can also be written as a virial expansion in density:

$$z = \sum_{i=0}^{\infty} \frac{b^i}{i!}\rho_{mol}^i \qquad 3.11$$

The virial coefficients are therefore easily determined by the following relation:

$$B_i = \frac{b^i}{i!} \qquad or \qquad \frac{B_i}{b_0{}^i} = \frac{4^i}{i!} \qquad 3.12$$

Where b_0 is the volume of one mole of hard sphere molecules.

The success of the cubic equations of state in describing real fluid systems over all densities have often been attributed to a fortuitous cancellation of errors of the hard sphere and perturbation approximations. However an often-overlooked fact is that despite the theoretical motivation behind the derivation of the Van der Waals free volume term, the actual value of the *b* parameter used in the equation of state, determined either by fitting experimental data or through the critical point criteria, through equation 2.117, is much smaller than 4 times the molar volume of that system [192], allowing the equations to be successful at higher densities. The relative sizes of b_0 as determined for argon are listed in Table 3.1. The Bondi volume is also known as the van der Waals volume, and is determined from X-ray diffraction data, the SRK and PR are examples of two cubic equations of state using the van der Waals hard sphere expression, and b_0 is determined by enforcing the accurate critical system pressure and temperature. The BACK EOS uses the Carnahan-Starling hard sphere equation (section 3.3.4 below) with a temperature dependent hard sphere diameter. It is clear that the cubic equations with the Van der Waals hard sphere model uses a hard sphere molar volume 2 to 3 times smaller than what can be observed experimentally or fitted with more realistic models.

Table 3.1 Argon molar volumes as determined by experimental methods and used in various EOS.

Argon Molar Volume b_0 [m^3/mol]	
Bondi [25]	16.76[1]
SRK [196]	5.56
PR [163]	5.02
BACK (100 K) [42]	11.99[2]

3.3.2 The Eyring free volume model

This free volume model was published by Eyring and Hirschfleder in 1937 [69]. It has a very limited practical application, but is discussed here a further example of deriving a hard-sphere equation of state from the free volume approximations.

When a cubical packing arrangement is considered with 6 molecules, two molecules bounding the central molecule on each axis, surrounding a central molecule, the distance that the central

[1] The Bondi van der Waals radius should ideally be the value that yields the correct packing density at 0 K. It was found that $V_{Bondi} \approx N_A(\pi/6)\sigma^3 = b_0$.

[2] The close packed volume of argon at 0 K, was obtained by fitting the BACK EOS to argon second virial coefficient data 42. S. S. Chen and A. Kreglewski, *Applications of the Augmented van der Waals Theory of Fluids. I. Pure Fluids.* Berichte de Bunsen-Gesellschaft, 1977. **81**(10): p. 1048-1053.. The original fitted parameter value was used to determine b_0.

molecule is free to move along each axis is equal to $2[(V/N)^{1/3} - \sigma]$. The total free volume can then be expressed as:

$$V_f = 8N\left[\left(\frac{V}{N}\right)^{1/3} - \sigma\right]^3 = 8N\left[\left(\frac{V}{N}\right)^{1/3} - \left(\frac{3b}{2\pi N_A}\right)^{1/3}\right]^3 \qquad 3.13$$

and the hard sphere pressure and compressibility (E) equations as:

$$P^{(0)} = NkT\left[V - \left(\frac{3Nb}{2\pi N_A}\right)^{1/3} V^{2/3}\right]^{-1} \qquad 3.14$$

and

$$z = \frac{1}{1 - \left(\frac{6\eta}{\pi}\right)^{1/3}} \qquad 3.15$$

It is however not possible to expand this equation as a virial equation of state.

3.3.3 Percus-Yevick solutions

The Percus-Yevick integral equation of the radial distribution function, as discussed in section 2.3.2.c, can be solved analytically for a hard sphere fluid and results in two different analytic hard sphere pressure equations of state, depending on whether the radial distribution function is coupled with the *pressure* or *compressibility functions*. (Equations 2.50 and 2.52 respectively).

$$z = \frac{1 + 2\eta + 3\eta^2}{(1-\eta)^2} \quad \text{(a)} \quad \text{or} \quad z = \frac{1 + \eta + \eta^2 - 3\eta^3}{(1-\eta)^3} \quad \text{(b)} \qquad 3.16$$

and

$$z = \frac{1 + \eta + \eta^2}{(1-\eta)^3} \quad \text{(a)} \quad \text{or} \quad z = \frac{1 + \eta^3}{(1-\eta)^4} \quad \text{(b)} \qquad 3.17$$

The (*b*) forms shown here are simply alternative expressions of the (*a*) equations, and are obtained by multiplying the (*a*) expressions by the ratio $(1-\eta)/(1-\eta)$.

Equation 3.16 is obtained through the *pressure function* [209, 230], and will be referred to as *PY-P*. Equation 3.17, *PY-C*, is the Percus-Yevick integral solution coupled with the *compressibility function* [209]. This same hard sphere compressibility expression has also been derived through a different approach, that of the *scaled particle theory* [176]. This method will not be discussed here, as further attempts to improve on equation 3.17 through this approach have not been successful [190].

3.3.4 Carnahan Starling hard sphere model

The Carnahan Starling equation, *CS*, is one of the most successful and widely applied hard sphere models [150, 190]. The equation was derived in 1969 by Carnahan and Starling [32], who approximated the first 5 reduced virial coefficients as integers, and found a recursive relation for these values:

$$z = 1 + 4\eta + 10\eta^2 + 18\eta^3 + 28\eta^4 + 40\eta^5 + \ldots \qquad 3.18$$

where $B_i=(i^2+i-2)$ for $i \geq 2$. This leads to a geometric series:

$$z = 1 + \sum_{i=0}^{\infty} \left(i^2 + 3i\right)\eta^i \qquad 3.19$$

By expressing equation 3.19 in a closed form, the *CS* compressibility equation may be obtained in its generally known form:

$$z = \frac{1 + \eta + \eta^2 - \eta^3}{(1-\eta)^3} \qquad 3.20$$

It has also been observed that the *CS* function can be obtained from the two Percus-Yevick expressions [33, 137]:

$$z^{CS} = \frac{1}{3}\left(2z^{PY-C} + z^{PY-P}\right) \qquad 3.21$$

The *CS* can be seen as a compromise between the assumptions made in the derivation of the *PY-C* and *PY-P* expressions, with a greater contribution from the first, indicating that the *PY-C* expression is the more correct of the two. This has been already been qualitatively proved by several authors [19, 125, 227]. (See section 3.4.4)

3.3.5 Kolafa Model

Kolafa, as quoted in [28], used a similar approach to the original method used to derive the CS equation, to derive a new hard sphere model. The hard sphere virial coefficients were again modelled as a geometric series, but with an improved virial coefficient approximation $B_i = 5/6*(i^2+3i-6)$ for $i \geq 3$. This leads to the following compressibility function, K :

$$z = \frac{1+\eta+\eta^2-\frac{2}{3}\eta^3-\frac{2}{3}\eta^4}{(1-\eta)^3} \qquad 3.22$$

This slightly more complex equation is in even better agreement with computer simulation data than the *CS* equation [28, 190].

3.3.6 Padé Approximants

Padé approximations of the hard sphere virial equation of state with its known virial coefficients are often used as hard sphere models. A Padé approximation is often more accurate than simply a truncated virial equation, even when developed using the same number of coefficients.

Of the better known Padé approximation equations are those of Ree and Hoover [174, 175], *RH*. The *RH*[3/3] approximant reproduces the first 6 (3+3) virial coefficients as determined by the Ree and Hoover[175], exactly, and can be expressed as:

$$z = \frac{1+1.75399\eta+2.31704\eta^2+1.108928\eta^3}{1-2.246004\eta+1.301056\eta^2} \qquad 3.23$$

Several Padé approximations have been developed by other authors, using different virial coefficient datasets and polynomials of different orders (i.e. different [n/m] designations) [67, 104, 135, 136, 183] resulting in equations of similar or higher complexity.

3.3.7 Guggenheim Equation

The Guggenheim hard sphere compressibility equation, *G*, was suggested as an improvement on the Van der Waals equation at higher densities whilst still being mathematically more simple than the *PY-C* and *PY-P* equations [87].

$$z = \frac{1}{(1-\eta)^4} \qquad 3.24$$

Equation 3.24 corresponds to the first term in equation 3.17(b) where the η^3 term has been neglected. This should be an acceptable approximation at low system densities. (See Table 3.6 for a confirmation of this.)

3.3.8 Shah Hard Sphere Compressibility

This model [192], *S*, was derived in order to provide a mathematically simple correct hard sphere equation, and was fitted to molecular simulation results in the packing fraction, η, range of 0.0 to 0.6.

$$z = \frac{1}{(1-k_0\eta)} + \frac{k_1\eta}{(1-k_0\eta)^2} \qquad 3.25$$

The parameters k_0 and k_1 were regressed from the simulation data, and were found to have values of 1.2864 and 2.8225 respectively.

3.3.9 CCOR Model

The *CCOR* model is so called because it was originally developed as part of the *Cubic-Chain-of-Rotators* equation of state [132]. It was fitted to the *CS* equation in the density range $0 \le \eta \le 0.5$ to derive a simpler expression that could be substituted into the original *Chain-of-Rotators* equation [43] and along with other simplifications would eventually result in a cubic equation of state. Since its development, it has been applied in many equations of state instead of more complex hard sphere expressions [123, 197, 226]. The *CCOR* equation has the following form:

$$z = \frac{V + k_1 b}{V - k_2 b} = \frac{1 + 4k_1\eta}{1 - 4k_0\eta} \qquad 3.26$$

Several authors have used this original functional form along with small modifications in the values for the parameters k_0 and k_1, in an attempt to improve the performance of the model in a variety of applications. Some of these parameter values are listed in Table 3.2

Table 3.2 Suggested parameter values for equation 3.26.

Source	k_0	k_1
CCOR [132]	0.42	0.77
Wang and Guo [227]	0.44744	0.6683
Elliot et al. [66]	0.476	0.525
Tochigi et al. [213]	0.625	0.375

3.3.10 Yelash-Kraska hard sphere models

Yelash et al. [243] derived their hard sphere models to have the correct limiting behaviour at high and low densities. The highest packing fraction, or reduced density, that a system of hard spheres can achieve is equal to $\pi\sqrt{2}/6$, or 0.74 (the packing fraction of a face-centred cubic lattice). The *CS*, *PY-C* and *PY-H* models all tend towards a maximum packing fraction of 1, whilst the *VDW* model tends towards a much lower value of 0.25.

The first of the Yelash-Kraska-Deiters models, *YKD-CS*, is a corrected *CS* model obtained by multiplying equation 3.20 by the ratio (3-4η)/(3-4η). This introduces a packing fraction limit of 0.75.

$$z = \frac{3 + 5\eta + 6\eta^2}{(1-\eta)(3-4\eta)} \qquad 3.27$$

The second equation, *YKD-VDW*, uses the *VDW* equation as a starting point. The equation has a packing fraction limit that is dependent on a parameter f_{pole} through the ratio $\eta_{limit}=1/f_{pole}$, and is constrained to always reproduce an accurate second virial coefficient:

$$z = \frac{1-(4-f_{pole})\eta + 7\left(1-\frac{f_{pole}}{4}\right)\eta^2}{1-f_{pole}\eta} \qquad 3.28$$

The virial coefficients of this equation are $B_i = (7+9/4f_{pole})\, f_{pole}^{\,i-3}$ for $i \geq 3$. By selecting f_{pole}= 4/3, or equivalently a packing fraction limit of 0.75, the third virial coefficient will also be exact and equation 3.28 can be simplified to the expression:

$$z = \frac{3 + 8\eta + 14\eta^2}{3 - 4\eta} \qquad 3.29$$

Recently Yelash and Kraska [242] derived a generic hard sphere model from which it can be shown that many of the well know hard sphere equations can be recovered depending on the choice of virial coefficients and packing fraction limit used in the model.

$$z = 1 + B_2\eta + \ldots + B_i\eta^{i-1} + \frac{C_1\eta^i}{(1-\eta)} - \frac{C_2\eta^i(i\eta - i - \eta)}{(1-\eta)^2} + \frac{C_0 f_{pole}\eta}{(1 - f_{pole}\eta)} \qquad 3.30$$

In this equation parameters B_2 up to B_i are the known the virial coefficient values, whilst the terms containing the coefficients C_1 and C_2 represent the crossover region between the higher and lower virial coefficients and the C_0 term the high density limit. The C_i coefficients can be determined from any three theoretically known virial coefficients B_{n+1},B_{n+2} and B_{n+3}. The authors propose an equation, *YK-1*, using the first four virial coefficients, and setting C_1=C_2=0 (resulting in a sharp transition from the lower virial coefficients to the high density limit), with parameters C_0 =9.090719 and f_{pole} = 1/0.747188 determined from the slope of the logarithm of a plot of the higher virial coefficients. Equation 3.30 can now be expressed as follows:

$$z = 1 + 4\eta + 10\eta^2 + 18.36448\eta^3 + \frac{9.090719(\eta/0.747188)^4}{(1 - 1/0.747188\eta)} \qquad 3.31$$

Rounding the parameters to C_0 = 9 and f_{pole} = 4/3, the expression can be simplified further, resulting in the following equation, *YK-2*:

$$z = \frac{3 + 8\eta + 14\eta^2 + 14\eta^3 + (40/3)\eta^4}{3 - 4\eta} \qquad 3.32$$

3.4 EVALUATION OF EXISTING AND ALTERNATIVE HARD SPHERE MODELS

3.4.1 Hard sphere evaluation criteria

In keeping with the aim of this work, to develop a practical equation of state, a compromise between model performance and simplicity has to be found. The hard sphere equations of state are generally evaluated against experimental hard sphere fluid data, obtained through computer

simulation [150, 240], and in their ability to accurately represent the hard sphere virial coefficients [32, 243]. A third criterion, that of model simplicity, will be now also be added.

3.4.1.a Computer simulation data

The various hard sphere compressibility equations are mainly compared to the simulation results of Alder and Wainwright [8, 174], Erpenbeck and Wood [67] and Speedy [203].

The computer simulations have shown that a hard sphere system can exist in two thermodynamically stable phases, a fluid and crystal phase. (As there are no attractive forces present in a hard sphere system, no gas-liquid phase transition can occur). Alder et al. [7] found the hard sphere system melting density at $\eta_m = 0.545$ and the freezing density at around $\eta_f = 0.493$. The system is however also able to exist in a metastable fluid state with no crystal structure at densities much higher than the freezing density. The hard sphere system therefore has two types of limiting densities or packing fractions, where the system pressure tends towards ∞, the crystal closest packed volume, $V_0 = N\sigma^3/\sqrt{2}$, where $\eta_{cp} = 0.740$, and the random closest packing limit, $\eta_{rcp} = 0.685$[212]. Most hard sphere theories have a limiting maximal packing faction of $\eta = 1$, which is much larger than either the closest packed or random packing densities, and instead corresponds to the limiting packing fraction of a system of perfectly packed *cubes* [242].

Alder and Wainwright [8] published Monte Carlo simulation data for systems with four to 500 particles in the reduced density range $0.0086 < \eta < 0.718$, and includes results from the fluid as well as the metastable and solid phases. They found that the simulation results of systems of more than 100 particles were indistinguishable from each other and therefore adequate to represent the hard sphere system. Their results were found to be in good agreement with the other publications except the highest density results of a system with 100 particles, where the data points appear to fall between the metastable and crystal phases. (These high-density results were not included in this study.)

The simulation data of Ergenbeck and Wood [67] covers the low density range of $0.0296 < \eta < 0.463$. The authors state that their data is statistically more precise than other previously published estimates because of the length of their calculations and because the dependence of pressure on system size have been taken into account correctly. The simulation results of a 5000 particle system were used in this work.

The high density hard sphere phase behaviour is not directly relevant to this study, as the aim is to develop an equation of state for a real system applicable to the a fluid phase of moderate to low densities. However, information on the hard sphere phase behaviour in this region, will provide additional means with which to evaluate the overall model performance and limiting behaviour. Alder et al. [7] reported high density simulation data of the solid phase up to a density of η= 0.737, whilst Speedy [203] studied the metastable phase up to η= 0.57.

The relevant computer simulation data of the various sources is shown in Figure 3.1 as a function of, ξ, the ratio between the closest packed and system volume, V_0/V.

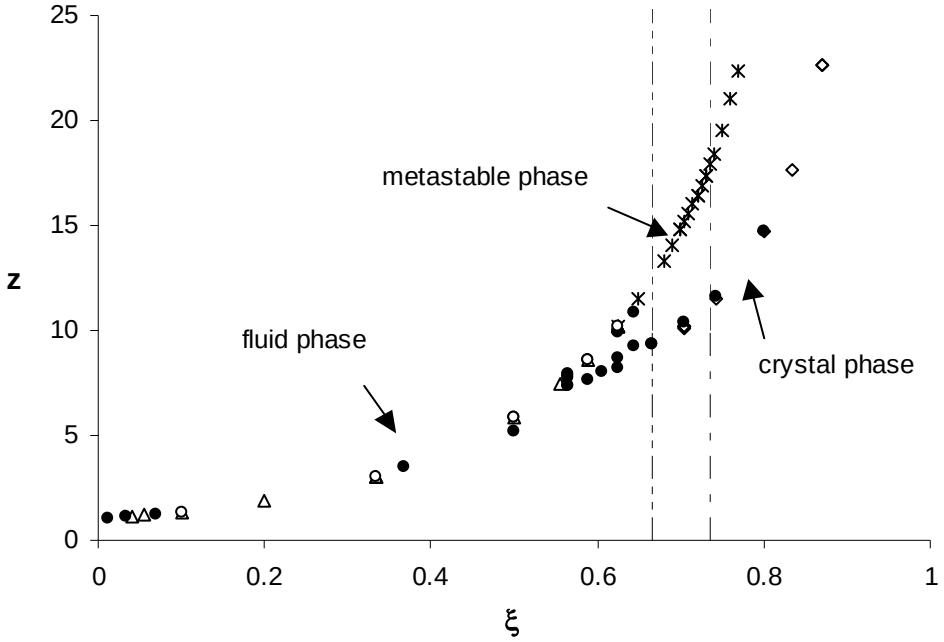

Figure 3.1 Molecular simulation data ● Alder and Wainwright [8] ○ Alder and Wainwright [174] ◇ Alder et al. [7] △ Ergenbeck and Wood [67] ✳ Speedy [203] _·_·_ η_f _·_·_ η_m

3.4.1.b Hard sphere virial coefficients

As discussed in section 2.3.1 the hard sphere virial coefficients can be determined through statistical mechanics by the evaluation of the sums of the integrals over the coordinates of i particles (i refers to the virial coefficient number B_i). Unfortunately the evaluation of these integrals very rapidly becomes very complex, and only the first four virial coefficients can be evaluated exactly. Determining the higher coefficients requires numerical integration

techniques. To date, hard sphere virial coefficients have only been determined up to B_8. These coefficients are listed in Table 3.3.

Table 3.3 Hard sphere virial coefficients

Virial Coefficients B_I			
B_2/b	4		
B_3/b^2	10		[24, 89, 175]
B_4/b^3	18.3648		[119, 157, 174, 175]
B_5/b^4	28.224512	±0.000256	[118]
B_6/b^5	39.739392	±0.05632	[104, 174]
B_7/b^6	53.53472	±0.28672	[104, 175]
B_8/b^7	70.77888	±1.6384	[104]

3.4.1.c Model simplicity and restrictions

A simple hard sphere model is classified here as a model that will result in a polynomial function in volume, or density, with analytically determinable roots (i.e. with an order smaller or equal to 4). The first requirement, that of a polynomial function in density, leads to a hard sphere compressibility expression in the form of a ratio of two polynomial functions:

$$z^{HS} = \frac{a_0 + a_1\eta + a_2\eta^2 + \ldots + a_i\eta^i}{1 + c_1\eta + c_2\eta^2 + \ldots + c_j\eta^j} \qquad 3.33$$

This is the most general expression possible with no constraints placed on the values of a_0, i or j. In order to ensure an analytical function in density the exponents must however adhere to the following restrictions: $j \leq 4$ and $i \leq 3$.

The residual Helmholtz free energy of the hard sphere fluid can be determined from the equation of state from the classical thermodynamic expression

$$d\frac{A^{resid}}{NkT} = \frac{z-1}{\eta}d\eta \qquad 3.34$$

by substituting equation 3.33 for the compressibility function and integrating between the zero and the actual reduced system density:

$$\frac{A^{resid}}{NkT} = \int_0^{\eta} \frac{\left(a_0 + a_1\eta + a_2\eta^2 + \ldots + a_i\eta^i\right) - \left(1 + c_1\eta + c_2\eta^2 + \ldots + c_j\eta^j\right)}{\eta\left(1 + c_1\eta + c_2\eta^2 + \ldots + c_j\eta^j\right)} d\eta \qquad 3.35$$

This immediately results in another restriction on the hard sphere equation parameters, in that in order for this expression to have a real solution, parameter a_0 must be equal to 1.

In developing an equation of state for real fluid systems, the hard sphere term will be used in conjunction with a perturbation expansion and a term accounting for the non-spherical nature of the actual molecules. The real system compressibility expression can be expressed as follows:

$$z = z^{HS} + z^{pert} + z^{non-sphere}$$

$$z = \frac{a_0 + a_1\eta + a_2\eta^2 + \ldots + a_i\eta^i}{1 + c_1\eta + c_2\eta^2 + \ldots + c_j\eta^j} + z^{pert} + z^{non-sphere} \qquad 3.36$$

Which leads to the following:

$$\frac{P}{kT}\frac{\pi\sigma^3}{6}\frac{1}{\eta}\left(1 + c_1\eta + c_2\eta^2 + \ldots + c_j\eta^j\right) = a_0 + a_1\eta + a_2\eta^2 + \ldots + a_i\eta^i + \left(z^{pert} + z^{non-sphere}\right)\left(1 + c_1\eta + c_2\eta^2 + \ldots + c_j\eta^j\right) \qquad 3.37$$

It is clear that the order of the denominator in the hard sphere compressibility, j, should be kept as low as possible, as it strongly influences the overall density dependence of the equation of state. The actual forms of the perturbation term and extension towards non-spherical systems have not been discussed up to this point, and it will be assumed that these terms will be kept as simple as possible. The perturbation and non-spherical terms are investigated in detail in chapters 4 and 5, however it needs to be considered here that certain approaches in accounting for the *real* properties of a fluid utilize expressions of the hard sphere equation of state and that that could place additional requirements on the form of the expression.

The according to the local compressibility approach of Barker and Henderson, the second perturbation term, equation 2.102, is a function of the hard sphere radial distribution function:

$$\frac{A_2^{(1)}}{NkT} = -\frac{\rho\beta^2}{4}\int_0^{\infty}\left[u^{(1)}(r_{12})\right]^2 \frac{1}{\beta}\left(\frac{\partial}{\partial P}\left(\rho g_0(r_{12})\right)\right)_0 4\pi r^2 dr \qquad 3.38$$

One possible approach to represent a real system, is to model it as a perturbed square well fluid with a well depth ε and a well width $\lambda\sigma$ (section 2.2.6.b). Equation 3.38 may then be expressed as [16]:

$$\frac{A_2^{(1)}}{NkT} = -\pi\eta\left(\frac{\varepsilon}{kT}\right)^2\left(z^{HS} + \eta\frac{\partial z^{HS}}{\partial\eta}\right)^{-1}\frac{\partial}{\partial\eta}\left(\int_{\sigma}^{\lambda\sigma} g_0(r_{12})r^2 dr\right) \qquad 3.39$$

The third term in this expression requires that z^{HS} be differentiable by η and that $z^{HS} \neq -\eta\frac{\partial z^{HS}}{\partial\eta}$.

A possible correction for the molecular shape is to model the molecules as consisting out of chains of spherical particles. Two possible corrections for the chain formation are discussed in section 5.2.2.b and will be introduced here in the form of additional compressibility contributions without further comment. Both these compressibility functions, the SAFT and PHSC chaining terms, are functions of the hard sphere radial distribution function at the hard sphere diameter, σ:

$$z^{SAFT} = -(r-1)\eta\frac{\partial\ln[g_0(\sigma+)]}{\partial\eta} \qquad \text{(a) } z^{SAFT} = -(r-1)\left(\frac{\frac{\partial}{\partial\eta}\left(z^{HS}\right)}{z^{HS}-1} - 1\right)\text{(b)} \qquad 3.40$$

and

$$z^{PHSC} = -(r-1)(g_0(\sigma+)-1) \qquad \text{(a) } z^{PHSC} = -(r-1)\left(\frac{z^{HS}-4\eta-1}{4\eta}\right)\text{(b)} \qquad 3.41$$

Parameter *r* represents the chain length in these equations, and the (*b*) forms were obtained by substituting equation 3.7 into the expressions.

Equation 3.40(*b*) introduces the trivial restriction that $z^{HS} \neq 1$.

The residual Helmholtz free energy contribution of the real system can be determined by substituting equation 3.36 into equation 3.34 and evaluating the integral. This leads to the following expression for the SAFT chaining Helmholtz energy contribution, which is valid for any realistic hard sphere function ($z^{HS} > 1$):

$$\frac{A^{SAFT}}{NkT} = -(r-1)\ln(g_0(\sigma+)) = -(r-1)\ln\left(\frac{z^{HS}-1}{4\eta}\right) \qquad 3.42$$

The expression for PHSC Helmholtz chaining contribution requires the evaluation of the following integral:

$$\frac{A^{resid}}{NkT} = -(r-1)\int_0^{\eta}\frac{z^{PHSC}}{\eta}d\eta = -(r-1)I \qquad 3.43$$

Where I represents the function:

$$I = \int_0^{\eta}\frac{z^{HS}-4\eta-1}{4\eta^2}d\eta$$

$$= \int_0^{\eta}\frac{\left(a_0+a_1\eta+\ldots+a_i\eta^i\right)-4\eta\left(1+c_1\eta+\ldots+c_j\eta^j\right)-\left(1+c_1\eta+\ldots+c_j\eta^j\right)}{4\eta^2\left(1+c_1\eta+\ldots+c_j\eta^j\right)}d\eta$$

$$= \int_0^{\eta}\frac{(a_0-1)+(a_1-c_1-4)\eta+(a_2-c_2-4c_1)\eta^2+\ldots}{4\eta^2\left(1+c_1\eta+\ldots+c_j\eta^j\right)}d\eta \qquad 3.44$$

It has already been determined that $a_0 = 1$, a further restriction $a_1 - c_1 = 4$ must be now be set in order to ensure a real value for I.

Although the requirements $a_0 = 1$ and $a_1 - c_1 = 4$ have been determined by ensuring real values of the residual Helmholtz energy hard sphere and PHSC contributions, these conditions are equivalent to constraining the hard sphere equation to accurate first and second virial coefficients.

3.4.2 Alternative hard sphere models

From the model requirements discussed above, two types of hard sphere models seem possible:

$$z^{HS} = 1+4\eta+a_2\eta^2+a_3\eta^3 \quad \text{(a)} \qquad z^{HS} = \frac{1+(4+c_1)\eta+a_2\eta^2+a_3\eta^3}{1+c_1\eta+c_2\eta^2+c_3\eta^3+c_4\eta^4} \text{ (b)} \qquad 3.45$$

Equation 3.45(*a*) has the form of a truncated virial coefficient expansion. If it is treated as such with $a_2 = B_3$ and $a_3 = B_4$, from the previous discussions of the virial equations of state, it can be said that due to the slow convergence of the expansion, this equation is not expected to perform well at liquid densities. The other alternative of treating the equation as purely a third order polynomial function that can be fitted to the simulation data, although it might result in a accurate fit of the fluid phase data, is highly empirical approach and cannot be used with confidence. This equation will therefore not be considered any further.

In order to ensure the simplest possible real equation of state, when using a hard sphere model of the form of equation 3.45*b*), it was decided to set parameters $c_2 = c_3 = c_4 = 0$, this is equivalent to setting *j* in section 3.4.1.c equal to 1. This assumption agrees well with the results of Tobochnik and Chapin [212] who found that $g(\sigma+) \propto (1 - \eta_{rcp}\eta)^{-1}$ for a hard sphere fluid system continuing along the metastable amorphous solid phase. (Their result for the radial distribution function will of course also hold true for z^{HS}.)

Out of the simplifications and parameter criteria, three alternative hard sphere equations of state can be suggested for use in the development of a simple real fluid model. These are listed in Table 3.4. Model *HS1* is similar to the *CCOR* type equations of state, and model *HS2* the *YKD-VDW* equation. The model parameters k_0 and k_1 used in the proposed equations will however be determined using a different method of simultaneously fitting the virial coefficient and molecular simulation data whilst adhering to the parameter restrictions as discussed in section 3.4.1.c..

Table 3.4 Proposed simple hard sphere equations of state

Simple hard sphere equations of state	
$z^{HS} = \frac{1+(4-k_0)\eta}{1-k_0\eta}$	HS1
$z^{HS} = \frac{1+(4-k_0)\eta+k_1\eta^2}{1-k_0\eta}$	HS2
$z^{HS} = \frac{1+(4-k_0)\eta+k_1\eta^2+k_2\eta^3}{1-k_0\eta}$	HS3

3.4.3 Hard sphere model fitting

In fitting the model parameters of equations *HS1*, *HS2* and *HS3*, three approaches were followed.

a. Fitting the simulation compressibility data.
b. Fitting the hard sphere virial coefficients
c. Using a combination of both of the above mentioned approaches.

The available hard sphere simulation datasets were interpolated by fitting a 6^{th} order polynomial through the available fluid and metastable phase data points whilst taking into account the relative uncertainties in the simulation data. (The datasets included were the fluid phase data of Alder and Wainwright [8, 174], Ergenbeck and Wood [67] and Speedy [203].) The fluid – solid (crystal) phase transition results in a discontinuity at the melting and freezing densities that cannot be modelled by any of the investigated hard sphere models. An attempt to model the phase transition with an equation of state requires that it produces a Van der Waals loop [174]. However, this would necessitate that some the hard sphere virial coefficients be negative, implying the attractive forces in the hard sphere fluid [227], which is, by definition, incorrect. It appears more likely that the virial coefficient series continues into the metastable fluid region [8]. The metastable phase was therefore included in the fitting procedure to ensure that the polynomial would follow a correct trend towards the higher densities.

The hard sphere models were fitted to the interpolated dataset up to a density of $\eta = 0.482$ which is close to the liquid freezing density of $\eta_f = 0.493$, and the parameters were optimised by reducing the absolute average error in the hard sphere compressibility:

$$z_{error} = \frac{1}{N_{data\ points}} \left(\sum_{n}^{data\ points} \frac{abs\left(z_{poly} - z_{\text{model}}\right)}{z_{poly}} \right) * 100 \qquad 3.46$$

In the second approach, *b*, the first 8 virial coefficients produced by the hard sphere model were fitted to the known coefficients as listed in Table 3.3. The first two coefficients will always be correct because of the constraints specified in section 3.4.2. As the higher virial coefficients only have a significant influence on the hard sphere phase behaviour at higher system densities, the virial coefficient error functions were scaled according to the coefficient number, to ensure that the accurate representation of the lower coefficients carried a greater weight:

$$B_{error} = \sum_{i}^{virial\ coefs} \left(\frac{1}{i} \frac{abs\left(B_{i\,data} - B_{i\,model}\right)}{B_{i\,data}} \right) * 100 \qquad 3.47$$

When combining the two approaches, in method *c*, the compressibility error is combined with the average error in the virial coefficient, and both are minimised simultaneously:

$$Total\ Error = z_{error} + \frac{1}{6} B_{error} \qquad 3.48$$

(The B_{error} function is scaled by 6 since only the third through eighth virial coefficients were used to fit the equations.)

The model parameters obtained by minimising these 3 error functions are listed in Table 3.5.

Table 3.5 Hard sphere model parameters

Model	Parameter	Method *a*	Method *b*	Method *c*
HS1	$\mathbf{k_0}$	1.7575	1.6818	1.7575
HS2	$\mathbf{k_0}$	1.4292	1.5231	1.4748
	$\mathbf{k_1}$	5.9475	3.9075	5.3571
HS3	$\mathbf{k_0}$	1.2555	1.4303	1.3990
	$\mathbf{k_1}$	4.9678	4.2789	4.4038
	$\mathbf{k_2}$	9.4144	4.0691	5.3635

The model hard sphere virial coefficients shown in Figure 3.1, includes the results of the three proposed equation of state models with the parameters listed in Table 3.5.

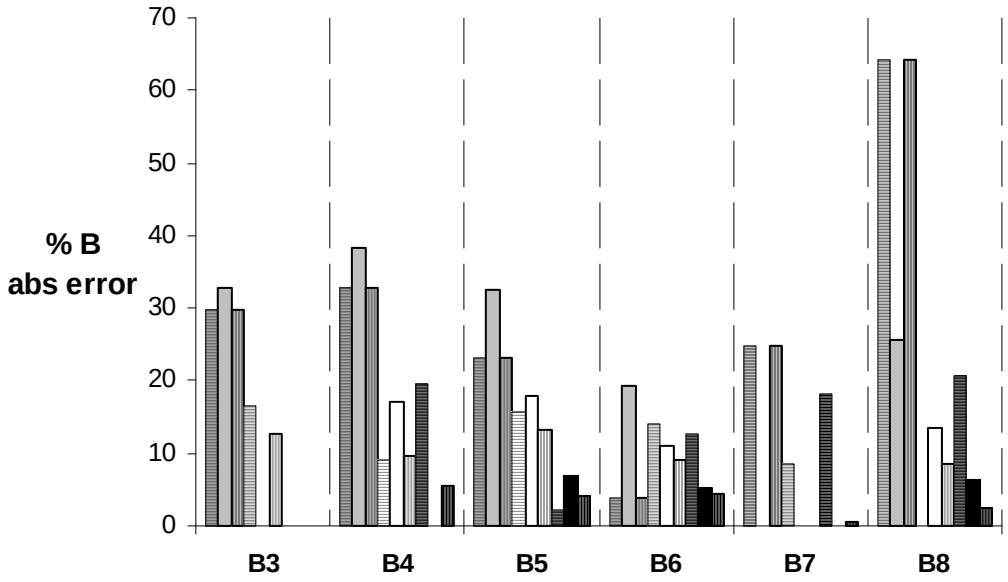

Figure 3.2 Absolute error in hard sphere virial coefficients, using the three model equations and three fitting procedures. *HS*1 : *a*, *b*, *c*; *HS*2; a b , c; *HS*3: *a*, *b*, *c*.

Methods *a* and *c*, optimising only the hard sphere compressibility and optimising both the compressibility and virial coefficient representation, both resulted in the same parameter values for equation *HS*1. It is also clear that even by solely minimising the error in the virial coefficients, method *b*, this proposed from is not suited to the representation of hard sphere virial coefficients.

The *HS*2 and *HS*3 models on the other hand are much more successful in modelling the virial coefficients, even when they are not explicitly fitted to the coefficients (method *a*). An encouraging result is the low overall errors that model *HS*3 delivers when fitted with method *c*. All the predicted virial coefficients fall within 5.4% of the region of accuracy of the theoretical values.

The errors in the modelled hard sphere compressibility are plotted in Figure 3.3. From the insert it can be seen that all the models perform similarly at low densities. This is the region where the lower virial coefficients would dominate the equation of state, and as stated before, the first two coefficients are correct for all the models.

Model *HS*1 again gives the largest errors. Using the model with parameters fitted with method *b*, results in the poorest performance, this is as expected, as method *b* did not even result in a significant improvement in the virial coefficient accuracies.

It can also be seen that including the virial coefficient errors in the fitting procedure, method *c*, did not significantly deteriorate the ability of either equation *HS*2 or *HS*3 to model the hard sphere fluid compressibility.

From Figure 3.4 it can be seen that there is very little to distinguish between these two models when they are optimised by either method *a* or *c*, with each equation being more accurate than the other in different density regions. However, when taking the results of the virial coefficient modelling (Figure 3.2) into account, it does seem that method *c* is the most suitable method to optimise the equation parameters.

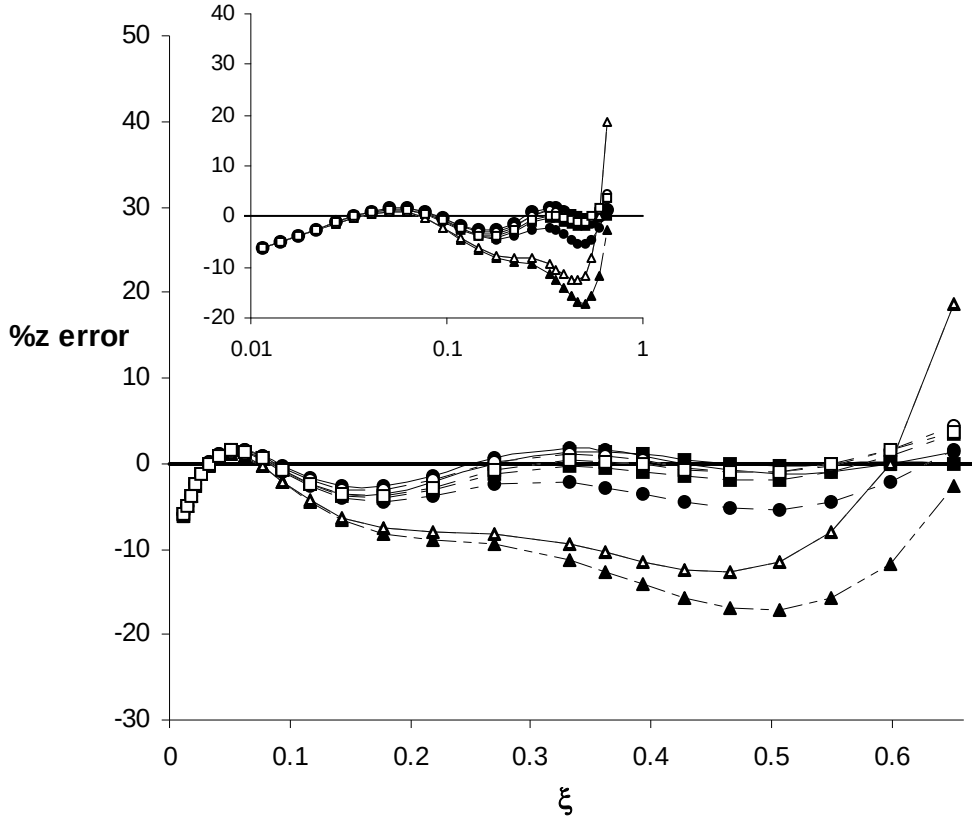

Figure 3.3 Percentage error in hard sphere compressibility vs. $\xi = (V_0/V)$, using the three model equations and three fitting procedures. Method *a* : *HS*1, *HS*2, *HS*3; Method *b*: *HS*1 *HS*2, *HS*3; Method *c* *HS*1, *HS*2 and *HS*3.

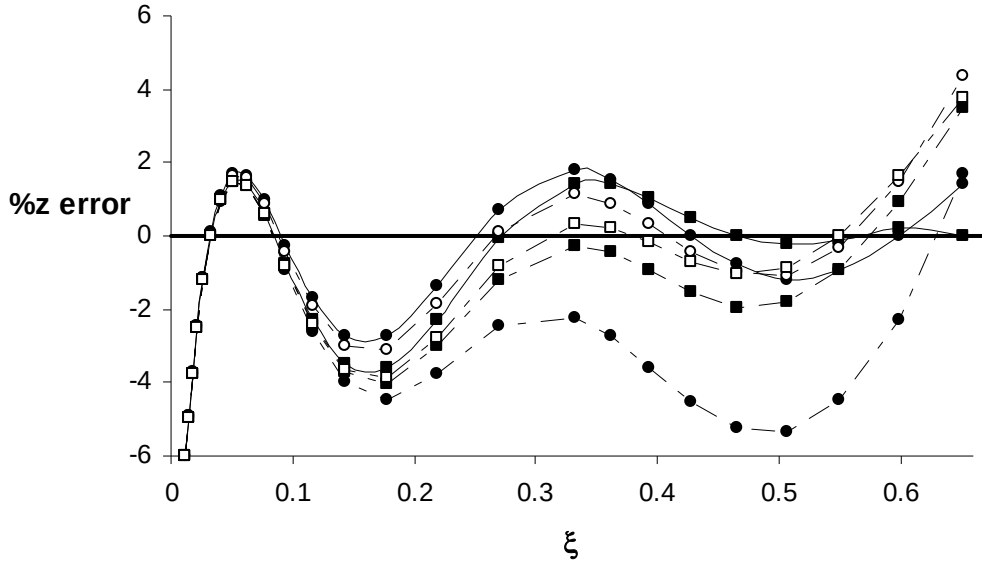

Figure 3.4 Percentage error in hard sphere compressibility vs. $\xi = (V_0/V)$, using the three model equations and three fitting procedures. (Similar to Figure 3.3, but with on a different scale) Method *a* : *HS*2, *HS*3; Method *b*: *HS*2, *HS*3; Method *c* : *HS*2 and *HS*3.

3.4.4 Hard sphere equation of state evaluation

The thirteen literature hard sphere equations of state, as discussed in section 3.3, together with the three new models optimised with method *c*, have been evaluated against their ability to represent the hard sphere phase behaviour and virial coefficients. These results are listed in Table 3.6 and Table 3.7.

Table 3.6 contains the average absolute percentage error in the hard sphere compressibility representation. Three different density ranges were evaluated, the low density range up to $\eta = 0.24$, an intermediate range, $0.24 \leq \eta \leq 0.4$, and a high density range $0.4 \leq \eta \leq 0.49 \approx \eta_f$. It should be noted that *VDW* equation fails at densities greater than 0.25. The discontinuities of all the other models occur at densities greater than the freezing density and will not affect this study.

Besides the *VDW* model, the Eyring equation, *E*, fares the worst in all the density intervals. This model was merely introduced to serve as an historical example of an alternative free volume approach in the hard sphere modelling, but is clearly an incorrect approximation as all the virial coefficients, other than the first, are undefined, and will not be considered further.

Table 3.6 The average absolute percentage error in the hard sphere compressibility

	Reduced Density Range			
	η: 0.007-0.24	η: 0.24-0.4	η: 0.4-0.49	
Model	**Ave. Abs. % Error**	**Ave. Abs. % Error**	**Ave. Abs. % Error**	**Σ**
VDW	153.97	—	—	153.97
E	46.35	51.87	152.33	250.55
PY-P	2.89	6.72	12.23	21.84
PY-C	2.17	1.35	5.94	9.45
CS	2.26	1.34	0.50	4.09
K	2.20	1.07	0.43	3.69
RH	2.80	5.65	9.54	17.99
G	2.24	5.50	17.15	24.89
S	2.93	3.43	2.78	9.13
CCOR	1.51	3.68	7.20	12.40
YKD-CS	2.21	0.42	4.71	7.35
YKD-VDW	3.49	10.11	16.64	30.24
YK-1	2.19	0.80	1.32	4.31
YK-2	2.26	1.47	0.68	4.42
HS1	5.95	11.39	9.74	27.08
HS2	1.87	0.73	2.46	5.06
HS3	2.13	0.58	2.33	5.04

Of interest is that, although the *PY-P* and *PH-C* equations were derived directly from statistical mechanical theory, they are not exact, indicating that the simplifying assumptions in the *Percus-Yevick* theory, as discussed in section 2.3.2.c, are not entirely valid. It is also obvious that the *PY-P* equation fares decidedly worse than *PY-C*,. This serves as a confirmation of the discussion of the *CS* model in section 3.3.4.

The *CCOR* model performs excellently in the low density and satisfactorily in the intermediate density regions, as this is the density range in which the *CS* equation performs well in and within which the model was optimised. (The *CCOR* model was fitted to the *CS* equation. See section 3.3.9.) The first and second virial coefficient restrictions placed on the *HS*1 equation, which has a similar form, reduces its flexibility, and hence its ability to model the hard sphere data. From Table 3.7 it can be seen that the *CCOR* model gives an inaccurate second virial

coefficient, indicating that no such restrictions were placed on its parameters, and resulting in a better fit of the compressibility data. The various *CCOR* type equations listed in Table 3.2 along with the *HS*1 model are plotted in Figure 3.5. All the model parameters, with the exception of those proposed by Tochigi et al. [213] are very similar (The *HS*1 method *c* parameters written in terms of k_0 and k_1 are equal to 0.4394 and 0.5606 respectively) and produce very similar hard sphere compressibility results.

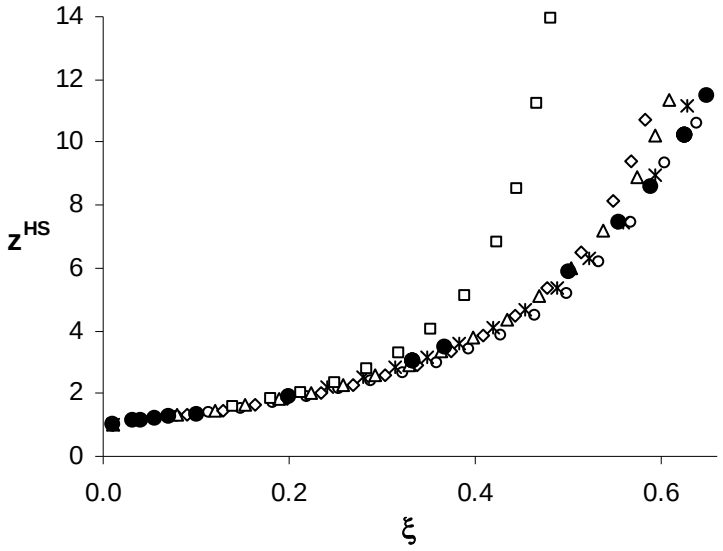

Figure 3.5 The fluid phase compressibility as represented by the equations of the *CCOR* form. ● Simulation data points, ✳ *CCOR*, ○ *HS*1, △ Wang and Guo [227], ◇ Elliot et al. [66], □ Tochigi et al. [213]

The *HS*2 and the *YKD-VDW* models also have a similar algebraic form, however here the restriction of an accurate third virial coefficient and a limiting value if $\eta = 0.75$, close to the structured closest packed limit $\eta_{cp} = 0.74$ restricts the latter model. From Table 3.7 it is clear that the requirement of an accurate third virial coefficient does not enhance the performance of the *YKD-VDW* equation in representing the higher virial coefficients and that in fact it is much more inaccurate than *HS*2 in representing the hard sphere virial coefficients greater than B_3, and also performs much worse in the representation of the hard sphere phase behaviour.

In general the Kolafa model, *K*, model is the most successful over the entire density range, however it is also the most complex model investigated. The *CS* model, as expected is only slightly less accurate, confirming the motivation for its broad application. The two new models by Yelash and Kraska, *YK*-1 and *YK*-2, also perform very well over the entire density range. They have however a reduced density order of 4 in the numerator (see equation 3.33), which is too high according, to the requirements set in section 3.4.2. The lower order proposed models

*HS*2 and *HS*3 are however only slightly less accurate in representing the hard sphere compressibility and produce comparable higher order virial coefficients.

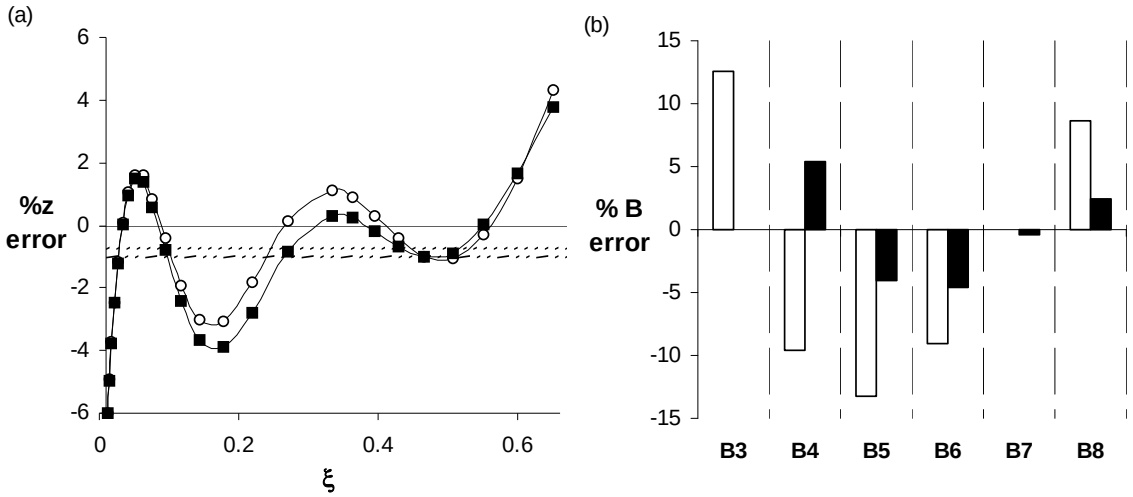

Figure 3.6 Comparison between ○ *HS*2 and ●*HS*3. (a) % Error in hard sphere compressibility average errors ..... *HS*2, _.._.. *HS*3 (b) % error in virial coefficients.

In Figure 3.4 the errors in hard sphere compressibility and virial coefficients as represented by the two proposed modes, *HS*2 and *HS*3 with parameters fitted by method *c*, are compared. It can be seen that the *HS*2 model has an overall average hard sphere compressibility error that is slightly lower than the *HS*3 model, but that it produces much larger virial coefficient errors. It should be noted that due to the cyclic nature of the compressibility error no clear conclusions can be drawn on the superiority of the model, as it is strongly dependent on the system density.

These two equations have limiting densities of η_{HS2}= 0.678 and η_{HS3} = 0.715. (See Figure 3.7(b)) The *HS2* limit agrees very closely to the amorphous solid phase random closest packed limit of 0.685. However in reality it is very difficult reach this density limit as is obvious from the work of Tobochnik and Chapin [212] and their investigation of the random closest packing where great care had to be taken to avoid the onset of crystal nucleation in the simulation process. They also state that upon freezing the hard sphere fluid phase is highly unlikely to nucleate into a single perfect crystal, and that usually a crystal with some defects will be produced. The closest packing limit of 0.715 produced by the *HS*3 model therefore appears to be a suitable compromise between the completely random solid, η_{rcp}=0.685, perfect crystal, η_{cp}= 0.740. It should be stressed that the model limiting behaviour was not explicitly enforced when fitting the equation parameters, and that these results were obtained only by fitting the fluid phase compressibility and virial coefficient data.(See Figure 3.7 (b))

It is therefore postulated that the *HS*3 equation provides in general a better model of the hard sphere fluid, and is not merely an accurate fit of a given dataset.

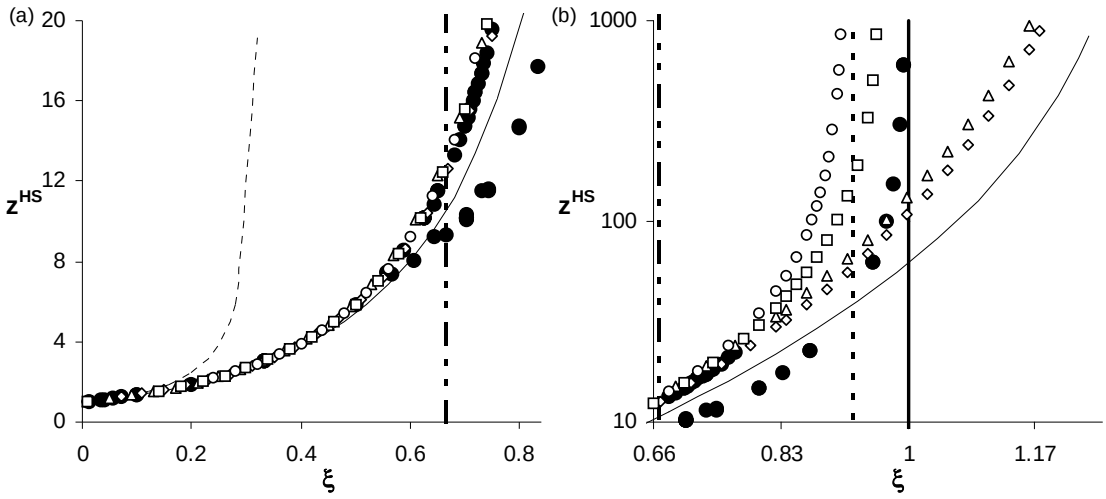

Figure 3.7 Hard sphere compressibility as represented by some of the hard sphere models ● Simulation data, ... *VDW*, Δ *PY-C*, —— *PY-P*, ◇ *CS*, ○ *HS*2, □ *HS*3, –·–·– Freezing density, ... Random closest packed density, —— Crystal closest packed density. (a) normal scale (b) high density limiting behaviour

In closing, Figure 3.7 is a plot of the hard sphere simulation data as represented by some of the models discussed in this section. The failure of the *VDW* model and the inaccuracy of the *PY-P* model at intermediate densities are apparent. The graph also serves as a confirmation that the proposed models, although they are mathematically less complex, are able to model the hard sphere simulation data to a similar extend than the *CS* equation. It can be furthermore also be seen that, all though the models *CS* and *PY*-C models have incorrect limiting values, they are still able to represent the liquid phase behaviour.

Table 3.7 Hard sphere virial coefficients and % errors as predicted by the various hard sphere models.

	B_2/b		B_3/b^2		B_4/b^3		B_5/b^4		B_6/b^5		B_7/b^6		B_8/b^7	
Exp	4		10		18.3648		28.224512 ±0.000256		39.73939 ±0.05632		53.53472 ±0.28672		70.77888 ±1.63840	
MODEL	**Value**	**% Err**	**Value**	**% Err**	**Value**	**% Err**	**Value**	**% Err**	**Value**	**% Err**	**Value**	**% Err**	**Value**	**% Err**
VDW	4	0	16	60	64	248.58	256.00	807.16	1024.00	2476.60	4096	7551.24	16384	23045.46
PY-P	4	0	10	0	16	-12.85	22.00	-22.04	28	-29.39	34	-35.94	40	-41.17
PY-C	4	0	10	0	19	3.49	31.00	9.85	46	15.60	64	19.02	85	17.77
CS	4	0	10	0	18	-1.96	28.00	-0.78	40	0.50	54	0.34	70	0.00
K	4	0	10	0	18.33	-0.15	28.33	0.40	40	0.50	53.33	0.00	68.33	-1.14
RH	4	0	10	0	18.36	0.00	28.20	-0.07	39.50	-0.45	52.02	-2.28	65.83	-4.68
G	4	0	10	0	20	8.93	35.00	24.03	56	40.76	84	56.38	120	67.22
S	4.11	2.75	8.92	-10.80	16.14	-12.09	26.76	-5.17	42.15	5.91	64.14	19.28	95.28	32.30
CCOR	4.76	19.00	8.00	-20.00	13.43	-26.85	22.57	-20.02	37.92	-4.43	63.7	18.46	107.02	48.88
YKD-CS	4	0	10	0	18	-1.96	28.67	1.59	42.89	7.78	61.85	15.00	87.14	20.80
YKD-VDW	4	0	10	0	13.33	-27.40	17.78	-37.00	23.7	-40.21	31.60	-40.43	42.14	-38.15
YK-1	4	0	10	0	18.36	0.00	29.17	3.37	39.03	-1.64	52.24	-1.87	69.92	0.00
YK-2	4	0	10	0	18	-1.96	28.44	0.78	37.93	-4.40	50.57	-4.99	67.42	-2.43
HS1	4	0	7.03	-29.70	12.36	-32.72	21.72	-23.06	38.17	-3.82	67.08	24.76	117.89	64.25
HS2	4	0	11.26	12.56	16.60	-9.61	24.48	-13.26	36.11	-9.00	53.25	0.00	78.53	8.64
HS3	4	0	10	0	19.35	5.39	27.08	-4.06	37.88	-4.53	53.00	-0.47	74.15	2.44

3.5 CONCLUSIONS AND SUMMARY

Three different hard sphere models have been investigated in this section. They were constrained to have an analytically determinable density dependence to accurately reproduce the first and second theoretical virial coefficients, and the model parameters determined by fitting hard sphere simulation results and the eight known virial coefficients.

It was found that the simplest model *HS*1 is too restricted by the constraints set on the model, and hence produced a worse hard sphere fluid representation than previously published models with a similar structure.

Although the second model *HS*2 was able to accurately represent the hard sphere compressibility behaviour and had a limiting density very close to the random closest packed density, it was not as successful in modelling the hard sphere virial coefficients, and it produced coefficients with errors up to 13.3%. It however was able to improve on the overall performance of a similar model in the literature.

The *HS*3 hard sphere equation was found to accurately represent the simulated hard sphere fluid phase behaviour, model the eight virial coefficients to within 5.4% and have a realistic limiting density intermediate to the random and closest packed hard sphere fluid limits, whilst satisfying all the requirements set in order to ensure its use in real fluid models.

$$z^{HS} = \frac{1 + 2.601\eta + 4.4038\eta^2 + 5.3635\eta^3}{1 - 1.399\eta} \qquad 3.49$$

This equation will be applied as the hard sphere fluid model throughout the remainder of this study.

Chapter 4 ***Perturbation***

4.1 INTRODUCTION

The two main approaches in the perturbation expansion of the fluid equation of state, the Barker and Henderson, *BH*, and the Chandler, Weeks and Andersen, *CWA*, methods, both express the attractive contributions of the intermolecular potential energies as perturbations on a well defined reference fluid, and in both cases the reference fluid can be approximated by a hard sphere equation of state with a temperature and/or density dependent effective hard sphere diameter. The development of a suitable hard sphere equation has been dealt with in the previous chapter.

In this chapter the various approaches towards representing the effective hard sphere diameter and the perturbation contribution will be investigated and used along with the hard sphere equation, equation 3.49, to model the real fluid behaviour of argon and methane as systems representative or small spherical non-polar particles. The ability of the proposed models to represent other small components such as and CO_2 and N_2 will also be investigated.

4.2 EFFECTIVE HARD SPHERE DIAMETER

The effective hard sphere diameter is a means through which the particular fluid potential model, that will be used to approximate the molecular interactions, is taken into consideration in the reference fluid. As described in section 2.3.3 the diameter is chosen, in both the *BH* and *CWA* approaches, to simplify the mathematical expressions of the perturbation terms by ensuring the cancellation of some integral terms.

The *BH* approach requires that the effective hard sphere diameter, d_{BH}, be defined as [15]:

$$\frac{d_{BH}}{\sigma} = \int_0^1 1 - \exp\left[-\frac{u(z)}{kT}\right] dz \qquad 4.1$$

where $z = r/\sigma$, and $u(z)$ is the intermolecular potential function. In this case the effective hard sphere diameter is a function of temperature.

The *CWA* perturbation theory defines the effective diameter, d_{CWA}, as the value that would satisfy equation 4.2 [228]. This specification results in a temperature and density dependent diameter.

$$\int_0^\infty \left(y_{HS}(r) \exp\left[-\frac{u_0(r)}{kT} \right] - 1 \right) r^2 dr = \int_0^\infty \left(y_{HS}(r) \exp\left[-\frac{u_{HS}(r)}{kT} \right] - 1 \right) r^2 dr \qquad 4.2$$

The subscript *HS* refers to a fluid property of a hard sphere fluid with a hard sphere diameter equal to d_{CWA} and u_0 refers to the reference energy as defined in the *CWA* theory. y_{HS} has been defined in section 2.2.4 equation 2.35 and is equal to:

$$y_{HS}(r) = g_{HS}(r) \exp\left[\frac{u_{HS}(r)}{kT} \right] \qquad 4.3$$

This function is continuous for $r \leq \sigma_{HS}$ and equal to the hard sphere radial distribution function g_{HS} for $r > \sigma_{HS}$.

Various approaches have been used to express the effective hard sphere diameter in a functional form, some of these will be discussed in the following sections.

4.2.1 The CWA effective hard sphere diameter expressions

Equation 4.2, as previously stated, requires that the *CWA* effective hard sphere diameter be dependent on temperature and density. A density dependent diameter greatly increases the complexity of any equation of state, as in most cases it has to be solved iteratively, complicating the determination of the density or compressibility roots at a given system temperature or pressure and making it less suited for everyday practical calculations.

The *CWA* approach has already been successfully applied to model Lennard-Jones fluids. In the case of a square well fluid model, the energy separation into a reference and perturbation contribution is identical to the *BH* separation, and the two perturbation theories are identical.

4.2.1.a Verlet and Weis Approach

Verlet and Weis [221] examined the *CWA* perturbation theory in detail and derived the following method to determine the effective hard sphere diameter, d_{CWA}.

$$d_{WCA} = d_B\left(1+\frac{\sigma_1}{2\sigma_0}\delta\right) \qquad 4.4$$

The d_B and δ parameters in equation 4.4 are integral functions of temperature, with the density dependence located in the terms σ_0 and σ_1. d_B is similar to the Barker and Henderson temperature dependent hard sphere diameter, equation 4.1:

$$d_B = \int_0^\infty 1-\exp\left[-\frac{u_0(r)}{kT}\right]dr \qquad 4.5$$

and

$$\delta = \frac{d_{CWA}}{d_B}\int_0^\infty\left(\frac{r}{d_{CWA}}-1\right)^2\frac{d}{dr}\left(\exp\left[-\frac{u_0(r)}{kT}\right]\right)dr \qquad 4.6$$

$$\approx \int_0^\infty\left(\frac{r}{d_B}-1\right)^2\frac{d}{dr}\left(\exp\left[-\frac{u_0(r)}{kT}\right]\right)dr \qquad 4.7$$

with

$$\sigma_0 = g_{HS}(d_{WCA}+) = \frac{z_{HS}-1}{4\eta} \qquad 4.8$$

and

$$\sigma_1 = 2\sigma_0 + \frac{\partial}{\partial r}g_{HS}(d_{WCA}+)\Big|_{d_{WCA}} \qquad 4.9$$

In this case $\eta = \rho\,\pi\,d^3_{CWA}/6$.

For a hard sphere fluid δ is equal to zero, and $d_{CWA} = d_B = d_{BH}$. Verlet and Weis evaluated the temperature dependent integral functions, equations 4.5 and 4.7 , for a Lennard-Jones fluid (with $u_0(r)$ as defined in equation 2.57) and found the following functions to correlate their results with the reduced temperature, $T^* = kT/\varepsilon$, [221]:

$$\frac{d_B}{\sigma_{LJ}} = \frac{0.3837T^*+1.068}{0.4293T^*+1} \qquad 4.10$$

$$\delta = \frac{T^*}{210.31T^* + 404.6} \qquad 4.11$$

They found these correlations reproduced the integrals with an error less than 2e-4 for $0.7 \leq T^* \leq 1.6$ and less than 8e-4 in the temperature range $1.6 \leq T^* \leq 4.5$ for equation 4.10 and a precision of order 8e-5 over the entire temperature range for equation 4.11. From these results it is clear that the δ parameter is between 800 and 260 times smaller than the d_B parameter in the range $0.65 \leq T^* \leq 5$. The validity of treating the density dependence as negligible has been investigated by some authors [51, 52]. They found that it gives a reasonable approximation of the radial distribution function only at high densities, but results in a Helmholtz free energy approximation with an error of less than 5% over a wider density range. The Helmholtz free energy is, however, still inaccurate at low densities.

4.2.1.b De Souza and Ben-Amotz CWA hard sphere diameter.

An approximate *CWA* hard sphere diameter has been proposed by de Souza and Ben-Amotz [57]. Their expression is explicit in d_{CWA}, and is a function of the reduced temperature, T^*, and reduced density, $\rho^* = \rho\sigma_{LJ}^3$.

$$d_{WCA} = 2^{1/6}\sigma_{LJ}\left\{1 + \left[\frac{T^* + a_2T^{*2} + a_3T^{*4}}{a_1\left(1 + a_4\rho^* + a_5\rho^{*2} + a_6\rho^{*3}\right)}\right]^{1/2}\right\}^{-1/6} \qquad 4.12$$

where a_i are universal constants: $a_1 = 1.5001$, $a_2 = -0.03367$, $a_3 = 0.0003935$, $a_4 = -0.09835$, $a_5 = 0.04937$ and $a_6 = -0.1415$. These parameters were determined by a least squares fit to the results of equation 4.2 over a range of $0 \leq \rho^* \leq 1.1$ and $0 \leq T^* \leq 5$. Equation 4.21 produces results of comparable accuracy to the iterative algorithm proposed by Verlet and Weis in section 4.2.1.a.

4.2.2 Barker and Henderson effective hard sphere diameter expressions

The *BH* perturbation theory has been applied to both square well and Lennard-Jones fluid models. The square well model, however, does not take the particle softness into account, and when used in equation 4.1 results in a effective hard sphere diameter, d_{BH}, that is independent of temperature, and equal to σ, the hard sphere diameter of the original model. The Lennard-Jones potential model on the other hand, results in an expression for d_{BH} that has to be

evaluated numerically. Several practical methods have therefore been developed to account for the model softness.

4.2.2.a Chen and Kreglewski diameter

Chen and Kreglewski modelled the real fluid systems as square well fluids, but included a correction to account for the softness of the molecules [42]. Their two-step potential model is depicted in equation 4.13 and Figure 4.1.

$$u(r)=\begin{cases}\infty & r\le(\sigma-s_1)\\ hu^0 & (\sigma-s_1)<r\le\sigma\\ -u^0 & \sigma<r\le\lambda\sigma\\ 0 & r>\lambda\sigma\end{cases} \qquad 4.13$$

In equation 4.14, u^0 represents the temperature independent well depth, as represented by ε in equation 2.55, λ the well width factor, s_1 the particle softness, or distance the particle can be penetrated and hu^0 the repulsive energy that must be overcome to allow the penetration. In their work Chen and Kreglewski found that the height of the repulsive step is about three times the depth of the attraction step, or h = 3, and that $s_1/\sigma = C \approx 0.12$ for most of the fluid systems except for systems exhibiting strong association.

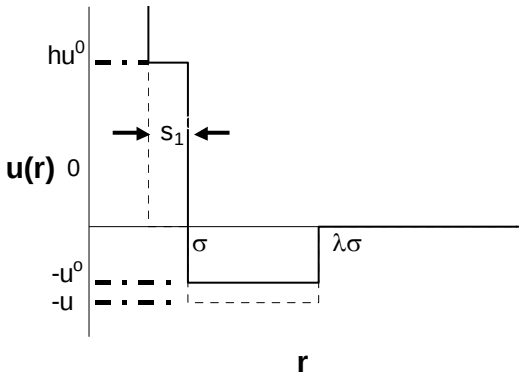

Figure 4.1 Two step CK potential function

By substituting equation 4.14 into equation 4.1 the following expression for the effective hard sphere diameter can be determined:

$$d_{BH} = \sigma\left(1 - C\exp\left(-\frac{hu^0}{kT}\right)\right) \qquad 4.14$$

4.2.2.b Cotterman Lennard Jones approximation

Cotterman et al. [49] evaluated equation 4.1 for a Lennard-Jones fluid in the reduced temperature rage $0 < T^* < 15$ and fitted the following function to their results:

$$\frac{d_{BH}}{\sigma_{LJ}} = \frac{1 + c_1 T^*}{1 + c_2 T^* + c_3 T^{*2}} \qquad 4.15$$

with c_1 = 0.29770, c_2 = 0.33163 and c_3 = 1.0477e-3. The expression matches the theoretical limits of a Lennard Jones fluid in that $d_{BH} = \sigma_{LJ}$ at $T^* = 0$ and that $d_{BH} \to 0$ as $T^* \to \infty$.

The Cotterman expression has been applied by other authors in representing the effective hard sphere diameter of Lennard Jones fluid systems [22]. Recently the parameters in equation 4.15 have been refitted [46], in order to improve the ability of the Cotterman equation of state [49] (section 4.3.5.b) to represent Lennard-Jones fluids over a wide range of temperatures and densities. The refitted parameters are: c_1 = 0.5495, c_2 = 0.6021 and c_3 = 3.0488e-3. These parameters were however fitted by optimising the overall *P-v-T* behaviour of the system and not to the values of the effective diameter of a Lennard-Jones fluid, which explains the poor performance of the refitted equation as seen in Figure 4.2.

4.2.2.c De Souza and Ben-Amotz BH Lennard Jones hard sphere diameter.

De Souza and Ben-Amotz [57] proposed the following analytical expression for the Lennard-Jones fluid effective hard sphere diameter determined through equation 4.1.

$$d_{BH} = 2^{1/6}\sigma_{LJ}\left\{1 + \left[1 + \frac{T^* + a_2 T^{*2} + a_3 T^{*4}}{a_1}\right]^{1/2}\right\}^{-1/6} \qquad 4.16$$

The parameter values were determined by a least squares fit to the numerically determined results of equation 4.1 over a range of $0 \le T^* \le 5$, and are a_1 = 1.1287, a_2 = -0.05536, a_3 = 0.0007278.

4.2.2.d Polynomial Lennard Jones approximations

In their work Morris et al. evaluated equation 4.1 for a Lennard Jones fluid up to a reduced temperature of $T^* = 2$ [149]. They represented the effective diameter as a polynomial function in reduced temperature:

$$\frac{d_{BH}}{\sigma_{LJ}} = a_0 + a_1 T^* + a_2 T^{*2} + a_3 T^{*3} + a_4 T^{*4} \qquad 4.17$$

with the following parameter values: a_0 = 0.9976, a_1 =-3.0554e+2, a_2 = 7.029e-3, a_3 = 1.1149e-3 and a_4 = 7.403e-5. Unlike the effective diameter approximation by Cotterman et al. (section 4.2.2.b), this model does not adhere to the correct boundary conditions as $T^* \rightarrow 0$ and $T^* \rightarrow \infty$ (section 4.2.2.b), and it has been found that the temperature dependence of the effective diameter given by Morris et al. is less accurate than the Cotterman approximation at low temperatures [46]. (Figure 4.2)

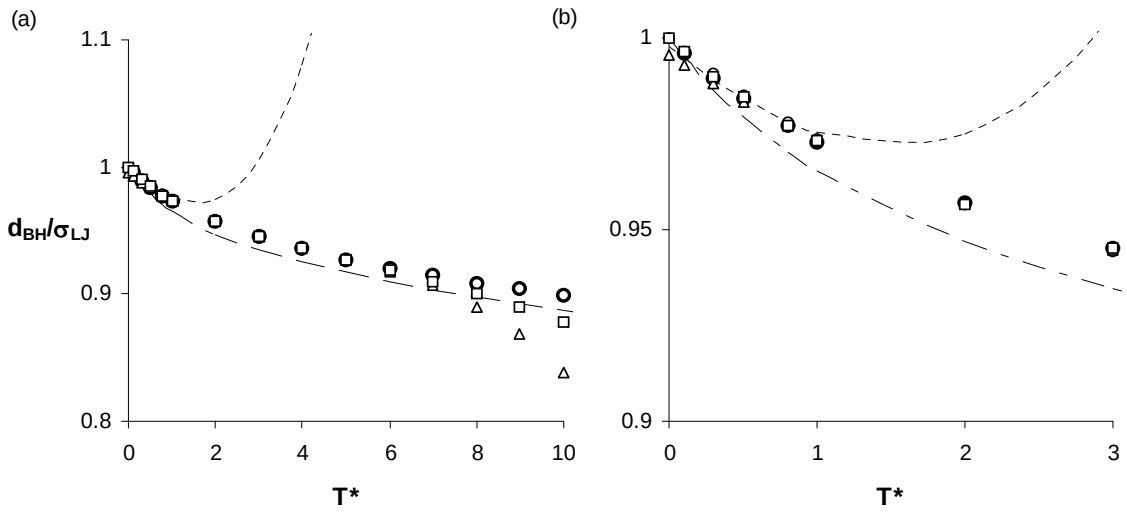

Figure 4.2 Effective Lennard-Jones hard sphere diameter on two temperature scales (a) and (b). ● Equation 4.1, ○ Cotterman, △ Gil-Villegas, □ De Souza, – – – refitted Cotterman and ..... Morris's approximations

Gil-Villegas et al. also developed a polynomial equation representing the Lennard-Jones effective hard sphere diameter [82]. Although their equation is less accurate than that of Morris in the low temperature region and it does not have the correct limiting values, this polynomial expression compares favourably with the original Cotterman approximation over a wider range of reduced temperatures, as can be seen in Figure 4.2. The third order polynomial coefficients are: a_0 = 0.995438, a_1 =-2.59917e-2, a_2 = 3.92254e-3 and a_3 = -2.89398e-3.

4.3 PERTURBATION TERM EVALUATION

According to the perturbation theory discussed in section 2.3.3, the Helmholtz free energy contribution of the attractive, or perturbation terms, can be expressed as a Taylor series expansion in temperature:

$$A^{Pert} = \frac{A^{(1)}}{kT} + \frac{A^{(2)}}{(kT)^2} + \frac{A^{(3)}}{(kT)^3} + \frac{A^{(4)}}{(kT)^4} + \ldots \qquad 4.18$$

The convergence of the perturbation expansion will be determined by the choice of the reference and perturbation potential energies. As already mentioned the *CWA* approach is rapidly convergent, and generally only the first perturbation term will be required, whilst with the *BH* perturbation approximation, higher order perturbation terms may be needed.

The expressions of the Helmholtz energy perturbation terms, $A^{(1)}$, $A^{(2)}$, etc., can be obtained through various approaches. In some limited cases analytical solutions of the actual perturbation equations, equations 2.92 and 2.93, may be obtained, but more generally the perturbation terms are obtained as approximations, either by functions fitted to simulation results or by making various simplifying assumptions.

4.3.1 Square Well Analytical Solution

Because of the simple nature of the square well potential function it is possible to express the perturbation expansion of this fluid in a much simpler form. The Barker and Henderson local compressibility second order perturbation expression for a square well fluid can be expressed as:

$$\frac{A^{Pert}}{NkT} = -\left(\frac{\varepsilon}{kT}\right) 12\eta \int_1^{\lambda} g_0(x) x^2 dx - \left(\frac{\varepsilon}{kT}\right)^2 6\eta kT \left(\frac{\partial P^{HS}}{\partial \rho}\right)^{-1} \frac{\partial}{\partial \eta}\left(\eta \int_1^{\lambda} g_0(x) x^2 dx\right) \qquad 4.19$$

where $x = r/\sigma$.

By introducing the isothermal compressibility as:

$$K^{HS} = kT\left(\frac{\partial P^{HS}}{\partial \rho}\right)^{-1} \qquad 4.20$$

and recognising equation 4.19 as an expansion in reduced temperature ($1/T^*=\varepsilon/kT$), the first and second perturbation terms may be written as:

$$\frac{A^{(1)}}{T^*} = -12\eta I \qquad 4.21$$

$$\frac{A^{(2)}}{T^{*2}} = -6\eta K^{HS}\left(I + \eta\frac{\partial I}{\partial \eta}\right) \qquad 4.22$$

where

$$I = \int_1^{\lambda} g_0(x)x^2 dx \qquad 4.23$$

Chang and Sandler developed an analytic equation of state from these expressions for a square well fluid with a variable well width ($1 \leq \lambda \leq 2$) by using the Percus-Yevic hard sphere compressibility approximation in the evaluation of the second term of equation 4.22 and solving the integral, equation 4.23 using the Percus-Yevic equation (section 2.3.2.c, equation 2.78) [35, 37]. They however observe that '*although the SW* (*square well*) *potential is simple, the final expressions for the thermodynamic properties obtained from the perturbation theory are lengthy and involve exponential and trigonometric functions, which arise from the definite integration of the RDF* (*radial distribution function*) *of hard spheres.*' [35].

Chang and Sandler expressed the solution of equation 4.23 as follows:

$$I = \sum_i^3 a_i t_i \qquad 4.24$$

with a_1, a_2 and a_3 representing expressions in reduced density, η, and the t_i terms, complex functions of the well width term, λ and η. (The reader is referred to the original articles [35, 37] for the complete functional expressions of these terns, should they be of interest.)

Due to the complex nature of the various expressions involved, the analytical solution of the square well fluid is of little practical value in the development of an equation of state. It should also be noted that although Chang and Sandler were successful in obtaining an analytical solution for the square well perturbation equation of state, the performance of this equation

will still be constrained by the accuracy of the underlying approximations of the Barker and Henderson local compressibility expression, the Percus-Yevic compressibility equation of state and the Percus-Yevic approximation of the radial distribution function.

4.3.2 Gil-Villegas Mean –Value approach

Gil-Villegas et al. [82] expressed the perturbation Helmholtz energy contributions in terms of the Van der Waals mean-field approximation and a mean hard sphere radial distribution function over the entire range of interaction, $g_0(\zeta)$.

As stated in section 2.4.2.b, Van der Waals attractive, or perturbation, contribution can be derived from a first order perturbation expansion by assuming a uniform molecular distribution over the entire fluid volume, i.e. $g_0(r) = 1$. This approach leads to the following expression:

$$\frac{A^{Pert}}{NkT} = -\frac{12\eta\varepsilon}{kT}\int_1^\infty \phi(x) g_0(x) x^2 dx = -\frac{3\varepsilon b^{VDW}\rho}{kT}\int_1^\infty \phi(x) x^2 dx = -\frac{a^{VDW}}{kT} \qquad 4.25$$

Where $\phi(x)$ represents the reduced perturbation energy and ε the maximum well depth, i.e. $u^{(1)}(x)=\varepsilon\phi(x)$. b^{VDW} is Van der Waals hard sphere volume term similar to b defined in section 2.4.2.b, with $b^{VDW}= 4*(N\pi\sigma^3/6) = N/N_A*b = nb$ and a^{VDW} the Van der Waals attractive parameter.

The applying the mean field theory to the Barker and Henderson local compressibility perturbation equation 2.102 can be written in the following form:

$$\begin{aligned}\frac{A^{Pert}}{NkT} &= -\frac{3\varepsilon b^{VDW}\rho}{kT} g_0(\varsigma)\int_1^\infty \phi(x) x^2 dx \\ &\quad -\frac{1}{2}\rho\left(\frac{\varepsilon}{kT}\right)kT\left(\frac{\partial P^{HS}}{\partial\rho}\right)^{-1}\frac{\partial}{\partial\rho}\left(-\frac{3\varepsilon b^{VDW}\rho}{kT} g_0(\varsigma)\int_1^\infty \phi(x)^2 x^2 dx\right)\end{aligned} \qquad 4.26$$

Where $\zeta \in [1,\infty]$. By defining a^{VDW*} as follows:

$$a^{VDW*} = -3\varepsilon b^{VDW}\rho\int_1^\infty \phi(x)^2 x^2 dx \qquad 4.27$$

and substituting equation 4.20 for the isothermal hard sphere compressibility term, equation 4.26 may be further reduced to the following:

$$\frac{A^{Pert}}{NkT} = -\frac{a^{VDW}}{kT} g_0(\varsigma) - \frac{1}{2}\rho\left(\frac{\varepsilon}{kT}\right) K^{HS} \frac{\partial}{\partial\rho}\left(-\frac{a^{VDW*}}{kT} g_0(\varsigma)\right) \qquad 4.28$$

In stead of determining the hard sphere radial distribution function at the intermolecular distance ς, Gil-Villegas et al. found that the mean radial distribution function could be represented by the simple hard sphere contact distribution function (equation 3.6) at an effective reduced density which is a is a function of the range of the attractive well:

$$g_0(\zeta,\eta) = g_0(1,\eta_{eff}) \qquad 4.29$$

For a square-well fluid with a well-width parameter λ the Van der Waals attractive parameter a^{VDW} is:

$$a^{VDW} = -4\eta\left(\lambda^3 - 1\right)\varepsilon \qquad 4.30$$

and $a^{VDW} = a^{VDW*}$. The perturbation expansion terms, $A^{(1)}$ and $A^{(2)}$, can therefore be expressed as:

$$\frac{A^{(1)}}{kT} = -\frac{a^{VDW}}{kT} g_0(1,\eta_{eff}) \qquad 4.31$$

and

$$\frac{A^{(2)}}{(kT)^2} = \frac{1}{2}\left(\frac{\varepsilon}{kT}\right) K^{HS} \eta \frac{\partial}{\partial\eta}\left(-\frac{A^{(1)}}{kT}\right) \qquad 4.32$$

where the effective reduced density, for square-well fluids with a well width parameters in the range of $1.1 \le \lambda \le 1.8$, is defined as follows:

$$\eta_{eff} = c_1\eta + c_2\eta^2 + c_3\eta^3 \qquad 4.33$$

and

$$\begin{bmatrix} c_1 \\ c_2 \\ c_3 \end{bmatrix} = \begin{bmatrix} 2.25855 & -1.50349 & 0.249434 \\ -0.669270 & 1.40049 & -0.827739 \\ 10.1576 & -15.0427 & 5.30827 \end{bmatrix} \times \begin{bmatrix} 1 \\ \lambda \\ \lambda^2 \end{bmatrix} \quad 4.34$$

For a Lennard-Jones fluid the temperature expansion is expressed in terms of the effective hard sphere diameter, d_{BH}, or packing fraction, $\eta_{BH}=\rho\pi d_{BH}^3/6$:

$$\frac{A^{(1)}}{kT} = 4\left[-a_1^s(\eta,\lambda=12)+a_1^s(\eta,\lambda=6)\right] \quad 4.35$$

and

$$\frac{A^{(2)}}{(kT)^2} = 4\left[-a_2^s(\eta,\lambda=12)+a_2^s(\eta,\lambda=6)\right] \quad 4.36$$

Where

$$a_1^s(\eta,\lambda) = -\frac{4\eta\varepsilon}{kT}\left(\frac{3\lambda}{\lambda-3}\right)g_0(1,\eta_{eff}) \quad 4.37$$

and

$$a_2^s(\eta,\lambda) = \frac{1}{2}\left(\frac{\varepsilon}{kT}\right)K^{HS}\eta\frac{\partial}{\partial\eta}\left(-a_1^s(2\lambda)\right) \quad 4.38$$

and the effective reduced density:

$$\eta_{eff} = c_1\eta + c_2\eta^2 \quad 4.39$$

and

$$\begin{bmatrix} c_1 \\ c_2 \end{bmatrix} = \begin{bmatrix} -0.943973 & 0.422543 & -0.0371763 & 0.000116901 \\ 0.370942 & -0.173333 & 0.0175599 & -0.000572729 \end{bmatrix} \times \begin{bmatrix} 1 \\ \lambda \\ \lambda^2 \\ \lambda^4 \end{bmatrix} \quad 4.40$$

The results of these expressions were compared to vapour liquid coexistence curves of simulation results of square-well fluids with various well-widths and it was found that the mean-value approach provides an accurate representation of the simulation data for several λ

values. It was also observed that this approach provides a description which is of comparable accuracy to the complex analytical solution provided by Chang and Sandler as discussed above, whilst being mathematically much more manageable [82]. It however is clear that, although not nearly as complex as the analytical solution, as a consequence of expressing the reduced effective density as a polynomial function of η or η_{BH}, the density dependence of the final equation of state is increased significantly.

4.3.3 Mathematical representation of Barker and Henderson local compressibility approximation

An alternative approach to the complex methods discussed above, is to represent the integral function (equation 4.23) in the Barker and Henderson square-well local compressibility approximation by an empirical but mathematically simple equation.

This approach was followed by Hino and Prausnitz [94] in the development of their monomer square-well perturbation expansion. They fitted a ninth order reduced density polynomial function to the analytical expressions by Chang and Sandler (section 4.3.1) for I (equation 4.23) in the range $1 \leq \lambda \leq 2$.

$$I = \sum_{i}^{10} c_i \eta^{i-1} \qquad 4.41$$

Gulati and Hall [88] used a similar approach by fitting a seventh order polynomial to hard sphere monomer and dimer molecular simulation results over a density range of $0.025 \leq \eta \leq 0.475$, whilst Gross and Sadowski [85] fitted two 6^{th} order polynomial functions to the integral function I and the derivative there of $\delta(\eta I)/\delta\eta$ as determined from the average hard chain radial distribution function results of Chiew [45]. (Although the dimer and hard chain fluids are not strictly of interest in this section, the approach followed to represent the perturbation terms is mentioned here as a practical example of the empirical representation if the integral term.)

The empirical expressions of the integral I and its density derivative $\delta(I)/\delta\eta$ or $\delta(\eta I)/\delta\eta$ are applied in equations 4.21 and 4.22 to obtain an expression for the first and second perturbation terms. Unfortunately the density order of the perturbation terms is still quite high, due partly to the high order of the polynomial function (9 in the case of Hino and Prausnitz or 7 in the

Gulati an Hall approach) but also due to the K^{HS} term in the second perturbation approximation. The K^{HS} expression is often determined from the Percus-Yevic compressibility hard sphere equation [35, 82, 88, 94], and has the following form:

$$K^{PY-C} = \frac{(1-\eta)^4}{1+4\eta+4\eta^2} \qquad 4.42$$

When using the simplified hard sphere equation *HS*3 as defined in equation 3.49, the isothermal compressibility term is expressed as:

$$K^{HS3} = \frac{(1-1.399\eta)^2}{1+5.202\eta+9.5726\eta^2+9.1322\eta^3+22.5106\eta^4} \qquad 4.43$$

The Barker and Henderson local compressibility approximation, on which this approach is based, has been found to be unreliable at high system densities [17], and coupled with the added complexity that this approximation brings to the evaluation of the equation of state in the form of the K^{HS} term, does not favour its application in a practical equation of state.

4.3.4 Empirical representation of molecular simulation results

An alternative approach to representing the integral of the hard sphere radial distribution function (equation 4.23) by empirical equations as discussed above (section 4.3.3), is to represent the *entire* perturbation expansion empirically. Some of the advantages of this approach are that it is not only applicable to the square-well fluid models and that, by empirically fitting molecular simulation results, the problem of the inaccuracies and mathematical complexities due to the simplifying assumptions (in the form of the K^{HS} term as an example), required to represent the second and higher perturbation terms analytically, is avoided.

In this approach the residual Helmholtz free energy of the system is expressed as:

$$\frac{A^{Resid}}{NkT} = \frac{A_0}{NkT} + \frac{A^{Pert}}{NkT} = \frac{A_0}{NkT} + \sum_{n=1}^{\infty} \frac{A_n}{T^{*n}} \qquad 4.44$$

Where T^* is the reduced temperature, $T^*=kT/\varepsilon$, with ε representing the maximum well depth, and the perturbation terms, A_n, functions of density.

4.3.4.a Alder square well approximation

Alder et al. [9] determined the first four perturbation terms (n=4 in equation 4.44) of a square-well fluid through thermodynamic and statistical mechanical calculations for a square well fluid with a well-width parameter, λ, of 1.5, and over a density and temperature range $0.104 \leq \eta \leq 0.494$ and $0.2 \leq T^* \leq \infty$. They represented the perturbation terms as polynomial functions in density, fitted to the various calculated values:

$$A_n = \sum_0^m \frac{D_{nm}}{(V/V_0)^m} = \sum_0^m D_{nm}\left(\frac{\eta}{\tau}\right)^m \qquad 4.45$$

V_0 represents the closest packed volume ($N\sigma^3/2^{1/2}$) and τ the value ($\pi 2^{1/2}/6 \approx 0.74048$). Alder et al. noted that it was necessary to keep the significant figures as published because of extensive cancellations amongst the terms [9]. Their coefficients are listed in Table 4.1.

Table 4.1 Alder perturbation expansion coefficients

	$D_{n\,m}$			
m	**n = 1**	**n = 2**	**n = 3**	**n = 4**
0	0	-1.2495816E-04	-5.1235572E-05	2.5364174E-03
1	-7.0346	-3.3015580	-1.1868777E+00	-5.1739049E-01
2	-7.2736	-0.98155782	7.2447507E+00	2.5259812E+00
3	-1.2520	2.2022115E+02	-1.7432407E+01	-4.1246808E+00
4	6.0825	-1.9121478E+03	1.9666211E+01	2.3434564E+00
5	6.8	8.6413158E+03	-8.5145188E+00	
6	1.7	-2.2911464E+04		
7		3.5388809E+04		
8		-2.9353643E+04		
9		1.0090478E+04		

4.3.4.b Barker and Henderson approximation

Barker and Henderson [17] fitted their first and second square well perturbation molecular simulation data (λ = 1.5) with the following equation:

$$A_n = C_n\left\{1 - \exp\left(\frac{-\alpha_n \rho^*}{\beta_n - \rho^*}\right) - \frac{\alpha_n}{\beta_n}\rho^*\right\} + P_n\rho^* + Q_n\rho^{*2} \qquad 4.46$$

Where $\rho^* = \sigma^3\rho$. The values of the constants C_n, α_n, β_n, P_n and Q_n are listed in Table 4.2.

Table 4.2 Barker and Henderson square-well parameters

n	C_n	α_n	β_n	P_n	Q_n
1	1.5	$2^{1/2}$	-8.460822	-4.974192	-2.427216
2	2.75	$2^{1/2}$	7.6956887	-2.487096	9.919624

4.3.4.c Cotterman Approximation Lennard Jones fluid perturbation approximation

Cotterman et al. [49] used the Barker and Henderson soft-repulsion approach with the first two perturbation terms of equation 4.44 to describe the phase behaviour of a Lennard-Jones fluid. They used Monte Carlo Lennard-Jones fluid simulations to determine the A_1 and A_2 perturbation terms and fitted the results with polynomial functions in reduced density, $\eta_{LJ} = 6\rho/(N\pi d^3)$:

$$A_n = \sum_{m=1}^{4} D_{nm}\left(\frac{\eta_{LJ}}{\tau}\right)^m \qquad 4.47$$

The coefficients D_{nm} are listed in Table 4.3.

Table 4.3 Cotterman et al. [49] Lennard-Jones parameters

	$D_{n\,m}$			
n	**m = 1**	**m = 2**	**m = 3**	**m = 4**
1	-8.5959	-4.5424	-2.1268	10.285
2	-1.9075	9.9724	-22.216	15.904

4.3.4.d The Padé approximation

A different approach was followed by Morris et al. [149] who approximated the first and second Lennard-Jones perturbation terms as follows:

$$A_1 = \sum_{m=1}^{6} A_{1m}\left(\frac{\eta_{LJ}}{\tau}\right)^m \qquad 4.48$$

And the second:

$$A_2 = \sum_{m=1}^{4}\left[\frac{C_{1m}}{2}\left(\frac{\eta_{LJ}}{\tau}\right)^m + C_{2m}\left(\frac{\eta_{LJ}}{\tau}\right)^{m+1} + \frac{C_{2m}}{2}\left(\frac{\eta_{LJ}}{\tau}\right)^{m+2}\right] \qquad 4.49$$

The coefficients of the first perturbation term were determined by fitting the results of equation 4.23, using Monte Carlo simulation results of the hard sphere fluid radial distribution function and the Barker and Henderson Lennard-Jones perturbation energy. The second perturbation coefficients were fitted to data reported by Smith et al. [195] on the evaluation of the higher order perturbation integrals through the use of the superposition approximation. The specific parameter values can be found in Table 4.4.

Instead of truncating the perturbation expansion after the second term, Morris et al. approximated the higher order perturbation terms through a Padé approximant. Their complete residual Helmholtz energy expression is then:

$$\frac{A^{Resid}}{NkT} = \frac{A_0}{NkT} + \frac{A_1}{T*}\left[\frac{\frac{A_1}{T*}}{\frac{A_1}{T*} - \frac{A_2}{T*^2}}\right] \qquad 4.50$$

The approaches used by Morris and Cotterman were investigated by Chunxi et al. [46], and they could not find any significant improvement in the calculation of the Lennard-Jones fluid pressure and internal energy by using the Padé approximant of the higher order perturbation terms. They however did not investigate the effect of the approximant on any other thermodynamic functions, and it may still result in an improvement in the representation of some of these properties.

Barker and Henderson also proposed the use of a Padé approximant for the higher order perturbation terms, because the perturbation expansion appears to be rapidly convergent [18] and hence ideal for such an approach. However, they found that the results of the Padé approximation are incorrect at low densities and that when it is applied to a simple square-well model results in higher order perturbation values that are incorrect even at high densities.

Table 4.4 The Morris Lennard-Jones fluid perturbation coefficients

m	1	2	3	4	5	6
$\mathbf{A_{1m}}$	-8.538	-5.276	3.73	-7.54	23.307	-11.2
$\mathbf{C_{1m}}$	-3.938	-3.193	-4.93	10.03		
$\mathbf{C_{2m}}$	11.703	-3.092	4.01	-20.2025		
$\mathbf{C_{3m}}$	-37.02	26.93	26.73			

4.3.4.e *CWA approximation approaches*

Cuadros et al. [51, 52] studied the *CWA* perturbation approximation of a Lennard-Jones fluid through extensive computer simulations in the liquid-vapour and supercritical regions and developed a simple analytical expression for the Helmholtz free energy perturbation term. In their approximation Cuadros et al included a correction term, C_3, to account for the truncation of the Lennard-Jones potential at an intermolecular distance r=2.5σ. The simulation results in the two different thermodynamic regions were unfortunately modelled using different parameter values, and hence limits the practical value of the analytical expression:

$$A^{Pert} = -\eta_{LJ}\left(C_1(T^*) + C_2(T^*)\eta_{LJ} + C_3\eta_{LJ}\right) \qquad 4.51$$

with

$$C_n = c_{n1} + c_{n2}T^* + c_{n3}T^{*2} + c_{n4}T^{*3} \qquad 4.52$$

The coefficient values for the liquid-vapour and supercritical regions are given in Table 4.5.

Table 4.5 Cuadros et al. parameters for the liquid-vapour and supercritical regions

	Liquid –Vapour Region				**Supercritical Region**			
i	**1**	**2**	**3**	**4**	**1**	**2**	**3**	**4**
$\mathbf{C_{1i}}$	5.107805	0.22211	0	0	5.7087	0.3602	-0.1578	0.0249
$\mathbf{C_{2i}}$	2.761161	-0.106594	0	0	2.3475	-0.1787	-0.0017	0.0037
$\mathbf{C_3}$	0.535432	0	0	0	0.5354343	0	0	0

Finally, Tan et al. [208] recently used the *CWA* perturbation approach to represent the first order perturbation term of a Lennard-Jones fluid. They evaluated the perturbation integral (equation 4.53)

$$\frac{A^{Pert}}{NkT} = \frac{2\pi}{NkT}\rho\int_{d_{LJ}}^{\infty} g_0(r)u^{(1)}(r)r^2 dr \qquad 4.53$$

by using a corrected hard sphere radial distribution function, which they obtained by applying the Verlet-Weis adjustment [221] on the analytical expression by Chang and Sandler [37], along with the perturbation Lennard-Jones energy, $u^{(1)}(r)$, as defined in section 2.2.6.d. The results of this perturbation term, in the range $0.1 \le \eta_{LJ} \le 0.5$ and $0.67 \le T^* \le 5$, were then

approximated by a double summation over the reduced temperature and density (The coefficient values are listed in Table 4.6):

$$\frac{A^{Pert}}{NkT} = 12\sum_{n=1}^{6}\sum_{m=1}^{4} D_{nm}\left(\frac{1}{T*}\right)^{n}\eta_{LJ}^{m} \qquad 4.54$$

Table 4.6 Tan et al. [208] CWA perturbation term approximation coefficients.

	$D_{n\,m}$					
m	**n = 1**	**n = 2**	**n = 3**	**n = 4**	**n = 5**	**n = 6**
1	-1.024028	0.363988	-0.570022	0.532256	-0.259057	0.050531
2	-0.598918	-1.277853	2.125006	-2.020867	0.991370	-0.194186
3	0.417149	-1.009886	0.770276	-0.436701	0.146287	-0.021159
4	0.113873	2.992720	-3.841951	3.260748	-1.507330	0.284955

4.3.5 Alternative approaches in perturbation approximation

Besides the methods discussed above, various other empirical approaches have been used to represent the perturbation expansion of real or theoretical systems more concisely, accurately or over a wider range of conditions. Some of these approaches will be discussed in this section.

4.3.5.a Fitting of pure component data

In section 4.3.4 various empirical equations, mostly polynomial functions in reduced density, have been fitted to the molecular simulation data or complex perturbation terms of theoretical models. These theoretical models are of course only approximations for the real fluid interactions and are not able to capture the fluid behaviour completely. In an attempt to improve the real fluid equations of state, many authors have fitted these empirical equations on real systems instead, thereby indirectly incorporating corrections to the simplifying assumptions in the theory into the equation of state.

Chen and Kreglewski [42] refitted the power series as derived by Alder et al. [9] for the four term square-well perturbation expansion (equations 4.44 and 4.45) to argon *P-v-T* and internal energy data. Their *BACK* equation of state reduces to the Carnahan-Starling hard sphere repulsive term and a power series expansion when applied to the spherical fluid system.

$$\frac{A^{Resid}}{NkT} = \frac{A_0^{CS}(\eta_{CK})}{NkT} + \sum_{n}\sum_{m} D_{nm}\left(\frac{\eta_{CK}}{\tau}\right)^{m}\left(\frac{u(T)}{kT}\right)^{n} \qquad 4.55$$

This equation of state is an improvement on the square-well fluid model, in that the softness of the molecules have been taken into account through the Chen and Kreglewski two-step potential model and the effective hard sphere diameter as defined in section 4.2.2.a. A further extension to the model is the use of a temperature dependent well-depth in the perturbation term (see Figure 4.1). The well-depth is determined through equation 4.56, where μ is a correction for the specific interactions between the particles in the fluid. (For the case of argon μ=0.):

$$u(T) = u^0\left(1 + \frac{\mu}{kT}\right) \qquad 4.56$$

The D_{nm} parameters were determined by fitting the entire equation of state to argon thermodynamic data. u^0 was taken to be equal to the argon critical temperature, whilst the hard sphere diameter, σ, or actually the specific hard sphere closest packed volume, v_0, and the D_{n1} parameters were fitted to argon virial coefficient data. The remainder of the D_{nm} parameters were fitted by simultaneously fitting the internal energy and *P-v-T* data of liquid and gaseous argon.

Table 4.7 Chen and Kreglewski perturbation power series terms

	$D_{n\,m}$			
m	**n = 1**	**n = 2**	**n = 3**	**n = 4**
1	-8.804	2.9396	-2.8225	0.3400
2	4.1646270	-6.0865383	4.7600148	-3.1875014
3	-48.203555	-40.137956	11.257177	12.231796
4	140.43620	-76.230797	-66.382743	-12.110681
5	-195.23339	-133.70055	69.248785	
6	113.51500	860.25349		
7		-1535.3224		
8		1221.4261		
9		-409.10539		

The Chen and Kreglewski, *CK*, power series expansion has been applied in many equations of state, most notably the *SAFT* equation as developed by Huang and Radosz [100, 101]. The parameters are listed in Table 4.7, and as in the case of the original Alder series, these parameters should not be rounded off as the system pressure and compressibility at low temperatures and high densities are very sensitive to these values.

Donohue and Prausnitz [60] also refitted the Alder power series in the derivation of the *Perturbed Hard Chain* equation of state (section 5.2.2.b). They reduced the perturbation parameter matrix size to a 4x6 matrix in order to facilitate faster machine calculations, and fitted the vapour pressure and liquid density data of methane whilst keeping the first perturbation term parameters and the parameters affecting the lower order virial coefficients constant. (See Table 4.8 for the parameters values) Donohue and Prausnitz found that the refitting of the parameters not only significantly improved the performance of their equation of state for methane, but also for most other fluids.

Table 4.8 Donohue and Prausnitz perturbation power series terms

	$D_{n\,m}$			
m	**n = 1**	**n = 2**	**n = 3**	**n = 4**
1	-7.0346	-3.5173	-1.1724	-0.29311
2	-7.2736	11.15	7.15	-1.32
3	-1.2520	-10.69	-31.3	32.9
4	6.0825	-3.5977	63.1073	-94.2481
5	6.8	7.4318	-40.6084	73.3867
6	1.7	0	0	0

Adidharma and Radosz [4] developed an interesting equation of state in which they applied the Gil-Villegas mean-value approach as discussed in section 4.3.2 to a square well fluid to account for the first two perturbation terms, whilst introducing power series expansion, equation 4.57, similar in form to the expansions used by Alder, Chen and Kreglewski and Donohue and Prausnitz, as an empirical correction to the truncation error of the second-order perturbation theory.

$$\frac{A^{trunc}}{NkT} = \sum_{n=1}^{4}\sum_{m=1}^{2} D_{nm}\left(\frac{\eta}{\tau}\right)^{m}\left(\frac{u(T)}{kT}\right)^{n} \qquad 4.57$$

In their equation of state the authors used a temperature dependent well-depth with a similar form as applied by Chen and Kreglewski (equation 4.56). The truncation correction term parameters, as listed in Table 4.9, were determined by simultaneously fitting the Adidharma-Radosz equation of state to ethane second virial coefficient and saturated vapour pressure and liquid volume data. (Only the perturbation approximation is of interest here and the reader is referred to the original article [4] for a complete discussion of the proposed equation of state.) From equation 4.57 it is clear that the empirical correction term will also affect the first and

second perturbation terms, and hence can be seen as a correction on the Barker and Henderson local compressibility approximation used in the Gil-Villegas approach.

Table 4.9 Adidharma and Radosz correction term parameters

	$D_{n\,m}$			
m	**n = 1**	**n = 2**	**n = 3**	**n = 4**
1	0.2933	2.8222	-8.9554	3.4764
2	0.9358	6.8199	0	0

It was mentioned in section 4.3.3 that Gross and Sadowski [85] applied molecular simulation data to determine the parameters of equation 4.41. Although this chapter is still concerned with the modelling of fluids with small spherical particles it should be noted that the *PC-SAFT* equation developed by Gross and Sadowski [85] is highly successful in representing real chained systems, and its success can, in part, be attributed to the fact that upon extending the equation to real fluid systems the perturbation parameters were refitted to real fluid thermodynamic data [86].

4.3.5.b Empirical second virial coefficient correction

From its theoretical basis, as essentially a MacLauren series expansion of fluid properties dominated by repulsive forces, the perturbation approach is generally more accurate at high system densities where these conditions prevail, whilst the virial expansion about an ideal gas is more accurate in the low density region. It has therefore been suggested that, in order to ensure the accurate representation of the fluid behaviour over a wide density range, these two approaches should be combined.

Cotterman and Prausnitz [49] developed an approach to separate the perturbation Helmholtz energy contribution into low-density (A^{virial}) and high-density (A^{liquid}) contributions and combine the two with a density and temperature dependent scaling function, F. (See equation 4.58). (In their original article Cotterman and Prausnitz allowed for other Helmholtz energy contributions from dipolar, quadrupolar and dipolar-quadrupolar forces, these interactions are however not of interest here, and the Cotterman-Prausnitz approach will be disused without further reference to the polar contributions.)

$$\frac{A^{Pert}}{NkT} = \frac{A^{virial}}{NkT}(1-F) + \frac{A^{liquid}}{NkT}F \qquad 4.58$$

The high-density contribution A^{liquid} is determined from the first two Barker and Henderson perturbation expansion terms represented by equation 4.47 and discussed in section 4.3.4.

The low-density contribution on the other hand was determined for simple spherical fluids, by fitting the virial coefficient data for methane.

$$\frac{A^{virial}}{NkT} = \eta_{BH}\left(B^{disp}\right) \qquad 4.59$$

Where B^{*disp} is the contribution to the second virial coefficient from the dispersion (non-polar) forces defined in equation 4.60, and η_{BH} is the temperature dependent reduced density (determined through equation 4.15 in [49]).

$$B^{disp} = -a_1\left[\exp\left(\frac{a_2}{T*}\right) - a_3\right] \qquad 4.60$$

With the fitted parameter values treated as universal constants: a_1 = 12.541, a_2 = 0.67372 and a_3 = 0.98071.

The scaling function, F, has to be such that it does not contribute to the second virial coefficient and meets the following boundary conditions: it must be zero at zero density and must approach unity at high densities and zero at high temperatures. Cotterman and Prausnitz used the following function:

$$F = 1 - \exp\left[-6\eta_{BH}\right] \qquad 4.61$$

(This equation appears in a slightly different form in [49] due to the polar contributions which are taken into consideration in the original work.)

Song and Mason [201] followed a different approach to ensure a good description of the fluid at low densities. Instead of a scaling function they split out the exact second coefficient from the equation of state (equation 2.60) and treated the remainder of the integral using an approach similar to the *CWA* perturbation theory. Equation 2.50 can therefore be written as:

$$\frac{PV}{NkT} = 1 - \frac{2\pi}{3}\frac{\rho}{kT}\int_0^\infty \frac{d\left(u(r)\right)}{dr} g(r) r^3 dr \qquad 4.62$$

$$= 1 + \rho B_2' + \rho I \qquad 4.63$$

Where

$$B_2' = -\frac{2\pi}{3}\frac{1}{kT}\int_0^\infty \frac{d(u(r))}{dr}\exp\left[-\frac{u(r)}{kT}\right]r^3 dr = -2\pi\int_0^\infty\left(\exp\left[-\frac{u(r)}{kT}\right]-1\right)r^2 dr \qquad 4.64$$

And

$$I = \frac{2\pi}{3}\int_0^\infty \psi(r)[y(r)-1]r^3 dr \qquad 4.65$$

with $y(r)$ as defined in equation 2.35, and the function $\psi(r)$ defined as follows:

$$\psi(r) = -\frac{1}{kT}\frac{d(u(r))}{dr}\exp\left[-\frac{u(r)}{kT}\right] \qquad 4.66$$

Song and Mason evaluated the integral I through the perturbation theory, using the *CWA* division of the potential function $u(r)$, and they show that I can be approximated as follows:

$$I \approx \alpha[g_{HS}(d+)-1] \qquad 4.67$$

$$\alpha = 2\pi\int_0^{r_m}\left(1-\exp\left[-\frac{u^{(0)}(r)}{kT}\right]\right)r^2 dr \qquad 4.68$$

In these equations r_m is intermolecular distance at which the minimum potential energy is found (the distance at which the potential model is separated into the reference and perturbation energies), $u^{(0)}(r)$ the unperturbed or reference energy and $g_{HS}(d+)$ the hard sphere radial distribution function evaluated at the dependent effective hard sphere diameter d. The effective hard sphere diameter is determined through the equation 4.69, an expression for the temperature dependent effective Van der Waals co-volume b, with $b=2/3\,\pi\, d^3$. Unlike in the *CWA* perturbation approach, the effective diameter is purely a function of temperature and not density.

$$b'(T) = 2\pi\int_0^{r_m}\left(1-\left[1+\frac{u_0(r)}{kT}\right]\exp\left[-\frac{u_0(r)}{kT}\right]\right)r^2 dr \qquad 4.69$$

Bokis and Donohue [22] derived their expression for the attractive contribution, or the perturbation expansion, of a square-well fluid by slightly modifying the third and fourth order perturbation terms derived by Alder et al. [9] so that the perturbation expansion conforms to an expansion of a mathematical series and the internal energy perturbation expansion can be expressed in a closed form:

$$\frac{U^{Pert}}{N\varepsilon} = \sum_{n=1}^{\infty} \frac{nA_n}{T^{*n-1}} = \sum_{n=1}^{\infty} \frac{U_n}{T^{*n}} = U_1 \exp\left[\frac{U_2}{U_1}\frac{1}{T^*}\right] \qquad 4.70$$

With U_n/T^{*n} representing the nth internal energy perturbation term.

Equation 4.70 is extended to a Lennard-Jones fluid through the Barker and Henderson approach of using a temperature dependent effective hard sphere diameter. (Equation 4.15). The ratio of U_2/U_1 is equal to 1 in the low density limit of a square-well fluid and results in the exact expression for the second virial coefficient. For a Lennard-Jones fluid this ratio tends towards constant α, which is used to ensure the correct Lennard-Jones second virial coefficient behaviour of this model. In the case where equation 4.15 was used as the effective hard sphere diameter function, Song and Mason determined α to be equal to 0.56.

Bokis and Donohue derived an expression for U_1 by refitting the first perturbation values of Morris et al. [149] (equation 4.48) with a polynomial function in $\underline{\rho}$, where $\underline{\rho}$ is defined as $\underline{\rho}=\rho\sigma^3$ and is temperature independent. The ratio U_2/U_1 was also expressed as a polynomial function in $\underline{\rho}$, with its coefficients determined by fitting equation 4.70 to Lennard-Jones molecular simulation data. The two polynomial functions are expressed in equations 4.71 and 4.72 and the values of the coefficients listed in Table 4.10.

$$U_1 = \sum_m C_{1m}\underline{\rho}^m \qquad 4.71$$

$$U_2 = \alpha\left(1 + \sum_m C_{2m}\underline{\rho}^m\right) \qquad 4.72$$

Table 4.10 Bokis and Donohue internal energy perturbation term coefficients

m	1	2	3	4	5	6
C_{1m}	-5.56	-0.49105	-2.073125	2.15	-0.04	-0.02917
C_{2m}	-1.99395	2.48585	-1.19714	0.06432	-0.05808	

The perturbation contribution to the overall fluid equation of state can be determined from the perturbation internal energy contribution through the normal thermodynamic relations:

$$\left(\frac{PV}{NkT}\right)^{pert} = \underline{\rho}\frac{\partial\left(A^{pert}/NkT\right)}{\partial\underline{\rho}} = \underline{\rho}\frac{\partial}{\partial\underline{\rho}}\left(\int_0^{1/T^*}\frac{U^{pert}}{N\varepsilon}d\frac{1}{T^*}\right) \qquad 4.73$$

By substituting equation 4.70 into this expression, the equation of state will contain terms that are exponential functions in density. Determining the density or volume roots of this equation will require an iterative approach, resulting in the repetitive evaluation of computationally expensive exponential functions and would therefore not be ideal for a practical equation of state.

4.3.5.c Local composition approximation

Sandler [184] derived the Van der Waals partition function, as discussed in section 2.4.2.a, in a slightly different way, through the use of a coordination number N_c. This approach applied to a square-well fluid leads to a unique approximation of the perturbation term through the use of local composition models.

The configurational integral, Z_{config}, of the generalised Van der Waals partition function can be expressed as follows (equation 2.122) :

$$Z_{config} = {V_f}^N\left[\exp-\frac{N\varphi}{2kT}\right] \qquad 4.74$$

where the mean intermolecular potential energy, φ, is defined by equation 2.123 as:

$$\varphi = \rho\int_0^\infty u^{(1)}(r_{12})g_0(r_{12})4\pi r^2 dr \qquad 4.75$$

and the average system potential energy, $\bar{U}$, of the system is defined through equation 2.37:

$$\overline{U} = kT^2\left(\frac{\partial\ln\left(Z_{config}\right)}{\partial T}\right)_{N,V} \qquad 4.76$$

Substituting equation 4.74 into 7.76, leads to the following expression:

$$\overline{U} = kT^2\left[\frac{N}{V_f}\frac{\partial V_f}{\partial T} - \frac{N}{2k}\frac{\partial \varphi}{\partial T}\right] \qquad 4.77$$

By assuming that V_f is independent of temperature, a valid assumption for a square-well fluid, the mean intermolecular potential energy can be expressed purely a function of the average system potential energy:

$$\varphi = -\frac{2k}{N}\int_{\infty}^{T}\frac{\overline{U}}{kT^2}dT \qquad 4.78$$

And by substituting equation 2.41 for $\bar{U}$:

$$\varphi = -\rho kT\int_{\infty}^{T}\frac{1}{kT^2}\left(\int_0^{\infty}u(r)g(r)4\pi r^2 dr\right)dT \qquad 4.79$$

For a square-well fluid the internal integral only needs to be evaluated over the well-width where the potential energy is equal to a constant value $u(r) = -\varepsilon$. Equation 4.79 can now be expressed as:

$$\varphi = \rho T\varepsilon\int_{\infty}^{T}\frac{1}{T^2}\left(\int_0^{\lambda\sigma}g(r)4\pi r^2 dr\right)dT \qquad 4.80$$

By defining the coordination number, N_c, as the average number of molecules that can be found in the interaction well about a central molecule:

$$N_c = \rho\int_{\sigma}^{\lambda\sigma}g(r)4\pi r^2 dr \qquad 4.81$$

the mean intermolecular potential energy of a square well fluid can be written as:

$$\varphi = \varepsilon T\int_{\infty}^{T}\frac{N_c(\rho,T)}{T^2}dT \qquad 4.82$$

The problem of expressing the first perturbation approximation of the equation of state has therefore been reduced to finding a suitable model to describe the density and temperature dependence of the coordination number.

From statistical mechanics [92] it can be shown that the radial distribution function for an ideal gas is equal to:

$$\lim_{\rho \to 0} g(r) = e^{-u(r)/kT} \qquad 4.83$$

This leads to the following low-density coordination number limit:

$$N_c = \frac{4\pi}{3}\rho\sigma^3\left(\lambda^3 - 1\right)e^{\varepsilon/kT} \qquad 4.84$$

At the other end of the density range, the closest packed limit, $\eta_{cp}=2^{1/2}\pi/6$, N_c should be equal to the Z_m, the maximum coordination number at all temperatures. For a face centred crystal of a square well fluid with λ=1.5 the maximum coordination number Z_m=18, and for λ= 1.85, Z_m = 42 [126]. It is clear that equation 4.84 does not approach these values, and when Lee et al. [126] investigated the use to the low-density limit over the entire density range and found that it was only accurate up to reduced density ($\underline{\rho}=\sigma^3\rho$) values of $\underline{\rho}$ = 0.1.

Using the local composition lattice theory to gain insight into the liquid phase behaviour, Lee et al. modelled the fluid as a lattice containing two components, the square-well particles (1) and holes (2). The distribution of these two components can be described through the local composition model:

$$\frac{N_{21}}{N_{11}} = \frac{N_2}{N_1}\frac{\sigma_{21}^3\int_1^\lambda g^{21}(x)4\pi dx}{\sigma_{11}^3\int_1^\lambda g^{11}(x)4\pi dx} \qquad 4.85$$

Where N_{ji} represents the number of particles j in the coordination sphere (interaction well) about a central particle i, N_i the total number of species i and ε_{ij} the well-depth of an i-j interaction. In the lattice theory the maximum coordination number, Z_m, is equal to the total number of lattice sites about the central particle:

$$Z_m = N_{ji} + N_{ii} \qquad 4.86$$

A function, ψ, can now be defined as:

$$\psi = \frac{\sigma_{21}^3 \int_1^{\lambda} g^{21}(x) 4\pi dx}{\sigma_{11}^3 \int_1^{\lambda} g^{11}(x) 4\pi dx} \qquad 4.87$$

In a system of particles and holes it is evident that the coordination number N_c is equal to N_{11}, the number of square well particles within the attractive well of a central particle, and can be determined through equations 4.86 and 4.87 to be:

$$N_c = \frac{Z_m}{1 + \frac{N_2}{N_1}\psi} \qquad 4.88$$

Lee et al. [126] related the number of holes in the lattice to the closest packed free volume:

$$N_2 = N_1\left(\frac{V}{V_0} - 1\right) = N_1\left(\frac{1-\xi}{\xi}\right) \qquad 4.89$$

where V_0 represents the closest packed volume, $V_0 = N\sigma^3/2^{1/2}$, and $\xi = V_0/V$. And proposed the following coordination number model:

$$N_c = \frac{Z_m \xi Y}{1 + \xi(Y-1)} \qquad 4.90$$

with

$$Y = \exp\left[\frac{\varepsilon}{2kT}\right] - 1 \qquad 4.91$$

Equation 4.91 can be derived from equation 4.88 by substituting equation 4.89 and by assuming that:

$$\psi = \exp\left[\frac{\varepsilon_{21} - \varepsilon_{11}}{2kT}\right] = \exp\left[\frac{-\varepsilon}{2kT}\right] \qquad 4.92$$

Substituting this coordination number expression (equation 4.90) into equations 4.82 and 4.74 leads to the following first order Helmholtz free energy and compressibility approximations, (*LLS* model):

$$\frac{A^{pert}}{NkT} = -Z_m \ln(1+\xi Y) \qquad 4.93$$

$$z_{pert} = -Z_m \frac{\xi Y}{(1+\xi Y)} \qquad 4.94$$

All of the required model parameters are related to the physical component properties through the well-depth, ε, the well-width, λ, and the hard sphere diameter σ as the coordination number Z_m, as already stated, is a function of the square-well fluid well-width parameter. The *LLS* model satisfies the high-density coordination number limit as $\rho \to \rho_{cp}$, or $V \to V_0$, $N_c \to Z_m$, however in the low-density limit $N_c \propto \exp(\varepsilon/2kT)$ instead of $N_c \propto \exp(\varepsilon/kT)$ [126].

Because *LLS* model provides a successful but very simple approximation of the perturbation contribution, it has been applied in a variety of equations of state [74, 78, 111]. Lee et al. [126] used the coordination number model along with a Carnahan Starling hard sphere equation of state, and found that a maximum coordination number $Z_m = 33.4$ used together with argon and methane square well parameters (σ and ε), determined from second virial coefficient data, produced an accurate representation of the real fluid *VLE* and *P-v-T* data. Kim et al. [111] used the *LLS* approximation in the perturbed hard chain theory (section 5.2.2.b) and concluded that the Z_m parameter does not have a significant effect on the thermodynamic properties as represented by their equation of state, but rather influences the values of the adjustable parameters of their model. They used $Z_m = 36$ as it resulted in realistic parameter values for the molecular size, shape and energy parameters of methane.

Lee et al. [128] also suggested the use of a slightly different coordination number model, that would adhere to both the low and high density limits. The new equation uses a different expression for Y (equation 4.91) :

$$Y = \exp\left[\frac{\varepsilon}{\alpha kT}\right] - 1 \qquad 4.95$$

where

$$\alpha = \frac{\rho_{cp}}{\rho_{cp} - \rho} \qquad 4.96$$

Where ρ_{cp} is the density in the closest packed limit ($\sigma^3/2^{1/2}$). Although using equation 4.95 in equations 4.93 and 4.94 ensures the correct limiting behaviour of the *LLS* model, it introduces a problematic density dependent exponential term in the perturbation compressibility expression. (See the discussion on the Bokis and Donohue approximation in section 4.3.5.b.)

It has been suggested that the *LLS* approximation be improved by introducing an empirical temperature dependence to the approximation. Gasem and Robinson tentatively suggested the use of a temperature dependent maximum coordination number, Z_m, and closest packed volume, V_0 [78]. (Whilst a temperature dependent Z_m may still be plausible, any attempts to attach temperature dependence to V_0 would imply the use of a temperature dependent hard sphere effective diameter, and would make the assumption, in equation 4.77, that V_f is independent of temperature incorrect, destroying the whole premise on which this perturbation approximation is based.)

In other approaches Shaver et al. [193] proposed the use of an empirical correction in the form of a polynomial function in $1/T^*$, or ε/kT, in the exponential term instead of the $\varepsilon/2kT$ term, whilst Vimalchand et al. [223] suggested the use of a density dependent parameter, ζ, instead of the closest-packed reduced density, ξ, in equation 4.89, to account for the effect of the changes in the fluid structure due to the hard sphere repulsive forces. They fitted ζ as a fifth order polynomial in η, to the results obtained form the Percus-Yevic solution for a square well fluid.

4.3.5.d Van der Waals perturbation approximation

The Van der Waals first perturbation approximation has already been discussed in detail in section 2.4.2.a. It has been shown that the attractive contributions of the well known cubic equations of state can be seen as empirical approximations of the integral function, equation 4.48, with the Van der Waals attractive term being the simplest instance where the integral is treated as a constant value.

This highly idealised Van der Waals attractive term has been applied in some studies where the investigation of the repulsive and/or non-spherical terms is of primary importance and a simple attractive term is required. Although in most cases it has been recognised that performance of these models could be improved by using a more realistic approximation [87, 113].

Most of the more complex temperature and density dependent variations were developed as empirical corrections to the overall equation of state behaviour when applied specifically with the Van der Waals hard sphere repulsive term. There is therefore no guarantee that an empirical form that resulted in a successful equation of state when applied with the Van der Waals hard sphere term would still be appropriate when applied with a more realistic hard sphere model. However, regardless of this uncertainty, many equations of state have been suggested where the incorrect Van der Waals term had merely been replaced by a more accurate expression, whilst keeping the form of the attractive term unchanged [34, 131].

Because of the empirical nature of the mathematical structure of the perturbation approximations and the uncertainty in the applicability of these relations to hard sphere approximations other than that of Van der Waals, these approximations will not be investigated in this study.

4.4 DEVELOPMENT OF NEW PERTURBATION MODEL

4.4.1 Perturbation approximation modelling approach and evaluation criteria

As is clear, from the overview of the various perturbation approximation methods in the literature, that there are a wide variety of approaches that can be followed to represent the attractive interactions in an equation of state. A suitable method needs to be found that is able to satisfy the main requirements of the proposed model: a mathematically simple form that is able to provide accurate results for non-polar systems over a wide temperature and pressure range including the in the higher pressure regions in the near critical and supercritical phases.

In deciding upon a suitable perturbation approximation various issues need to be addressed, and these will be discussed in this section:

4.4.1.a Choice of the perturbation approximation model

Of the two perturbation approaches discussed in this work, the *CWA* approach and the *BH* method, it is clear that the main difference between these two models lie in the division of the intermolecular potential into an unperturbed and perturbation contribution. The principal consequence of choice of the unperturbed or reference state is the rate at which the perturbation expansion converges, with the CWA approach converging rapidly and requiring

only the first perturbation term whilst the *BH* approximation converges more slowly and generally requires higher order perturbation terms to provide satisfactory results.

On a practical level however there is very little to be gained from using the *CWA* approach to model a real system, as the functions used to represent the first perturbation are polynomial functions in reduced temperature, T^*, and are from a mathematical perspective identical to some of the functions used to represent the higher order *BH* perturbation expansions. (Compare equations 4.51 and 4.52 or 4.54 with equations 4.44 and 4.45).

A further argument against the *CWA* approach is the use of a density dependent effective hard sphere diameter, d_{CWA}, which will significantly complicate the determination of the volume roots of the equation.

Therefore, because of the additional complexity involved in the *CWA* approach without any real explicit mathematical benefit, the Barker and Henderson perturbation approximation with a density independent effective hard sphere diameter will be used in this study.

4.4.1.b Intermolecular potential model

The next important choice is that of the type of theoretical intermolecular potential model to be used to model the real fluid interactions. The choice of theoretical model will affect the nature of the temperature dependence of the effective hard sphere diameter.

Nezbeda [153] noted that the use of simple approximations of the intermolecular potentials (such as square well potential) in the first order perturbation approximation might in fact result in a more complicated and incorrect required density dependence of the perturbation integral. This finding will be investigated by comparing the density dependence of the required perturbation contribution as determined for the square well model, the simplified Chen and Kreglewski two-step potential model and the more realistic Lennard-Jones intermolecular potential.

The Chen and Kreglewski hard sphere diameter is given by equation 4.14, and will be used with the parameters as reported in the original article [42]. (h=3, C=0.12).

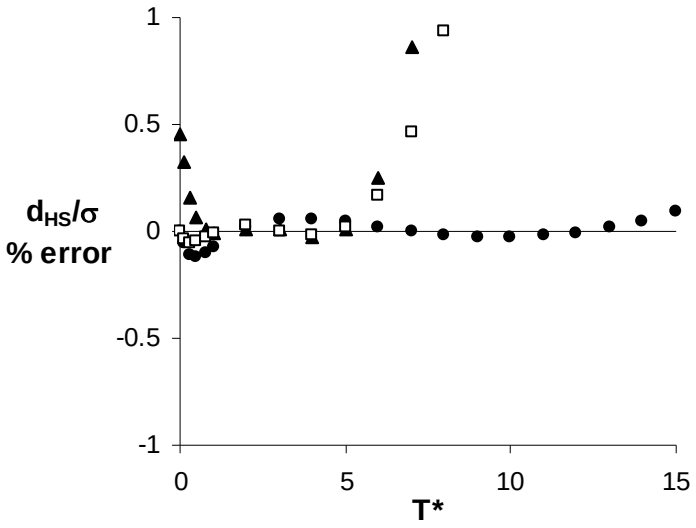

Figure 4.3 % Error in the evaluation of equation 4.1 for a Lennard-Jones potential model.
● Cotterman, ▲ Gil-Villegas and □ De Souza approximations

The Cotterman approximation (section 4.2.2.b) will be used to represent the Lennard Jones effective hard sphere diameter. As can be seen from Figure 4.3, the Cotterman equation is accurate over a much wider temperature range, and although it is slightly less accurate than the De Souza approximation in the lower temperature region, it is a mathematically a lot less complicated. (Compare equations 4.15 and 4.16.)

4.4.1.c Temperature dependence of the London attractive energies

According to Rowlinson the London attractive energy (section 2.2.6) includes a non-central temperature dependent part [120, 179]. The London energy may therefore be written as:

$$u^{L}(r,T) = u^{L0}\left(1 + \frac{\mu}{kT}\right) \qquad 4.97$$

μ represents the non-central contribution to the London dispersion forces in a non-polar system and may also the dipole-dipole or mulitpole interaction contributions in systems where these forces are present. [121].

As stated in section 4.3.5.a Chen and Kreglewski used equation 4.56 to incorporate the temperature dependence of London forces into their two-step square well approximation, which effectively increases the well-depth of the potential model (Figure 4.1).

Due to the structure of the Lennard-Jones potential model the incorporation of the non-central London forces for a non-polar fluid is more complex as the repulsive contribution remains temperature independent [120]:

$$u(r) = 4\varepsilon\left(\left(\frac{\sigma}{r}\right)^{12} - \left(\frac{\sigma}{r}\right)^{6}\left(1 + \frac{\mu}{kT}\right)\right) \qquad 4.98$$

Incorporating this temperature dependence will therefore not only affect the attractive well-depth, but also the slopes of the attractive and repulsive energies and the value of the collision diameter σ, where these energies cancel out (Figure 4.4). The temperature dependent collision diameter, σ, will consequently affect the effective Lennard-Jones hard-sphere diameter, d_{BH}, as equation 4.1 is evaluated between $r = 0$ and $r = \sigma$, and a unique numerical solution for each μ value has to be determined.

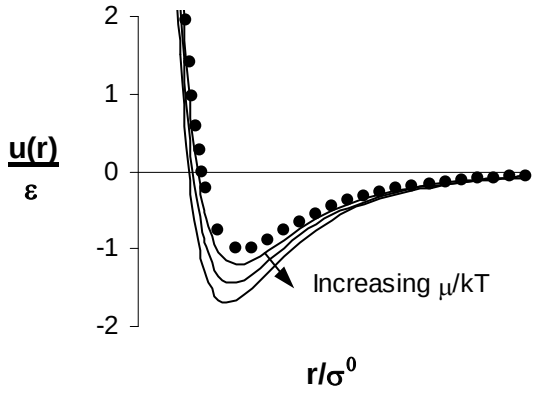

Figure 4.4 Effect of incorporating the temperature dependent non-central London energies (σ^0 is the temperature independent collision diameter)
● Original Lennard-Jones fluid, —— Equation 4.96 (μ/kT = 0.1, 0.2 and 0.3)

As this work is mostly focussed on non-polar, spherical systems, either in the form of spherical molecules, mono-atomic particles or chains of spherical segments, the non-central London energies are expected to be quite small. Chen and Kreglewski proposed μ/k values of 0 for argon, 1 for methane and 3 for N_2 in their equation of state [42], whilst in many applications for the *SAFT* equation of state μ/k = 10 is recommended for chain segments [5, 100]. A value of μ/k = 10 is equivalent to a change of 3.7%-2% in the square well depth in the temperature range 272K-500K.

Therefore, because the expected effect of the non-central London forces is relatively small, and the incorporation of equation 4.98 into the perturbation theory relatively complex, the

Lennard-Jones model will be treated as temperature independent. The effect of neglecting the non-central London forces will be investigated through the use of the Chen and Kreglewski two-step model.

4.4.1.d Mathematical representation of the Perturbation expansion

From the discussion in section 4.3 it is clear that there is a wide variety of possible approaches to represent the perturbation approximations. Two of these approaches will be investigated in this work, the first the representation of the perturbation terms through a double summation in reduced density and temperature, and the second the local composition approximation.

- ***The polynomial expansion of the perturbation term.***

Upon inspection of the mathematical structure of the various perturbation approximation approaches discussed in sections 4.3.4 and 4.3.5.a it is clear that the majority of the approximations can be represented by the same mathematical expression

$$\frac{A^{Pert}}{NkT} = \sum_n \sum_m D_{nm} \left(\frac{\eta}{\tau}\right)^m \left(\frac{1}{T*}\right)^n \qquad 4.99$$

$$z_{pert} = \sum_n \sum_m m D_{nm} \left(\frac{\eta}{\tau}\right)^m \left(\frac{1}{T*}\right)^n \qquad 4.100$$

each varying only in the values of the parameters *n* and *m*. It will be the aim of this study to determine the minimum values of these parameters, i.e. the lowest order density polynomial and perturbation expansion, required to provide a satisfactory representation of the systems of interest.

As discussed previously, the theoretical potential models used in this study, the two step Chen and Kreglewski model and the Lennard-Jones potential are not able to accurately capture the real fluid effective pair interactions. By fitting equation 4.99 to real fluid systems, the uncertainties in the intermolecular interactions can be, in part, accounted for.

Chen and Kreglewski [42] fitted their D_{nm} parameters to argon thermodynamic data as a representative non-polar, spherical system, whilst Donohue and Prausnitz [60] used methane as a basis for their fit. Although in this study we are primarily concerned with the modelling of hydrocarbon systems, argon will still be used as real fluid model system. There are several factors on which this choice is based.

Firstly, although the homologous alkane series is of primary concern the resulting equation of state will also be required to model other fluid systems. By using methane as reference fluid, because of its already more complex hydrocarbon structure and intramolecular interactions, the perturbation expansion might be unduly biased towards hydrocarbons systems, and hence result in unrealistic molecular parameters, σ and ε/k, for other fluids systems. Argon atoms also have the advantage that they do not exhibit any non-central London forces, hence the perturbation parameters will not be subjected to any uncertainty regarding the treatment thereof.

- ***The local composition perturbation approximation***

The local composition approximation of Lee et al. [126] (*LLS* approximation) is included in this study, largely because of its success in representing real fluid systems despite very simple mathematical structure and overall density dependence of the perturbation compressibility contribution.

The *LLS* approximation is however at a disadvantage to the other perturbation approximation models, in that on a strictly theoretical basis the molecular diameter must be treated as temperature independent. The *LLS* approximation is inherently an approximation of the perturbation expansion of a square well fluid, and the particle softness cannot be taken into account. (See section 4.3.5.c for the assumptions made during the derivation of the approximation.)

Some of the issues that will be addressed regarding the *LLS* approximation are: the determination of an appropriate maximum coordination number, Z_m, and the effects of the first perturbation approximation at low system densities and the incorrect low density limit of the coordination number approximation (equation 4.90).

- ***Accurate 2nd virial coefficient representation***

Some perturbation approximation methods, such as those discussed in section 4.3.5.b, place a considerable amount of stress on the accurate representation of the second virial coefficient. Determining the second virial coefficient contribution from a perturbation approximation such as equation 4.99, is very simple as equation 4.101 illustrates:

$$\frac{B^{pert}}{v^0} = \sum_n D_{n1}\left(\frac{1}{T^*}\right)^n \qquad 4.101$$

The structure of equation 4.101 will however be problematic when the equation of state is extended to mixtures, as it will require n unique mixing rules to satisfy the statistical mechanical second virial coefficient mixing rule (See 6.1.1.a):

$$B^{mix} = \sum_i \sum_j x_i x_j B_{ij} \qquad 4.102$$

One possible solution to the problem is by requiring that n=1 for m =1. This of course will have a detrimental effect on the ability of equations 4.98 and 4.101 to represent the pure component perturbation expansion and second virial coefficients respectively.

The impact of a reduced accuracy in the pure component representation versus a correct or simple mixing rule will be investigated in this chapter and in Chapter 6.

4.4.2 Data and Fitting procedure

Two types of parameters need to be determined in this section, the global perturbation term parameters, the D_{nm} parameters for the double summation approximation and Z_m in the *LLS* approach, and two component specific equation of state parameters related to the intermolecular potential model, the component hard sphere diameter,σ , or equivalently the specific temperature independent hard sphere volume, v_{00}, and the maximum attractive well-depth ε/k. (All the relevant pure component and D_{nm} parameters are reported in Appendix A)

As in discussed section 4.4.1.d, argon is used as the model non-polar, spherical particle to which the various perturbation term parameters are fitted. The general applicability of this perturbation approximation is then tested by applying it to model methane thermodynamic data and only fitting the two equation of state parameters.

Three other molecules were also used in this investigation. Nitrogen *VLE* data and methane and carbon dioxide saturated and supercritical data were used to determine the effect of the inclusion of temperature dependent energy contributions to the London attractive energies.

Table 4.11 Pure component data ranges

Component	VLE Data	Supercritical PVT Data		Source
	T [K]	P [1e5 Pa]	T [K]	
Argon	100 – 148	50 – 975	160 – 700	[11, 130]
Methane	96 – 189	65 – 495	210 – 630	[130]
Nitrogen	80 – 120			[130]
Carbon Dioxide	218 – 289	102 – 489	330 – 600	[130]

The various parameters are fitted to literature saturated and supercritical phase data. In many studies only the saturated fluid properties are considered when fitting pure component parameters, however in this study, where the ultimate aim is to develop an equation of state for application at higher system pressures, above the critical pressures of components such as methane and ethane. The accurate representation of the supercritical phase will facilitate the description of the mixture properties at these elevated (near critical) pressures, as it addresses one possible source of uncertainty, the accurate pure component behaviour, and leaves only the uncertainty in the mixing rules that need to be addressed.

Reducing the error in two different thermodynamic properties, the saturated pressure and fluid volume, simultaneously ensures that realistic parameter values are obtained and that the equation of state is not merely being forced into an unrealistic form in order to represent a specific property accurately. The actual fitting techniques used are discussed in section 8.3, and the temperature and pressure ranges over which the equation of state parameters were fitted for the various components are listed in Table 4.11.

A further safeguard against unrealistic parameters is the calculation of the pure component enthalpy as represented by the equation of state. Because this information is not included in the fitting of the equation parameters, a reasonable representation of these enthalpy values would indicate a realistic model. As the energy properties (enthalpy and internal energy) are determined through the first order temperature derivative of the equation of state, they also provide an indication as to the correctness of the temperature dependence of the model, both

directly, through the perturbation term, and indirectly through the use of an effective hard sphere diameter in the hard sphere and perturbation contributions. It should however be noted that the primary aim of this work is to develop a model that is able to provide accurate and rapid phase equilibrium information and not the optimisation of the predicted energetic properties, small inaccuracies in the energy values can there be tolerated but they must however display the correct trends.

Besides the representation of the *P-v-T* and energetic properties, the performance of the equation of state performance will be judged according to the representation of the pure component second virial coefficient data. The relevant pure component second virial coefficients are taken from the compilation by Dymond and Smith [64]. The accurate representation of second virial coefficients can be seen as an indication of the correct low pressure behaviour of the model. In certain instances the second virial coefficient data were used in the fitting of the actual model parameters, whilst in other cases it was used as a measure to compare different equations.

4.4.3 Perturbation term development

4.4.3.a Equations of State

The hard sphere equation of state, equation *HS3*, as developed in Chapter 3, is used in conjunction with the various perturbation approximations to form a complete equation of state for spherical non-polar systems. The *EOS* that are investigated in this chapter are listed in Table 4.12.

Table 4.12 Equations of state used in the perturbation term development

Name	$z_{Hard\ sphere}$	$z_{pert.}$	d_{BH}/σ	Potential Model
HS3CK	Equation 3.49	Equation 4.100	Equation 4.14	Two step
HS3LJ	Equation 3.49	Equation 4.101	Equation 4.15	Lennard Jones
HS3LLS	Equation 3.49	Equation 4.94	1	Square Well
HS3SW	Equation 3.49	Equation 4.100	1	Square Well

The *HS3SW* equation is included not as a proposed real fluid equation of state, but rather to facilitate the comparison between the various types of potential models for the sake of completeness.

4.4.3.b *Double summation perturbation approximation*

- ***Parameter determination***

Initially the *HS3CK* and *HS3LJ* equations will be used with a 4x6 double summation in equation 4.99 with $n = 4$ and $m = 6$, which translates into the modelling of the first four perturbation terms with polynomial functions that are 6^{th} order in density. The matrix size was chosen based on the excellent results that can be obtained by using the Chen and Kreglewski fourth order perturbation expansion, whilst still limiting the expansion to a manageable size of 24 perturbation parameters that have determined. The 4x6 perturbation parameter matrix along with the two component specific equation of state parameters translates into a total of 26 parameters that have tot bee fitted to argon *P-v-T* data.

In order to ensure the accurate second virial coefficient representation, and to facilitate the fitting of the perturbation matrix parameters by incorporating a real limit to the parameter values, the *HS3CK* and *HS3LJ* equations were first fitted to the argon second virial coefficient data [64]. The parameters determined through this fit (v_{00}, ε/k and D_{11}, D_{21}, D_{31} and D_{41}) are then kept constant whilst the remainder of the D_{nm} parameters are fitted to the argon saturated and supercritical data. (A similar approach was followed by Chen and Kreglewski in the determination of the parameters for the *BACK* equation of state [42].)

The argon determined D_{nm} parameters are then treated as global parameters, and the equations of state are extended to other fluids by only fitting the v_{00} and ε/k parameters to the relevant pure component *P-v-T* data.

A similar procedure was followed when determining the perturbation matrix parameters for other matrix configurations (other n and m values).

- ***Investigation into the effect of the potential model***

The theoretical square well and Lennard-Jones potential models have been extensively studied through computer simulation [9, 106, 156, 194]. The reduced critical properties determined for these models have been determined and are listed in Table 4.13. The theoretical v_{00} and ε/k values of argon can therefore be determined from the component critical pressure and density

.

Table 4.13 Theoretical fluid critical properties

	Square Well Fluid (λ=1.5) [3] [9]			Lennard Jones Fluid		
	N=32	**N=108**	**N=500**	**Nicolas et al. [156]**	**Smit [194]**	**Johnson et al. [106]**
$\rho_c.v_0$	0.215	0.227	0.235	0.18	0.159	0.162
$T_c/(\varepsilon/k)$	1.308	1.29	1.26	0.741	0.760	0.762

It has been noted [42, 120] that the experimentally determined mean potential well depths of small molecules and atoms, such as argon, are very close to their critical temperatures. For a square well or two-step potential fluid this means that $\varepsilon/k \approx T_c$ (or $T_c.\varepsilon/k \approx 1$) and λ is component specific. In this study a ε/k = 150.86 K is therefore used for argon in the *HS3CK* equation of state. Enforcing this value on the Lennard-Jones fluid is in essence incorrect given the set relation between the fluid critical temperature and the maximum well depth (Table 4.13), however a more realistic intermolecular potential may lead to a more successful real fluid equation of state. The ε/k value that would result in the *mean* Lennard-Jones interaction potential of argon equal to 150.86 K is $\varepsilon/k \approx$ 1040 K which is very far removed form the theoretical value (see Table 4.15), and hence the effect of setting *maximum* Lennard-Jones interaction potential to 150.86 K instead is also investigated. (Throughout this work *HS3LJ-LJ* will refer to the *HS3LJ* equation, using the parameters determined with from an unconstrained argon well depth, *HS3LJ-Mean* the parameters determined by setting ε/k = 1039.5 K for argon, and *HS3LJ-Real* using the parameters determined by using a more realistic value of $\varepsilon/k = T_c$ for argon.)

Table 4.14 contains the pure component parameters determined for argon and methane for the *HS3CK* and *HS3SW* equations of state. The argon parameters were determined as discussed above, by fitting the argon virial coefficient data and setting ε/k=150.86 K (argon T_c) and the methane parameters, by fitting the methane *P-v-T* data using the argon determined perturbation parameters. The *BACK* parameters are determined in a similar way by Chen and Kreglewski [42] for their two-step potential model. Lee et al. [126] determined the *LLS* parameters for a square well fluid with λ=1.85 by fitting virial coefficient data. The Alder parameters on the other hand are determined from square well critical properties listed in Table 4.13.

[3] N refers to the number of particles used in the simulations

Table 4.14 Pure component EOS parameters for square-well and two-step potential models

Square-Well and Two-step Potential models				
	Argon		Methane	
	v_{00} [1e6 m^3/mol]	ε/k [K]	v_{00} [1e6 m^3/mol]	ε/k [K]
HS3CK	15.70	150.86	20.80	190.57
HS3SW	10.94	150.86	—	—
BACK [42]	16.29	150.86	21.57	190.29
LLS λ=1.85 [126]	13.46	69.40	16.74	88.80
Alder N=32 λ=1.85 [9]	16.04	115.34	21.20	145.72
Alder N=108 λ=1.85 [9]	16.95	116.95	22.41	147.75
Alder N=500 λ=1.85 [9]	17.55	119.73	23.20	151.27

By specifying the argon ε/k to be 150.86 K and essentially assigning an unknown value to λ, the direct comparison between the *HS3CK* and *HS3SW* parameters and the theoretical parameters determined at $\lambda = 1.5$ and $\lambda = 1.85$ is not possible. It is however encouraging to see that the v_{00} parameters are all of the same order of magnitude. The *HS3CK* and the *BACK* equations, which use similar potential models but with different perturbation parameters and hard sphere equations, have very similar v_{00} and ε/k parameters. It is also encouraging to see that the fitted methane ε/k value is very close to the critical temperature of methane (T_c = 190.6 K). This is in agreement with the experimental observations for small molecules [42, 121].

Table 4.15 Pure component EOS parameters for Lennard-Jones potential models

Lennard-Jones Potential models				
	Argon		Methane	
	v_{00} [1e6 m^3/mol]	ε/k [K]	v_{00} [1e6 m^3/mol]	ε/k [K]
HS3LJ-LJ	15.65	112.58	20.85	142.95
HS3LJ-Mean	11.87	1039.5	—	—
HS3LJ-Real	14.94	150.86	20.09	191.02
Nicolas et al. [156]	13.67	111.75	18.07	141.19
Smit [194]	11.87	114.64	15.69	144.83
Johnson et al. [106]	12.10	114.90	16.00	145.16

The v_{00} and ε/k parameters determined for the Lennard-Jones potential models are listed in Table 4.15. It should be noted that the *HS3LJ-Real* ε/k for methane, which is again determined

by the unconstrained fitting of the *P-v-T* data, is now also closer to the methane critical temperature. It is also clear whilst the v_{00} parameters determined for the *HS3LJ-LJ* equation of state are slightly larger than the theoretical values (determined from Table 4.14), the ε/k values are fall with the theoretical Lennard-Jones values. This is an indication that the Lennard-Jones potential model is well suited to represent the real fluid data of these small component real fluid systems, and can be fitted to represent the real fluid behaviour without the distortion of its parameters.

As observed in section 4.4.1.b the use of an inappropriate potential model may result in the unnecessary and incorrect complex density dependence of the perturbation contribution. The required perturbation compressibility contribution that will result in a perfect fit of the experimental data can easily be determined by subtracting the hard sphere compressibility, determined from the known fluid volume, temperature and pressure and the *EOS* parameters listed in Table 4.14 and Table 4.15, from the total compressibility value determined at the known fluid conditions:

$$z_{pert} = z_{total} - z_{HS}(\eta) = \frac{Pv}{RT} - z_{HS}\left(\frac{\tau v_0}{v}\right) \qquad 4.103$$

The effect of the potential model is brought into equation through the temperature dependent specific hard sphere closest packed volume, $v_0 = d_{BH}^3/2^{1/2} = v_{00}(d_{BH}/\sigma)^3$. The density dependence of the compressibility term is used as a measure of the required density dependence of the perturbation Helmholtz energy contribution through equation 4.104, as it can be determined without the perturbation term having to be already specified in the equation of state.

$$z_{pert} = \eta \frac{\partial}{\partial \eta}\left(\frac{A_{pert}}{NkT}\right) \qquad 4.104$$

In the specific case of a double summation perturbation approximation, the density dependence of z_{pert} is of the same order in density as the A_{pert} approximation (equations 4.99 and 4.100), this will however not always be the case for all perturbation approximations, but in general a simple z_{pert} density dependence would still indicate a relatively simple A_{pert} relation.

Figure 4.5 is a plot of the required z_{pert} values for argon against the reduced system density η, at temperatures above the critical temperature. At these conditions the perturbation

contribution is expected to be relatively simple, as the molecules are far removed from each other and the intermolecular interaction is small. This is confirmed by the various near linear z_{pert} plots for the various potential models, indicating that $\partial A_{pert}/\partial\eta \approx$ constant. The *HS3SW* and the *HS3LJ-Mean* equations can however be seen to deviate from the simple linear behaviour, especially at the lower near-critical temperatures.

Upon investigating required z_{pert} at higher system densities, in Figure 4.6, it is clear that the compressibility can no longer be treated as a simple linear function in density. This effect is most pronounced at T = 100K (the highest liquid density). It is apparent that the perturbation contribution of the *HS3CK* equation has the lowest density dependence, with z_{pert} deviating from a linear η dependence only at the highest densities, whilst the *HS3SW* and *HS3LJ-Mean* equations again, displaying the greatest deviation form a simple linear dependence.

It is apparent that by neglecting the softness of the argon atoms molecules in the *HS3SW* model the density dependence of the required perturbation contribution is increased, and is in agreement with the observation by Nezbeda [153]. Furthermore by distorting the Lennard-Jones potential model to provide the correct mean energy value for argon the overall required complexity of the perturbation term is raised. No detrimental effect at either the low or high density conditions can however be observed as a result of using a more realistic $\varepsilon/k = T_c$ for argon in the Lennard-Jones potential model as opposed to the more theoretically correct value. (See Figure 4.5 and Figure 4.6 (b) and (c))

The *HS3CK*, *HS3LJ-LJ* and *HS3LJ-Real* models appear to be the most promising in the development of a simple perturbation approximation, and will be investigated further in the upcoming sections.

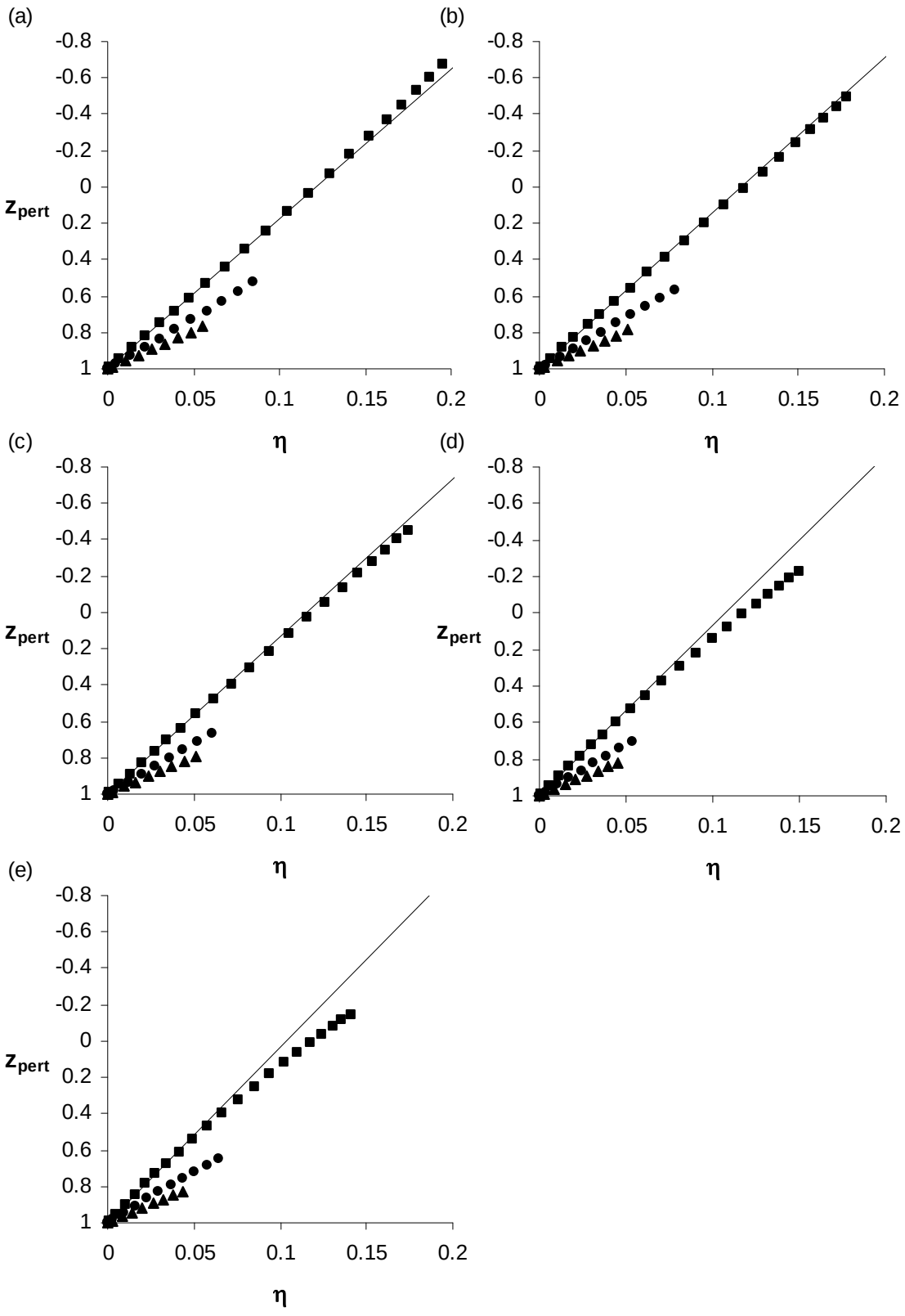

Figure 4.5 Required perturbation compressibility as determined for (a) *HS3CK* (b) *HS3LJ-LJ* (c) *HS3LJ-Real* (d) *HS3LJ-Mean* and (e) *HS3SW* equations for argon at $T > T_c$. ■ T = 200 K, ● T = 300 K, ▲ T = 400 K. —— Linear extrapolation of low-density z_{pert} values at T = 200K.

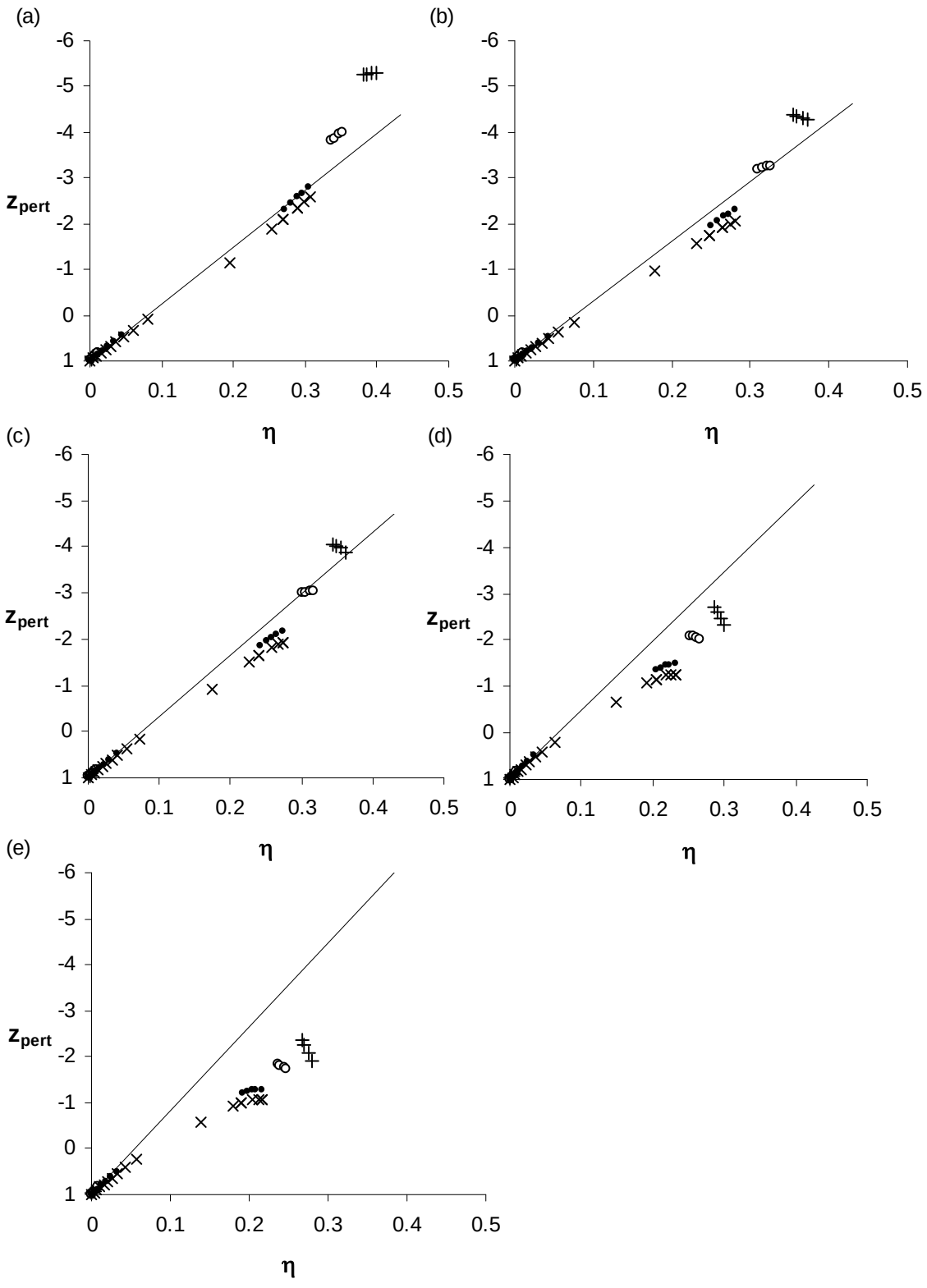

Figure 4.6 Required perturbation compressibility as determined for (a) *HS3CK* (b) *HS3LJ-LJ* (c) *HS3LJ-Real* (d) *HS3LJ-Mean* and (e) *HS3SW* equations for argon at $T < T_c$. + T = 100K, ○ T = 120 K, • T = 140 K, × T = 150 K, —— Linear extrapolation of vapour phase z_{pert} values at T = 140K.

- ***Investigation into the effect of the inclusion of the non-central London interactions***

As discussed in section 4.4.1.c, the square well and two-step potential models lend them selves to the easy incorporation of the temperature dependent non-central London energies. The effect of the inclusion of these energies will now be investigated.

Two sets of *HS3CK* parameters were fitted to methane, nitrogen and carbon dioxide saturated and supercritical data whilst using the same global perturbation parameters fitted to the argon *P-v-T* data. The first set of parameters were determined by neglecting the non-central forces and the second set by using the μ/k values as determined by Chen and Kreglewski [42]. The optimal values in saturated pressure and fluid volumes errors that were obtained by fitting the pure component data are listed in Table 4.16.

Table 4.16 Comparison of %AAD in saturated pressure, liquid and vapour volumes and super critical fluid volumes obtained with and without the non-central London energies.

			Average Absolute % Deviation			
		μ/k [K]	**$P_{sat.}$**	**$v_{liq\ sat.}$**	**$v_{vap\ sat.}$**	**$v_{super\ crit.}$**
Methane	**HS3CK**	1	0.54	1.68	2.69	0.46
	HS3CK	0	1.00	2.09	3.41	0.72
	HS3LJ-LJ	—	1.10	0.49	2.90	0.32
N_2	**HS3CK**	3	0.22	1.31	0.86	0
	HS3CK	0	2.03	1.77	3.07	0
	HS3LJ-LJ	—	2.22	0.53	3.13	0
CO_2	**HS3CK**	40	2.76	2.28	4.38	4.25
	HS3CK	0	8.73	4.76	11.26	11.41
	HS3LJ-LJ	—	8.88	4.46	11.40	11.00

It is clear that even for methane, where μ/k is very small, the inclusion of the non-central London energies greatly improves the overall performance of the *HS3CK* equation of state. The results of the *HS3LJ* equation, which neglects the non-central energies, are similar to those obtained by the *HS3CK* with $\mu/k = 0$, indicating the need for the inclusion of the non-central energies even with the Lennard-Jones potential model.

The modelling of carbon dioxide with the *HS3CK* and *HS3LJ* equations, is an extreme test for the proposed equations of state, as these equations approximate CO_2 as spherical molecule and

are not able to account for the quadrupolar interactions present in the fluid system in anyway other than through the μ/k parameter. From the results in Table 4.16 it is obvious that by introducing the temperature dependent interaction energies through the μ/k parameter, CO_2 can be modelled much more accurately. It can therefore be said that by including the temperature dependent London energies the flexibility of the proposed equation of state can be improved, enabling, to a certain degree, interaction energies other than purely non-polar London energies to be taken into account without significantly chancing the mathematical structure of the equation of state.

- ***Direct comparison of proposed perturbation approximation models***

The average absolute percentage deviation in the various thermodynamic properties of argon and methane are listed in Table 4.17 and Table 4.19.

Table 4.17 Average absolute percentage deviation in the predicted values of argon.

		Average Absolute % Deviation							
		$P_{sat.}$	$v_{liq\ sat.}$	$v_{vap\ sat.}$	$v_{super\ crit.}$	$H_{liq\ sat.}$	$H_{vap\ sat.}$	$H_{super\ crit.}$	Σ
Argon	**HS3LJ-LJ**	0.25	0.13	0.30	0.54	4.24	3.36	5.10	13.92
	HS3LJ-Real	0.20	0.20	0.12	0.71	4.04	2.84	2.40	10.51
	HS3CK	0.34	0.58	0.41	0.36	1.11	1.79	1.15	5.74

The large enthalpy errors in the methane liquid phase can be attributed to the poor representation of the methane saturated properties at high system densities. Figure 4.7 (b) is a plot of the errors in the methane saturated liquid volume as a function of density in which the poor performance of the equations of state at low densities is immediately obvious. This behaviour indicates that the sixth order density polynomial of the perturbation term may not be suitable to represent the required density dependence of the perturbation contribution at these conditions. A similar trend, although not as pronounced, can be seen for argon at temperatures below 110K. (Figure 4.7(a)) Fortunately the optimal performance of the models in the lower temperature regions is not important in non-cryogenic applications, and is therefore not of consequence in this work. The average absolute percentage deviations tabulated in Table 4.18 and Table 4.20 are determined by ignoring the lower temperature regions for both the argon and methane systems.

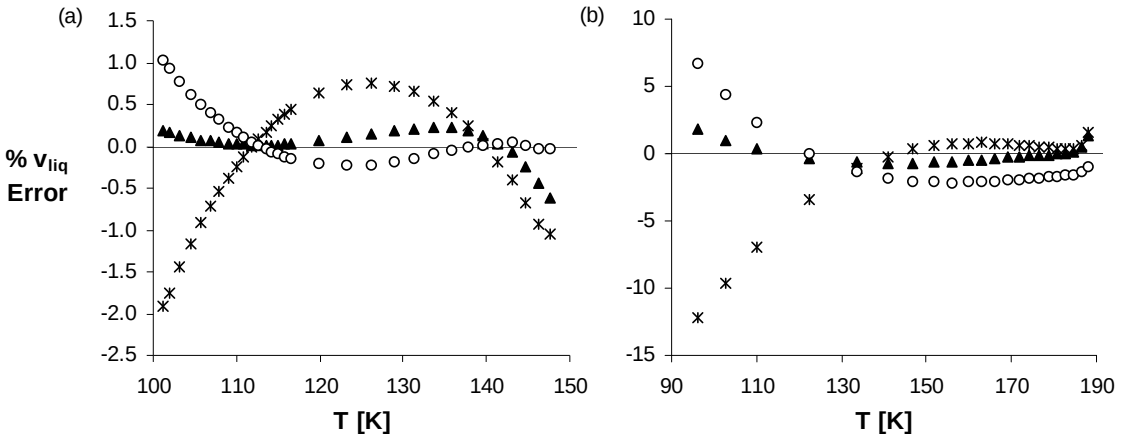

Figure 4.7 Percentage error in the saturated liquid volume for (a) argon and (b) methane, determined with ▲ *HS3LJ-LJ*, ○ *HS3LJ-Real* and ✳*HS3CK* (μ/k = 1 for methane).

Table 4.18 Average absolute percentage deviation in the saturated argon properties evaluated at T>110K

		Average Absolute % Deviation							
		$P_{sat.}$	$v_{liq\ sat.}$	$v_{vap\ sat.}$	$v_{super\ crit.}$	$H_{liq\ sat.}$	$H_{vap\ sat.}$	$H_{super\ crit.}$	Σ
Argon	**HS3LJ-LJ**	0.32	0.14	0.38	0.54	4.75	4.46	0.32	10.91
	HS3LJ-Real	0.26	0.09	0.15	0.71	4.58	3.76	0.26	9.81
	HS3CK	0.44	0.45	0.49	0.36	1.30	2.40	0.44	5.88

From the results of the Lennard-Jones based equations of state, *HS2LJ-LJ* and *HS3LJ-Real*, it appears as if the use of a more realistic although theoretically incorrect Lennard-Jones maximum well depth leads to an improvement in the representation of the saturated vapour pressure and volumes, and a lower general or total error in all thermodynamic values evaluated. However, when only considering the accuracies in the vapour pressure and fluid volumes, there is very little to choose between the various proposed models. The *HS3CK* equation is slightly less accurate than the Lennard-Jones type equations in its representation of argon saturated *P-v-T* data, but more accurate in the supercritical phase. These differences between the models become even less pronounced when applied to the methane system. Fortunately when the accuracy in the enthalpy representation is included in the evaluation, it becomes clear that the *HS3CK* has much more realistic temperature functionality than the Lennard-Jones models. (This is apparent even when the temperature dependent London energies do not play a role in the case of argon or where they are neglected in the methane system.)

Table 4.19 Average absolute percentage deviation in the predicted values of methane.

		Average Absolute % Deviation							
		$P_{sat.}$	$v_{liq\ sat.}$	$v_{vap\ sat.}$	$v_{super\ crit.}$	$H_{liq\ sat.}$	$H_{vap\ sat.}$	$H_{super\ crit.}$	Σ
Methane	**HS3LJ-LJ**	1.10	0.49	2.90	0.32	38.14	1.72	0.37	45.04
	HS3LJ-Real	0.78	1.92	1.47	0.51	20.43	1.28	0.42	26.81
	HS3CK (μ/k = 0)	1.00	2.09	3.41	0.72	22.62	1.29	0.15	31.28
	HS3CK (μ/k = 1K)	0.54	1.68	2.69	0.46	15.81	1.14	0.10	22.42

Table 4.20 Average absolute percentage deviation in the methane evaluated at T>130K

		Average Absolute % Deviation							
		$P_{sat.}$	$v_{liq\ sat.}$	$v_{vap\ sat.}$	$v_{super\ crit.}$	$H_{liq\ sat.}$	$H_{vap\ sat.}$	$H_{super\ crit.}$	Σ
Methane	**HS3LJ-LJ**	0.34	0.46	2.54	0.29	5.85	2.05	0.35	11.88
	HS3LJ-Real	0.34	1.76	1.13	0.46	7.16	1.52	0.39	12.76
	HS3CK (μ/k = 0)	0.26	1.23	3.21	0.68	0.56	1.53	0.14	7.61
	HS3CK (μ/k = 1K)	0.16	0.67	2.75	0.43	0.90	1.36	0.09	6.36

The ability of the *HS3CK* to represent the methane dataset so successfully is highly significant as the methane pressure and volume data were only fitted by modifying the two equation of state parameters (v_{00} and ε/k) whilst the enthalpy data were not included in the optimisation procedure at all. This indicates that the *HS3CK* perturbation term is not merely a polynomial that is forced to fit the argon data, but that the perturbation parameters are transferable to other systems and that the double summation approximation is successful in capturing the true perturbation contribution of a small spherical non-polar fluid.

- ***Simplification of Double summation approximation***

The 4x6 perturbation term parameter matrix although successful in representing the perturbation contribution in a real fluid system, is not conducive to rapid computer calculations, especially with the sixth order density polynomial, which will be especially problematic in the determination of the equation of state volume roots. The next step in the development of the perturbation term is therefore to investigate the effect of the simplification of the double summation matrix on the ability of the equations of state to represent the fluid thermodynamic behaviour.

Four different matrix configurations are investigated, a 4x2, 4x3, 3x3 and a 2x3 matrix. (The first integer indicates the order of the perturbation expansion, the *n* parameter, and the second, the order of the density polynomial used to model each perturbation term, the *m* term.) The procedure used to fit the required parameters has already been discussed in earlier in the section Because of the known inability of the equations to model the high density methane thermodynamic behaviour, the data points at temperatures below 130K were excluded from the fitting of the methane parameters. The results for argon and methane are listed in Table 4.21and Table 4.22.

Table 4.21 Argon average percentage deviation obtained as a result of the simplification of the double summation matrix of the perturbation approximation.

Argon Average Absolute Percentage Deviation

Matrix	Model	$P_{sat.}$	$v_{liq\ sat.}$	$v_{vap\ sat.}$	$v_{super\ crit.}$	$H_{liq\ sat.}$	$H_{vap\ sat.}$	$H_{super\ crit.}$	∑
4x2	**HS3LJ-LJ**	1.20	17.43	2.31	1.62	12.02	4.58	7.92	47.08
	HS3LJ -Real	1.20	16.06	2.40	0.94	11.69	4.86	8.05	45.2
	HS3CK	1.51	20.84	2.92	1.63	8.76	3.27	28.05	66.98
4x3	**HS3LJ -LJ**	0.37	2.47	1.00	1.67	6.85	4.26	28.05	44.67
	HS3LJ -Real	0.26	2.65	0.85	1.34	6.71	4.71	33.46	49.98
	HS3CK	0.46	1.99	1.01	1.14	3.19	2.79	17.40	27.98
3x3	**HS3LJ -LJ**	0.37	2.40	1.27	1.99	6.65	3.70	30.18	46.56
	HS3LJ -Real	0.50	3.33	1.35	2.57	7.11	3.34	35.82	54.02
	HS3CK	0.38	2.43	1.33	1.46	3.27	2.58	22.06	33.51
2x3	**HS3LJ -LJ**	0.33	5.63	0.43	2.36	8.59	2.60	29.78	49.72
	HS3LJ-Real	0.44	4.52	0.49	2.93	8.32	2.28	34.53	53.51
	HS3CK	0.77	4.68	0.68	2.89	4.78	0.60	32.94	47.34

It is apparent from the results that the density dependence of the 4x2 approximation is too low, resulting in large errors in the liquid volume of argon. These errors are large over the entire temperature range, and not specifically at the high system densities (See Figure 4.8.) By increasing the density order in the matrix to 3 the performance of all the equations is greatly improved, except for the large increase in the errors in the argon supercritical enthalpy values. It appears therefore that a polynomial of a third order in density (m=3) is the lowest perturbation term density dependence that will result in the suitable representation of a simple fluid system.

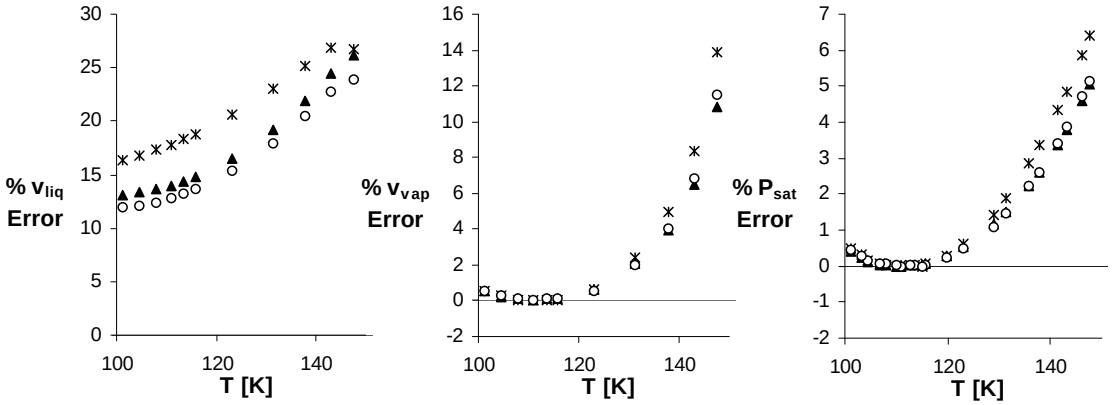

Figure 4.8 Plot of the percentage errors in the argon fluid properties for the 4x2 perturbation approximation matrix ▲ *HS3LJ-LJ,* ○ *HS3LJ-Real* and ✳*HS3CK*

Furthermore, it was also found that the fourth perturbation term could be neglected without significantly affecting the overall ability of the models to represent the real fluid thermodynamic behaviour. However using only two perturbation terms resulted in a increase in the errors in the liquid and more seriously the supercritical fluid volumes. The perturbation expansion clearly does not converge fast enough in the supercritical phase to allow the truncation after the second term, and as this region is of particular interest in this work the third perturbation term will be retained in this study. Fortunately a higher order in the perturbation expansion does not have such a serious effect on the overall complexity of the equation of state as what a higher density dependence would have, because, in practical calculations, the finding of the volume roots is much more prevalent and time consuming than the actual calculation of the fluid properties at a specific temperature.

From the results of this investigation a 3x3 double summation perturbation approximation used in the *HS3CK* equation of state seems to provide an ideal compromise between model simplicity, flexibility and performance.

Table 4.22 Methane average percentage deviation obtained as a result of the simplification of the double summation matrix of the perturbation approximation. (T > 130 K and μ/k=1 in *HS2CK*)

Methane Average Absolute Percentage Deviation

Matrix	Model	$P_{sat.}$	$v_{liq\ sat.}$	$v_{vap\ sat.}$	$v_{super\ crit.}$	$H_{liq\ sat.}$	$H_{vap\ sat.}$	$H_{super\ crit.}$	∑
4x2	**HS3LJ-LJ**	2.40	2.79	6.45	1.88	6.34	3.71	0.75	24.32
	HS3LJ -Real	2.44	3.03	6.42	2.46	6.96	3.62	0.73	25.66
	HS3CK	2.61	3.38	7.13	3.02	4.20	3.20	0.89	24.43
4x3	**HS3LJ -LJ**	1.13	2.92	2.94	1.18	7.68	2.35	0.63	18.83
	HS3LJ -Real	1.18	3.00	3.12	0.84	7.59	2.40	0.65	18.78
	HS3CK	1.12	2.25	2.92	1.22	3.00	1.55	0.69	12.75
3x3	**HS3LJ -LJ**	0.74	2.83	3.00	0.95	7.25	2.21	0.62	17.6
	HS3LJ -Real	0.49	3.16	3.34	1.62	6.75	2.24	0.87	18.47
	HS3CK	0.70	2.85	2.90	0.74	2.57	1.63	0.45	11.84
2x3	**HS3LJ -LJ**	1.04	4.67	2.74	1.49	8.42	2.06	0.61	21.03
	HS3LJ-Real	0.67	4.22	2.24	1.64	7.94	1.91	0.72	19.34
	HS3CK	0.29	4.39	1.91	1.64	2.67	1.17	0.84	12.91

4.4.3.c The local composition approximation

- ***Parameter determination***

In this section the local composition perturbation approximation is investigated as an alternative to the double summation approach. This approximation leads to a very simple expression for the overall equation of state and requires only three parameters, one perturbation parameter, the maximum coordination number, Z_m, and two component specific equation of state or potential model parameters, the temperature independent specific closest packed volume, v_{00}, and the square well depth parameter, ε/k.

Because of the small number of parameters that need to be determined, all the parameters are fitted directly to the argon saturated pressure and fluid volume data without first fitting some parameters to second virial coefficient data. (See the parameter fitting procedure in section 4.4.3.b) In fact, by first fitting the argon second virial coefficient data, the equation of state parameters would be over specified, as all the parameters can be determined directly form the virial coefficient data without taking any other thermodynamic properties into consideration.

As the accurate *P-v-T* representation was deemed mode important the parameters were fitted to this data.

Four different parameter sets were determined by using Z_m=18, the theoretical value for a square well fluid with λ=1.5, Z_m = 33.4, the optimal value found in the original article on the coordination number approximation by Lee et al. [126], Z_m=36 the value proposed by Kim et al. [111], and lastly fitting Z_m along with the other parameters to the argon data and using this value as a global parameter for other systems. The fitted parameters are listed in Table 4.23. (To facilitate the unbiased comparison to the simplified double summation perturbation approximation evaluated in the previous section, the *HS3LLS* equations were fitted to the same high temperature methane dataset (T>130K)).

Table 4.23 Local composition approximation parameters, as fitted to argon and methane data.

Equation		Argon		Methane	
	Z_m	v_{00} [1e5 mol/m^3]	ε/k [K]	v_{00} [1e5 mol/m^3]	ε/k [K]
HS3LLS	15.7	13.036	138.73	16.986	176.43
HS3LLS	18	13.225	122.79	17.258	155.99
HS3LLS	33.4	13.931	69.43	18.182	87.89
HS3LLS	36	13.982	64.71	18.265	81.86
Lee et al. [126]	33.4	12.800	67.37	16.924	85.12
Kim et al. [111]	36			19.408	81.46

The equations by Lee et al. [126] and Kim et al. [111] use the Carnahan and Starling hard sphere equation [32], whilst the *HS3LLS* equations use the *HS3* equation derived in Chapter 3. The parameters fitted in this work are however very similar to those used in the published equations. With a decrease in the model maximum coordination number, the optimum fitted closest packed volume was found to decrease whilst the well depth parameter increased. This trend is similar to that observed by Kim et al. [111] for ethane, octane and eicosane.

- ***Investigation into the effect of the inclusion of the non-central London interactions***

Although the local composition approximation is strictly only applicable to a hard sphere model, and the temperature dependence of the hard sphere diameter of closest packed volume cannot be accommodated, it is still theoretically possible to extend the square well potential model to include the temperature dependent non-central London energies.

The same procedure as used in section 4.4.3.b to investigate the effect of the inclusion of these energies on the performance of the *HS3CK* equation, using equation 4.95 and the μ/k parameters as determined by Chen and Kreglewski [42] to correct the square well depth. The results obtained for the *HS3LLS* equation of state with a coordination number of Z_m=36, are listed in Table 4.24. Similar results were obtained with the other coordination number equation of state parameter sets.

Table 4.24 Comparison of %AAD in saturated pressure, liquid and vapour volumes and super critical fluid volumes obtained with and without the non-central London energies for *HS3LLS* with (Z_m=36).

		Average Absolute % Deviation			
	μ/k [K]	**$P_{sat.}$**	**$v_{liq\ sat.}$**	**$v_{vap\ sat.}$**	**$v_{super\ crit.}$**
Methane	1	3.34	3.99	7.17	1.40
	0	3.67	3.92	7.52	1.28
N_2	3	1.73	3.46	2.80	
	0	2.98	3.12	4.82	
CO_2	40	4.47	1.82	6.92	3.66
	0	9.90	1.51	13.66	10.95

The inclusion of the non-central London energies in the *HS3LLS* equation when applied to methane, even by treating μ/k as an equation of state parameter and fitting it to the methane data, did not result in a similar overall improvement in the model performance as was observed with the *HS3CK* equation. On the other hand including these energies when modelling the nitrogen and carbon dioxide systems enabled the *HS3LLS* equation to represent these systems much more accurately.

By including the non-central energies, the flexibility of the *HS3LLS* equation of state seems to be improved, allowing it to more successfully accommodate deviations from the ideal spherical non-polar fluid particles for which this model has originally been derived. Care should however be taken when applying this correction, as in cases where the non-central energy contribution is small, including it in the equation of state may in fact have a detrimental effect on the model performance, as in the case of methane observed here.

- ***Comparison between the simplified HS3CK and HS3LLS equations***

The average absolute percentage deviations of the argon and methane thermodynamic properties as represented by the 3x3 simplified *HS3CK* and the various *HS3LLS* equations are listed in Table 4.25 and Table 4.26.

Table 4.25 Average absolute percentage deviation in the predicted values of argon.

Argon Average Absolute Percentage Deviation								
Model	$P_{sat.}$	$v_{liq\ sat.}$	$v_{vap\ sat.}$	$v_{super\ crit.}$	$H_{liq\ sat.}$	$H_{vap\ sat.}$	$H_{super\ crit.}$	$\sum$
HS3CK (3x3)	0.38	2.43	1.33	1.46	3.27	2.58	22.06	33.51
HS3LLS (Z_m=15.7)	1.12	4.54	2.25	2.08	6.55	5.40	16.31	38.25
HS3LLS (Z_m=18)	1.21	4.34	2.50	2.10	6.15	6.23	15.91	38.44
HS3LLS (Z_m=33.4)	1.83	3.66	4.03	2.32	4.79	8.97	14.43	40.03
HS3LLS (Z_m=36)	1.93	3.61	4.21	2.33	4.66	9.21	14.38	40.33

From the average errors it is clear that the variation of the Z_m value does not significantly affect the accuracy of the *HS3LLS* equation of state. This is in agreement with the observation made by Kim et al. [111] that the actual value of the maximum coordination number has little effect on the thermodynamic properties of a the equation of state, but rather influences the values of the required equation of state parameters (v_{00} and ε/k).

Table 4.26 Average absolute percentage deviation in the predicted values of methane. (T > 130 K)

Methane Average Absolute Percentage Deviation								
Model	$P_{sat.}$	$v_{liq\ sat.}$	$v_{vap\ sat.}$	$v_{super\ crit.}$	$H_{liq\ sat.}$	$H_{vap\ sat.}$	$H_{super\ crit.}$	$\sum$
HS3CK (3x3)	0.70	2.85	2.90	0.74	2.57	1.63	0.45	11.84
HS3LLS (Z_m=15.7)	1.99	3.41	5.46	0.95	4.90	3.17	0.44	20.32
HS3LLS (Z_m=18)	2.36	3.21	6.02	1.00	4.84	3.47	0.45	21.35
HS3LLS (Z_m=33.4)	3.38	2.67	8.14	1.22	5.76	4.46	0.58	26.21
HS3LLS (Z_m=36)	3.52	2.64	8.29	1.25	6.00	4.53	0.60	26.83

Overall the *HS3CK* equation performs significantly better than the *HS3LLS* models in the representation of the pure component thermodynamic data, especially in the modelling of the saturated pressures and vapour volumes. Although the local composition perturbation approximation has been applied to great success as a very simple expression for the perturbation contribution, the model may not be flexible enough to represent all the phase regions simultaneously to a similar degree of accuracy as the 3x3 simplified *HS3CK* equation. Furthermore the comparatively high errors in the vapour volumes (especially for the methane system) could be an effect of the incorrect low density limit of the coordination number model (see section 4.3.5.c) or indicate that the first order perturbation approximation of the *HS3LLS* is insufficient in the low density regions. (Because these two inaccuracies in the model will affect the equation of state performance in the same density region, it is impossible to

determine the primary cause of the errors in the predicted values from the information available.)

Figure 4.9 is a plot of the argon and methane second virial coefficients as represented by the *HS3LLS* equation with Z_m = 15.7. Although the virial coefficient data were not included in the fit of the parameters, the *HS3LLS* equation is still able to represent the second virial coefficient values accurately and only deviating from the reported values at very low temperatures.

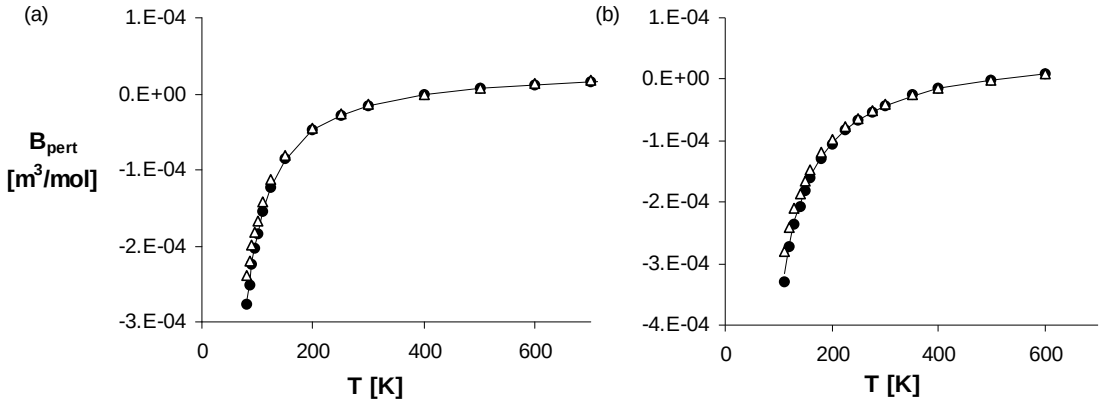

Figure 4.9 (a) Argon and (b) methane second virial coefficients. ● Literature data [64] and —— 3x3 *HS3CK* ▵ *HS3LLS* (Z_m = 15.7) representation.

4.4.3.d Double summation approximation conducive to the correct second virial coefficient mixing rule

From the investigations in the previous two sections it appears as if the *HS3CK* equation with a 3x3 perturbation approximation provides a suitable compromise between model flexibility and simplicity. However as discussed in section 4.4.1.d the mathematical structure of the double summation approximation is not conducive to simple mixing rules if the theoretically correct second virial coefficient mixing rules are to be satisfied.

As suggested in section 4.4.1.d, one possible solution to this problem is to set D_{n1}=0 for all values of n>1. This would necessarily result in less accurate pure component second virial coefficient values, but would only require one simple mixing rule to ensure the correct composition dependence of a fluid mixture at lower densities.

Table 4.27 Regressed EOS parameters of Argon and Methane for the HS3CK-ltd EOS

HS3CK-ltd pure component parameters			
	v_{00} [1e6 m^3/mol]	ε/k [K]	μ/k [K]
Argon	17.346	23	0
Methane	150.86	190	1

The perturbation approximation parameters are again determined using the same approach as before, by fitting the v_{00}, ε/k and D_{11} parameters to the argon virial coefficient data, and the remainder of the perturbation term parameters to the argon saturated and supercritical pressure and volume data. However because limiting the first perturbation term to a linear dependence in density will decrease the flexibility of the approximation, and the lower temperature, high density methane data has been found difficult to model, the low temperature methane data ($T <$ 130K) were again excluded from the fitting procedure. The regressed pure component parameters are listed in Table 4.27 and the results obtained in Table 4.28.

Table 4.28 Average absolute percentage deviation in the predicted values of argon (T>110K) and methane (T>130K).

		Average Absolute % Deviation							
		$P_{sat.}$	$v_{liq\ sat.}$	$v_{vap\ sat.}$	$v_{super\ crit.}$	$H_{liq\ sat.}$	$H_{vap\ sat.}$	$H_{super\ crit.}$	Σ
Argon	**HS3CK 3x3 full**	0.28	3.01	1.54	1.46	2.91	3.45	22.06	34.71
	HS3CK 3x3 ltd.	1.06	1.00	1.49	1.54	4.29	7.30	10.77	27.45
Methane	**HS3CK 3x3 full**	0.70	2.85	2.90	0.74	2.57	1.63	0.45	11.84
	HS3CK 3x3 ltd.	1.42	1.10	3.27	0.87	4.83	3.08	0.75	15.32

The respective errors in the saturated pressure, liquid and vapour volumes and the supercritical volumes for methane are plotted in Figure 4.10. It can be seen that the constrained HS3CK equation is in fact more successful than the unconstrained model in the representation of the saturated liquid volumes, even in the high density regions (below 130 K) where the model parameters have not been explicitly fitted on. Furthermore, whilst constrained equation is on average less accurate than the unconstrained version in the supercritical phase, it displays in fact a smaller range of errors in the temperature range $200<T<325$.

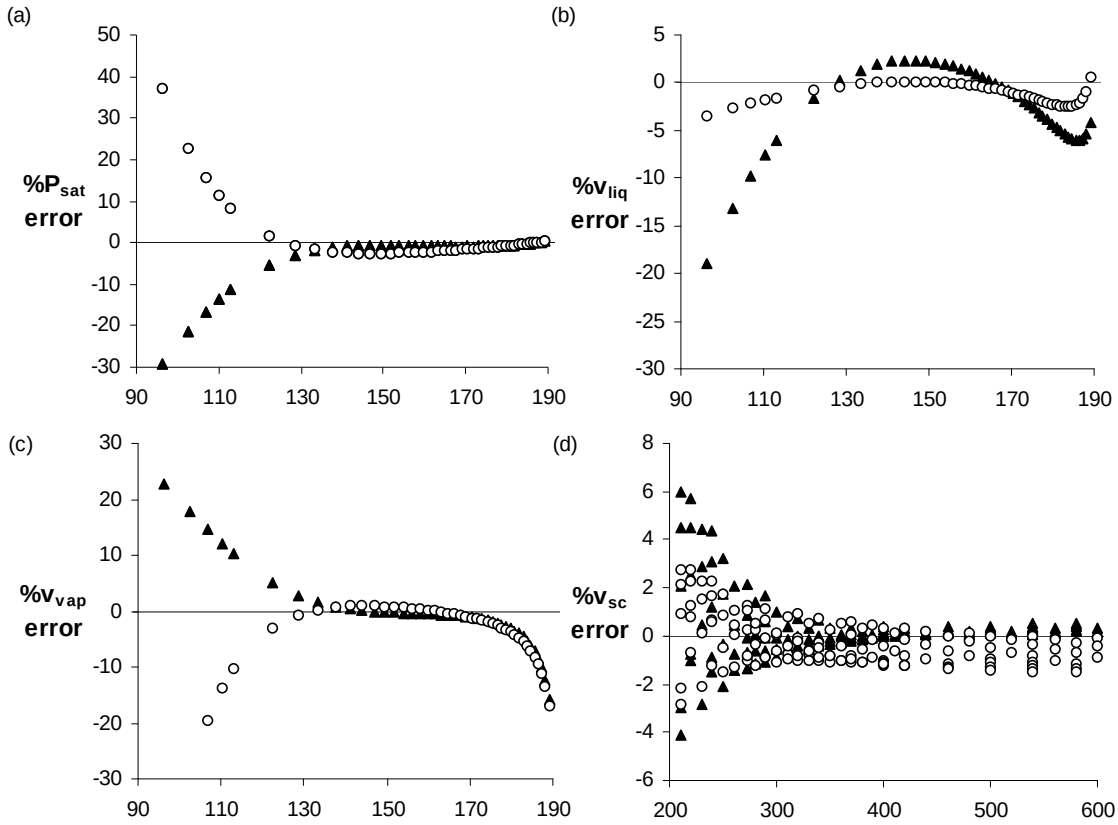

Figure 4.10 % Error plots in (a) saturated pressure error, (b) saturated liquid volume, (c) saturated vapour volume and (d) supercritical fluid volume for the methane system as determined by the ▲ unconstrained and ○ constrained 3x3 *HS3CK* equations.

The empirical modification of the double summation approximation of course also has a detrimental effect on the accuracy of the pure component virial coefficients. Figure 4.11 (a) and (b) are plots of the second virial coefficients of argon and methane respectively as represented by the two 3x3 *HS3CK* equations of state.

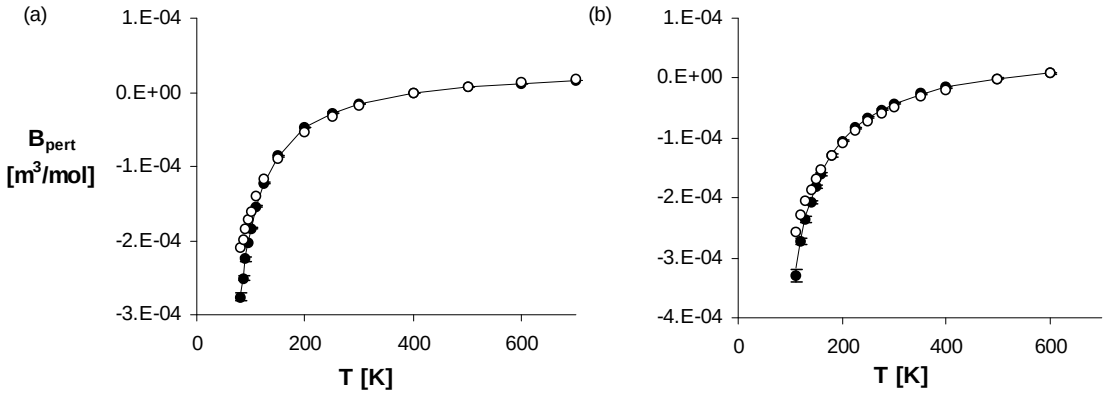

Figure 4.11 (a) Argon and (b) methane second virial coefficients. ● Literature data [64] and —— unconstrained 3x3 *HS3CK* ○ constrained 3x3 *HS3CK* representation.

It can be seen that by using only the first perturbation approximation to represent the virial coefficient data the equation becomes less accurate in the low temperature region, but that at high temperatures the model still performs satisfactorily. The accuracy in the methane virial coefficients is especially encouraging, as the methane virial coefficient data were not used in determining the equation of state parameters.

The full effect of the slight loss in the accuracy of the limited model versus the advantage of simple and theoretically correct mixing rules will be investigated further in later chapters.

4.5 SUMMARY AND CONCLUSIONS

In this chapter several possible perturbation approximations were investigated with the aim of finding a simple expression able to represent the attractive contributions in a real fluid system consisting of small spherical nonpolar molecules or atoms.

The Barker and Henderson perturbation approximation was found to be more suited to the development of a simple equation of state than the Chandler Weeks and Anderson approach, as it requires the use of a temperature dependent, but density independent effective hard sphere diameter.

During the investigation into the effect that the choice of the theoretical intermolecular potential model has on the required perturbation term, it was found that the incorporation of the softness of the atoms or molecules is important to ensure a simple perturbation term density dependence. Furthermore by deforming the Lennard-Jones potential model to ensure the correct mean interaction energy, the required complexity of the equation is actually increased.

Two possible methods to represent the perturbation approximation, the double summation and the local composition approaches were studied. The double summation approach was chosen, because the majority of the most successful methods in the literature use a similar mathematical structure, and the local composition approximation because of its very simple mathematical structure. The double summation approach was applied with two types of intermolecular potentials, the Chen and Kreglewski two-step potential and the Lennard-Jones model, whilst the local composition approximation is based on a square well fluid. With both of these perturbation approaches the required parameters were fitted to argon *P*-*v*-*T* data, to

indirectly compensate for the inaccuracies and simplifying assumptions in the underlying theory on which the equations are based.

It was found that the inclusion of the temperature dependent non-central London interaction energies in the fluid potential model greatly increased the flexibility of the proposed equations of state with both the double summation and the local composition approximations. The non-central energies are readily introduced into a square well and two-step potential models, but problematic in a Lennard-Jones fluid.

However it was found that even without the non-central energies, the two-step potential model double summation approximation, *HS3CK*, provides an overall better representation of the pure component thermodynamic data.

Upon the simplification of the double summation approximation a 3x3 parameter matrix was found to provide the optimal compromise between model simplicity and performance.

During the investigation into the local composition approximation the specific value of the maximum coordination number model did not significantly affect the accuracy of the representation of the fluid thermodynamic data, but rather influenced the size of the equation of state component specific parameters.

The local composition approximation is at a distinct disadvantage to the alternative approach in that it is unable to accommodate the particle softness. The model was also found to be less flexible than the double summation perturbation approximation in that it is unable to simultaneously represent the various fluid phase regions to a satisfactory degree of accuracy.

From the above mentioned results, it has been decided to use the double perturbation approximation with a 3x3 parameter matrix which in effect represents the first three perturbation terms as cubic functions in density. The Chen and Kreglewski effective hard sphere diameter will be used to incorporate the particle softness into the model, and the non-central temperature dependent contributions to the equation's energy parameter will also be taken into consideration.

Finally, a further possibility to constrain the first order perturbation term to a linear function in density in order to ensure the theoretically correct mixing rules appears to hold some promise, and will be investigated further in the upcoming chapters in this work.

Chapter 5 ***Non-Spherical Chainlike Systems***

5.1 INTRODUCTION

The primary aim of this work has, up to this point, been the development of an equation of state capable of representing spherical non-polar systems and has lead to the development of the simple hard sphere equation, *HS3*, and the 3x3 double summation two-step potential perturbation approximation. In this study it is however also of interest to be able to represent chainlike molecules, such as hydrocarbons, with geometries that differ significantly from simple spheres.

Not only will the chainlike structure of the molecules significantly influence the system free volume, but the intermolecular potential energy will also be a function of the relative molecular orientations. Furthermore, the rotational and vibrational partition functions that up to this point have been neglected, as they had no influence on the equation of state, are functions of the system density of chained particle systems and should now be taken into account.

Various approaches have been used to incorporate these features associated with the molecular structure in the various fluid models, some of these will be investigated in this chapter in order to find the ideal method to extend the proposed *HS3CK* equation of state to chained systems whilst still maintaining, as far as possible, the model simplicity.

5.2 NON-SPHERICAL APPROXIMATIONS IN EOS

The perturbation theory, according to which the short range (mostly repulsive) interactions are accounted for by a simple equation of state for the reference fluid and the weaker long range energies are treated as perturbations, is still valid for a non-spherical fluid system. The generalised Van der Waals partition function for a such a system can therefore be expressed as:

$$Q = \frac{1}{N!}\frac{1}{\Lambda^{3N}} {q_{rot}}^{N} {q_{vib}}^{N} {V_f}^{N} \left[\exp - \frac{\varphi}{2kT} \right]^{N} \qquad 5.1$$

Here the nuclear and electric partition functions have been neglected as they are still independent of the system volume and φ represents the mean intermolecular potential over the system volume.

There are a wide variety of approaches to determine expressions for q_{rot}, q_{vib}, V_f and $\exp[-\varphi/(2kT)]$ for chainlike molecules. Some of the principal methods will be reviewed it this section, however, as this is such a vast field it is a virtually impossible task to provide a complete overview of all the methods that have been reported in the literature, and the review is not claimed to be extensive.

5.2.1 Hard convex body

One approach to account for the non-sphericity of the molecular particles could be to use an equation of state with a hard convex body instead of the hard sphere as the reference fluid in the perturbation expansion. The development of the various hard convex body equations of state is closely related to the scaled particle theory (section 3.3.3) has been reviewed by Boublík and Nezbeda in [28].

One of the most generally applied hard body equations is:

$$Z_{CB} = \frac{1+(3\alpha-2)\eta+(3\alpha^2-3\alpha+1)\eta^2-\alpha^2\eta^3}{(1-\eta)^3} \qquad 5.2$$

with α a nonsphericity parameter, defined as:

$$\alpha = \frac{R_{CB}S_{CB}}{3V_{CB}} \qquad 5.3$$

where R_{CB} represents the $(1/4\pi)$ multiple of the mean curvature integral, S_{CB} the surface area and V_{CB} the volume of one molecule or convex body. For spheres α = 1, and for all other convex bodies α >1. Equation 5.2 reduces to the Carnahan-Starling hard sphere equation of state for α=1 (equation 3.20).

These hard convex body models retain the complex density dependence of the theoretical hard sphere equations of state and have the limitation that they treat the molecules as rigid [66]. Furthermore the hard convex body equations derived from the scaled particle theory and its

modifications, such as equation 5.2, have been found to generally provide a poor approximation of the phase behaviour of larger molecules with $\alpha > 2$ [225].

5.2.2 Chains of tangent spheres

A different approach to modelling the entire chained particle as a convex body is to approximate it as a series or chain of spherical particles. This approach has received much attention in the literature because of the similarity of the model to the actual geometry of hydrocarbons and polymer systems.

5.2.2.a Lattice based equations of state

In the lattice theory, the liquid behaviour is approximated as that of a pseudo solid phase in which the particles have a greater degree of freedom of movement than in the original ordered solid crystal lattice. This is in contrast to approximating the liquid as a "dense" gas in the off-lattice theories.

The Flory-Huggins model is a well known method used to represent the excess Gibbs energy in solutions of polymer systems and models the system as mixtures of flexible chain molecules in a quasi-crystalline lattice liquid [170, 185]. This model, however, does not account for the compressibility of the fluid system, and is only applicable to liquid systems.

There are however various approaches through which the concept of compressibility can be incorporated into the lattice model and thereby extending it from a solution theory to an equation of state [191].

- ***Cell models***

In the cell model, the chainlike molecule is treated as consisting out of r segments. These r segments occupy r neighbouring sites on the lattice. In a system containing N molecules there are therefore rN lattice sites available. At finite temperatures each of the segments may be displaced from the central position in the lattice site, but this segment displacement is restricted by the segments in the neighbouring sites to which the particular segment is connected (to form the chained molecule) and the background dispersion forces exerted by all the segments in the lattice. The segments are therefore effectively confined within a *cell*

volume in the lattice. The compressibility is brought into the system by allowing the cell volume to change with temperature.

The canonical partition function of a lattice cell system can be expressed as follows:

$$Q = Q_{comb}\left(\frac{V_f}{\Lambda^3}\right)^N {q_{rot}}^N {q_{vib}}^N\left[\exp-\frac{E_0}{kT}\right] \qquad 5.4$$

Where Q_{comb} is the combinatorial factor, which represents the number of ways of arranging the N particles in the lattice, and E_0 the potential energy of the system with every segment located in the central position of the lattice site. In this expression only Q_{comb} is independent of the overall system volume.

As already mentioned in section 5.1, the rotational and vibrational motions of chained systems are dependent on the system volume or density. (On other words the free motions may be restricted by the presence of other particles in the system.) The exact density dependence is however very difficult to determine for large polyatomic molecules. Prigogine proposed that the rotational and vibrational partition functions be factored into an internal part that is dependent only on the system temperature and an external part that is a function of the system volume (or density) as well:

$$q_{rot}q_{vib} = q_{int}(T)q_{ext}(V,T) \qquad 5.5$$

The q_{ext} partition function is a function of the degree of freedom of the segments making up a molecule. A completely rigid molecule will only have three degrees of freedom (for each translational coordinate), whilst at the other extreme, a completely flexible molecule with no restrictions on its bond lengths, bond angles and torsional angle has $3r$ degrees of freedom (each segment has an unrestricted translational motion). The motions of a real chain molecule will have a degree of freedom somewhere between these two extremes, $3 \leq 3c \leq 3r$. ($3c$ therefore represents the number of effective external degrees of freedom.)

Prigogine assumed that the external density and vibrational partition functions could be treated as equivalent to the translational partition function. Applying this approximation to equation 5.4 leads to the following canonical partition function:

$$Q = Q_{comb} q_{int}{}^{N} \left(\frac{V_f}{\Lambda^3} \right)^{cN} \left[\exp - \frac{E_0}{kT} \right] \qquad 5.6$$

In order to derive an equation of state from this equation, expressions need to be derived for V_f and E_0.

Commonly used forms of Prigogine's cell model for a face-centred cubic arrangement of segments around a central segment are [191]:

$$V_f = Nrv^* \gamma \left(\tilde{v}^{1/3} - 2^{-1/6} \right)^3 \qquad 5.7$$

and

$$E_0 = \frac{1}{2} N \varepsilon q Z \left[\frac{A}{\tilde{v}^4} - \frac{B}{\tilde{v}^2} \right] \qquad 5.8$$

where γ is a geometrical constant, Z the lattice coordination number, q the external surface are of the molecule and with qZ the number of unbonded nearest-neighbour segments surrounding a molecule. $\tilde{v}$ is the reduced cell volume, v_{cell}/v^*, with v^* the characteristic segment volume. The parameters A and B are determined from the Lennard Jones potential and are equal to 1.2045 and 1.011 for a face-centred cubic lattice geometry.

The equation of state for the Prigogine cell model can therefore be determined to be:

$$\frac{\tilde{P}\tilde{v}}{\tilde{T}} = \frac{\tilde{v}^{1/3}}{\tilde{v}^{1/3} - 2^{-1/6}} + \frac{2}{\tilde{v}\tilde{T}} \left(\frac{A}{\tilde{v}^3} - \frac{B}{\tilde{v}} \right) \qquad 5.9$$

with

$$\tilde{P} = \frac{P}{P^*} = \frac{Prv^*}{qz\varepsilon} \qquad 5.10$$

and

$$\tilde{T} = \frac{T}{T^*} = \frac{ckT}{qz\varepsilon} \qquad 5.11$$

Various other cell models can be derived by using different lattice geometries and expressions for V_f and E_0 [170, 191].

A major flaw of the Prigogine and many of the other cell models are that the derived equation of state does not adhere to the correct ideal gas limit $V_f \rightarrow V$ as $V \rightarrow \infty$. Equation 5.7 specifically also does not display the correct behaviour at the closest packed limit that requires that the free volume in the system be equal to zero in the closest packed configuration ($V_f = 0$).

- ***Lattice Fluid Models***

Lattice fluid models incorporate compressibility into the lattice structure, not by allowing the volume occupied per molecular segment to vary with temperature as in the case of the cell models, but rather by incorporating empty sites or voids into the lattice matrix.

The Sanchez-Lacombe model is essentially identical to the Flory-Huggins but uses using holes as one of the "components" in the fluid mixture [170, 191]. The total number of lattice sites, N_r, in a system with N r-segment molecules is therefore equal to:

$$N_r = N_0 + rN \qquad 5.12$$

Where N_0 represents the number of vacancies or empty sites in the lattice.

The closest packed volume of a molecule is equal to rv^*, where v^* is a again the characteristic segment volume, and is equal to the volume of one lattice site. The total system volume is therefore equal to:

$$V = (N_0 + rN)v^* \qquad 5.13$$

A reduced density for this model can be defined as:

$$\tilde{\rho} = \frac{1}{\tilde{v}} = \frac{v^*}{v} = \frac{rN}{N_0 + rN} \qquad 5.14$$

where v is equal to the volume per segment, $V/(rN)$, and $\tilde{v}$ is the reduced volume, v/v^*.

The canonical partition function for the lattice fluid model is as follows:

$$Q = Q_{comb} \exp\left[-\frac{E}{kT}\right] \qquad 5.15$$

with E as the lattice energy, which is assumed to be only dependent on the nearest-neighbour interactions.

The Sanchez-Lacombe model further assumes the random mixing of segments and holes. For a pure system the lattice energy can be therefore be expressed as:

$$E = -\frac{Z}{2} N_r \varepsilon \tilde{\rho}^2 \qquad 5.16$$

With ε is equal to the segment-segment interaction energy and Z the coordination number.

In contrast to the cell model, the combinatorial factor, Q_{comb}, of a lattice fluid is a function of the system volume because of the presence of voids in the matrix. For the Sanchez-Lacombe model the Q_{comb} is that of the Flory-Huggins lattice, with one of the components replaced by a vacancy:

$$Q_{comb} = (constant)^N \frac{(N_0 + rN)!}{N_0! N!} \frac{1}{(N_0 + rN)^{N(r-1)}} \qquad 5.17$$

By substituting equations 5.16 and 5.17 into equation 5.15 the Sanchez-Lacombe equation of state can be derived:

$$\frac{\tilde{P}\tilde{v}}{\tilde{T}} = \frac{1}{r} - \left[1 + \tilde{v} \ln\left(1 - \frac{1}{\tilde{v}}\right)\right] - \frac{1}{\tilde{v}\tilde{T}} \qquad 5.18$$

Where the previously undefined reduced properties are:

$$\tilde{P} = \frac{P}{P^*} = \frac{P}{(Z\varepsilon)/(2v^*)} \qquad 5.19$$

and

$$\tilde{T} = \frac{T}{T^*} = \frac{T}{(Z\varepsilon)/(2k)} \qquad 5.20$$

Besides the Sanchez-Lacombe equation various other lattice fluid models have been developed using different approximations for the lattice energy and the combinatorial terms. Some of these equations, such as the Costas and Sanctuary, the Panayiotou and Vera and the Mean-Field lattice gas, are discussed in [191].

- ***Hole models***

Hole models can be seen as a combination of the cell and lattice fluid methods [191]. In these models the system volume is a function of the volume per lattice site or cell volume, *w*, and fraction of occupied lattice sites, *y*.

$$w = \frac{V}{N_0 + rN} \tag{5.21}$$

and

$$y = \frac{rN}{N_0 + rN} \tag{5.22}$$

The canonical partition function of a hole model can be expressed as:

$$Q = Q_{comb}(N, y)\left[V_f(V, y, w)\right]^{cN}\left[\exp - \frac{E_0(V, y, w)}{kT}\right] \tag{5.23}$$

Various approaches to develop equations of state based on the hole models are discussed in [191].

5.2.2.b Off-Lattice models

Since the early 1980's there has been an increased interest in developing an equation of state for chainlike molecules that is not based on a lattice-like fluid structure [170]. Although the statistical mechanical description of a chainlike molecule is much more complex than a spherical particle system, the perturbation theory (section 2.3.3) allows relatively simple theoretically based chain reference equations to be extended to real fluid systems. The equation of state derived from the perturbation theory can be expressed as:

$$\frac{PV}{NkT} = \left(\frac{PV}{NkT}\right)_{reference} + \left(\frac{PV}{NkT}\right)_{perturbation} \tag{5.24}$$

Often with chainlike systems a hard sphere chain equation of state is used as a reference system, representing the short-range repulsive forces and accounting for the free volume and

effects of chain connectivity whilst the long-range attractive interactions are treated as perturbations on the reference system.

Some of the main off-lattice or continuous-space models are reviewed in this section.

- ***Perturbed Hard Chain Theory, PHCT***

The perturbed hard chain theory is often discussed as a variation of the Lattice-cell theory. However the actual expressions of the free volume and perturbation terms used in this model are derived for continuous phase (off-lattice) systems.

The *PHCT* was developed by Beret and Prausnitz [20] and Donohue and Prausnitz [60] using the approach of Prigogine in the Lattice-cell theory to separate the rotational and vibrational partition functions into an internal density independent and external density dependent contributions (equation 5.5) and applying it to the off-lattice canonical partition function. This approach leads to the following expression for equation 5.1:

$$Q = \frac{1}{N!}\frac{1}{\Lambda^{3N}} {q_{\text{int}}}^N {q_{ext}}^N {V_f}^N \left[\exp -\frac{\varphi}{2kT}\right]^N \qquad 5.25$$

Furthermore, still following Prigogine, they approximated the external partition functions at liquid like densities as being equivalent to translational partition functions with 3(c-1) degrees of freedom. (Note the slight difference in the definition of the c parameter in the *PHCT* and cell theory.)

The *PHCT* however incorporates additional constraints into the model, other than those imposed in the Prigogine cell theory, to ensure the correct behaviour at gaseous densities. The external partition function has to satisfy the following boundary conditions:

- In the ideal gas limit as $V \to \infty$:

$$V_f q_{ext} \to V \qquad 5.26$$

- In the closest packed limit, as $V \to V_0$, where V_0 is the closest packed volume.

$$V_f q_{ext} \to 0 \qquad 5.27$$

- For spherical or simple fluids where the density dependence of the rotational and vibrational motions are negligible, i.e. where $c \rightarrow 1$:

$$q_{ext} = 1 \qquad 5.28$$

- At liquid like densities q_{ext} must be equivalent to the translational partition function, so that:

$$\frac{V_f}{\Lambda^3} q_{ext} \rightarrow \frac{V_f}{\Lambda^3}\left(\frac{V_f}{\Lambda^3}\right)^{c-1} = \left(\frac{V_f}{\Lambda^3}\right)^{c} \qquad 5.29$$

Beret and Prausnitz [20] found that the following expression adhered to the required boundary conditions:

$$q_{ext} = \left(\frac{V_f}{V}\right)^{c-1} \qquad 5.30$$

whilst Donohue and Prausnitz [60] included the effect of the attractive interactions on the rotational and vibrational motions:

$$q_{ext} = \left(\frac{V_f}{V}\exp\left[-\frac{\phi}{2kT}\right]\right)^{c-1} \qquad 5.31$$

Substituting equation 5.31 into equation 5.25 the following canonical partition function is obtained:

$$Q = \frac{1}{N!}\frac{V^N}{\Lambda^{3N}} {q_{\text{int}}}^N {V_f}^{cN}\left[\exp -\frac{c\varphi}{2kT}\right]^N \qquad 5.32$$

(Using equation 5.30 a similar equation would be obtained, but without the c term in the mean potential energy term.)

Beret and Prausnitz [20] and Donohue and Prausnitz [60] used the Carnahan-Starling hard sphere equation to determine the free volume term, and approximated the mean intermolecular potential energy over the fluid volume with double summation perturbation approximations based on the square-well fluid approximation by Alder et al. [9] and refitted to methane *P-v-T* data [60] respectively.

Kim et al. [111] simplified the *PHCT* of Donohue and Prausnitz by replacing the double summation perturbation approximation by the local composition approximation developed by Lee et al. [126]. Shaver et al. [193] investigated slight modifications to this simplified *PHCT* by incorporating volume translation strategies and modifying the local composition approximation as discussed in section 4.3.5.c.

Wang and Guo [226] simplified the *PHCT* of Kim et al. [111] even further by replacing the Carnahan-Starling free volume term by a simpler form proposed by Lin et al. [132] (see section 3.3.9). When this simple free volume expression is applied along with the local composition approximation, resultant equation of state is cubic in volume.

Kubic [123] developed a quartic hard chain equation of state based on the *PHCT* as proposed by Beret and Prausnitz [20], by using the free volume expression of Lin et al. [132] and an empirical expression for the mean intermolecular potential, ϕ. Ciocca et al. [47] used the simplified *PHCT* of Kim et al. [111] with a density dependent *c* parameter.

Cotterman et al. [48, 49] extended the *PHCT* to better represent fluids at low and high densities by using the Cotterman perturbation term discussed in section 4.3.4.c. They also introduced the molecular softness into the equation through the use of an effective hard sphere diameter (section 4.2.2.b). (The effective temperature dependent molecular volume is then equal to the product of the temperature independent volume with the ratio d_{HS}/σ.) Morris et al. [149] developed a similar model, the perturbed soft chain theory, *PSCT,* using equation 4.17 to introduce the softness and a second order perturbation expansion to represent the attractive interactions.

- ***Chains of Rotators, COR,* approach**

Chien et al. [43] devised a method through which the partition function of the rotational motions could be determined from an equation of state describing the behaviour of a hard dumbbell instead of using the Prigogine approach and approximating it to be equal to the translational partition function.

The rotational movement of a hard dumbbell has two degrees of freedom, and the volume dependent part of the canonical partition function of hard dumbbells with no attractive potentials can be expressed has:

$$Q_{db} = {q_r}^{2N} {V_f}^{N} \tag{5.33}$$

Where q_r is the partition function *per degree of motion* and Q_{db} the *complete* translational partition function (including all three degrees of freedom). Boublík and Nezbeda [27] extended the hard convex body equation of state, equation 5.2, to describe hard dumbbells. Using equation 2.18 and integrating the dumbbell equation between the boundary conditions $V = 0$ and $V = \infty$ with $Q_{db}=V^N/N!$ at $V = \infty$ the Chien et al obtained the following expression:

$$Q_{db} = \frac{V^N}{N!}\left\{\left(\frac{\eta}{\eta-1}\right)^{\alpha^2-1} \exp\left[-\frac{\left(\alpha^2+3\alpha\right)\eta-3\alpha}{(\eta-1)^2}\right]\right\}^N \tag{5.34}$$

The nonsphericity parameter, α, for the hard dumbbells is defined as a function of L, the ratio between l, the centre to centre distance between the two spheres, and σ the diameter of the spheres that form the dumbbell:

$$L = \frac{l}{\sigma} \tag{5.35}$$

$$\alpha = \frac{(L+1)(L+2)}{2+3L-L^3} \tag{5.36}$$

Using the Carnahan-Starling hard sphere equation to determine the free volume term:

$$V_f = \frac{V^N}{N!}\exp\left[-\frac{N(4\eta-3)}{(\eta-1)^2}\right] \tag{5.37}$$

a function describing q_r can be derived, by substituting equations 5.37 and 5.34 into equation 5.33:

$$q_r = \left(\frac{\eta}{\eta-1}\right)^{\left(\alpha^2-1\right)/2} \exp\left[-\frac{\left(\alpha^2+3\alpha-4\right)\eta-3(\alpha-1)}{2(\eta-1)^2}\right] \tag{5.38}$$

Equation 5.1, the canonical partition function for a real fluid can now be expressed as:

$$Q = \frac{1}{N!}\frac{1}{\Lambda^{3N}} {q_{int}}^{N} {q_r}^{cN} {V_f}^{N} \left[\exp - \frac{\varphi}{2kT} \right]^{N} \qquad 5.39$$

Chien et al. [43] used a double summation perturbation approximation to represent the attractive interactions, the Carnahan-Starling hard sphere equation of state to determine the free volume term, and equation 5.38 as the rotation partition function, and determined the rotator parameter α=1.078 for a single bond between two carbon atoms and applied it as a universal constant. Their approach resulted in three characteristic parameters that had to be fitted to the real fluid data: a molecular volume term, an energy term and the *c* parameter that represents the degrees of rotational freedom of the molecule.

Because of the complicated mathematical structure of the equation of state resulting from equation 5.47 Lin et al. [132] simplified the *COR* equation by fitting simpler empirical functions to the respective hard sphere, rotation and perturbation terms to derive an equation of state that is cubic in volume.

- ***Generalized Flory Methods***

Dickman and Hall [58] derived generalizations of the Flory [72] and Flory-Huggins [102] lattice theories applied to continuous space. They accomplished this by replacing the site occupation fraction ϕ with the reduced density of a continuous system η, where $\eta = \rho\, r\pi\sigma^{3}/6$ and σ is the spherical segment diameter, and by developing the insertion probability[4] equations according to the same approach as used in the Flory and Flory-Huggins theories.

The osmotic equation of state, derived from the insertion probability, is expressed as follows:

$$\frac{PV}{NkT} = 1 - \ln p_r(\eta, r) + \frac{V}{N}\int_0^{\eta} \ln p_r(\eta, r)\, d\eta \qquad 5.40$$

where $p_r(\eta,r)$ is the chain insertion probability (the probability of inserting a chain with *r* segments into the fluid without creating an overlap).

Dickman and Hall expressed the generalized Flory insertion probability as follows:

---

[4] The probability of adding an additional particle to the system into a volume or space not already physically occupied by the system particles.

$$p_{GF} = [p_1(\eta)]^{v_e(r)/v_e(1)} \qquad 5.41$$

Where $p_1(\eta)$ is the insertion probability of a monomer in a monomer fluid, and v_e represents the exclusion volume: with $v_e(1)$ referring to the exclusion volume of a single segment and $v_e(r)$ the volume excluded by the entire chain.

The values of the excluded volumes depend on the particular molecular model used to approximate the chained system. For chains of freely jointed hard spheres with diameters σ, $v_e(r)$ is obtained by averaging over all the possible configurations of an isolated *r*-chain. This leads to the following exclusion volumes:

$$\begin{aligned} v_e(1) &= (4/3)\pi\sigma^3 \\ v_e(2) &= (9/4)\pi\sigma^3 \\ v_e(3) &\approx 9.82605\sigma^3 \\ v_e(r) &\approx v_e(3) + (r-3)[v_e(3) - v_e(2)] \qquad for \quad r \geq 4 \end{aligned} \qquad 5.42$$

By substituting equation 5.41 into equation 5.40 the generalized Flory, *GF*, equation of state can be derived:

$$\left(\frac{PV}{NkT}\right)_{GF} = \frac{v_e(r)}{v_e(1)}\left[\left(\frac{PV}{NkT}\right)_1 - 1\right] + 1 \qquad 5.43$$

Here $(PV/(NkT))_1$ refers to the compressibility of a single segment or spherical particle. Dickman and Hall used the Carnahan Starling [32] equation of state to represent this term.

The generalized Flory-Huggins, *GFH*, equation of state is a much more complicated expression than equation 5.43, but is also a similar function of the excluded volume ratio, $v_e(r)/v_e(1)$, and the hard sphere compressibility. The reader is referred to the original article for the derivation and expression of the *GFH* equation of state [58].

The *GF* theory has been extended by Honnell and Hall [95] to be able to account for the chain connectivity more directly than only through the excluded volume. Honnell and Hall incorporated the dimer insertion probability into the *GF* equation to derive the generalized Flory-dimer, *GF-D*, model. They expressed the chain insertion probability as follows:

$$p_{GF} = p_1(\eta)\left[\frac{p_2(\eta)}{p_1(\eta)}\right]^{[v_e(r)-v_e(1)]/[v_e(2)-v_e(1)]} \qquad 5.44$$

where $p_2(\eta)$ refers to the dimer insertion probability in a dimer fluid.

Equation 5.44 leads to the following *GF-D* EOS when used in equation 5.40:

$$\left(\frac{PV}{NkT}\right)_{GF-D} = (Y_r+1)\left(\frac{PV}{NkT}\right)_2 - Y_r\left(\frac{PV}{NkT}\right)_1 \qquad 5.45$$

with:

$$Y_r = \frac{v_e(r)-v_e(1)}{v_e(2)-v_e(1)} \qquad 5.46$$

$(PV/(NkT))_2$ refers to the hard dimer fluid compressibility and $(PV/(NkT))_1$ to the compressibility of hard spheres.

Honnell and Hall used the Carnahan Starling hard sphere [32] and the Tildesley-Streett [204] dimer equations of state in their model.

Yethiraj and Hall [246] extended the *GF* and *GF-D* equations to square-well chains. They found that the excluded volume dependence of the attractive contribution to the equation of state is similar to that of the hard sphere chain fluid. The attractive contribution to the real chain equation can be expressed as:

$$\left(\frac{PV}{NkT}\right)_{att\,GF-D} = (Y_r+1)\left(\frac{PV}{NkT}\right)_{att\,2} - Y_r\left(\frac{PV}{NkT}\right)_{att\,1} \qquad 5.47$$

Yethiraj and Hall used the integral equation theory with a mean spherical approximation, *MSA*, to obtain equations of state for square-well monomers and dimers [246]. Bokis et al. [23] similarly applied the *GF-D* equation to square-well fluids, but used the local composition theory to derive the monomer and dimer equations instead, in an attempt to derive a more practical equation of state.

The *GF*, *GFH* and *GF-D* equations were originally derived for chains of tangent hard spheres, but can easily be extended to a more realistic system of fused hard spheres, by using the

correct excluded volume expressions for this type of molecule and a suitable expression for a fused diatomic particle [246].

- ***SAFT***

The Statistical Associating Fluid Theory, *SAFT*, has received a considerable amount of interest over the past decade as a method to not only account for chain formation but also association in non-spherical fluid systems. There have been a vast number of articles published on the approach and very many modifications and improvements proposed. The development of the *SAFT* equations has been reviewed in articles such as [65, 152, 229].

Traditionally the development of the *SAFT* approach has been described as following two distinct routes. The first, based on the approach to develop a real-fluid equation, is generally referred to as the Statistical Associating Fluid Theory, whilst the second route that of the Thermodynamic Perturbation Theory, *TPT*, is based on the original theory behind the *SAFT* approach, and generally refers to the development of equations describing theoretical or model fluids [65]. The *TPT* models can however be easily extended to real systems, and both approaches will be treated under the same heading in this work.

The Thermodynamic Perturbation Theory was originally developed in a series of articles by Wertheim [231-235] in an attempt to quantify the relationship between the well defined site-site interactions present in associating fluid systems and the bulk fluid properties through the perturbation theory. Wertheim developed the *TPT* approach by expanding the fluid Helmholtz energy in a series of integrals of molecular distribution functions and the association potential. It can be shown that many of these integrals must be zero and that by resuming the expansion series (through cluster or graph theory) a simplified expression for the Helmholtz energy of the system can be obtained [39]. The first order perturbation theory allows for the formation of chain- or tree-like clusters of associating molecules, but does not account for the bond-angle or allow the formation of double bonds or ring-like structures.

Chapman [38, 39] and Wertheim [236] independently extended the *TPT* to the formation of chained systems, by imposing strong covalent-like bonds on spherical equisized segments with one or two bonding (association) sites. (With a maximum of two bonding sites the formation of branched chains cannot be directly accommodated in this theory.) Chapman proposed the following expression for the residual Helmholtz energy of a chained, associating system:

$$\frac{A^{Resid}}{NkT} = \frac{A^{seg}}{NkT} + \frac{A^{chain}}{NkT} + \frac{A^{assoc}}{NkT} \qquad 5.48$$

Where A^{seg} refers to the unbonded segment Helmholtz energy and is generally equal to the product of the chain length, r, with the individual segment Helmholtz energy ($A^{seg}=rA^{indiv\ seg}$), A^{chain} the Helmholtz energy contribution due to the chain formation and A^{assoc} the association Helmholtz energy. Because only non-associating systems are of interest in this work the association Helmholtz energy will not be discussed further and A^{assoc} will treated as equal to zero.

The chain term in equation 5.48 can be expressed as [38, 39]:

$$\frac{A^{chain}}{NkT} = -(r-1)\ln g^{seg}(\sigma) \qquad 5.49$$

where r refers to the number of segments in the chain, and $g^{seg}(\sigma)$ is the segment radial distribution function evaluated at the segment contact.

Equation 5.48 has been applied in two ways to model real fluids, the first to develop a hard sphere chain (*HSC*) reference term that could then be extended to real systems through the perturbation theory: (d_{HS} refers to the effective hard sphere contact diameter.)

$$\frac{A^{Resid}}{NkT} = \left[r\frac{A^{HS}}{NkT} - (r-1)\ln g^{HS}(d_{HS}) \right]_{HSC} + \left[\frac{A^{pert}}{NkT} \right]_{HSC} \qquad 5.50$$

Or alternatively by directly applying equation 5.50, incorporating the attractive interactions into the segment term initially, e.g. in the form of a square-well or Lennard-Jones segment, and then extending it to a chained system. This approach requires the use of the segment radial distribution function in equation 5.49, e.g. $g^{SW}(\sigma)$ or $g^{LJ}(\sigma)$.

A vast number of *SAFT* equations have been proposed in the literature, using various method potential models, perturbation contributions and both of the approaches discussed above.

The original article by Chapman et al. [38] used an equation of state developed by Twu et al. [216] to represent the segment term, and approximated the g^{seg} as g^{HS} using the hard sphere contact radial distribution function as derived from the Carnahan-Starling [32] equation. In a later publication the authors used the Carnahan-Starling hard sphere model to determine the

hard sphere chain term, and the perturbation term and effective hard sphere diameter as developed by Cotterman et al. [49].

One of the most widely applied versions of the *SAFT* equation was developed by Huang and Radosz [100]. They used the hard sphere chain approach with the Carnahan-Starling hard sphere equation along with the Chen and Kreglewski [42] two-step potential model and perturbation term. Fu and Sandler [74] derived a simplified SAFT equation using the *HSC* reference term determined from the Carnahan-Starling equation of state with a square well potential model and the local composition perturbation approximation by Lee et al. [126].

Banaszak et al. [13] developed an equation of state for Lennard-Jones chains based on the *TPT* theory. Their approach referred to as *TPT-LJ* is derived from equation 5.48 with Lennard-Jones segments. (A^{assoc}=0). The compressibility of the Lennard Jones spheres and the Lennard-Jones radial distribution function were determined from Monte Carlo simulation data. Müller and Gubbins [151] and Kraska and Gubbins [117] developed a *SAFT-LJ* equation of state with a Lennard-Jones segment term represented by the Lennard-Jones equation of state as developed by Kolafa and Nezbeda [116] and the results of Johnson and Gubbins [105] for the Lennard-Jones radial distribution function. Chen et al. [40] developed a similar equation using the Johnson [106] Lennard-Jones equation of state and a g^{LJ} term fitted to Monte Carlo simulation data instead. Blas an Vega [21] developed a *Soft-SAFT* equation in an approach that is essentially identical to the *SAFT-LJ* model, using the Lennard-Jones equation of state by Johnson et al. [106] to represent the segment term, and the results of Johnson and Gubbis [105] for the radial distribution function. They however also extended their model to be able to handle heteronuclear chains.

The *SAFT* equation has also been applied to square-well segments to derive *SAFT-SW* and *TPT-SW* equations. Banaszak et al. [14] developed the *TPT-SW* equation using the Barker and Henderson [17] second order square well fluid approximation for the square well segment and the Barker and Henderson [14] first order perturbation approximation of the square-well radial distribution function. Adidharma and Radosz [5] used similar approximations in the development of their *SAFT-SW* equation, but included a truncation correction in the square-well segment perturbation approximation fitted to ethane data (see section 4.3.5.a) and extended their model to heteropolymeric fluids.

Gil-Villegas et al. [82] and Adidharma and Radosz [6] in an expansion of the *SAFT* approach proposed *SAFT-VR* equations that allow the attractive well width of the segment term to be varied.

A further modification to the *SAFT* equation is the inclusion of the effect of the interdependency of the bonds during chain formation. Equation 5.49 only contains information about the monomer system. Ghonasgi and Chapman [81] and Chang and Sandler [36] developed the *SAFT-D* and *TPT-D* theories that include the structural information on the dimer fluid. The chain contribution towards the total residual Helmholtz energy of the system can now be expressed as:

$$\frac{A^{chain}}{NkT} = -\frac{r}{2}\ln g^{monomer}(\sigma) - \frac{(r-2)}{2}\ln g^{dimer}(\sigma) \qquad r \geq 2 \qquad 5.51$$

A normal hard sphere equation of state is used to determine $g^{monomer}$ whilst g^{dimer} is normally determined by a polynomial fitted to molecular simulation results such as used by Chiew [45] and Yethiraj and Hall [245, 247]. Sadus investigated the simplification of the *TPT-D* equation through an approximation of the dimer distribution function and the use of a simpler hard sphere equation of state [181, 182], whilst . Yeom et al. [244] extended equation 5.51 to include the effects of successive polymerisation. They express the chain contribution as:

$$\frac{A^{chain}}{NkT} = -\ln g^{monomer}(\sigma) - (r-2)\ln g^{monomer-dimer}(\sigma) \qquad r \geq 2 \qquad 5.52$$

where $g^{monomer\text{-}dimer}$ is the radial distribution function of a monomer-dimer mixture, which is composition independent in the first order theory [244] and can be determined from:

$$g^{monomer-dimer}(\sigma) = g^{monomer}(\sigma) - \frac{1}{4(1-\eta)} \qquad 5.53$$

There have been various other attempts to improve the performance of the *SAFT* type equations. Pfohl and Brunner [167] extended the *SAFT* equation as proposed by Huang et al. [100] to allow mixtures of hard convex bodies as represented by the *BACK EOS* [42] and hard sphere chains. This approach was taken further by Chen and Mi [41] in the development of an equation for hard convex body chains. This was accomplished by replacing the expressions for hard spheres in equation 5.50 in the segment and chaining term by the hard convex body equation of state, equation 5.3.

Another attempt at improving the *SAFT* equations of state is specifically focussed on improving the perturbation term of the *HSC* type equations. Very often the perturbation term is simply taken the product of the segment number, *r*, and the perturbation terms developed for spherical particles. This approach neglects the effect of the chain-connectivity on the perturbation term. Several authors have proposed methods to correct this approximation [40, 85, 86, 180]. The *HSC* perturbation term will be discussed in detail in section 5.3.1.b.

The extension of the *TPT* and *SAFT* approaches to chains consisting out of segments of different sizes, heterosegmented chains, and branced molecules have also been investigated [4, 6, 12, 21]. As this study is mostly concerned with the description of unbranched simple hydrocarbon chains such as n-alkanes, these extensions to the statistical associating fluid theory will not be considered further in this work.

- ***Perturbed hard sphere chain theory* (*PHSC*)**

The perturbed hard sphere chain theory was developed form the solution of the Percus-Yevick integral theory for athermal hard sphere chains as reported by Chiew [44] in 1990.

Chiew solved the direct correlation function through the Percus-Yevick approach for spherical particles or segments whilst imposing several conditions on the particle behaviour to incorporate the effect of chain formation [44] and obtained the following *HSC* equation [44, 198]:

$$\left(\frac{PV}{NkT}\right)_{HSC} = \left(\frac{PV}{NkT}\right)_{HS} + \left(\frac{PV}{NkT}\right)_{bond}$$

$$= 1 + \rho\left[rg_{HS}(\sigma)\right] - (r-1)\left[g_{bond}(\sigma) - 1\right] \qquad 5.54$$

Chiew determined an expression for the hard sphere radial distribution function at contact, $g_{HS}(\sigma)$, through the compressibility function (equation 2.52) which leads to the *PY-C* hard sphere equation (equation 3.17), and obtained a Percus-Yevick solution of the bond contribution of the folliwing form::

$$\left(\frac{PV}{NkT}\right)_{bond} = -(r-1)\left[g_{bond}(\sigma) - 1\right] = -(r-1)\left(\frac{1 + (1/2)\eta}{(1-\eta)^2}\right) \qquad 5.55$$

In an attempt to improve the *HSC* equation, Chiew proposed the use of the more accurate Carnahan-Starling hard sphere equation instead of the *PY-C* expression, but kept equation 5.55 the same. This modification however resulted in a poorer performance at higher system densities.

Song et al. [198] recognised the fact that had the *Percus-Yevick* integral theory been exact the expressions for the *PY-C* g_{HS} and g_{bond} would have been identical and replaced the both these contact radial distribution functions with that of the Carnahan-Starling equation of state. This approach resulted in a significant improvement in the performance of the *HSC EOS.*

The *HSC* equation can be extended to a perturbed hard sphere chain, *PHSC*, capable of representing real fluid systems by using the perturbation theory along with the *HSC* equation describing the reference fluid. Song et al. [199, 200] used the *HSC* with the Carnahan-Starling hard sphere fluid model along with the perturbation approximation as proposed by Song and Mason [201], whilst Hino and Prausnitz applied it with the exact solution of the second order perturbation theory for a square well fluid derived by Chang and Sandler [35].

5.3 SELECTION OF SUITABLE APPROACH

Of the various methods reviewed in section 5.2, many approaches result in complex equations that are impractical for use in practical applications. A suitable approach needs to be identified that will lead to a simple accurate equation of state capable of describeing non-spherical non-polar fluid systems.

The *HCB* models discussed in section 5.2.1 that have been explicitly developed to account for the molecular shape have been developed primarily out of the scaled-particle-theory, and in their simplest form, when applied to spherical systems, reduce to the normal Carnahan-Starling and *PY-C* equations of state. These hard sphere equations, as has been discussed in Chapter 3, are already too complex for use in a simple equation of state. The simplified forms of the hard sphere models, on the other hand, cannot be derived through the scaled particle theory, and hence do not lend themselves to the extension towards hard convex bodies in this manner. Furthermore, as have been discussed in section 5.2.1, the application of the hard convex body equations of state to long chainlike molecules becomes problematic. Therefore as there are other more efficient ways to account for the non-sphericity of the system particles, this approach will not be considered further.

The lattice fluid models will also not be considered for the development of a simple equation of state, as the molecular distribution structure on which these models are based is inherently incorrect and will contribute to the uncertainty in the model performance, especially in the vapour phase.

On the other hand various off-lattice tangent sphere models are based on the accurate description of the spherical segments. This provides an excellent opportunity for the simplification of these models, as the simple equation of state for spherical systems developed in the previous chapters can be used to replace the more complex models that may have been used in the original theories. Of the five off-lattice methods discussed, three approaches will be investigated further, *SAFT*, *PHSC* and *PHCT*.

The *COR* off-lattice model, besides a hard sphere equation, also requires an explicit expression for the hard dimer fluid. This was originally determined through the use of the *HCB* equation, equation 5.2. As discussed above, this expression needs to be simplified for applications in practical equations of state. In a previous attempt to simplify the *COR* model, an empirical equation was fitted to the results obtained from equation 5.2 using a non-sphericity parameter of $\alpha = 1.078$ indicative of a C-C bond [132]. It was decided not to follow a similar approach of fitting a simplified function to hard dumbbell simulation data, as unlike the *PHCT*, the *COR* approach is not able to explicitly not account for the vibrational density dependence or the effect of the attractive interactions on the rotational and vibrational motions of the fluid.

It has been noted [23, 222] that the *GF* equations have a similar mathematical structure to the *PHCT* model as proposed by Donohue and Prausnitz [60] with the external degrees of freedom parameter *c* replaced by the excluded volume ratio. It has also further been observed that the expressions for the exclusion volume terms as determined for tangent spheres through equation 5.42 will be too large for real fluid systems where there is a considerable degree of overlap of the exclusion volumes, and that smaller values are needed to describe these systems [246] which are expected to result in a volume ratio close to the value of the *c* parameter [222]. As these two models can be considered to be equivalent the *GF* equation will not be studied explicitly. The structure of the *GFH* equation of state, on the other hand, differs considerably from that of the *PHCT*, but as this equation has an inherently complex density dependence it does not lend itself to the development of a practical equation of state.

The inclusion of information on dimer or higher order chain behaviour has been proposed for several models, e.g. in the *GF-D, SAFT-D* and *TPT-D* equations, in order to improve the actual representation of the chained systems. This approach, however, raises the density dependence of the resultant *EOS* significantly. Although the inclusion of this information may slightly improve the performance of the theoretical hard sphere chain model, it will not be used in this study, as the cost in the additional complexity is too high given the ability of the chain models, such as the normal *SAFT* equations, to represent real fluids without this correction. In fact in their study of the *SAFT-SW* models Adidharma and Radosz [6] found that the inclusion of the dimer structure seemed to have no significant benefit for representing real substances. This observation has later been confirmed by Zhang et al. [249] in their investigation of the square-well *TPT* and *TPT-D* models.

By applying the three promising tangent sphere theories to the *HS3CK* equation developed in the previous chapters, three possible simple chained models can be derived, the *simple-SAFT,* the *simple-PHSC* and the *simple-PHCT* equations. The actual derivation of these models will be discussed in the remainder of this section:

5.3.1 The simple-SAFT equation

As discussed in section 5.2.2.b, there are two methods to apply the *SAFT* approach to model the real fluid system: by treating the segment as a soft segment with attractive interactions, or alternatively by developing a hard spherical chain reference equation and then applying it in the perturbation theory.

5.3.1.a Chains of Two-step potential segments

Within the scope of this study, the approach of representing chains of attractive segments, implies that the 3x3 *HS3CK* equation, developed in Chapter 3, must be used to represent the segment term. This approach further requires an expression for the radial distribution function of the *HS3CK* segment, $g^{3x3\ HS3CK}$, at the contact or bonding distance, d_{BH}, which will be used to determine the Helmholtz energy contribution of the bond formation through equation 5.49.

According to Barker and Henderson [18] the radial distribution function may be approximated through the perturbation theory:

$$g(r) = g^{HS}(r) + \frac{\varepsilon}{kT} g_1(r) + \left(\frac{\varepsilon}{kT}\right)^2 g_2(r) + \ldots \qquad 5.56$$

where ε is the well-depth and $g_n(r)$ represents the n^{th} perturbation term. In the first perturbation approximation term $g_1(r)$ can be determined from [82]:

$$g_1(\sigma) = \frac{1}{4\varepsilon}\frac{\partial A^{(1)}}{\partial \eta} - \frac{1}{\varepsilon}\int_1^\infty x^3 \frac{\partial u^{(1)}}{\partial x} g^{HS}(x) dx \qquad 5.57$$

Where $A^{(1)}$ refers to the first perturbation term in the notation of equation 4.18, $u^{(1)}$ to the perturbation intermolecular energy and x to the intermolecular distance.

Equation 5.57 requires the knowledge of the hard sphere radial distribution function over the entire system volume, but because of the nature of the two-step potential the integral may be solved following Gil-Villegas et al. [82]. It is however clear that the even the first order approximation of the radial distribution function will result in a highly complex equation of state, and that the *HSC* approach will result in a mathematically much more simple model.

5.3.1.b Hard Sphere Chain Approach

This approach entails the development of a hard chain equation based on the simplified hard sphere model developed in Chapter 3 and uses the perturbation theory to extend it to real fluid systems.

The chain contribution using *HS3* can be expressed as follows:

$$\frac{A^{chain}}{NkT} = -(r-1)\ln\left[g^{HS3}(\sigma)\right] = -(r-1)\ln\left[\frac{1 + \frac{b}{4}\eta + \frac{e}{4}\eta^2}{(1-d\eta)}\right] \qquad 5.58$$

$$z^{chain} = -(r-1)\eta\frac{\partial\left(\ln\left[g^{HS3}(\sigma)\right]\right)}{\partial\eta} = -(r-1)\frac{\left(d + \frac{b}{4}\right)\eta + \frac{e}{2}\eta^2 - \frac{ed}{4}\eta^3}{(1-d\eta)\left(1 + \frac{b}{4}\eta + \frac{e}{4}\eta^2\right)} \qquad 5.59$$

with b = 4.4038, e = 5.3635 and d = 1.399. η still represents the reduced density of the spherical segments and is defined as the ratio of the physical volume occupied by a total

number of segments in the fluid to the system volume, $\eta = (rN)\tau\, v_0/V$, where v_0 is the closest packed segment volume, N the number of molecules in the system and r the number of segments per molecule.

The complete hard sphere chain equation of state according to the *SAFT* approach determined from equation 5.50 is therefore:

$$z^{HSC} = 1 + r\frac{4\eta + b\eta^2 + e\eta^3}{(1-d\eta)} - (r-1)\frac{\left(d+\frac{b}{4}\right)\eta + \frac{e}{2}\eta^2 - \frac{ed}{4}\eta^3}{(1-d\eta)\left(1+\frac{b}{4}\eta+\frac{e}{4}\eta^2\right)} \qquad 5.60$$

(Note that equation 5.50 is in the residual form, whilst equation 5.60 describes the actual *HSC* compressibility.)

The next step in the model development is to extend equation 5.60 to a real fluid system through the perturbation theory. The perturbation expansion of equation 5.60 would therefore be a function of the perturbation energy and the *HSC* radial distribution function. The first perturbation term (equation 2.92) can therefore be expressed as follows:

$$\frac{A^{(1)}}{kT} = 2\pi\rho N\int_{\sigma}^{\infty} u^{(1)}(r_{12})g^{HSC}(r_{12})r^2 dr \qquad 5.61$$

In many applications of the *SAFT* approach [38, 39, 74, 100] the perturbation term as simply been determined as r times the segment perturbation term:

$$\frac{A^{HSC\ pert}}{NkT} = r\left(\frac{A^{HS\ pert}}{NkT}\right) \qquad 5.61$$

This of course does not take the chain connectivity into account.

Sadowski [180] used the number of segment-segment interactions, $N_{r\text{-}r}$, in a chain system to determine the perturbation compressibility contribution:

$$z^{HSC\ pert} = N_{r-r}z^{HS\ pert} \qquad 5.62$$

$N_{r\text{-}r}$ is estimated by assuming that the ratio of $N_{r\text{-}r}/N_{1\text{-}1}$ is equivalent to the ratio of the contact radial distribution functions of hard chain fluids, $g^{HSC}(\sigma)$, and hard spheres, $g^{HS}(\sigma)$. Here $N_{1\text{-}1}$

is the number of interactions in a system of unconnected spheres with $N_{1\text{-}1} = r(2r\text{-}1)$. By determining the expressions for $g^{HS}(\sigma)$ from the *PY-P* equation of state and for $g^{HSC}(\sigma)$ from the analytical solution of the *Percus-Yevic* theory for hard sphere chains determined by Chiew [45], Sadowski obtained the following relation:

$$\frac{z^{HSC\ pert}}{z^{HS\ pert}} = \frac{N_{r-r}}{N_{1-1}} = (2r-1)\frac{2+(3r-2)\eta}{2+\eta} \qquad 5.63$$

This empirical correction is dependent on the system density and increases the complexity of the proposed perturbation term.

Following a different approach Chen and Mi [41] proposed an empirical correction to the *SAFT* perturbation term through which the intramolecular segment interactions can be excluded from the perturbation term:

$$\frac{A^{chain\ pert}}{A^{segment\ pert}} = f = \varpi\left(\frac{A^{chain}}{A^{seg}}\right) \qquad 5.64$$

where A^{chain} is given by equation 5.49, and ϖ is a constant for fluids with the same interaction potential. Chen and Mi [41] determined $\varpi = 1.75$ for all non-polar fluids for their equation of state. Like the correction proposed in equation 5.63 the correction term f is density dependent and will increase the density functionality of the final equation of state.

Following a theoretically based approach, Gross and Sadowski [85] developed the *PC-SAFT* equation in which they applied the Barker and Henderson second perturbation theory based on the *local compressibility* approximation to square well chains (see section 2.3.3.a). They used the *SAFT HSC* equation of state determined from the Carnahan Starling hard sphere equation of state as reference fluid and the mean *HSC* radial distribution function as determined by Chiew [45] in the evaluation of the perturbation integrals. Because the second perturbation term of the local compressibility approximation requires the pressure derivative of the reference equation (see equations 2.102 and 2.105), in this case the *HSC* equation, the *PC-SAFT* equation is mathematically very complex and has a very high overall density dependence.

Of interest in their work is the fact that they simplified their equation by approximating the perturbation integrals with polynomial functions in density in an approach similar to those

discussed in section 4.3.5.a, but that in this case the polynomial coefficients a_i and b_i are functions of the chain length.

$$\int_1^{\lambda} g^{HSC}(x)x^2 dx = \sum_{i=0}^{6} a_i(r)\eta^i \qquad 5.65$$

$$\frac{\partial}{\partial \rho}\left[\rho \int_1^{\lambda} g^{HSC}(x)x^2 dx\right] = \sum_{i=0}^{6} b_i(r)\eta^i \qquad 5.66$$

Gross and Sadowski [85] used a relation developed by Hu et al. [96] and Liu and Hu [133] to describe the segment number dependence of these coefficients:

$$a_i(r) = a_{0i} + \frac{r-1}{r}a_{1i} + \frac{r-1}{r}\frac{r-2}{r}a_{2i} \qquad 5.67$$

$$b_i(r) = b_{0i} + \frac{r-1}{r}b_{1i} + \frac{r-1}{r}\frac{r-2}{r}b_{2i} \qquad 5.68$$

This parameterisation significantly increases the number of coefficients that need to be determined for the perturbation approximation. (From 12 (6 per perturbation term) to 36 (18 per perturbation term).)

In a later work Gross and Sadowski [86] extended their *PC-SAFT* equation to real fluid systems by first determining the equation of state parameters, the segment number, segment diameter and well-depth by fitting the equation of state to alkane *P-v-T* data using the complex analytical expression for the mean g^{HSC} [45] in the perturbation term, and then using these fitted parameters in the simplified equation to regress the perturbation parameters. It should however be noted that in the extension of the *PC-SAFT* equation to mixtures the *r* parameter is dependent on the overall mixture composition. Equations 5.67 and 5.68 therefore need to be re-evaluated for each new mixture composition in the multi-component flash calculations.

As shown in Chapter 4, the double summation perturbation approximation is better suited to represent real fluid systems than the Barker and Henderson local compressibility perturbation approximation [18]. Unfortunately this approach does not lend itself to the method proposed by Gross and Sadowski to incorporate the chain connectivity in the perturbation term because of the complexity in determining the perturbation parameters.

Being guided by the satisfactory performance of the *SAFT* equation of state in representing real fluids whilst neglecting the chain connectivity, it was decided to use equation 5.61 along with the 3x3 double summation perturbation approximation of the two-step potential, developed in Chapter 4, to represent the hard sphere chain perturbation:

$$\frac{A^{HSC\ pert}}{NkT} = r\sum_{n}\sum_{m} D_{nm}\left(\frac{\eta}{\tau}\right)^{m}\left(\frac{1}{T^{*}}\right)^{n} \qquad 5.69$$

$$z^{HSC\ pert} = r\sum_{n}\sum_{m} mD_{nm}\left(\frac{\eta}{\tau}\right)^{m}\left(\frac{1}{T^{*}}\right)^{n} \qquad 5.70$$

with reduced temperature $T^{*} = kT/\varepsilon$, the ratio of the kinetic energy to the potential energy of each segment.

The complete equation of state for the *simple-SAFT* model can therefore be obtained by combining equations 5.60 and 5.70 and results in an equation that has a 7^{th} order density functionality. The proposed equation has four characteristic parameters: three segment parameters: the temperature independent closest packed segment volume, v_{00}, the temperature independent well-depth, ε_0/k, and the non-central contribution to the London dispersion forces, μ/k; and one chain parameter, r, the segment number or chain length.

5.3.2 The simple-PHSC equation

The *PHSC* theory is based on an exact solution for hard sphere chains within the assumptions of the *Percus-Yevick* theory and those made to allow for chain connectivity. This is in contrast to the *SAFT-HSC* that is determined from a first perturbation expansion of the resummed cluster expansion or graph theory.

Song et al. [198] and Kim and Bae [112] compared the ability of the two *HSC* models, the *SAFT-HSC*, or *TDT*, and that used in the *PHSC* model to represent the phase behaviour of hard sphere chains of various lengths determined through molecular simulation. Song et al found that the *PHSC-HSC* is more accurate than the *SAFT-HSC* in the representation of the mixtures of binary chains of different lengths, where as Kim and Bae reported the superior performance of the *SAFT-HSC EOS* in the modelling of pure hard sphere chain systems. Feng et al. [71], on

the other hand, in their comparison of the *SAFT* and *PHSC* square well model representation of real fluid hydrocarbons and polymers found the *PHSC* model superior.

Applying the *PHSC* theory to the *HS3* equation results in the following chain contribution term:

$$\frac{A^{resid}}{NkT} = -(r-1)\int_0^{\eta} \frac{g^{HS3}(\sigma)-1}{\eta} d\eta$$

$$= (r-1)\left[\frac{e}{4d}\eta + \left(1+\frac{b}{4d}+\frac{e}{4d^2}\right)\ln(1-d\eta)\right] \qquad 5.71$$

$$z^{chain} = -(r-1)\left[g^{HS3}(\sigma)-1\right] = -(r-1)\frac{\left(\frac{b}{4}+d\right)\eta + \frac{e}{4}\eta^2}{(1-d\eta)} \qquad 5.72$$

with b = 4.4038, e = 5.3635 and d = 1.399.

The complete hard sphere chain equation can then be expressed as:

$$z^{HSC} = 1 + r\frac{4\eta + b\eta^2 + e\eta^3}{(1-d\eta)} - (r-1)\frac{\left(\frac{b}{4}+d\right)\eta + \frac{e}{4}\eta^2}{(1-d\eta)} \qquad 5.73$$

The discussion in section 5.3.1.b on the expansion of the hard chain term to real fluids through the perturbation theory and the inclusion of the chain-connectivity in the perturbation term is fully applicable to equation 5.73. The perturbation approximation as represented by equations 5.69 and 5.70 will therefore also be applied to this hard sphere chain equation.

The final *simple-PHSC* equation can now be expressed as:

$$z^{simple-PHSC} = 1 + r\frac{4\eta + b\eta^2 + e\eta^3}{(1-d\eta)} - (r-1)\frac{\left(\frac{b}{4}+d\right)\eta + \frac{e}{4}\eta^2}{(1-d\eta)} + r\sum_n\sum_m mD_{nm}\left(\frac{\eta}{\tau}\right)^m\left(\frac{1}{T^*}\right)^n \qquad 5.74$$

This model is quintic in volume and has the same equation of state parameters as the *simple-SAFT* equation: the segment parameters: v_{00}, ε_0/k and μ/k; and the chain length r.

5.3.3 The simple-PHCT equation

The *perturbed hard chain theory* will be investigated because of its inherent simplicity, as it requires no additional terms to account for the chain connectivity as opposed to the *SAFT* and *PHSC* approaches, and the fact that it explicitly takes the density dependence of the rotational and vibrational motions into account.

In the derivation of the *simple-PHCT* the approach of Donohue and Prausnitz [60] will be followed, by including the effect of the attractive interactions on the rotational and vibrational movement. It will further be assumed that the free volume of the chained system can be represented by the simple hard sphere equation of state, *HS3* (equation 3.49), and that the mean intermolecular potential energy can be represented by the 3x3 double summation approximation for a two-step potential model as developed in Chapter 4. The molecular structure, as in the case of the *SAFT* and *PHSC* approaches, can be seen as consisting out of r tangently bonded spherical segments. A new property, $3c'$, is defined to represent the external degrees of freedom per segment such that $c = rc'$. Applying these approximations to equation 5.23 leads to the following expression for the *simple-PHCT* equation of state:

$$Z = 1 + c'r\left(\frac{4\eta + b\eta^2 + e\eta^3}{1 - d\eta}\right) + c'r\left(\sum_n^3 \sum_m^3 mD_{nm}\left(\frac{\eta}{\tau}\right)^m \left(\frac{1}{T'^*}\right)^n\right) \qquad 5.75$$

with b = 4.4038, e = 5.3635 and d = 1.399 and η the reduced density per spherical segment of the molecule. It should be noted that in this equation the reduced temperature T'^* has a slightly different definition to the T^* terms used in equation 5.69, 5.70 and in Chapter 4. T'^* may be interpreted as the ratio of the total kinetic energy and the intermolecular potential energy of the molecular segment. According to the assumption of Prigogine the rotational and vibrational motions increase the effective kinetic energy of the segment (or molecule). T'^* should reflect this, therefore:

$$T'^* = \frac{c'kT}{\varepsilon} = c'T^* \qquad 5.76$$

In order to reduce the number of parameters that need to be specified for each molecule equation 5.75 can be expressed on a molecular, instead of a segmental basis, by making use of the equivalence of the reduced segmental and molecular densities, η, and the definition of $c' = c/r$. It can also be shown that the reduced segment temperature is equivalent to the reduced molecular temperature through $T'^* = (c'kT)/(\varepsilon) = cTk/(r\varepsilon) = ckT/(q\varepsilon')$ where r is the chain length or number of segments per chain, ε/k the segment energy term and, following the original *PHCT* [20], defining q as the surface area of the molecule and ε'/k the molecular energy term per surface area. Equation 5.75 may therefore be expressed as:

$$Z = 1 + c\left(\frac{4\eta + b\eta^2 + e\eta^3}{1 - d\eta}\right) + c\left(\sum_n^3 \sum_m^3 mD_{nm}\left(\frac{\eta}{\tau}\right)^m \left(\frac{1}{T'^*}\right)^n\right) \qquad 5.77$$

It should also be noted that the effective hard sphere diameter, equation 4.1, is a function of the kinetic energy of the system and hence of T'^* and not T^* as in sections 5.3.1 and 5.3.2 should be used when determining the effective diameter through equation 4.14. The temperature dependent well depth or energy parameter ε/k is however still determined through equation 4.97.

For pure components the *simple-PHCT* EOS will have 4 characteristic parameters: the temperature independent molecular volume, rv_{00}, the molecular energy term $r\varepsilon_0/k$ or $q\varepsilon_0'/k$, the parameter accounting for the degrees of motion, c, and a parameter μ/k to account for the temperature dependent London dispersion energies, and has a 5th order density dependence.

5.4 MODEL EVALUATION

The three chaining approaches in as proposed in section 5.3, will be evaluated in this section. There were however two perturbation parameter matrices suggested in Chapter 4, the first the full 3x3 matrix, which results in a more accurate argon and methane virial coefficient representation, and the second the constrained 3x3 matrix that with slightly less accurate vapour pressure and virial coefficient results for the two systems, but that facilitates the development of the theoretically correct mixing rules. Both these matrices will be investigated. The chained equations with the full matrix will be referred to as the *simple-SAFT*, *simple-PHSC* and the *simple-PHCT* models, whilst the equations using the constrained matrix will be identified using a *–ltd* suffix.

5.4.1 Evaluation criteria

The various proposed equations of state will be evaluated according to their ability to represent theoretical and real chainlike systems and the ease with which the equation of state parameters can be generalized for a homologous species.

The investigation into the representation of theoretical hard sphere chain systems is used to confirm whether the methods proposed to account for the non-sphericity are indeed applicable to the simplified empirically derived *HS3* equation.

The ability of the various models to represent the real chained systems will be investigated by evaluating the accuracy with which the equations can represent the normal alkane saturated vapour pressure and fluid volume data. This homologous hydrocarbon series has been selected as the basis of the investigation as it is the simplest possible chained system, without any undue complications due to branching, polarity or multiple bond formation, there is also a fair amount of saturated data available for these systems up to a carbon number of about 36 (hexatriacontane).

The third criterion, that of the ease with which the model parameters can be generalized is vitally important to the practical application of the equation of state. Because of the high costs, both in terms of financial expense and time, and difficulty of experimentally generating acute pure component data to which the parameters can be fitted, especially in the case of the heavier hydrocarbons and ill defined polymers, it is necessary that the *EOS* parameters be well behaved to facilitate the estimation of values for systems without the use of pure component data. It has been found that in chained systems the *EOS* parameters generally are simple functions of the chain-length or molecular weight [78, 86, 101, 149, 200]. The nature of the parameters determined for the proposed models will be investigated to determine whether they display similar trends.

5.4.2 Experimental Data

As mentioned above, the chained equations will be evaluated against theoretical hard body and hard sphere chain compressibility and n-alkane *P*-*v*-*T* data.

Table 5.1 Hard body simulation data

Hard Sphere Chains	
Chain length	**Source**
4	[36, 59]
8	[36, 59]
16	[36, 59, 75]
51	[75]
201	[75]
Prolate Spherocylinders	
γ (length/beadth)	**Source**
2	[28]
3	[28]
Prolate Ellipsoids	
λ (ratio of axis)	**Source**
2	[28]
3	[28]

Three types of theoretical particle geometries will be investigated, prolate spherocylinders, prolate ellipsoids and hard sphere chains. In the proposed models the hard sphere chain serves as the reference system in the perturbation expansion, it is therefore important that the models are indeed able to provide an accurate description of such a reference system. Hard sphere chain simulation data used in this study are listed in Table 5.1. The representation of the other non-spherical hard body systems, the prolate spherocylinders and ellipsoids, is investigated as a test of the flexibility of the proposed models to represent more realistic particle geometries that cannot be classified explicitly as chained systems. (The structure of carbon dioxide could be seen as an example of such a geometry.)

The extension of the equations of state to real chained systems is investigated through the ability of the proposed models to represent the phase behaviour of the normal alkane homologous series. For the n-alkanes up to heptane the saturated pressure, liquid and vapour volumes as well as the supercritical phase data were used in the regression of the equation of state parameters to ensure the optimal performance of the model over as wide as possible a range of conditions. For the heavier alkane systems, because of their low vapour pressures and the degradation of the components at higher system temperatures, the amount of data reported is much less and of varying degrees of accuracy. In this work smoothed data of the saturated

vapour pressures and liquid volumes were obtained for n-alkanes up to hexatriacontane from the work of Morgan and Kobayashi [148], Piacente et al. [168] and Tobler [211]. The various datasets and ranges are reported in Table 5.2.

Table 5.2 N-Alkane data sets used in the fitting of the proposed chained equations.

Component		Mr	VLE Data	Supercritical PVT Data		Source
		[g/mol]	T [K]	P [1e5 Pa]	T [K]	
Ethane	**C_2H_6**	16.04	150-295	52.5-600	310-620	[130]
Propane	**n-C_3H_8**	30.07	182-360	50.0-450	380-620	[130]
Butane	**n-C_4H_{10}**	44.1	215-420	54.4-397	440-580	[130]
Pentane	**n-C_5H_{12}**	58.12	237-465	44.6-500	480-540	[130]
Hexane	**n-C_6H_{14}**	72.15	244-500	32.0-370	520-600	[130]
Heptane	**n-C_7H_{16}**	86.18	266-532	33.5-100	560-600	[130]
Hexadecane	**n-$C_{16}H_{34}$**	100.2	330-445			Smoothed
Eicosane	**n-$C_{20}H_{42}$**	226.44	335-450			Smoothed
Octacosane	**n-$C_{28}H_{38}$**	282.55	345-460			Smoothed
Dotriacontane	**n-$C_{32}H_{66}$**	394.76	350-460			Smoothed
Hexatriacontane	**n-$C_{36}H_{74}$**	450.87	355-460			Smoothed

*** Smoothed data obtained from [148, 168, 211]**

5.4.3 Hard body representation

Of the three proposed chained equations, the *simple-SAFT* and *simple-PHSC* equations lend themselves directly to the modelling of the theoretical hard sphere chain simulation results by using the same chain length, r, and reduced segment density, η, as that for which the simulated data points were obtained. For the *simple-PHCT* model, due to the nature of its definition, the exact value of the total external degrees of freedom c is unknown for the theoretical system. In this study c is approximated by the following relation:

$$c = 1 + \frac{2}{3}(r - 1) \qquad 5.78$$

This equation implies a highly flexible hard sphere chain, with each segment losing only one translational degree of freedom due to the bond formation because of the fixed bond-length, but is able to move freely about the spherical surface area of the spherical segment to which it is bonded. This relation of course neglects the volume physically occupied by the other

segments in the same chain, but nevertheless results in a quite adequate model performance, especially at high densities. (See Figure 5.1). (Elliot et al. [66] estimated their c parameter using a more rigid hard sphere chain model with $c = 1 - 1/2(r\text{-}1)$ instead. Their estimation results in a slightly better performance of the *simple-PHCT* at low densities, but accompanied by very poor results at values of $\eta > 0.25$.)

The simulation results of the hard sphere chain compressibilities for systems with 4, 16, 51 and 201 tangent hard spheres are plotted Figure 5.1. (The results of the chain length $r = 8$ are not shown, but display a similar trend.)

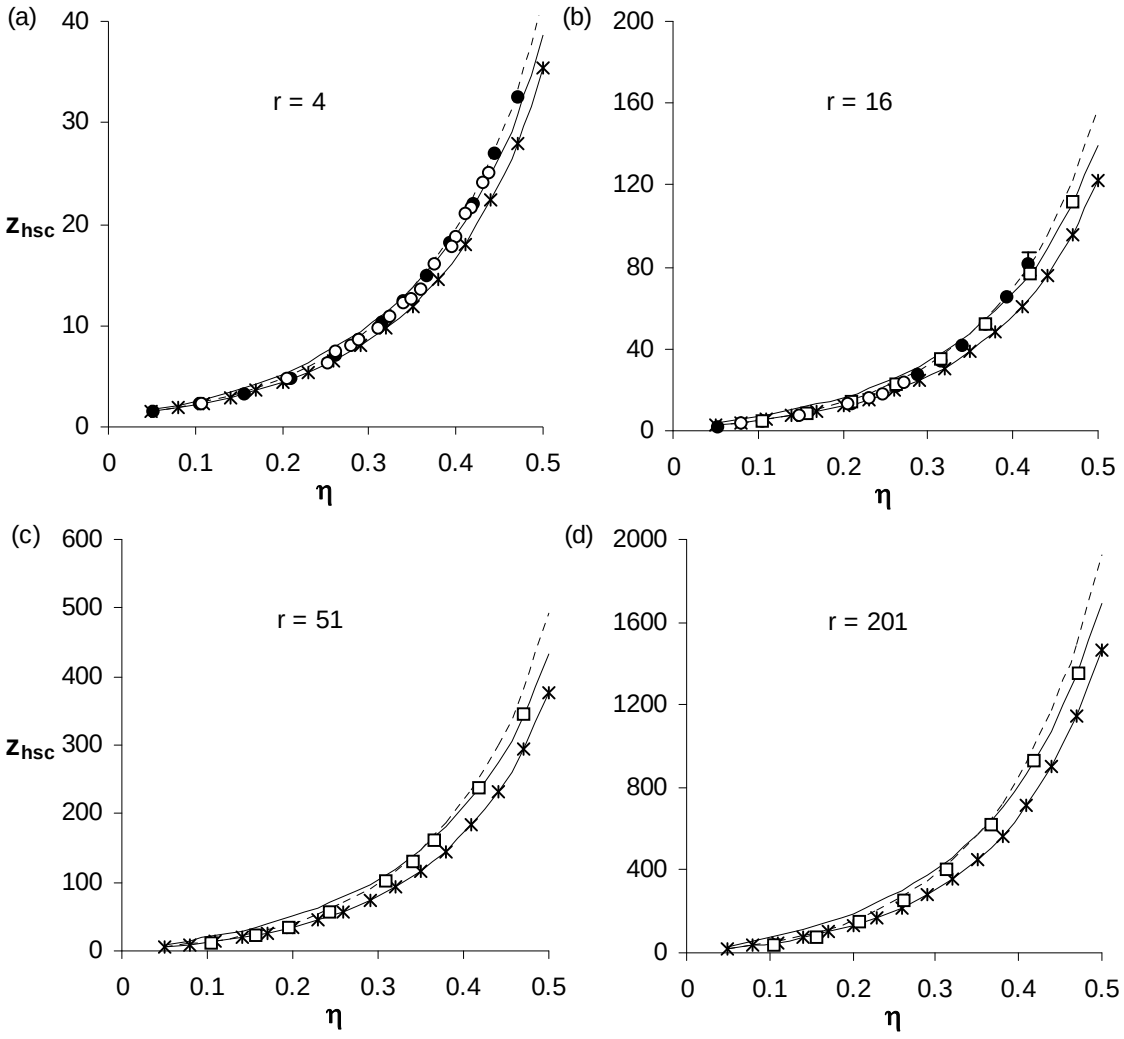

Figure 5.1 Hard sphere chain compressibility for particles with chain lengths of (a) r = 4, (b) r = 16, (c) r = 51 and (d) r = 201. With simulation data of ● [36] ○ [59] □ [75] and modelled by _____ *simple-SAFT,* —✳— *simple-PHSC,* and ____ *simple-PHCT*

From Figure 5.1 it can be seen that all three of the chain models are able to provide a reasonable representation of the hard sphere chained system. The *simple-PHSC* equation is

slightly less accurate than the *simple-SAFT* model at higher system densities. This observation is in agreement with the conclusions of Kim and Bae [112] based on their study of the *SAFT* and *PHSC* approaches using the Caranhan-Starling and Kolafa equations (see section 3.3) to represent the hard sphere phase behaviour.

As mentioned above, the *simple-PHCT* using equation 5.78 provides a highly accurate estimate of the hard sphere chain simulation results at higher densities, but is less accurate at low system densities. This could possibly be attributed to the fact that equation 5.78 neglects the restrictive effect that the presence of other segments in the chain segment has on the freedom of motion of a particular segment. At high densities this restriction will be overshadowed by the presence of other chained molecules in the fluid, but will become more significant at lower densities. The results are nevertheless satisfactory.

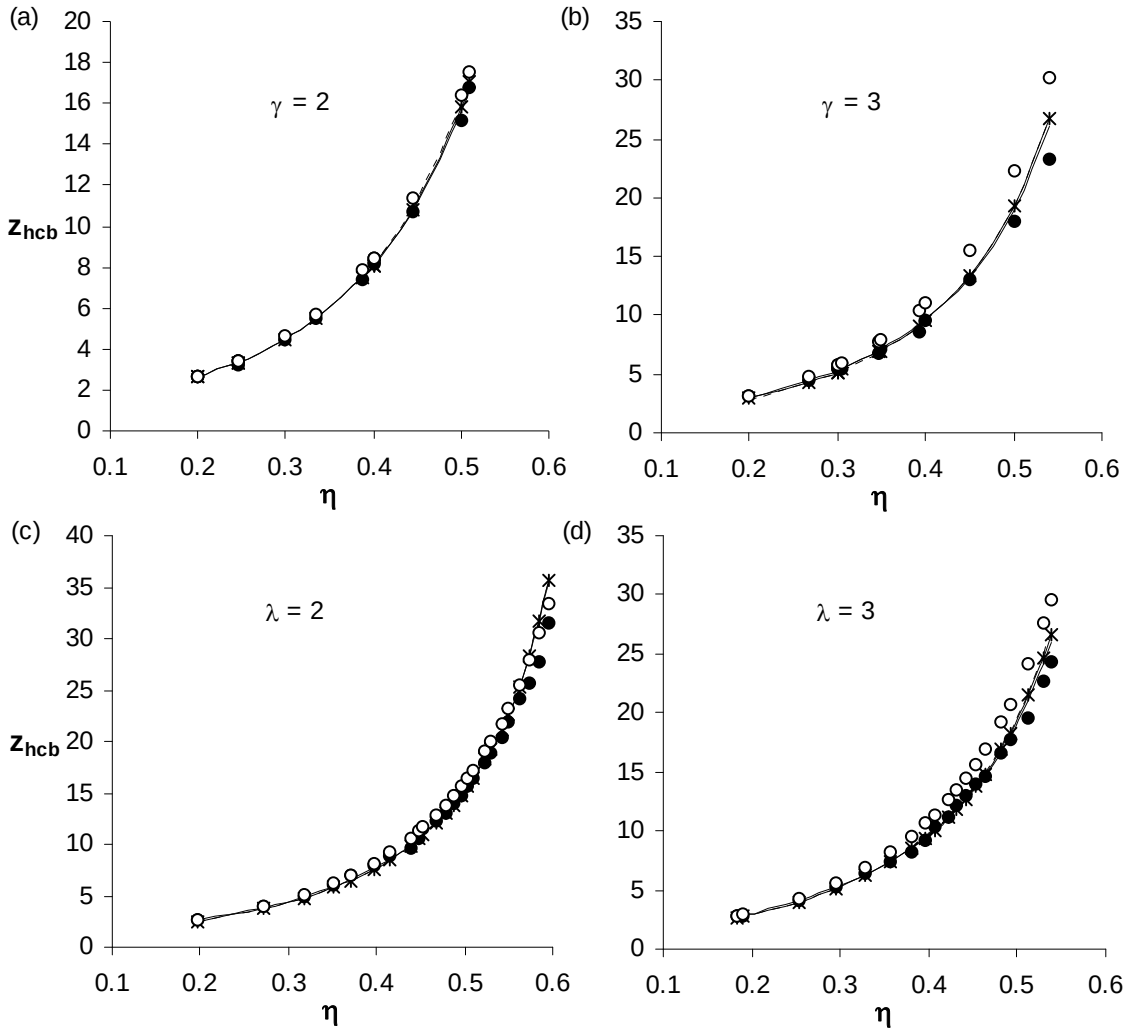

Figure 5.2 Hard body compressibilities for (a) and (b) prolate spherocylinders and (c) and (d) prolate ellipsoids. ● simulation data [28], ○ predicted by equation 5.2 and modelled by fitted by _____ *simple-SAFT*, —✳— *simple-PHSC*, and ——— *simple-PHCT*

Figure 5.2 is a plot of the simulated hard body phase behaviour. Figure 5.2 (a) and (b) contain results obtained for prolate spherocylinders with γ, *a* length : diameter ratio, of 2 and 3, and Figure 5.2 (c) and (d) results for a system of hard prolate ellipsoids with a characteristic parameter, $\lambda = 2$ and $\lambda = 3$, which represents the ratio of the ellipsoid axes. The γ and λ ratios are reported for a normalized system with the breadth of the hard body, $\sigma = 1$. The results obtained using *hard convex body* equation of state, equation 5.2 as discussed in section 5.2.1, with the nonsphericity parameter, α, determined by using the relations listed in Table 5.3 in equation 5.3. From the various plots is obvious that the *hard convex body* equation becomes less accurate as the nonsphericity increases as has been observed in the literature [28, 225].

It should however be noted that the *hard convex body* equation is applied here in a purely predictive capacity, and that better results could have been obtained by using the α parameter as an adjustable parameter to fit the model to the simulated data. This however would nullify the theoretical basis of the model.

In the case of the proposed chained models, the effective chain length, *r*, the segment diameter, σ, and the external degrees of freedom, *c*, are undefined (or unknown in the case of the *simple-PHCT EOS*) for hard convex bodies. For the *simple-PHCT c* was used as an adjustable parameter in the fitting of the simulation data, whilst for the *simple-SAFT* and *simple-PHCT* the effective segment diameters were fitted to the data and the segment length, *r*, determined from the number of segments required to form a hard sphere chain with the same molecular volume as the convex hard body, V_{CB}:

$$r = \frac{V_{cb}}{\pi\sigma^3/6} \qquad 5.79$$

The various fitted parameters are listed in Table 5.4.

Table 5.3 Geometric functionals for the hard convex bodies.

Hard Body	R_{CB}	S_{CB}	V_{CB}
prolate spherocylinder	$\frac{1}{4}[\gamma+1]\sigma$	$\gamma\pi\sigma^2$	$(3\gamma-1)\pi\sigma^3/12$
prolate ellipsoid	$\frac{1}{4}\left[\lambda+\frac{\ln\left[\lambda+\sqrt{\lambda^2-1}\right]}{\sqrt{\lambda^2-1}}\right]\sigma$	$\frac{1}{2}\left[1+\frac{\lambda^2\arccos\lambda^{-1}}{\sqrt{\lambda^2-1}}\right]\pi\sigma$	$\pi\lambda\sigma^3/6$

From Figure 5.2 it is clear that the proposed models are indeed flexible enough to represent other non-spherical geometries. The fitted parameters listed in Table 5.4 appear to be realistic, with the hard convex bodies that deviate more from the spherical geometries requiring larger *r* and *c* values to represent the phase behaviour. The effective segment diameters determined for the *simple-SAFT* and *simple-PHSC* models, which have the same underlying geometric structure, are comparable, indicating that the model parameters were not subjected to unrealistic distortions.

Table 5.4 Fitted chain parameters of proposed models.

		Prolate Spherocylinder		Prolate Ellipsoid	
		γ = 2	γ = 3	λ = 2	λ = 3
Simple-SAFT	**r**	1.25	1.60	1.17	1.63
	σ	1.26	1.36	1.20	1.23
Simple-PHSC	**r**	1.32	1.80	1.22	1.80
	σ	1.24	1.31	1.18	1.18
Simple PHCT	**c**	1.17	1.43	1.18	1.48

5.4.4 Normal-alkane representation

In the investigation of the ability of the proposed models to represent the n-alkane homologous series, the models were fitted to the relevant *P-v-T* data by adjusting the three equation of state parameters to simultaneously reduce saturated vapour pressure and fluid volume error and thus incorporating the representation of different thermodynamic properties in the data fitting procedure ensures the regression of realistic equation of state parameters as discussed in section 8.3. For the *simple-SAFT* and *simple-PHSC* the v_{00}, ε_0/k and *r* parameters were fitted to the data whilst the rv_{00}, $q\varepsilon_0'/k$ and *c* parameters were adjusted in the *simple-PHCT*. Most of the successful chained equations of state are able to represent the fluid systems with only three regressed parameters [60, 100, 200]. In keeping with this approach the μ/k parameters were not regressed along with the other parameters and unless explicitly stated otherwise the following values were used to account for the temperature dependent London energies: μ/k=1 for methane [42] and μ/k = 10 per n-alkane segment (or surface area) as proposed by Huang and Radosz [100]. The fitted *EOS* parameters are listed in Table 5.5 and Table 5.6.

Table 5.5 Fitted equation of state parameters for unconstrained *simple-SAFT*, *simple-PHSC* and *simple-PHCT* equations of state.

	Simple-SAFT			Simple-PHSC			Simple-PHCT		
	r	v_{oo} [m^3/mol]	ε_0/K [K^{-1}]	r	v_{oo} [m^3/mol]	ε_0/K [K^{-1}]	c	rv_{oo} [m^3/mol]	$q\varepsilon_0'$/K [K^{-1}]
C_2H_6	1	1.970E-05	190.0	1	1.970E-05	190.0	1	1.970E-05	190.0
n-C_3H_8	1.57	1.748E-05	220.8	1.16	1.924E-05	222.7	1.26	2.776E-05	343.3
n-C_4H_{10}	1.93	1.888E-05	240.1	2.09	2.118E-05	240.2	1.43	3.647E-05	456.1
n-C_5H_{12}	2.39	1.865E-05	246.4	3.10	2.240E-05	250.7	1.59	4.555E-05	564.8
n-C_6H_{14}	3.14	1.613E-05	235.9	3.73	2.103E-05	244.4	1.80	5.408E-05	680.3
n-C_7H_{16}	3.95	1.417E-05	228.4	3.62	1.703E-05	222.4	2.03	6.113E-05	802.0
n-$C_{16}H_{34}$	4.64	1.332E-05	227.1	3.75	1.767E-05	228.3	2.14	6.699E-05	893.6
n-$C_{20}H_{42}$	7.52	2.075E-05	265.1	8.07	2.708E-05	263.6	4.07	1.659E-04	1884.5
n-$C_{28}H_{38}$	10.22	1.829E-05	252.6	10.46	2.404E-05	249.3	5.12	2.035E-04	2377.2
n-$C_{32}H_{66}$	16.18	1.510E-05	236.4	15.23	1.971E-05	230.2	7.18	2.767E-04	3350.4
n-$C_{36}H_{74}$	19.87	1.381E-05	227.7	17.74	1.845E-05	222.9	8.24	3.147E-04	3839.6

Table 5.6 Fitted equation of state parameters for constrained *simple-SAFT*, *simple-PHSC* and *simple-PHCT* equations of state.

	Simple-SAFT-ltd			Simple-PHSC-ltd			Simple-PHCT-ltd		
	r	v_{oo} [m^3/mol]	ε_0/K [K^{-1}]	r	v_{oo} [m^3/mol]	ε_0/K [K^{-1}]	c	rv_{oo} [m^3/mol]	$q\varepsilon_0'$/K [K^{-1}]
C_2H_6	1	2.299E-05	190.2	1	2.299E-05	190.2	1	2.299E-05	190.2
n-C_3H_8	1.96	1.522E-05	186.6	1.57	3.126E-05	286.8	1.09	3.400E-05	312.0
n-C_4H_{10}	2.61	1.451E-05	192.3	1.93	3.359E-05	328.7	1.31	4.402E-05	430.7
n-C_5H_{12}	3.11	1.493E-05	201.6	2.39	3.474E-05	358.5	1.54	5.356E-05	552.7
n-C_6H_{14}	3.73	1.453E-05	203.5	3.14	3.524E-05	378.7	1.78	6.269E-05	673.6
n-C_7H_{16}	4.32	1.424E-05	205.5	3.95	3.483E-05	393.3	2.02	7.042E-05	795.0
n-$C_{16}H_{34}$	4.79	1.414E-05	210.8	4.64	3.409E-05	411.1	2.23	7.594E-05	915.7
n-$C_{20}H_{42}$	9.45	1.761E-05	218.5	7.52	4.511E-05	468.8	4.05	1.829E-04	1900.6
n-$C_{28}H_{38}$	12.22	1.653E-05	213.3	10.22	4.303E-05	466.3	5.18	2.230E-04	2417.1
n-$C_{32}H_{66}$	18.06	1.497E-05	206.4	16.18	3.895E-05	457.2	7.68	2.992E-04	3512.0
n-$C_{36}H_{74}$	21.07	1.457E-05	203.5	19.87	3.651E-05	445.7	9.30	3.394E-04	4142.8

5.4.4.a Second virial coefficient modelling

As shown in section 5.4.3, the proposed models are able to satisfactorily represent the thermodynamic phase behaviour of the hard sphere chained fluid that forms the basis of the *perturbation* expansion. In this section the ability of the equations of state to represent the *virial* expansion of chained systems will be determined, by investigating the ability of the proposed models to represent the second virial coefficient of normal alkanes.

Because of the low vapour pressures of the heavy n-alkanes the determination of accurate virial coefficients is very difficult and the reported values of heavier n-alkanes very limited. The of ethane and hexane second virial coefficients as reported by Dymond and Smith [64] are used in this study. It should be noted that the virial coefficients data were not included in the determination of the equation of state parameters. Furthermore the functional form of the *simple-SAFT* and *simple-PHSC* second virial coefficient expressions are identical, and any difference in the predicted coefficients will be solely due to the differences in the regressed parameters.

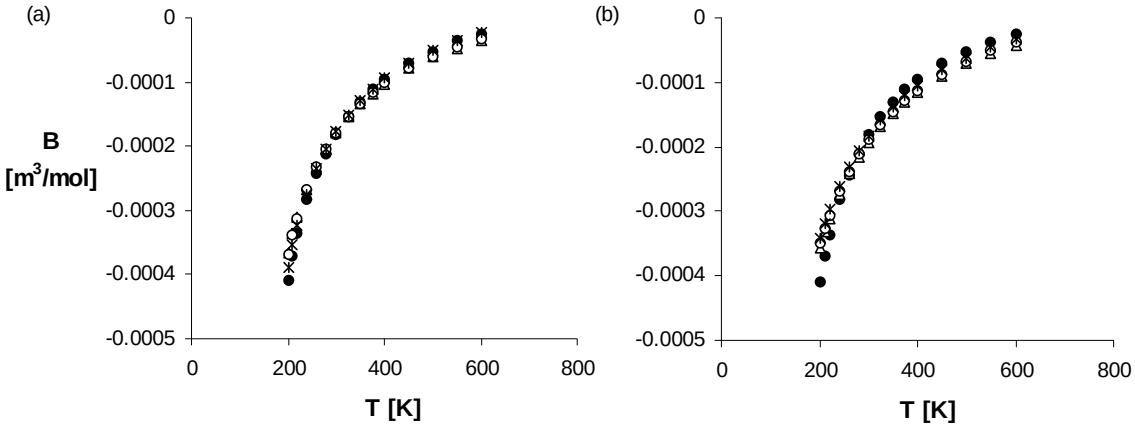

Figure 5.3 Ethane second virial coefficients as represented by proposed chained models using (a) the unconstrained and (b) the constrained perturbation. ● Published virial coefficients [64], △ *simple-SAFT*, ○ *simple-PHSC* and ✱ *simple-PHCT*

In Figure 5.3 the second virial coefficients of ethane as represented by the proposed models are plotted. As can be seen from Table 5.5 and Table 5.6, the ethane molecular structure is modelled by all the equations with the possible exception of the *simple-SAFT-ltd EOS* as not deviating much from a spherical particle, and from the predicted virial coefficients it is clear that the all the proposed models are able to represent the correct virial coefficient behaviour. The effect of constraining the perturbation parameter matrix to represent the virial coefficient contribution of the perturbation expansion with a linear function in density (D_{n1} = 0 for all

n>1) can be seen in Figure 5.3 (b), with slightly larger errors in the low and high temperature regions.

Figure 5.4 is a plot of the hexane second virial coefficients. Here the effect of the non-spherical structure is more obvious. The second virial coefficients as predicted by the original *SAFT* equation as proposed by Huang and Radosz [100] are also included in the plot to provide insight into the ability of the more complex chained equations of state using the Carnahan Starling [32] hard sphere reference term and the original double summation perturbation of Chen and Kreglewski [42].

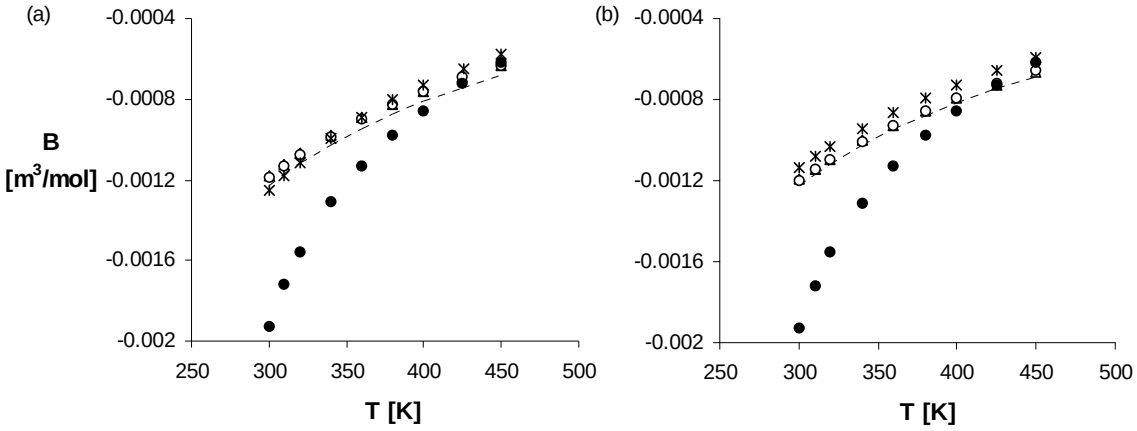

Figure 5.4 Hexane second virial coefficients as represented by proposed chained models using (a) the unconstrained and (b) the constrained perturbation. ● Published virial coefficients [64], △ *simple-SAFT*, ○ *simple-PHSC*, ✱ *simple-PHCT*, _____ original *SAFT* [100]

From Figure 5.4 it can be seen that the simplification of the original *SAFT* equation of state did not significantly influence the ability of the *simple-SAFT* equation of state to represent the hexane second virial coefficients. It is also clear that all three proposed chaining methods are able to represent the virial coefficients with a comparable accuracy.

Upon closer inspection of Figure 5.4 (b) it appears as if the predicted virial coefficients of the *simple-SAFT-ltd* and *simple-PHSC* models have been merely shifted downwards to slightly lower values, whilst the slope of the *simple-PHCT-ltd* predicted values appears to have been altered slightly. There is however very little difference between the constrained and unconstrained proposed models. It therefore appears as if any effect that using the constrained perturbation parameter matrix might have had on the ability of the proposed models to represent the second virial coefficients of the chained system has been compensated for by the difference in the equation parameters determined for the constrained and unconstrained models (see Table 5.5 and Table 5.6).

5.4.4.b P-v-T behaviour

The results of the proposed equations of state using the optimum values listed in Table 5.5 and Table 5.6, are represented in Figure 5.5 and Figure 5.6 as plots of the average absolute percentage error in the saturated vapour pressure, saturated liquid and vapour volume and supercritical fluid volume of the n-alkane series.

The step change in the errors in the representation of the methane to heptane and hexadecane to hexatriacontane systems, as can be seen in Figure 5.5 (b), Figure 5.6 (b) and Figure 5.7, can be attributed to the fact that representation of the supercritical fluid volumes were included in the parameter regressions of the lighter components (methane to heptane) whilst only saturated data were used in the regression of the heavier n-alkane parameters.

From Figure 5.5 (a) and (b) it appears as if the *simple-PHCT EOS* is significantly more accurate in the representation of the heavier n-alkane systems (hexadecane and higher). This equation further appears to represent the saturated properties of the lighter alkanes more successfully than the *simple-SAFT* and *simple-PHSC* models, but is slightly less accurate that than these models in the supercritical phase. There is very little difference in the accuracy of the *simple-SAFT* and *simple-PHSC* models, with the *simple-PHSC* appearing on average result in slightly smaller errors overall. (This is in agreement with the observation by Feng et al. [71] in their study of the *SAFT* and *PHSC* square well models.)

Unfortunately with the constrained models (Figure 5.6) there is no model that is obviously superior in all the thermodynamic properties.

By comparing the results in Figure 5.6 (a) to those in Figure 5.5 (a) it can be seen that the *simple-PHCT-ltd* equation of state is less successful than the unconstrained model (*simple-PHCT*) in the representation of the saturated vapour pressures. The *simple-SAFT-ltd* model is significantly more accurate than the other models in the representation of the lighter alkane vapour pressures, whilst the *simple-PHSC-ltd* equation has the smallest heavy alkane vapour pressure errors.

It is furthermore apparent that the constrained models in fact result in an improvement in the representation of the saturated liquid volumes. (See Figure 5.5(b), Figure 5.6(b) and Figure 5.7.) This is in agreement with the observations made in Chapter 4 where the 3x3 *HS3CK* and 3x3*HS3CK ltd. e*quations were fitted to the argon and methane *P-v-T* data. The *simple-PHCT-*

ltd equation as with the unconstrained models, provides the most accurate representation of the heavy alkane systems liquid volumes.

Furthermore, from the representation of the lighter alkane saturated vapour and supercritical fluid volumes in Figure 5.6 (c) and (d) it appears as if the *simple-SAFT-ltd* and the *simple-PHCT-ltd* models perform better that the *simple-PHSC-ltd* equation.

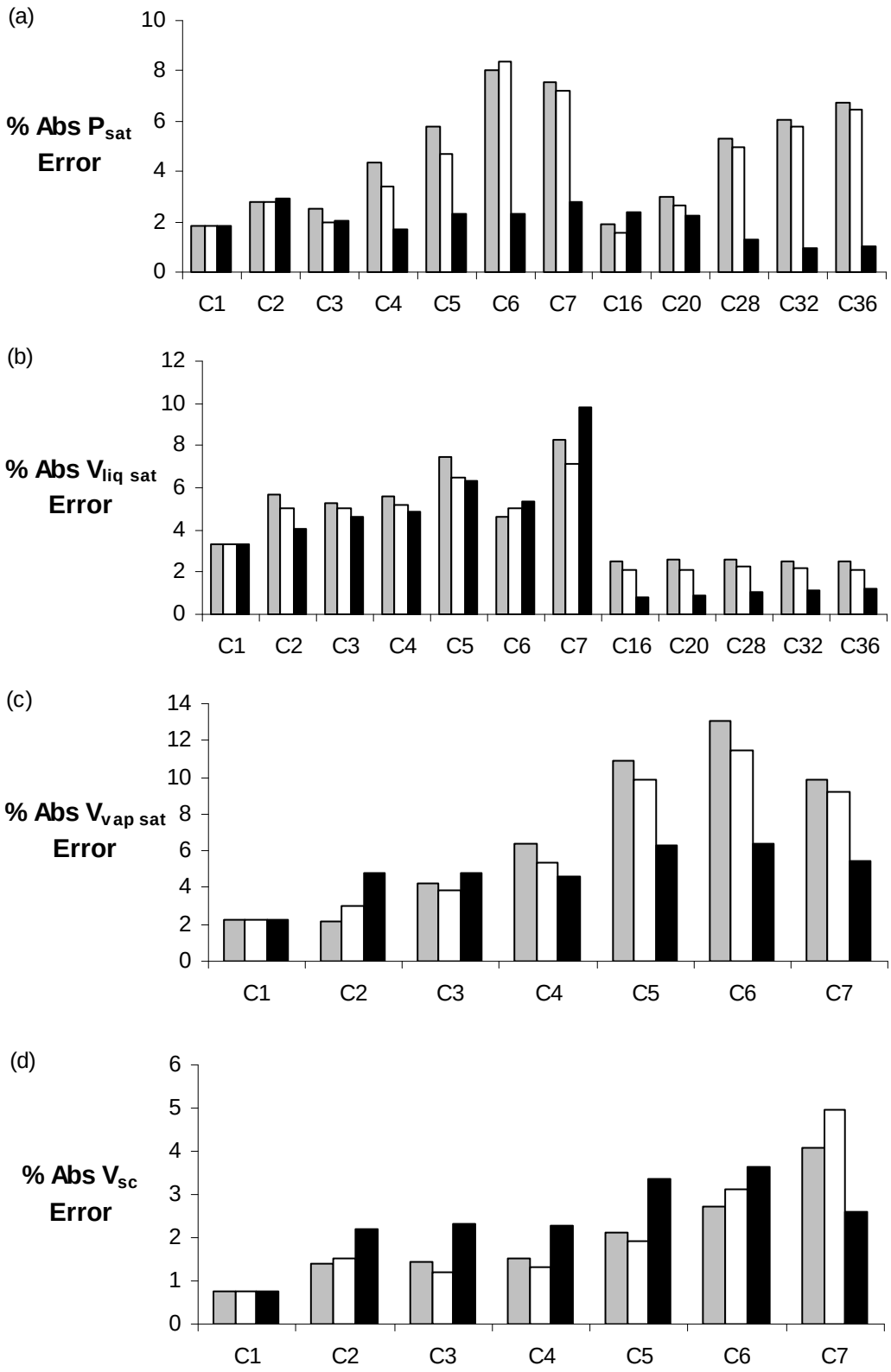

Figure 5.5 Absolute % errors in the representation for the n-alkane homologous series by the unconstrained models. (a) vapour pressure, (b) saturated liquid volume, (c) saturated vapour volume and (d) supercritical fluid volume. ▒ *simple-SAFT*, □ *simple-PHSC* and ■ *simple-PHCT*

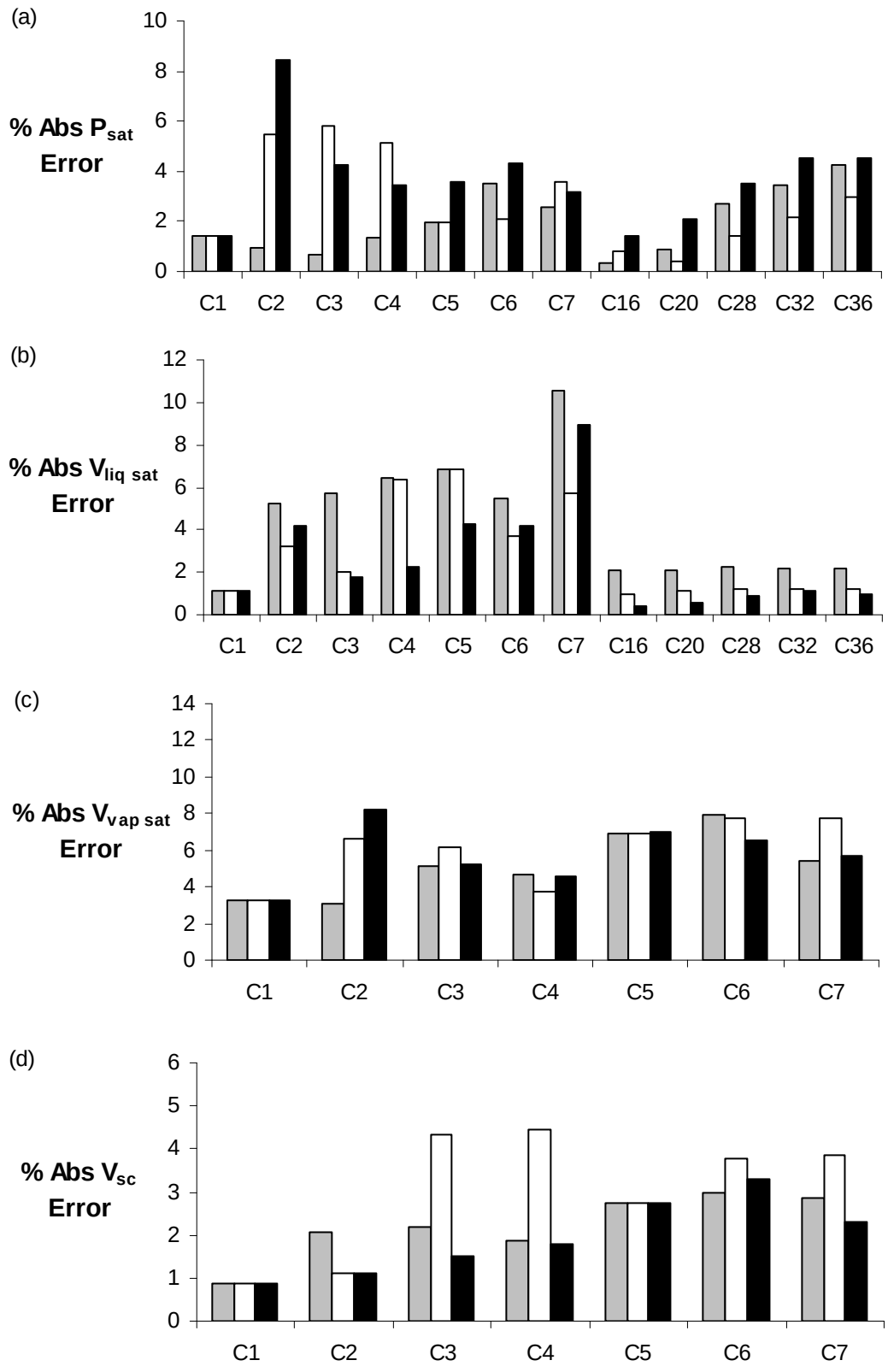

Figure 5.6 Absolute % errors in the representation for the n-alkane homologous series by the constrained models. (a) vapour pressure, (b) saturated liquid volume, (c) saturated vapour volume and (d) supercritical fluid volume. ■ *simple-SAFT-ltd,* □ *simple-PHSC-ltd* and ■ *simple-PHCT-ltd*

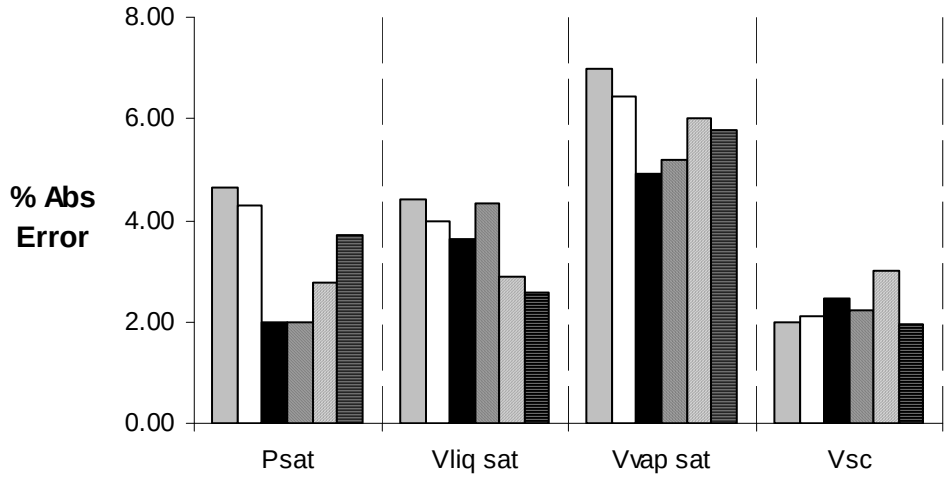

Figure 5.7 Avereage absolute % errors of the n-alkane systems investigated. . ▒ *simple-SAFT,* □ *simple-PHSC,* ■ *simple-PHCT, .* ▪ *simple-SAFT-ltd,* ▫ *simple-PHSC-ltd* and ▒ *simple-PHCT-ltd*

The comparison between the various proposed models is further facilitated in Figure 5.7, which is a plot of the average absolute percentage deviations over the alkane components investigated. From this figure it is clear that the *simple-PHCT* equation is the most promising unconstrained equation of state with the smallest average error the vapour pressure and saturated liquid and vapour volumes, with only a slightly larger average error in the supercritical phase.

From the constrained equations a choice has to be made between the *simple-SAFT-ltd* equation with a small average error in the saturated pressure and vapour volume, and the *simple-PHCT-ltd* model which is more accurate in the liquid and supercritical fluid volumes.

5.4.4.c Temperature dependence of dispersion energies

Up to this point all the proposed models were fitted using a value of μ/k=10 to account for the temperature dependent part of the London interaction energies in equation 4.97. This convention has been applied to many proposed chained models [4, 41, 100]. In this section the validity of setting μ/k=10 for n-alkane segments will be investigated. For each model the three sets of equation of state parameters were regressed using μ/k=10, μ/k=5 and μ/k=0. For the non-polar n-alkane series a decreasing μ/k value would imply a decrease in the need to account for non-spherical London attractive forces per segment.

The average of the absolute % errors of the entire n-alkane under investigation are listed in Table 5.7 and Table 5.8.

Table 5.7 Average absolute % errors over the n-alkane series for the unconstrained models with μ/k=10 and μ/k=0.

Average Absolute % Errors									
	Simple-SAFT			**Simple-PHSC**			**Simple-PHCT**		
	μ/k=10	μ/k=5	μ/k=0	μ/k=10	μ/k=5	μ/k=0	μ/k=10	μ/k=5	μ/k=0
$\mathbf{P_{sat}}$	4.90	5.21	4.77	4.54	4.55	4.53	2.00	1.97	1.94
$\mathbf{v_{sat\ liq}}$	4.51	4.60	4.72	4.05	4.15	4.32	3.65	3.89	4.18
$\mathbf{v_{sat\ vap}}$	7.77	8.42	8.05	7.12	7.26	7.43	5.39	5.43	5.46
$\mathbf{v_{sc}}$	2.21	2.58	2.20	2.34	2.23	2.32	2.74	2.80	2.88
Total	**19.40**	**20.80**	**19.75**	**18.05**	**18.19**	**18.60**	**13.78**	**14.09**	**14.47**

From the error values in Table 5.7 it appears a decreasing the μ/k has an overall detrimental effect on the performance of the unconstrained models. By setting μ/k =0 a slight improvement in the overall average vapour pressure representation may be obtained but this effect is offset by an increasing error in the saturated fluid volumes.

The effect on the μ/k on the constrained models is illustrated in Table 5.8. Here again although using μ/k=5 leads to a slight decrease in average errors in vapour pressure as determined with the *simple-SAFT-ltd* and *simple-PHSC-ltd* models, using a smaller value for μ/k results in an overall decrease in the performance of the models.

Table 5.8 Average absolute % errors over the n-alkane series for the constrained models with μ/k=10 and μ/k=0.

Average Absolute % Errors										
	Simple-SAFT-ltd			**Simple-PHSC-ltd**			**Simple-PHCT-ltd**			
	μ/k=10	μ/k=5	μ/k=0	μ/k=10	μ/k=5	μ/k=0	μ/k=10	μ/k=5	μ/k=0	μ/k=1
$\mathbf{P_{sat}}$	2.06	1.95	2.62	2.89	2.53	2.93	3.94	3.30	2.73	2.83
$\mathbf{v_{sat\ liq}}$	4.64	4.91	4.65	3.06	3.49	3.88	2.69	2.79	3.23	3.12
$\mathbf{v_{sat\ vap}}$	5.52	5.65	6.97	6.48	6.43	8.15	6.21	5.55	5.04	5.12
$\mathbf{v_{sc}}$	2.45	2.58	2.54	3.37	3.52	3.19	2.13	2.30	2.50	2.46
Total	**14.67**	**15.08**	**16.78**	**15.81**	**15.98**	**18.14**	**14.97**	**13.93**	**13.49**	**13.53**

From the results listed in Table 5.8 it is however apparent that the overall performance of the *simple-PHCT-ltd* model can be significantly improved by using a smaller μ/k value. The results of the parameter regression with μ/k=1 are also included in the table, as this is the value

for methane as suggested by Chen and Kreglewski [42]. As can be seen using this value for μ/k does not significantly decrease the overall accuracy of the model compared to using μ/k =0 and has the added advantage that the same μ/k value can be used for the entire n-alkane homologous series.

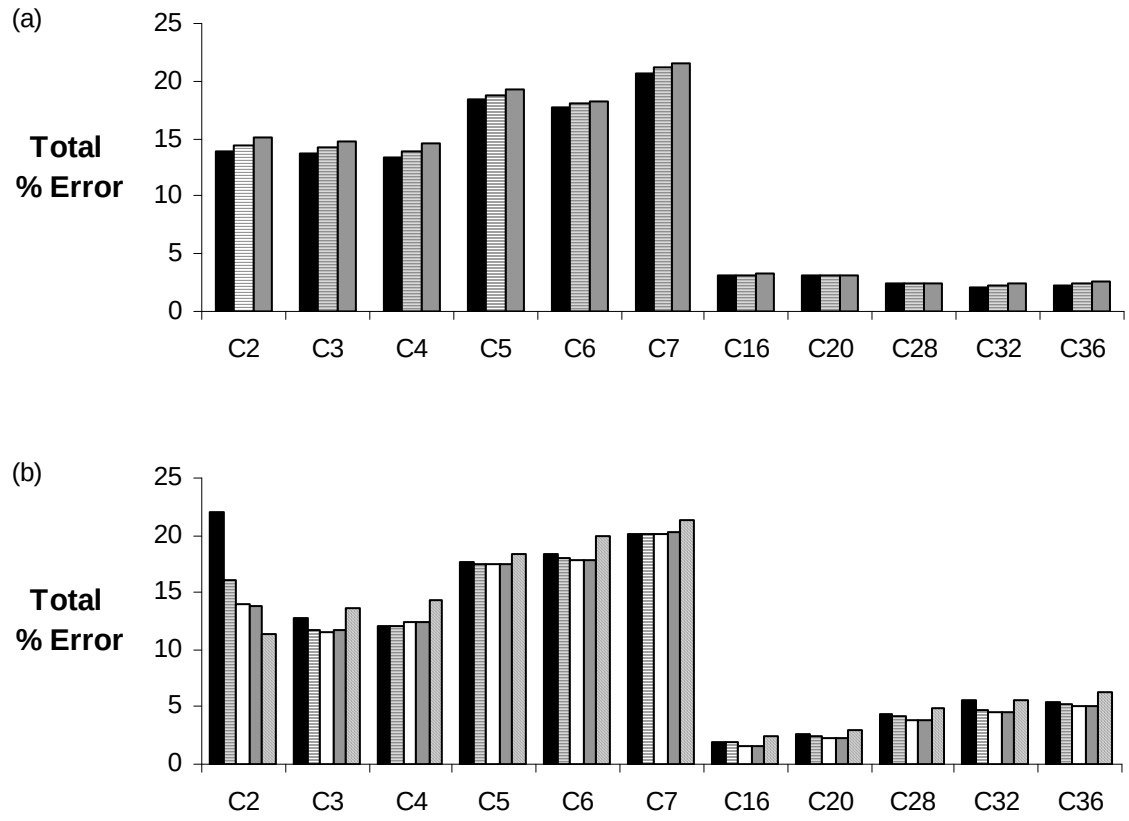

Figure 5.8 Total errors for the n-alkane series as determined with the (a) *simple-PHCT* (b) *simple-PHCT-ltd* with ■ μ/k = 10, ▩ μ/k = 5 ,□ μ/k = 1 ▩ μ/k = 0 and ▩ *simple-SAFT-ltd* (μ/k = 10)

Figure 5.8 is a plot of the total errors in the representation of the n-alkane series, as determined with the *simple-PHCT* and the *simple-PHCT-ltd* equations using the various proposed values for the μ/k parameter. Form Figure 5.8 (a) it is clear that the *simple-PHCT* equation of state is not very sensitive to the actual value of the μ/k parameter, but the general increase in the error with a decreasing μ/k as observed in Table 5.7 can still be detected. Similar trends were observed for the *simple-SAFT* and *simple-PHSC* models.

It is also apparent that the significant improvement in the *simple-PHCT-ltd* model performance can mostly be attributed to the large decrease in the total error of the ethane system when using μ/k values smaller than 10 (Figure 5.8 (b)). The overall model performance can be seen to be

relatively insensitive to whether $\mu/k = 5$, $\mu/k = 1$ or $\mu/k = 0$ is used. (This can also be seen from the total average error values in Table 5.8.).

The results of the *simple-SAFT-ltd EOS* with $\mu/k = 10$ are also included in Figure 5.8 (b) for comparative reasons. It can be seen that the *simple-PHCT-ltd* using the smaller μ/k values consistently outperforms the optimum *simple-SAFT-ltd* model except in the representation of the ethane fluid system. The small error value of the *simple-SAFT-ltd* model for the ethane system can be mainly attributed to the exceptionally good representation of the ethane saturated vapour pressure and volume in comparison to the other proposed models (Figure 5.6 (b) and (d)). These accurate results are however not consistent over the entire n-alkane homologous series, resulting in the comparatively poorer performance of the *simple-SAFT-ltd* model to the *simple-PHCT-ltd* equation with $\mu/k \neq 10$ over the remainder of the n-alkane series.

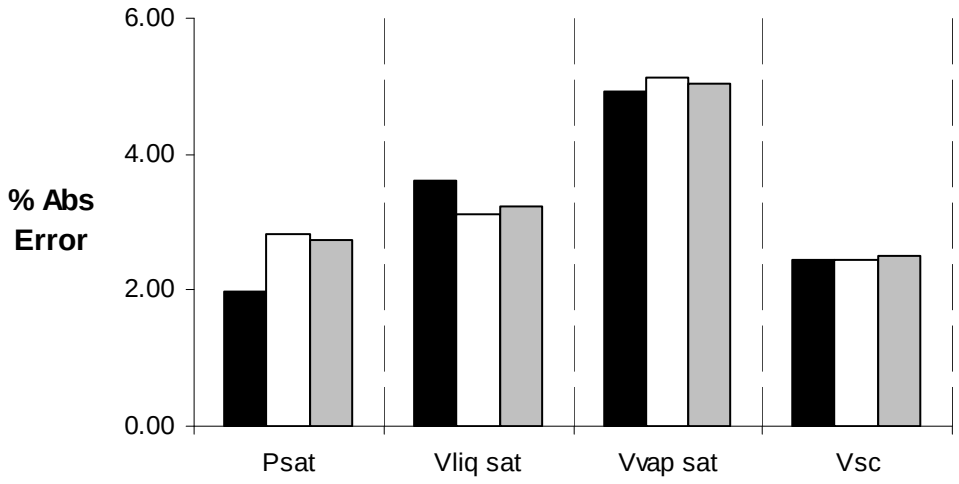

Figure 5.9 Average absolute % errors of the n-alkane systems as determined using the ■ *simple-PHCT* (μ/k = 10) □ *simple-PHCT-ltd* (μ/k = 1) and ▒ *simple-PHCT-ltd* (μ/k = 0) models

Figure 5.9 is a comparison between the performance of the optimal *simple-PHCT* and *simple-PHCT-ltd* models. It can be seen that the major advantage of the unconstrained model is the high accuracy of the vapour pressure presentation, whilst as has been observed before, the constrained models result in an improved saturated liquid volume representation.

5.4.4.d The Generalization of the equation parameters

It is important that the equation of state parameters display a simple relationship with a characteristic feature of the homologous series in order to facilitate the interpolation of the

parameters to enable the estimation of the equation of state parameters without the regression of any experimental data. In this study it is also especially important that there should be a high degree of confidence in the parameter behaviour to enable the extrapolation of parameter values because of the lack of accurate vapour pressure data of the heavy n-alkanes suitable for parameter regression.

The various equation of state parameters are plotted against the n-alkane molecular weight in Figure 5.10 - Figure 5.15. The parameter values of the *simple-PHCT-ltd* model determined for μ/k = 0 and μ/k = 1 are shown. (In these figures the two sets of *simple-PHCT-ltd* parameter values are virtually indistinguishable, whilst in Figure 5.12 the *simple-SATF-ltd* and both sets of *simple-PHCT-ltd* parameters lie on top of each other.)

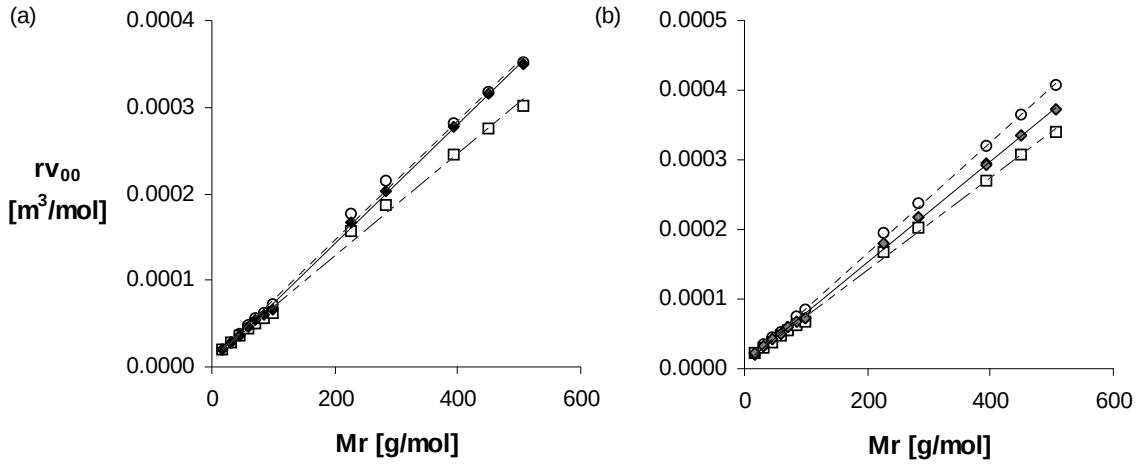

Figure 5.10 The regressed molecular volume, rv_{00}, as a function of n-alkane molecular weight, for the (a) unconstrained and (b) constrained equations. □ *simple-SAFT* (–·–·– trend line), ○*simple-PHSC* (– – – – – trend line) and ◆, *simple-PHCT* (μ/k=10), ◇ *simple-PHCT-ltd* (μ/k=0) and ◇ *simple-PHCT-ltd* (μ/k=1) (——*simple-PHCT* trend line in (a) and(b))

From Figure 5.10, Figure 5.11 and Figure 5.12 it can be seen that the required parameters of all proposed models display a linear relationship with the n-alkane molecular weight.

The molecular properties of the *simple-SAFT* and *simple-PHSC* equations are plotted as they are expected to increase with the molecular chain length, whilst the segment volume and energy terms, v_{00} and ε_0, are expected to stay fairly constant, especially with the larger n-alkanes where effect of the difference in the end, CH_3–, and internal, –CH_2–, building blocks become negligible due to the large number of internal carbon atoms. (See Figure 5.13).

The *r* parameter for the *simple-PHCT* and *simple-PHCT-ltd* was determined by approximating a segment volume as being equal to the methane molecular volume ($r = rv_{00}/(rv_{00})_{methane}$).

Methane was chosen as the segment volume in order to ensure that $r = 1$ for methane as this value was enforced on the other two models. The various *EOS* parameters will therefore be evaluated on the same scale. (In the next chapter the effect of using different segment volumes will be investigated.) It can be seen that the chain length determined in this way is of the same order of magnitude as the fitted parameters for the *simple-SAFT* and *simple-PHSC* models.

From the various graphs it appears as if the constrained *simple-SAFT-ltd* and the *simple-PHSC-ltd* model parameters have a slightly improved linear behaviour with less scatter than the unconstrained versions, which will be advantageous in the parameter generalization. The *simple-PHCT* parameters are already well behaved and no additional improvement in the parameter behaviour of *simple-PHCT-ltd* equation can be seen.

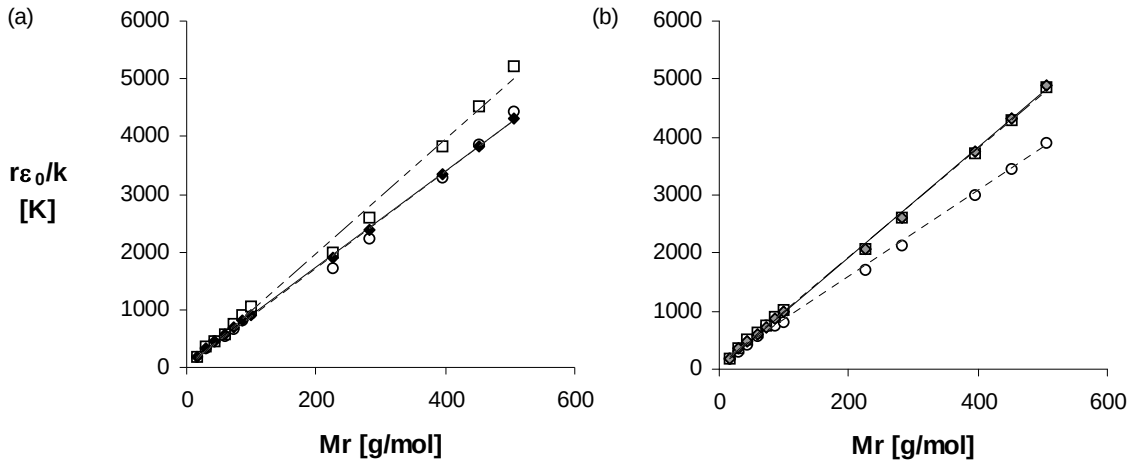

Figure 5.11 The regressed molecular energy parameter, $r\varepsilon_0$/k or $q\varepsilon_0$'/k, as a function of n-alkane molecular weight, for the (a) unconstrained and (b) constrained equations. With legend as defined in Figure 5.10

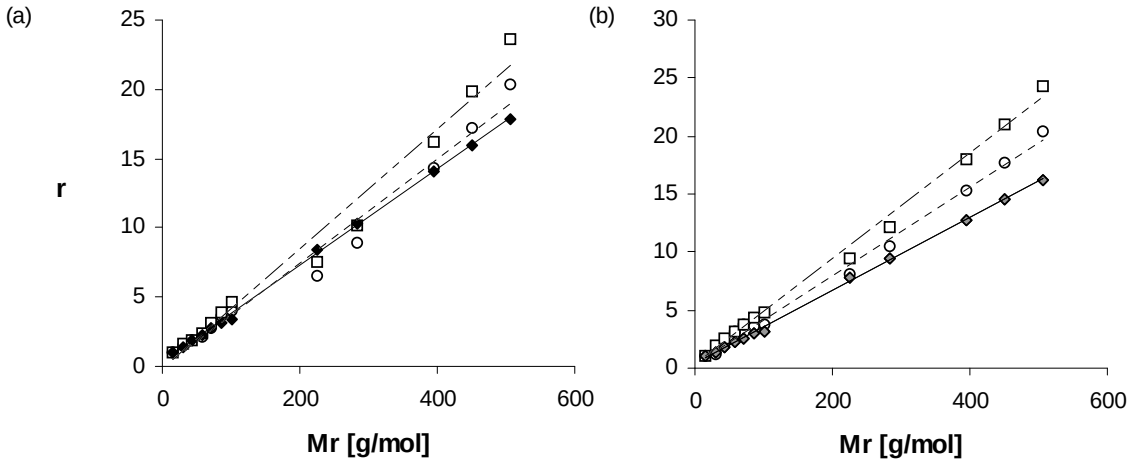

Figure 5.12 The regressed segment parameter, *r*, function of n-alkane molecular weight, for the (a) unconstrained and (b) constrained equations. With legend as defined in Figure 5.10

Figure 5.12 depicts the relationship of the chain length with the alkane molecular weight. The deviations of the hexadecane and eicosane chain length parameters for the *simple-SAFT* and the *simple-PHSC* coincide with the large segment volumes and energy terms as depicted in Figure 5.13. As mentioned before, the effective segment length of the *simple-PHCT* models display a linear dependence on the hydrocarbon molecular weight, similar to the *simple-SAFT* and *simple-PHSC* models, with the *simple-PHCT-ltd* chain length parameters having a much smaller slope than that of the other models when plotted on an identical scale. This is especially encouraging since as observed by Adidharma and Radosz [6], in their study of square well statistical association fluid theory, parameters with a smaller dependence on the component molecular weight will lead to better mixture behaviour as the differences between the parameters values will be smaller and hence require simpler mixing rules.

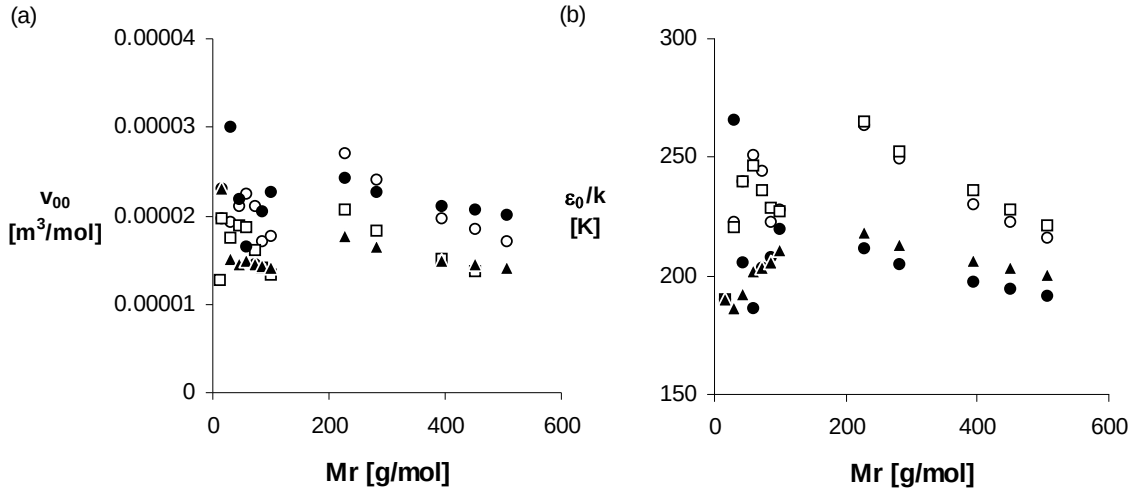

Figure 5.13 (a) Segment volume, v_{00}, and (b) Segment energy, ε_0/k, terms of the □ *simple-SAFT,* ○ *simple-PHSC,* ▲*simple-SAFT-ltd* and ◆ *simple-PHSC-ltd* models as a function of molecular weight.

Figure 5.13 depicts the segment properties for the n-alkanes as fitted directly by the *simple-SAFT* and *simple-PHSC* models. A considerable amount of scatter can be observed for the segment values at the lower molecular weights. It is however clear that the constrained parameters (the solid symbols) of both models are generally more well-behaved and coincides with the improvement in the performance of the modes as discussed in section 5.4.4.b. It is also encouraging to note that the constrained segment parameter values display a much smaller dependence on the heavy alkane molecular weight as these values are theoretically expected to be constant. The residual dependence on molecular weight can be attributed to the fact that both the segment parameters were allowed to vary freely during the parameter regression.

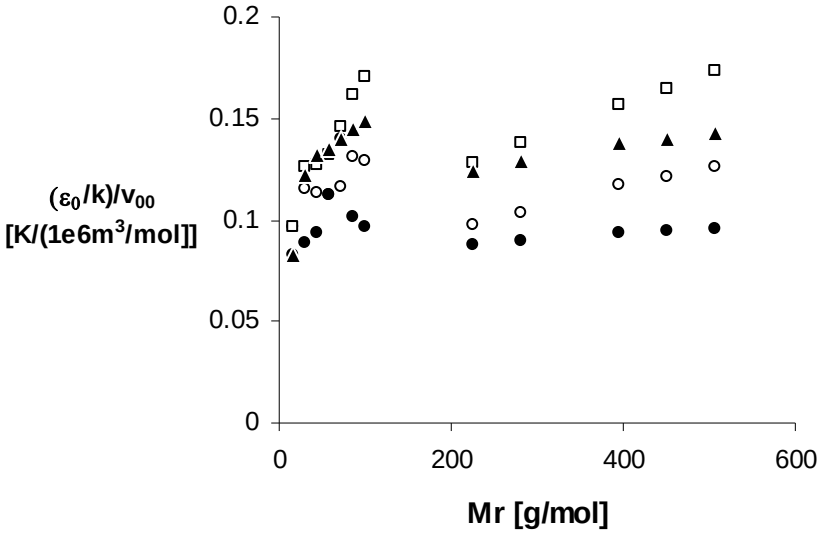

Figure 5.14 Scaled segment energy as a function of molecular weight. With legend as defined in Figure 5.13.

When the reduced segment energy, the energy contribution per segment volume ($\varepsilon_0/k/v_{00}$) is plotted against the alkane molecular weight in Figure 5.14, it can be seen the parameters of the constrained models to do in fact display the expected correct trends, although the heavy alkane parameter of unconstrained models are still dependent on the n-alkane molecular weight.

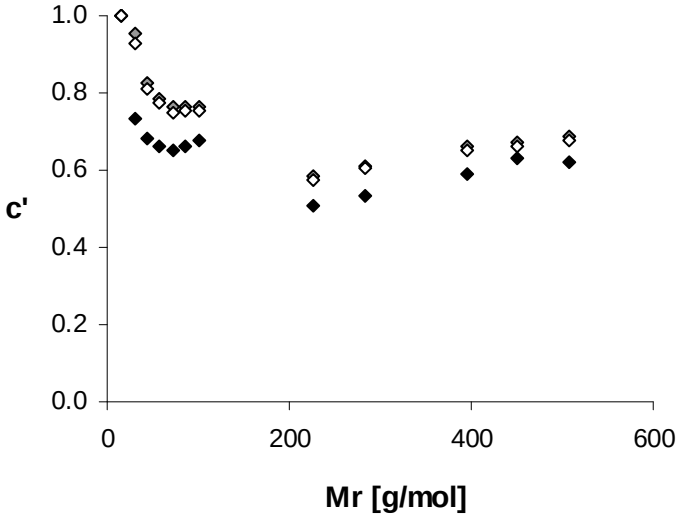

Figure 5.15 External degree of freedom contribution per segment vs. molecular weight. ◇ *simple-PHCT*, ◆ *simple-PHCT-ltd*.

Figure 5.15 is a plot of the effective contribution to the external degrees of freedom per segment, *c'*, where *c=rc'*. As the molecules become large enough that the difference between the end and internal carbon CH_3– and $–CH_2$– groups become negligible, the addition of each successive segment adds a constant value to the external degrees of freedom of motion, which

is as expected due to the similar strengths of the bonds between the carbon groups throughout the entire the homologous series. Out of all the plots of the parameter values, the effect of using different μ/k values can only be observed in the *c'* values, and even here is only really significant at the lower molecular weights.

5.5 SUMMARY AND CONCLUSIONS

In this section three methods to extend the proposed *HS3CK* equation of state for spherical molecules to non-spherical and specifically chainlike systems were investigated. These methods, the Statistical Associating Fluid Theory, the Perturbed Hard Sphere Chain model and the Perturbed Hard Chain Theory, were used to develop the *simple-SAFT*, *simple-PHSC* and the *simple-PHCT* equations of state. The *simple-SAFT* model reduces to a polynomial that is a 7^{th} order function in density, whilst the other two proposed models reduce to 5^{th} order density functions.

It has been shown that all three proposed models are able to represent the computer generated hard sphere chain phase behaviour. The *simple-PHCT*, through the use of a simple estimation of the external degrees of freedom of the hard sphere chain, was found to accurately represent the simulation results at high densities, whilst the *simple-PHSC* and *simple-SAFT* models are more accurate at the lower system densities. In a direct comparison of the abilities of the *simple-PHSC* and the *simple-SAFT* models to represent pure hard sphere chained systems, the latter model has been found to be more accurate over a wider density range.

During the evaluation of the performance of the various models in representing the real n-alkane homologous series, it was found that as the n-alkane chain length is increased, the ability of the proposed models to represent the virial coefficients at the lower temperatures become less accurate. This loss in accuracy however cannot be attributed to the simple structure of the proposed models but are rather inherent to the techniques used to account for the deviations from the spherical structure, as mathematically, the second virial coefficients of the proposed models are nearly identical to the more complex *SAFT* equation of state proposed by Huang and Radosz [100].

The two different chaining approaches, that of accounting for the rotational and vibrational density dependence through the concept of an increased external degree of freedom of motion, in the *simple-PHCT*, that of accounting for the Helmholtz energy contribution due to the chain

formation used in the *simple-SAFT* and *simple-PHSC* models, are both able to represent the n-alkane second virial coefficients to a similar degree of accuracy.

Furthermore it was found that the restrictive effect of constraining the perturbation matrix to represent the attractive contribution as linear in density has sufficiently been compensated for by the actual equation of state parameters, and no detrimental effect could be observed on the modelling of the second virial coefficients.

Upon the investigation of the ability of the regressed models to represent the n-alkane saturated pressure and fluid volumes of the *simple-PHCT* was found to provide the most consistently accurate results in both the constrained and unconstrained forms. It was however shown that the *simple-PHCT-ltd* model parameters need to be regressed using a μ/k parameter smaller than 10 as commonly used in the literature. It was found that there is very little difference between the overall model performance and the actual values of the regressed parameters when using either $\mu/k = 0$ or $\mu/k = 1$ in the *simple-PHCT-ltd* model. Setting $\mu/k = 1$ however is preferable because this enables the entire homologous series including methane to be modelled using the same parameter.

It was also shown that the equation of state parameters of both the *simple-PHCT* models as well as the constrained *simple-SAFT-ltd* and *simple-PHSC-ltd* model parameters display the expected dependence on the n-alkane molecular weight, which would greatly facilitate the generalization of the model parameters.

Because of its optimal performance in the representation of the n-alkane *P-v-T* data and the nature of the required equation parameters the *simple-PHCT* will be used throughout the remainder of this study to represent the real fluid phase behaviour. The effect of the reduced accuracy in the pure component vapour pressure versus possible advantages of simple theoretically correct mixing rules when using the *simple-PHCT-ltd* model needs to be investigated further before a choice can be made between the two versions of the model.

Chapter 6 ***Mixtures and Mixing Rules***

One of the strengths of using equations of state to represent the thermodynamic fluid properties lies in the fact that the same model may be used to describe pure fluid and fluid mixture systems.This is generally accomplished by determining the relevant equation of state parameters for the mixture fluid from those of the individual mixture components.

In this chapter the proposed *simple-PHCT* and *simple-PHCT-ltd* equations developed in the previous chapter will be extended to represent fluid mixtures. Various mixing rules used to determine the mixture equation of state parameters will be investigated to determine the most suitable method to provide accurate mixture properties whilst still maintaining the computational simplicity and speed.

6.1 OVERVIEW OF APPROACHES TO MIXTURES

The theory regarding the representation of fluid mixtures by equations of state is not nearly as extensively developed as that of the pure fluid systems and most of the mixture equations of state are to some degree empirical [190].

In this section an overview of some of the approaches towards mixtures will be given. There will be mainly focussed on the most important and generally applied concepts in the mixture theory, with some examples of the application thereof.

Generally a mixture fluid property, θ_m, is determined from a mixing rule such as:

$$\theta_m = \sum_{i=1}^{nc}\sum_{j=1}^{nc} x_i x_j \theta_{ij} \qquad 6.1$$

With x_i the mole fraction of component i in the mixture with $x_i = N_i/N$, nc the total number of species in the fluid and θ_{ij}, a combinatorial property determined from the pure component parameters, θ_i and θ_j through a combination rule such as:

$$\theta_{ij} = \frac{\theta_i + \theta_j}{2}\left(1 - l_{ij}\right) \qquad 6.2$$

Equation 6.2 implies that θ_{ij} is the arithmetic average of component *i* and *j*. The parameter, l_{ij}, is a binary interaction parameter that serves as a correction to the contributions of the two pure components to the mixture property.

6.1.1 Theoretically correct mixing rules

From a strictly theoretical basis an equation of state of a fluid mixture can be derived from the grand canonical ensemble (section 2.2.1, equation 2.15), however this would require a detailed knowledge of the mixture radial distribution function and the intermolecular potential between the different species. These properties are not known for real fluid systems and hence precludes the possibility of a purely theoretical model. It is however possible to determine the correct mixing rules and expressions for highly simplified or idealised systems, and these may serve as guidelines for the extension of the equations of state to real mixtures.

6.1.1.a Virial Equation of State

As discussed in section 2.3.1 the virial equations of state can be derived directly from the statistical mechanical theory, with each successive virial coefficient the result of the interaction of an increasing number of particles. From the derivation of the virial equation of state it follows directly that virial coefficients of the fluid mixture must have the following composition dependence:

$$B_{2\,m} = \sum_{i=1}^{nc}\sum_{j=1}^{nc} x_i x_j B_{2\,ij} \qquad 6.3$$

$$B_{3\ m} = \sum_{i=1}^{nc}\sum_{j=1}^{nc}\sum_{k=1}^{nc} x_i x_j x_k B_{3\,ijk} \qquad 6.4$$

etc.

Where $x_i=n_i/n$ is the mole fraction of component *i* in the mixture, *nc* the total number of species in the fluid, and $B_{2\,ij}$ and $B_{3\,ijk}$ the second and third interaction coefficients, determined through the evaluation of the Meyer function integrals of equations 2.67 and 2.68 for different components.

Although, as discussed in section 2.3.1, the virial equation of state cannot represent the real fluid behaviour at high densities, it is however able to successfully represent the gaseous or vapour phase behaviour at low system pressures and densities. The mixture virial coefficient composition dependence as depicted in equations 6.3 and 6.4 is therefore valid in this region and applicable to any equation of state applied under these conditions.

6.1.1.b Mixtures of Hard Spheres

As in the case for pure fluids, expressions for the radial distribution function for mixtures of hard spheres can be obtained through the direct correlation function. (See sections 2.3.2.c and 3.3.3) Lebowitz [124] obtained a solution of the *Percus-Yevic* equation for hard sphere mixtures. As in the case of the pure hard sphere fluids, this solution results in two slightly different equations of state when applied with the pressure or compressibility equations (equations 2.50 and 2.52):

$$z^p = \frac{\left(1+\eta+\eta^2\right)-3\eta\left(y_1+y_2\eta\right)-3\eta^3 y_3}{\left(1-\eta\right)^3} \qquad 6.5$$

$$z^c = \frac{\left(1+\eta+\eta^2\right)-3\eta\left(y_1+y_2\eta\right)}{\left(1-\eta\right)^3} \qquad 6.6$$

With

$$\eta'_i = \rho\frac{1}{6}\pi\sigma_i^3 \qquad 6.7$$

$$\eta = \sum_{i=1}^{nc} x_1\eta'_i \qquad 6.8$$

and

$$y_1 = \sum_{j>i=1}^{nc}\Delta_{ij}\frac{\sigma_i+\sigma_j}{\sqrt{\sigma_i\sigma_j}} \qquad 6.9$$

$$y_2 = \sum_{j>i=1}^{nc}\Delta_{ij}\sum_{k=1}^{nc}\frac{\eta'_k}{\eta}\frac{\sqrt{\sigma_i\sigma_j}}{\sigma_k} \qquad 6.10$$

$$y_3 = \left[\sum_{i=1}^{nc} x_i^{1/3} \left(\frac{\eta'_k}{\eta} \right)^{2/3} \right]^3 \qquad 6.11$$

and

$$\Delta_{ij} = \left(x_i x_j \right)^{1/2} \frac{\sqrt{\eta'_i \eta'_j}}{\eta} \frac{\left(\sigma_i - \sigma_j \right)^2}{\sigma_i \sigma_j} \qquad 6.12$$

Mansoori et al. [137] applied the relation (equation 3.21) between the two pure hard sphere Percus-Yevic equations and the Carnahan-Starling compressibility to the mixture equations, to derive expression for hard sphere mixtures that would reduce to the Carnahan-Starling equation of state for mixtures of identical spheres. Boublík independently developed an identical equation of state using the contact radial distribution function derived from the Scaled Particle Theory as starting point. The equation is referred to as the Boublík-Mansouri-Carnahan-Starling, *BMCS*, mixing rule:

$$z^{BMCS} = \frac{6}{\pi\rho} \left(\frac{\eta_0}{1-\eta_3} + \frac{3\eta_1\eta_3}{\left(1-\eta_3\right)^2} + \frac{\left(3-\eta_3\right)\eta_2^{\,3}}{\left(1-\eta_3\right)^3} \right) \qquad 6.13$$

with

$$\eta_k = \sum_{i=1}^{nc} x_i \rho \frac{1}{6} \pi \sigma_i^k \qquad 6.14$$

(Note the difference in the definitions of η'_k (equation 6.7) and η_k (equation 6.14) and that $\eta_3 = \eta$.)

6.1.1.c Perturbation expansion

Henderson [91] developed expressions for the first two perturbation expansion terms for mixtures of hard-spheres and square-well fluids with equal hard sphere diameters: (In the notation of section 4.3.4, equation 4.44)

$$\frac{A^{(1)}}{NkT} = \frac{\rho}{2} \left(\sum_{i=1}^{nc} \sum_{j=1}^{nc} x_i x_j \varepsilon_{ij} \right) I \qquad 6.15$$

With

$$I = \int_{\sigma}^{\infty} u'^{(1)}_{12}(x) g^{(0)}(x) \pi r^2 dr \qquad 6.16$$

where $u'^{(1)} = u^{(1)}/\varepsilon_2$ refers to the reduced perturbation energy and ε the attractive well depth.

The expression for the second perturbation term is significantly more complicated:

$$\frac{A^{(1)}}{NkT} = \frac{\rho}{4}\left(\sum_{i=1}^{nc}\sum_{j=1}^{nc} x_i x_j (\varepsilon_{ij})^2\right) J_1 - \frac{\rho^2}{2}\left(\sum_{i=1}^{nc}\sum_{j=1}^{nc}\sum_{k=1}^{nc} x_i x_j x_k \varepsilon_{ij}\varepsilon_{jk}\right) J_2 - \frac{\rho^3}{8}\left(\sum_{i=1}^{nc}\sum_{j=1}^{nc}\sum_{k=1}^{nc}\sum_{l=1}^{nc} x_i x_j x_k x_l \varepsilon_{ij}\varepsilon_{kl}\right) J_3 \qquad 6.17$$

With

$$J_1 = \int_{\sigma}^{\infty} \left(u'^{(1)}_{12}\right)^2 (x) g^{(0)}(x) \pi r^2 dr \qquad 6.18$$

and J_2 and J_3 complicated terms requiring expressions for three and four body radial distribution functions respectively. The J_2 term can be evaluated by the use of the superposition approximation and J_3 evaluated from its relation with J_1 and J_2. The reader is referred to the original article [91] for the complete derivation of the approximations of these terms.

It should be noted that the virial coefficient contributions determined equations 6.15 and 6.17 display the theoretically correct composition dependence.

Donohue and Prausnitz [60] extended the mixture perturbation expansion to four terms and developed theoretically correct mixing rules for the double summation perturbation approximation for use in their Perturbed Hard Chain equation of state. Their approach however requires the determination of 10 mixture properties through double summation over the component mole fractions which is prohibitive in practical calculations.

6.1.2 One Fluid Approximation

The one fluid approximation is the most commonly applied method to extend pure fluid equations of state to fluid mixtures. These mixing rules approximate fluid mixtures as fluids with uniform composition over the entire system volume with fluid properties determined from the individual fluid components.

6.1.2.a Van der Waals mixing rule

These mixing rules were originally used by Van der Waals in the classical Van der Waals equation of state [217], and are generally applied in the cubic equations of state of the form:

$$P = \frac{RT}{v-b} - \frac{a(T)}{f(v^2,b)} \qquad 6.19$$

where b is the Van der Waals co-volume parameter ($\eta=b/(4V)$) and $a(T)$ the temperature dependent attractive parameter. Equation 6.19 can be applied directly to fluid mixtures:

$$P = \frac{RT}{v-b_m} - \frac{a_m(T)}{f(v^2,b_m)} \qquad 6.20$$

with the mixture parameters, a_m and b_m, are traditionally defined as:

$$a_m = \sum_{i=1}^{nc}\sum_{j=1}^{nc} x_i x_j a_{ij} \qquad 6.21$$

$$b_m = \sum_{i=1}^{nc} x_i b_i \qquad 6.22$$

The geometric mean of the two pure component parameters is generally used as the combination rule for a_{ij}:

$$a_{ij} = \left(a_i a_j\right)^{1/2}\left(1-k_{ij}\right) \qquad 6.23$$

The adjustable binary interaction parameter k_{ij} is used to ensure the accurate representation the fluid system by introducing a slight correction to the mixing rule.

The linear combination of the Van der Waals co-volume term b_m can also be extended to include a binary interaction parameter to improve the flexibility of the mixture model and is generally applied with a arithmetic mean combination rule:

$$b_m = \sum_{i=1}^{nc}\sum_{j=1}^{nc} x_i x_j b_{ij} \qquad 6.24$$

and

$$b_{ij} = \frac{b_i + b_j}{2}\left(1 - l_{ij}\right) \qquad 6.25$$

Equation 6.24 and 6.25 reduce to equation 6.22 if the binary interaction parameter $l_{ij} = 0$ for all the components.

For the simple Van der Waals equation of state equations 6.21 and 6.24 result in the correct second virial coefficient composition dependence:

$$B_{2m} = \left(b_m + \frac{a_m}{RT}\right) = \sum_{i=1}^{nc}\sum_{j=1}^{nc} x_i x_j \left(b_{ij} + \frac{a_{ij}}{RT}\right) \qquad 6.26$$

The third and higher virial coefficients of the cubic equations of state are however purely functions of the co-volume, *b*. The third virial coefficient for example is:

$$B_{3m} = b_m^2 \qquad 6.27$$

From equations 6.26 and 6.27 it is clear that there is no combination rule for b_m to ensure the simultaneous correct composition dependence of the second and higher virial coefficients.

6.1.2.b Composition dependent combination rules

In an attempt to extend the flexibility of the mixture equation of state to enable the representation of more complex fluid mixtures many authors suggested the use of *empirical* composition dependent combination rules. This approach has generally been applied to cubic equations of state where more complex combination rules were proposed for the *a* parameter whilst keeping the co-volume combination term as proposed in equation 6.25.

Some of the more widely known combination rules for use in equation 6.21 are those developed by Adachi and Sugie [3], Stryjek and Vera [205-207], Schwartzentruber and Renon [186, 187] etc. Schwartzentruber however showed that many of these proposed combination rules in fact reduce to the same functional form [188]:

$$a_{ij} = \left(a_i a_j\right)^{1/2}\left[1 - k_{ij} - n_{ij}\left(x_i - x_j\right)\right] \qquad 6.27$$

where

$$k_{ij} = k_{ji} \qquad 6.28$$

$$n_{ij} = -n_{ji} \qquad 6.29$$

Many of these combination rules have some serious deficiencies and result in the thermodynamically incorrect behaviour of the equations of state.

Michelsen and Kistenmacher [145] first recognised a serious flaw in these combination rules that has become known as the Michelsen-Kistenmacher syndrome. Many of the proposed composition dependent combination rules are not conservative when two components are made identical in a fluid mixture, i.e. if the mixture parameters were to be determined for a binary mixture of component 1 and 2 and for a hypothetical ternary mixture consisting out of components 1, 2 and 2, different equation of state parameters would be obtained. This incorrect behaviour will have a particularly serious effect when modelling multi-component fluid mixtures where some the components are very similar.

A further problem identified by Michelsen and Kistenmacher [145] is that of the dilution effect. The binary interaction parameter n_{ij} is multiplied by the difference in the mole fractions, however as the number of components in the fluid mixture are increased the mole fractions will decrease and the effect of the interaction parameter will become negligible, and the mixing rule will reduce to the original quadratic form.

Finally the additional compositional dependence in the combination rule results in the violation of the constraint that the equation of state second virial coefficient should display the theoretically correct quadratic compositional dependence.

Mathias et al. [141] and Schwartzentruber and Renon [188] proposed methods through which these problems can be overcome, however they have found that these corrections limit the flexibility of the equations to such an extent that the improvement on the traditional quadratic mixing rules is greatly reduced.

6.1.2.c Excess Gibbs Energy mixing rules

The equations of state using excess Gibbs energy mixing rules, G^E-*EOS*, were developed in an attempt to incorporate the performance of the existing excess Gibbs energy or activity coefficient models used in the solution theory into the equations of state.

Unlike the theoretical quadratic composition dependence of the virial coefficients at low system densities there is no known theoretical boundary condition for the equation of state mixing rules at high densities. On the other hand the existing excess Gibbs energy models were specifically developed for high-density systems.

Huron and Vidal [103] first proposed that the excess Gibbs energy determined from an activity coefficient model, G_γ^E, be set equal to the excess energy determined from an equation of state, G_{EOS}^E, at infinite pressure:

$$G_\gamma^E\left(T, P=\infty, x_1 \ldots x_n\right) = G_{EOS}^E\left(T, P=\infty, x_1 \ldots x_n\right) \qquad 6.30$$

In order to determine the *EOS* excess energy at infinite pressure it must be assumed that there is no free volume in the fluid in order to ensure that the excess volume is equal to zero, i.e. for a Van der Waals type cubic equation of state $v = b_m$ where b_m is determined through equation 6.22. This leads to the following:

$$v^E = v - \sum_{i=1}^{nc} x_i v_i = b_m - \sum_{i=1}^{nc} x_i b_i = 0 \qquad 6.31$$

and

$$g^E = a^E + Pv^E = a^E \qquad 6.32$$

where g^E is the molar excess Gibbs and a^E the molar excess Helmholtz energy.

By determining the excess Gibbs energy of the equation of state and equating it to the activity coefficient model the following expression can be obtained:

$$g_{\gamma}^{E} = -C\left(\frac{a_m}{b_m} - \sum_{i=1}^{nc} x_i \frac{a_i}{bi}\right)$$
$$a_m = b_m\left(\sum_{i=1}^{nc} x_i \frac{a_i}{bi} - \frac{1}{C} g_{\gamma}^{E}\right) \qquad 6.33$$

Where C is a constant characteristic of the equation of state. Any activity coefficient model may be used to obtain g_{γ}^{E}.

The excess Gibbs energy of a system is however not independent of system pressure, and the activity coefficient parameters determined at atmospheric conditions are not valid at infinite pressure. The parameters must therefore be refitted at higher system pressures if they are to be used in the Huron-Vidal mixing rule. This severely limits the general applicability of the proposed mixing rule. Furthermore it is apparent from equation 6.33 that the Huron-Vidal mixing rule violates the second virial coefficient composition dependence requirement.

In an attempt to utilise the vast database of activity coefficients determined atmospheric conditions, Mollerup proposed a method of equating the two different excess Gibbs energies (G_{γ}^{E} and G_{EOS}^{E}) at zero pressure [147]. The most well known mixing rules of this type are those developed by Michelsen [143] and Dahl and Michelsen [53], known as the modified Huron-Vidal mixing rules or *MHV1* and *MHV2*:

$$q(\alpha) = \sum_{i=1}^{nc} x_i q(\alpha_i) + \frac{g_{\gamma}^{E}}{RT} + \sum_{i=1}^{nc} x_i \ln\frac{b_m}{bi} \qquad 6.34$$

where $\alpha = a_i/(b_i RT)$ and q is defined as follows:

$$q(\alpha) = -\ln\left[\frac{v(T, P=0)}{b} - 1\right] + \alpha C(v(T, P=0)) \qquad 6.35$$

$v(T,P = 0)$ is the fluid specific volume at zero pressure, and $C(v)$ is a characteristic function of the equation of state.

The zero pressure excess energy mixing rules however have a disadvantage in that equation 6.34 is only defined at conditions where the equation of state has a valid liquid volume root.

To overcome this problem various extrapolation functions and estimation methods have been proposed for $q(\alpha)$[53, 90, 143]. The zero-pressure excess energy mixing rules furthermore also violate the second virial coefficient composition constraint.

Wong and Sandler [239] proposed a different mixing rule by equating the excess *Helmholtz* energy of an activity coefficient model and equation of state at infinite pressure and ensured the correct second virial coefficient behaviour.

For a general cubic equation of state to display the correct second virial coefficient composition dependence the equation of state parameters, *a* and *b* must adhere to the following relation:

$$b_m + C\frac{a_m}{RT} = \sum_{i=1}^{nc}\sum_{j=1}^{nc} x_i x_j \left(b_{ij} + \frac{a_{ij}}{RT} \right) \qquad 6.36$$

A possible solution to this expression is the following:

$$b_m + \frac{a_m}{RT} = \sum_{i=1}^{nc}\sum_{j=1}^{nc} x_i x_j \left(b + \frac{a}{RT} \right)_{ij} \qquad 6.37$$

with

$$\left(b + \frac{a}{RT} \right)_{ij} = \frac{\left(b_i + \frac{a_i}{RT} \right) + \left(b_j + \frac{a_j}{RT} \right)}{2} \left(1 - k_{ij} \right) \qquad 6.38$$

Wong and Sandler used this combination rule along with the approximation that the fluid excess volume at infinite pressure is equal to zero through equation 6.31. This assumption enables the calculation of a finite excess Helmholtz energy value for the equation of state at infinite pressure. By requiring that this value be equal to the excess energy value determined from an activity coefficient model the following relation is obtained:

$$\frac{a_m}{b_m} = \sum_{i=1}^{nc} x_i \frac{a_i}{b_i} - C a_\gamma^E \qquad 6.39$$

(C is a constant specific to the relevant equation of state, a_m is the mixture Van der Waals attractive term whilst ${a_\gamma}^E$ represents the molar excess Helmholtz energy as determined from the activity coefficient model.)

From the classical thermodynamic relation for the excess Gibbs energy (equation 6.40)

$$G^E = A^E + PV^E \qquad 6.40$$

Wong and Sandler showed that at atmospheric conditions where the excess volume of mixing is generally small, the excess Gibbs energy is approximately equal to the excess Helmholtz energy. Furthermore they claimed that the excess Helmholtz energy is much more independent of the system pressure than the Gibbs energy. This ensures that the activity coefficient parameters determined at atmospheric conditions can be used to determine the excess Helmholtz energy at infinite pressure as opposed to the *Huron-Vidal* mixing rules. The activity coefficient model excess Helmholtz energy can therefore be determined as follows:

$$G_\gamma^E\left(T, P = low, x_i \ldots x_n\right) \approx A_\gamma^E\left(T, P = low, x_i \ldots x_n\right) \approx A_\gamma^E\left(T, P = \infty, x_i \ldots x_n\right) \qquad 6.41$$

Orbey and Sandler [159] suggested the use of a different combination rule to equation 6.38 to ensure the smooth transition between the Wong-Sandler excess Helmholtz energy mixing rule and the traditional Van der Waals mixing rules as discussed in section 6.1.2.a. This combination rule allows for the use of two binary interaction parameters:

$$\left(b + \frac{a}{RT}\right)_{ij} = \frac{\left(b_i + b_j\right)}{2}\left(1 - l_{ij}\right) + \frac{\sqrt{a_i a_j}}{RT}\left(1 - k_{ij}\right) \qquad 6.42$$

The capability of the Wong-Sandler mixing rules, used in conjunction with various cubic equations of state and different activity coefficient models, to represent a vast variety of complex fluid mixtures have been widely investigated [68, 158, 160, 238, 241]. It has however been observed that the ability of the Wong-Sandler mixing rules to represent fluid mixtures decreases with an increase in the as the size asymmetry of the mixture components [50]. This inability to represent asymmetric components can be attributed to the fact that the cubic equation of state with the Wong-Sandler mixing rule does not reproduce the activity coefficient excess Gibbs free energy at the same conditions and that this discrepancy increases as the component asymmetry increases [50, 144]. In their original article Wong and Sandler

[238] stated that the binary interaction parameter k_{ij} can be adjusted freely to improve the *VLE* representation of the binary systems, however in a later work they suggested that the k_{ij} parameter be used to minimise the discrepancy between the G_{γ}^{E} and the G_{EOS}^{E} values[239]. Wong and Sandler suggested an entirely predictive model by adjusting k_{ij} to ensure $G_{\gamma}^{E} = G_{EOS}^{E}$ at an equimolar binary composition ($x_1 = x_2 = 0.5$). This approximation is approximately correct for symmetric systems, but the G^E plot for an asymmetric fluid mixture is biased towards one component, and $x_i = 0.5$ would not be a suitable position to enforce the agreement between the excess properties. In fact Coutsikos et al. [50] found that k_{ij} should be composition dependent to accomplish this.

Coutsikos et al. [50] further found that the assumption that the excess Helmholtz energy is independent of the system pressure is valid for symmetrical systems, but that the A^E displays a significant pressure dependence for asymmetric systems, hence rendering the last equality in equation 6.41 invalid. Brandani et al. [29, 30] furthermore showed that the Wong-Sandler mixing rules are inapplicable to equations using hard sphere reference terms where the denominator in the hard sphere term is raised to a power greater than 1, as in the case of the Carnahan-Starling hard sphere equation of state (equation 3.20).

Although excess Gibbs energy mixing rules have received a considerable amount of attention in the recent years, they have only been applied to the empirical cubic equations of state. The mathematical structure of the more realistic models is too complex to readily apply the same approach. Furthermore the requirement that the excess properties determined from the equations of state and activity coefficient models be identical has no strict theoretical basis and by using this approach the success of the G^E-*EOS* is made dependent on the performance of the specific activity coefficient model used.

6.1.3 Two Fluid Approximation

In contrast to the one fluid approximation whereby it is assumed that the entire fluid mixture has a uniform composition, the two fluid approach recognises that there may be differences in the local compositions within the fluid mixtures because of the formation of clusters with a higher concentration of a specific component. The local composition differences will become especially significant when there are large differences in the component properties, e.g. a polar - non-polar mixture or a mixture of two components that differ significantly in size. Anderko [10] provides a detailed review of these mixing rules.

Whiting and Prausnitz [237] and Mollerup [146] showed how the local composition concept could be incorporated into an equation of state. In a binary mixture of components *i* and *j* two hypothetical fluid regions can exist. The first consists out of particles interacting with species *i* and the second with species *j*. The local composition in the first region is described by the mole fractions x_{ii} and x_{ji}, the fraction of molecules *i* and *j* interacting with species *i* respectively with $x_{ii} + x_{ji} = 1$. Similarly the second region is described by the mole fractions x_{ij} and x_{jj}. Whiting and Prausnitz used the following relation to relate the local mole fractions to the overall fluid composition of a system with different sized particles:

$$\frac{x_{ji}}{x_{ii}} = \frac{x_j}{x_i} \exp\left[-\frac{\alpha q_i \left(\varepsilon'_{ji} - \varepsilon'_{ii} \right)}{RT} \right] \qquad 6.43$$

$$\frac{x_{ij}}{x_{jj}} = \frac{x_i}{x_j} \exp\left[-\frac{\alpha q_j \left(\varepsilon'_{ij} - \varepsilon'_{jj} \right)}{RT} \right] \qquad 6.44$$

where q_i is the surface area of component *i*, ε'_{ij} is the attractive or perturbation Helmholtz energy per surface area between component *i* and *j* and α is the degree of non-randomness perturbation parameter.

In the simplest case when these equations are applied to the Van der Waals equation of state the following mixing rule for the attractive parameter, *a*, is obtained:

$$a_m = \sum_{i=1}^{nc} x_i \left\{ \frac{\sum_{j=1}^{nc} x_j \frac{a_{ji} b_{ii}}{b_{ji}} \exp\left[\frac{\alpha a_{ji} b_{ii}}{b_{ji} RT} \rho \right]}{\sum_{k=1}^{nc} x_k \exp\left[\frac{\alpha a_{ki} b_{ii}}{b_{ki} RT} \rho \right]} \right\} \qquad 6.45$$

As can be seen the mixing rule in equation 6.45 is density dependent. This is a characteristic feature of the local composition mixing rules. As the system density is decreased equation 6.45 will tend towards the traditional quadratic mixing rule which when used along with a correct mixing rule for the co-volume term will result in the correct second virial coefficient composition dependence.

The density dependent local composition mixing rules, *DDLC* mixing rules, have been investigated by several authors [97, 127, 129, 140], whilst all these proposed mixing rules perform reasonably satisfactory they are not generally suited for practical calculations. As has

been observed by Mathias and Copeman [140] and shown by Topliss et al. [214] the majority of the computational time in the determination of the phase equilibria of multi-component fluid systems is the determination of the mixture properties which increases exponentially with an increase in the number of components in the system (see section 6.2.1.c). With density dependent rules this problem will be compounded, as the mixture properties will have to be revaluated for each fluid density iteration.

6.1.4 Mixing rules for non-cubic equations of state

Although the approaches in the development of the various mixing rules discussed above could theoretically also be applied to non-cubic equations of state, the often complex mathematical structure of these models make the general discussion of the required mixing rules difficult, as these are often specific to the equation of state. As the aim of this chapter is the development of mixing rules for the proposed *simple-PHCT* a brief review of approaches towards the mixing rules for similar equation of state parameters will be given in this section.

It is a characteristic feature of the various non-cubic equations of state that different mixing rules are used for the different contributing terms in the model, e.g. the *SAFT* type equations uses different mixing rules in the reference, perturbation and associating terms [101]. The various mixing rules will therefore be discussed according to the mixing rules used for the hard sphere reference term and the perturbation approximation.

6.1.4.a Hard sphere reference term

The hard sphere reference terms of the *simple-PHCT* and *simple-PHCT-ltd* equations, as in the case of the other *PHCT* models in the literature, are functions of the *PHCT* degrees of freedom parameter c and the effective molecular closest packed volume rv_0.

Cotterman and Prausnitz [48] state that the physical significance of the c parameter requires that the mixture parameter should be determined by a simple linear mixing rule, and used a similar mixing rule for the molecular closest packed volume. Similar mixing rules were used by Kim et al. [111] in the extension of the Simplified Perturbed Hard Chain Theory, *SPHCT*, towards mixture systems:

$$c_m = \sum_{i=1}^{nc} x_i c_i \qquad 6.46$$

$$(rv_0)_m = \sum_{i=1}^{nc} x_i (rv_0)_i \qquad 6.47$$

These mixing rules are of course identical to the simple Van der Waals one fluid mixing rule (equation 6.22).

6.1.4.b Perturbation Contribution

The proposed models require three equation of state parameters in the determination of the perturbation contribution, the *c* parameter, the molecular energy parameter, $q\varepsilon'/k$ or $r\varepsilon/k$, and the molecular closest packed volume rv_0.

As discussed in 6.1.1.c Donohue and Prausnitz used the theoretical first and second perturbation mixing rules for mixtures of hard spheres and square well fluids of similar size [91] to develop mixing rules for the first four perturbation terms of perturbed hard chains of differing sizes that interact according to a square well potential model. Although these mixing rules are too complex for practical calculations (see section 6.2.1.c) some of the concepts originally developed in these models were used by other authors in simplified versions of the *PHCT* equation of state.

Donohue and Prausnitz suggested that the molecular volume be represented by the product of a segment volume with a specific segment number, and the interaction energy by the product of the molecular surface area with the energy per surface area. One of the mixing rules developed by them has the following form:

$$\left(c\left(\frac{q\varepsilon'}{k}\right)^n rv_0 \right)_m = \sum_{i=1}^{nc}\sum_{j=i}^{nc} x_i x_j c_i \left(\frac{q_i \varepsilon'_{ij}}{c_i k}\right)^n r_j v_{0ij} \qquad 6.48$$

where *n* refers to the perturbation order. The combinatorial parameters in equation 6.48 are defined as follows:

$$\varepsilon'_{ij} = \sqrt{\varepsilon'_i \varepsilon'_j}\left(1 - k_{ij}\right) \qquad 6.49$$

and

$$v_{0ij} = \left(\frac{v_{0i}^{1/3} + v_{0j}^{1/3}}{2} \right)^3 \qquad 6.50$$

Equation 6.50 represents the linear combination of the effective segment diameters.

The perturbation term mixing rule of the simplified Perturbed Hard Chain Theory, *SPHCT*, with a local composition perturbation approximation (section 4.3.5.c) as developed by the Kim et al. [111] is based on the work of Donohue and Prausnitz as discussed above. The *SPHCT* mixing rule is as follows:

$$\left(crv_0 \exp\left[\frac{q\varepsilon}{2ckT} - 1 \right] \right)_m = \sum_{i=1}^{nc} \sum_{j=i}^{nc} x_i x_j c_i r_j v_{0ij} \exp\left[\frac{q_i \varepsilon'_{ij}}{2c_i k} - 1 \right] \qquad 6.51$$

with equation 6.49 and 6.50 as the combination rules. It should be noted that in the original article by Kim et al. [111] equation 6.49 was used without a binary interaction parameter, but that it was included by Gasem and Robinson [78] in their evaluation of the model.

The application of equation 6.51 in the *SPHCT* model leads to the correct second virial coefficient composition dependence.

Cotterman and Prausnitz [48], as discussed in section 4.3.4.c, use a double summation approximation of the first two perturbation terms and their perturbation compressibility term will have the following form:

$$z^{pert} = \sum_{n=1}^{2} \sum_{m=1}^{4} mD_{nm} c(rv_0\rho)^m \left(\frac{q\varepsilon}{ckT} \right)^n \qquad 6.52$$

They used the Donohue and Prausnitz mixing rule, equation 6.48 along with equation 6.47 to extend their perturbation approximation to fluid mixtures. This approach results in a second virial coefficient perturbation contribution that displays the theoretically correct quadratic composition dependence.

Boublík and Lu [26], as cited by Kemény et al. [109], proposed slightly different mixing rules for the double summation perturbation approximation developed by Chen and Kreglewski [42] which also lead to a second virial coefficient contribution with a quadratic composition dependence:

$$z^{pert} = \sum_{i=1}^{nc}\sum_{j=1}^{nc} x_i x_j \sum^{n}\sum^{m}\left(\frac{v_{0ij}}{v}\right)^m \left(\frac{\varepsilon_{ij}}{kT}\right)^n \qquad 6.53$$

In this equation, v_0, represents the closest packed molar volume and, ε, the energy parameter of an entire molecule. The energy combination term ε_{ij} is the geometric mean of the two pure component properties, and the v_{0ij} term can be taken either as the arithmetic mean or determined with equation 6.50.

Using the Boublík-Lu approach (equation 6.53) in fact implies the usage of a total *m* x *n* different mixing rules, each of the form:

$$v_0^m \varepsilon^n = \sum_{i=1}^{nc}\sum_{j=1}^{nc} x_i x_j v_{0ij}^m \varepsilon_{ij}^n \qquad 6.54$$

The generally applied version of the *SAFT* equation of state as developed by Huang and Radosz [100] also use a double summation approximation to represent the fourth order perturbation expansion (see section 4.3.5.a, equation 4.55):

$$z^{pert} = r\sum^{n}\sum^{m} mD_{nm}\left(\frac{\eta}{\tau}\right)^m \left(\frac{\varepsilon}{kT}\right)^n \qquad 6.55$$

here r is the chain length or segment number, ε/k the segment energy and η the reduced segment density. The η/τ term is equivalent to the $rv_0\rho$ term used in equation 6.52.

Huang and Radosz [101] determined the mixture reduced density as follows:

$$\eta_m = \rho\sum_{i=1}^{nc} x_i \frac{\pi}{6} r v_{0i} \qquad 6.56$$

and proposed two different types of mixing rules for the energy term in equation 6.55. The first, a Van der Waals one fluid averaging equation:

$$\left(\frac{\varepsilon}{kT}\right)_m = \frac{\sum_{i=1}^{nc}\sum_{j=1}^{nc} x_i x_j r_i r_j \left(\frac{\varepsilon_{ij}}{kT}\right) v_{0ij}}{\sum_{i=1}^{nc}\sum_{j=1}^{nc} x_i x_j r_i r_j v_{0ij}} \qquad 6.57$$

with the combination terms ε_{ij} and v_{0ij} defined as in equations 6.49 and 6.50 respectively.

The second approach is to determine the mixture energy term as a function of the molecular volume fraction, f, instead of the normal composition fraction. This approach is in agreement with the mixing rules used in the activity coefficients models such as the Flory-Huggins and UNIFAC models [185] [170] where the molecules are considered as consisting out of segments or specific groups [101]:

$$\left(\frac{\varepsilon}{kT}\right)_m = \sum_{i=1}^{nc}\sum_{j=1}^{nc} f_i f_j \left(\frac{\varepsilon_{ij}}{kT}\right) \qquad 6.58$$

ε_{ij} is again defined by equation 6.49 and the volume fractions are determined as follows:

$$f_i = \frac{x_i r_i v_{0i}}{\sum_{j=0}^{nc} x_j r_j v_{0j}} \qquad 6.59$$

Using a volume fraction to weigh the overall intermolecular interaction of the fluid mixture has an intuitive appeal especially in the instances where there is a large size asymmetry between the mixture components, as the presence of a very large molecule even if present in small molar quantities will experience a significant degree of interaction with the smaller components in the mixture due to the large volume it occupies.

Huang and Radosz further proposed that the mixture segment number or chain length, r_m, be determined through a simple linear combination of the individual component parameters, and allowed for the inclusion of a second binary interaction parameter in their model although it is not often used [101]:

$$r_m = \sum_{i=1}^{nc}\sum_{j=1}^{nc} x_i x_j r_{ij} \qquad 6.60$$

and

$$r_{ij} = \frac{r_i + r_j}{2}\left(1 - l_{ij}\right) \qquad 6.61$$

(As stated in section 6.1.2.a the mixing and combination rules of the forms of equations 6.60 and 6.61 reduce to a simple linear combination rule if the binary interaction parameter is set to zero.)

These mixing rules for the *SAFT* perturbation contribution are of such a form that the second virial coefficient composition dependence is violated. In spite of this fact the Huang and Radosz version of the *SAFT* equation is remains very popular and has been successfully used to represent the phase behaviour of various fluid mixture systems [170].

6.2 EVALUATION CRITERIA

From the investigation of the mixing rules above, certain criteria can be identified that the proposed mixing rules for the *simple-PHCT* and *simple-PHCT-ltd* models should meet. Adherence to the criteria will ensure that the mixing rules are practical and free from any fundamental flaws and allow the developed mixture *EOS* to be used with greater confidence when representing fluid mixtures of different fluid systems or at conditions what were not explicitly used in the evaluation of the proposed mixing rules.

6.2.1.a Second virial coefficient composition dependence

As discussed in section 6.1.1.a the quadratic composition dependence of the second binary virial coefficient forms the zero density boundary condition of any theoretically correct equation of state mixing rule.

This is the only known theoretical constraint that can be practically applied to the proposed model mixing rules. The perturbation expansion mixing rules as discussed in section 6.1.1.c are too complex to use in a practical equation of state, furthermore, although the perturbation mixing rules were developed from a theoretical basis, they still require the use of simplifying assumptions and approximations to obtain an analytical solution.

The theoretically derived hard sphere mixture equations 6.5 and 6.6 (section 6.1.1.b) are constrained by the accuracy of the Percus-Yevick theory from which it is derived, and display the same inaccuracies as the pure *PY-C* and *PY-P* hard sphere models [137]. The *HS3* hard sphere equation of state as developed in Chapter 3 also does not lend itself to the extension towards fluid mixtures in the same way as the Carnahan-Starling does in the development of

the mixture *BMCS* equation of state. (The *HS*3 cannot be written as an algebraic function of the *PY-C* and *PY-P EOS*.)

There has been some discussion relating to the importance of the adherence to the second virial coefficient boundary condition, as the equations of state are generally unable to accurately represent the pure fluid virial coefficients and hence could not be expected to do so in fluid mixtures. The virial coefficients are also related to the ideal gas behaviour of a system, and it is argued that the actual equations of state are generally applied at conditions removed from this stata. Many of the proposed mixing rules in the literature have therefore been allowed to violate this requirement, because of their supposed superior performance. (See the discussion of the mixing rules in section 6.1.) However it should be noted that during the calculation of the fugacity coefficient of a species in a fluid mixture an integral of the compositional derivative of the equation of state between $V = \infty$ and V the actual system volume needs to be determined as shown in equation 6.62:

$$\ln \hat{\phi}_i = \int_{V=0}^{V} \frac{1}{v} - \left(\frac{\partial P/RT}{\partial n_i} \right)_{T,V,N_{j \neq i}} dV - \ln Z \qquad 6.62$$

Here n_i represents the mole number of species i in the fluid mixture and $\hat{\phi}_i$ the fugacity coefficient of species i in the mixture.

Evaluating equation 6.62 between $V = \infty$ and V is of course equivalent to taking the integral between $\rho = 0$ and ρ. The theoretically incorrect compositional dependence at zero pressure will therefore affect the calculated fugacity coefficient, and hence the entire model performance, at all system conditions, neccecitating the accurate representation of this behaviour. The correct virial coefficient composition dependence and the accurate representation of the coefficients should be seen as two different problems [190] that can be addressed individually.

6.2.1.b Michelsen-Kistenmacher Syndrome and the Dilution effect

As discussed in section 6.1.2.b many empirical mixing and combination rules lead to thermodynamically incorrect mixture behaviour. The Michelsen-Kistenmacher syndrome especially is expected to have a serious detrimental effect on the representation of the fluid mixtures of interest in this work: mixtures of relatively small molecules as solvents and solutes

consisting out of long chained molecules belonging to the same homologous groups with very similar thermodynamic properties.

To avoid the possibility of these problems occurring composition independent combination rules will be used and unnecessarily complex empirical mixing rules will be approached with care.

6.2.1.c Computational simplicity and speed

As mentioned earlier, the calculation of the thermodynamic properties of a fluid mixture the determination of the equation of state composition dependent *EOS* parameters contributes a considerable amount to the total computational time [214]. This contribution will increase exponentially with an increase in the number of mixture components. It is therefore important that the *EOS* mixing rules be kept as simple and few as possible.

The majority of the mixing rules, excluding those using the composition dependent combination rules, can be classified as belonging to two types: the single summation mixing rule, *SSMR*, without any cross-interaction parameters (equation 6.63), and the double summation mixing rules, *DSMR*, that incorporates cross-interaction and binary interaction parameters (equation 6.64):

$$\theta_m = \sum_{i=1}^{n} x_i \theta_i \qquad 6.63$$

$$\theta_m = \sum_{i=1}^{n} \sum_{j=1}^{n} x_i x_j \theta_{ij} \left(1 - k_{ij}\right) \qquad 6.64$$

In a system with n components each *SSMR* requires a minimum of n calculations whilst the *DSMR* requires n^2 calculations[5]. During the calculation of the thermodynamic properties of a multi-component mixture the number of double summation mixing rules will therefore have a much more significant influence on the computational time and should be kept to a minimum.

[5] With certain combination rules when the interaction parameter k_{ij} is equal to zero, the double summation mixing rule may be simplified to eliminate unnecessary nested calculations and less than n^2 calculations will be required. E.q. equation 6.24 with the combination rule 6.25 reduces to equation 6.22 if l_{ij}=0.

An analysis of the various mixing rules used in the extension of some of the equations of state found in literature is given in Table 6.1. Two cubic equations, the two parameter *SRK* [196] and the three parameter Patel-Teja [162], *PT*, models, are listed along with some of the more popular three parameter non-cubic models. In these models the binary interaction parameters are used to correct the mixing rules of the attractive and co-volume terms.

Table 6.1 The number of single and double summation mixing rules in some of the generally applied equations of state.

Equation of State	Interact. Params.	SSMR	DSMR	Reference
SRK	2	0	2	[196]
PT	2	1	2	[162]
SAFT (1 fluid)*	2	3	3	[101]
SAFT (vol. fraction)*	2	3	2	[101]
SAFT (1 fluid)*	1	4	2	[101]
SAFT (vol. fraction)*	1	4	1	[101]
PC-SAFT*	1	4	2	[86]
PHCT (attractive term)	1	2	10	[60]
SPHCT	1	2	1	[111]

*** Without association**

The non-cubic models with one binary interaction parameter use it to correct the mixture energy term or attractive parameter mixing rule, whilst the second parameter in the *SAFT* equation is used in the chain length or segment number mixing rule (equations 6.60 and 6.61).

Only the attractive term mixing rules of the *PHCT* equation are listed in Table 6.1, as the original article by Donohue and Prausnitz [60] does not explicitly provide the mixing rules for the hard sphere repulsive terms. However simply from the attractive term mixing rules it is already apparent that the *PHCT* will be at a serious disadvantage in terms of computational speed compared to the other proposed models.

The high number of *SSMR* used in the *SAFT* and *PC-SAFT* equations is attributable to the fact that these models use the *BMCS* mixing rule to represent the mixture hard sphere repulsive term. By using the original Carnahan-Starling equation with a reduced density determined from a simple linear combination of the chained segments (equation 6.65) the number of *SSMR* can be reduced by two.

$$\eta_m = \rho \frac{\pi}{6} \sum_{i=1}^{n} x_i r_i d_i^3 \qquad 6.65$$

This approach is followed by Von Solms et al. [224] in order to simplify the *PC-SAFT* equation without a significant loss in accuracy of the model.

Using purely the complexity and number of mixing rules used in the equations listed in table Table 6.1 as criteria to differentiate between the various mixing rules it appears as if the *SAFT EOS* with the volume fraction mixing rule for the energy term and the *SPHCT* model are the most suited equations of state for use in the representation of the multi-component fluid mixtures during practical calculations. It should be noted that the *SPHCT* model only allows the use of one binary interaction parameter and furthermore requires the evaluation of a costly exponential function (see equation 6.51) which will be detrimental to the computational speed when the mixture consists out of a large number of components.

6.3 APPROACH TO MIXING RULE DEVELOPMENT FOR THE PROPOSED EQUATIONS OF STATE

The *simple-PHCT* and *simple-PHCT-ltd EOS* developed in the previous chapter have the following form (equation 5.77):

$$Z = 1 + c\left(\frac{4\eta + b\eta^2 + e\eta^3}{1 - d\eta}\right) + c\left(\sum_{n}^{3}\sum_{m}^{3} mD_{nm}\left(\frac{\eta}{\tau}\right)^m \left(\frac{1}{T'^*}\right)^n\right) \qquad 6.66$$

Following the approach by Donohue and Prausnitz [60] to express the molecular closest packed volume and energy parameter in terms of segment volume and number and energy per surface area, the reduced density and temperature are expressed as $\eta = rv_0\rho$ and $T^* = ckT/(q\varepsilon')$ respectively.

The differences between *simple-PHCT* and *simple-PHCT-ltd* models lie in the actual D_{nm} perturbation approximation parameters as well as the fitted *EOS* parameter values. The much simpler second virial coefficient expression of the *simple-PHCT-ltd* is obtained as a result of the fact that $D_{n1} = 0$ for all $n>1$ in the perturbation approximation:

$$B_2 = 4crv_0 + cD_{11}rv_0\frac{q\varepsilon'}{ckT} + cD_{21}rv_0\left(\frac{q\varepsilon'}{ckT}\right)^2 + cD_{31}rv_0\left(\frac{q\varepsilon'}{ckT}\right)^3 \qquad 6.67$$

$$B_2 = 4crv_0 + cD_{11}rv_0\frac{q\varepsilon'}{ckT} \qquad 6.68$$

Equation 6.67 is the expression for the second virial coefficient of the *simple-PHCT* equation of state and equation 6.68 for the *simple-PHCT-ltd* model.

In the development of mixing rules for these models a compromise needs to be found between model performance, confidence (theoretically correct form), flexibility (the number of interaction parameters) and computational efficiency. The proposed mixing and combination rules, the definition of the segment terms and some of the relevant concepts regarding use of the interaction parameters will be discussed in the remainder of this section.

6.3.1 Equation of State parameter mixing and combination rules

6.3.1.a Simple-PHCT mixing rules

In order to achieve the correct second virial coefficient quadratic composition dependence in the repulsive term it is necessary to determine the mixture c and rmv_0 parameters through the simple linear combination of the pure component parameters (equations 6.46 and 6.47):

$$c_m = \sum_{i=1}^{nc} x_i c_i \qquad 6.69$$

$$(rv_0)_m = \sum_{i=1}^{nc} x_i (rv_0)_i \qquad 6.70$$

For the attractive term there are two approaches that will result in the correct second virial coefficient behaviour. The first approach used by Boublík and Lu [26] to is to use a unique mixing rule for each *n-m* combination, however this will result in 6 *DSMR*.

The second possibility is the approach followed by Cotterman and Prausnitz [48] to use three unique mixing rules for the attractive term second virial coefficient contributions (equation 6.47) along with the mixture closest packed volume as determined through equation 6.70:

$$\left(c\left(\frac{q\varepsilon'}{k} \right)^n rv_0 \right)_m = \sum_{i=1}^{nc} \sum_{j=i}^{nc} x_i x_j c_i \left(\frac{q_i \varepsilon'_{ij}}{c_i k} \right)^n r_j v_{0\,ij} \qquad 6.71$$

The combination terms for the ε_{ij} and v_{0ij} are defined as follows:

$$\varepsilon'_{ij} = \sqrt{\varepsilon'_i \varepsilon'_j}\left(1 - k_{ij}\right) \qquad 6.72$$

and

$$v_{0\,ij} = \left(\frac{v_{0\,i}^{1/3} + v_{0\,j}^{1/3}}{2} \right)^3 \qquad 6.73$$

This is the simplest form of the mixing rules for the *simple-PHCT* that will correctly represent the second virial coefficient composition dependence and consists out of 2 *SSMR* and 3 *DSMR* and allows for the use of one binary interaction parameter. In this study these mixing rules will be identified as the *CP* mixing rules.

The only possibility to include a second binary interaction coefficient into the model without violating the second virial coefficient boundary condition is to either include it in equation 6.73 or to use a *DSMR* with an interaction parameter for the mixture *rvo* term used in the *perturbation* approximation in stead of equation 6.70. The latter method would increase the number of required mixing rules to 2 *SSMR* and 4 *DSMR*. Furthermore, in both cases the two binary interaction parameters would only affect the perturbation approximation and not the reference term, and would therefore be highly correlated.

And alternative mixing rule approach is to, similarly to Huang and Radosz [101], use volume fraction mixing rules in the model and to allow the equation of state to violate the second virial coefficient boundary condition. These mixing rules will be referred to as the *VF* mixing rules.

Three *SSMR* are required to determine the mixture c_m parameter, surface area q_m, and closest packed volume, rv_{0m} :

$$c_m = \sum_{i=1}^{nc} x_i c_i \qquad 6.74$$

$$q_m = \sum_{i=1}^{nc} x_i q_i \qquad 6.75$$

$$rv_{0m} = \sum_{i=1}^{nc} x_i r_i v_{0i} \qquad 6.76$$

and one additional *DSMR* for the mixture energy term:

$$\left(\frac{q\varepsilon'}{ckT}\right)_m = \frac{q_m}{c_m}\sum_{i=1}^{nc}\sum_{j=1}^{nc} f_i f_j \left(\frac{\varepsilon'}{k}\right)_{ij} = \frac{q_m}{c_m}\frac{\sum_{i=1}^{nc}\sum_{j=1}^{nc} x_i x_j r_i r_j v_{0i} v_{0j}\left(\frac{\varepsilon'}{k}\right)_{ij}}{\left(\sum_{i=1}^{nc} x_i r_i v_{0i}\right)^2} = \frac{q_m}{c_m}\frac{\sum_{i=1}^{nc}\sum_{j=1}^{nc} x_i x_j r_i r_j v_{0i} v_{0j}\left(\frac{\varepsilon'}{k}\right)_{ij}}{\left(rv_{0m}\right)^2} \qquad 6.77$$

The energy combination term, ε_{ij}, used in this equation is defined by equation 6.72.

The volume fraction mixing rules can be extended to include a second binary interaction parameter in the mixture volume term, but this would require two additional mixing rules, one *SSMR* and one *DSMR*.

A third set of mixing rules, the 2*D* mixing rules, will also be investigated. These mixing rules have been developed specifically for the *simple-PHCT-ltd* equation of state (see 6.3.1.b below). When applied to the *simple-PHCT EOS* the suggested mixing rules, similarly to the *VF* approach, violate the second virial coefficient constraint.

6.3.1.b Simple-PHCT-ltd mixing rules

The *simple-PHCT-ltd* equation of state has been developed specifically with the aim to simplify the mixing rules required to provide the correct second virial coefficient composition dependence. (See sections 4.4.1.d and 4.4.3.d) As can be seen from equation 6.68 the expression for the second virial coefficient of the *simple-PHCT-ltd* is much simpler than that of the *simple-PHCT* equations of state, and mixing rules other than those suggested by the Cotterman and Prausnitz [48] or Boublík and Lu [26] will result in the correct second virial coefficient boundary condition.

Mixing rules similar to those used in the *CP* approach are used for the c_m and rv_{0m} terms (equations 6.69 and 6.70) to ensure the correct compositional dependence of the reference virial coefficient contribution. The second virial coefficient contribution of the perturbation term is given by the following mixing rule:

$$\left(c\left(\frac{q\varepsilon'}{ck}\right)rv_0\right)_m = \sum_{i=1}^{nc}\sum_{j=i}^{nc} x_i x_j c_i \left(\frac{q_i \varepsilon'_{ij}}{c_i k}\right) r_j v_{0ij} = \sum_{i=1}^{nc}\sum_{j=i}^{nc} x_i x_j \left(\frac{q_i \varepsilon'_{ij}}{k}\right) r_j v_{0ij} \qquad 6.78$$

This leaves the remaining mixture energy terms in the higher order perturbation terms free to be determined by any mixing rule without affecting the second virial coefficient boundary condition. The following volume fraction mixing rule, identical to the *VF* expression, equation 6.77, was used for these terms:

$$\left(\frac{q\varepsilon'}{ckT}\right)_m = \frac{q_m}{c_m}\sum_{i=1}^{nc}\sum_{j=1}^{nc} f_i f_j \left(\frac{\varepsilon'}{k}\right)_{ij} = \frac{q_m}{c_m}\frac{\sum_{i=1}^{nc}\sum_{j=1}^{nc} x_i x_j r_i r_j v_{0i} v_{0j}\left(\frac{\varepsilon'}{k}\right)_{ij}}{\left(\sum_{i=1}^{nc} x_i r_i v_{0i}\right)^2} = \frac{q_m}{c_m}\frac{\sum_{i=1}^{nc}\sum_{j=1}^{nc} x_i x_j r_i r_j v_{0i} v_{0j}\left(\frac{\varepsilon'}{k}\right)_{ij}}{\left(rv_{0m}\right)^2} \qquad 6.79$$

In both equations 6.78 and 6.79 the ε_{ij} term is determined through equation 6.72, the q_m term through equation 6.75 and the c_m term as normal through equation 6.69 or 6.74.

The volume fraction mixing rule of the higher order energy term is reminiscent of the mixing rules used in the lattice fluid activity coefficient models used to represent the liquid phase thermodynamic properties [170]. These mixing rules for the *simple-PHCT-ltd* equation of state can therefore be seen as incorporating the mixing rules at two density conditions, the ideal gaseous state and liquid-like densities, and will therefore be referred to as the 2*D* mixing rules.

The 2*D* mixing rules consist out of 3 *SSMR* and 2 *DSMR* and use one binary interaction parameter. The extension of the model to incorporate two binary interaction parameters is subject to the same constraints as the *CP* mixing rules as discussed in section 6.3.1.a.

In addition to the 2*D* mixing rules the *simple-PHCT-ltd* model will also be evaluated using the *CP* and *VF* mixing rules as developed for the *simple-PHCT EOS*.

6.3.2 Definition and determination of the segment volume and molecular surface area.

All the mixing rules proposed in section 6.3.1, require the definition of a segment volume, v_0, chain length, r, interaction surface area, q, and the interaction energy per surface area ε'. In the fitting of the pure component properties it is not possible to determine these properties individually, as they are always found in the molecular from i.e. rv_0 and $q\varepsilon'$. Another aspect that should be considered is that from the definition of the *simple-PHCT* and *simple-PHCT-ltd* models both the molecular volume and interaction energy parameters are in fact temperature dependent. The question therefore arises as to how the segment and surface are properties should be defined and which property should display the relevant temperature dependence.

6.3.2.a Temperature dependence of the equation of state properties

From the Barker and Henderson theory [15] and the definition of the proposed intermolecular interaction energy (section 4.2.2.a) the effective molecular volume is defined as follows:

$$rv_0 = rv_{00}\left(1 - 0.12\exp\left(-\frac{3\varepsilon_0'}{ckT}\right)\right) \qquad 6.80$$

The effective hard sphere model incorporates the effect of the molecular softness into the perturbation theory. If conceptually, the molecule is seen as consisting out of spherical segments, the number of segments would remain constant and be independent of the degree of softness of the relevant segments. It is therefore clear that the temperature dependence of equation 6.80 should reside in the effective segment volume and not the chain length.

Similarly the temperature dependence of the interaction energy, equation 6.81, is a measure of the effect of the non-central forces of interaction on the total *strength* of the intermolecular potential, and unrelated to the actual surface *area* of the molecule, and should reside in the ε' parameter.

$$q\varepsilon' = q\varepsilon_0'\left(1 + \frac{\mu}{kT}\right) \qquad 6.81$$

6.3.2.b *Definition of the v_{00} and ε'_0 parameters*

In the application of the *PHCT* Donohue and Prausnitz [60], Kim et al. [111] and Wang and Guo [226] suggested the use of the volume of a $-CH_2-$ segment as the segment volume and determined this value form the slope of the rv_{00} values plotted against the carbon numbers of the n-alkane series (Donohue and Prausnitz [60] included some information on aromatics and fused rings in their determination of the segment volume as well), whilst Cotterman and Prausnitz simply used a fixed segment volume for all the molecules. The interaction energy per surface area can also be determined by plotting the $q\varepsilon'_0/k$ parameter values for n-alkanes against the carbon number [60, 111, 225].

The relevant segment volumes of the various equations of state are listed in Table 6.2. The Bondi [25] Van der Waals volume for a $-CH_2-$ segment as well as the parameters reduced from the *simple-PHCT* and *simple-PHCT-ltd* n-alkane pure component parameters are included for comparative purposes. It can be seen that all the methods result in segment volumes of similar magnitude.

Table 6.2 Various proposed $-CH_2-$ segment closest packed volumes

$-CH_2-$ segment volumes	
Source	v_0 [1e-6 m^3/mol]
Bondi [25]	10.23
Kim et al. [111]	8.67
Wang and Guo [226]	9.23
SAFT (n-alkanes >n-$C_{20}H_{42}$) [100]	12.00
Cotterman and Prausnitz [49]	10.00
simple-PHCT	9.49
Simple-PHCT-ltd	10.06

The question however arises as to how to define the v_{00} and ε'_0 parameters for chemical species that cannot be said to consist out of $-CH_2-$ segments such as CO_2 or N_2. Kim et al. [111] used the parameters determined from the n-alkane homologous series as universal constants. Cotterman and Prausnitz [48] similarly used a universal segment volume, but determined the ε'_0/k parameter from binary phase equilibrium data where the chemical species

is the one component and the second component is an n-alkane, a ε'_0/k value was chosen that resulted in the smallest binary interaction coefficient needed to represent the data. Finally Wang and Guo [226] reduced both the v_{00} and ε'_0/k parameters from binary *VLE* and density data.

By defining component specific v_{00} and ε'_0/k parameters the actual number of *EOS* parameters needed for the representation for a fluid mixture is increased from 3 to 5, this will complicate the generalization of the equation of state parameters, as additional property correlations will be required. Furthermore by determining these values through the minimization of the errors in binary mixture data they in effect serve as additional interaction parameters and will be correlated to the specific binary system used to regress the parameter value. This will further limit the general applicability of the equation of state parameters.

However when treating the v_{00} and ε'_0/k parameters as universal constants along with the mixing rules as discussed in section 6.3.1, it can easily be shown that the mixture properties are independent of the actual values of the v_{00} and ε'_0/k parameters and that the combination terms are in effect merely involve the combination of the relevant temperature dependence functions.

A third possibility is to set $q_i=ri$ [164] and to define the r_i parameter not as a segment number, but rather as a measure of how much one particle "sees" of another particle. This definition is especially relevant for highly asymmetric chained systems, because as there is a limiting size difference beyond which a smaller particle cannot distinguish between segments of differing chain length [60]. In this approach r_i can be determined by the ratio of the molecular volumes with the smallest volume in the fluid mixture, as in equation 6.82. The v_{00} parameter now represents the smallest molecular volume in the mixture and the ε'/k parameter the interaction energy scaled by the ratio in the molecular volumes (equation 6.83).

$$q_i r_i = \frac{rv_{0i}}{rv_{0\,smallest}} \qquad 6.82$$

$$\frac{\varepsilon'_i}{k} = \frac{\varepsilon'_i}{k}\frac{rv_{0\,smallest}}{rv_{0i}} \qquad 6.83$$

Both cases, using universal constants to describe the segment volume and interaction energy per surface area (arbitrarily defined as the properties of the smallest component) and setting $q_i = r_i$ and using the smallest molecular volume as the reference, will be investigated in this study.

6.3.3 Binary interaction parameters

The binary interaction parameters are used to modify the relevant combinatorial terms in the mixing rules in order to improve the representation of the relevant binary systems. For the sake of consistency all the proposed models will be fitted to the experimental data using only one interaction parameter to adjust the cross interaction energy in equation 6.72.

The temperature dependence of the interaction parameter will also be investigated as it is important that the interaction parameters are generally well behaved in order to enable the estimation of parameters at conditions where binary *VLE* data is unavailable.

6.4 EXPERIMENTAL DATA USED

In this chapter there will only be focussed on the modelling of binary *VLE* data. The modelling of multi-component systems will be investigated in the next chapter.

The representation of the phase behaviour of high-pressure asymmetric systems consisting out of hydrocarbons and supercritical solvents are of primary importance in this study. The various mixing rules will be evaluated according to their ability to represent the binary vapour-liquid equilibrium data of n-alkanes where there is a significant difference between the two component sizes, primarily focussing on binary systems with methane, ethane or propane as one of the components. Furthermore the representation of the CO_2-n-alkane binary systems will be studied as a measure of the ability of the various mixing rules to handle mixtures of unlike components.

The relevant binary *VLE* data sets used in this study are listed in Table 6.4. The desired range of application of the final model for asymmetric systems would typically be at conditions above the critical point of the smaller component or solvent, whilst the model is also expected to be able to represent asymmetric mixtures and mixtures of non-spherical components at lower system pressures. Binary data at lower system pressures as well as near the mixture

critical point are therefore included in the evaluation to ensure the overall correct behaviour of the model.

Table 6.3 Pure component parameters for the simple-PHCT-ltd EOS regressed for methane and CO_2.

Simple-PHCT-ltd pure component parameters				
	v_{00} [1e6 m^3/mol]	ε/k [K]	μ/k [K]	c
Methane	150.86	190	1	1
CO_2	20.85	306.26	40	1.204

The pure component parameters for methane and CO_2 used in this study are listed in Table 6.3, whilst the remainder of the n-alkane parameters are used as reported in Table 5.6.

Table 6.4 Binary VLE data used in the evaluation of the EOS mixing rules

Solute	Solvent	T [K]	P [1e5 Pa]	Source
CH_4	n-C_5H_{12}	377	13-104	[56]
CH_4	n-C_6H_{14}	373	50-185	[139]
CH_4	n-$C_{16}H_{34}$	300 – 360	21-704	[83]
C_2H_6	n-$C_{16}H_{34}$	360	12-114	[55]
C_2H_6	n-$C_{20}H_{42}$	320 – 450	3-168	[165]
C_2H_6	n-$C_{36}H_{74}$	363	160-227	[61]
C_3H_8	n-$C_{36}H_{74}$	340	68-100	[189]
n-C_5H_{12}	n-C_6H_{14}	309	0.317-1.0063	[177]
n-C_6H_{14}	n-$C_{16}H_{34}$	472 – 623	7-40	[107]
n-C_6H_{14}	n-$C_{36}H_{74}$	573	7-54	[107]
CO_2	n-$C_{16}H_{34}$	393	101-256	[202]
CO_2	n-$C_{20}H_{42}$	323-573	9-51	[99]
CO_2	n-$C_{28}H_{38}$	373	8-94	[77]

6.5 EVALUATION OF PROPOSED MIXING RULES

In this section the three proposed mixing rules the *CP*, *VF* and the 2*D* approaches, will be evaluated for the two forms of the newly developed equation of state, the *simple-PHCT* and the *simple-PHCT-ltd* models.

All three mixing rules have a simple mathematical structure with no empirically introduced density or composition dependence, and hence do not suffer from the Michelsen-Kistenmacher syndrome or the dilution effect as discussed in section 6.2.1.b. The other model criteria, the

model performance, simplicity and reliability will therefore be used to select a suitable fluid model.

In the following discussions, unless explicitly stated, the various equations of state are applied without binary interaction parameter (l_{ij}=0) using the pure component parameters as determined in Chapter 4 and Chapter 5.

6.5.1 The correct second virial coefficient composition dependence

As discussed in section 6.2.1.a the quadratic composition dependence of the mixture second virial coefficient is the only theoretically known boundary condition of the equations of state mixing rules, and affects the thermodynamic performance of the model over all densities through equation 6.62. The effect of adhering to this limit can be seen in Figures 6.1 to 6.3.

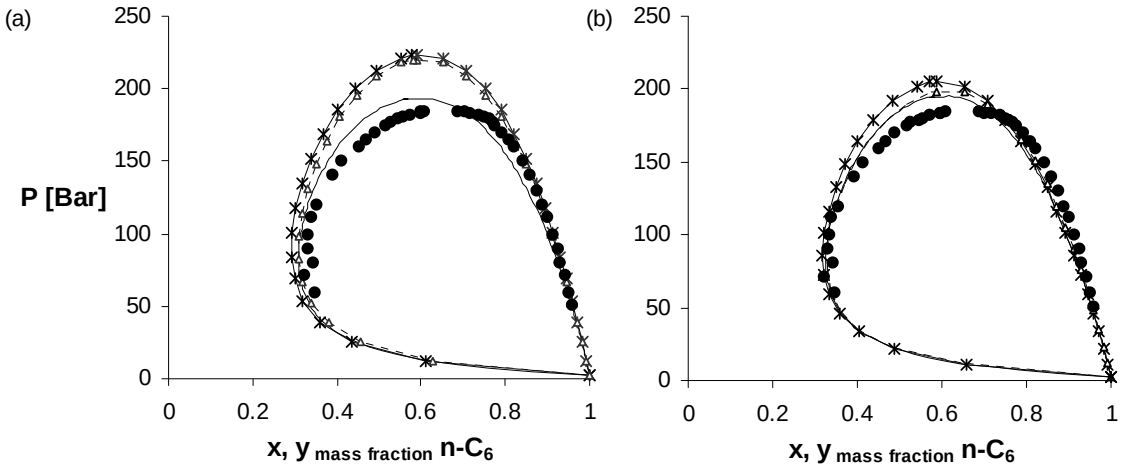

Figure 6.1 Methane – n-Hexane VLE at 373 K as represented by the (a) *simple-PHCT* and (b) *simple-PHCT-ltd* EOS. ● Experimental data [56], —— *CP* , —✳— VF and - - - *2D* mixing rules.

From Figure 6.1 to Figure 6.3 it appears as if the mixing rules that adhere to the correct second virial coefficient boundary conditions are successful in describing the phase behaviour of the lighter phase (lower heavy component mass fractions). This effect is especially pronounced in the case of the *simple-PHCT CP* equation of state, although the theoretically correct *simple-PHCT-ltd CP* and *2D* equations are also slightly more accurate than the respective model with the *VF* mixing rule.

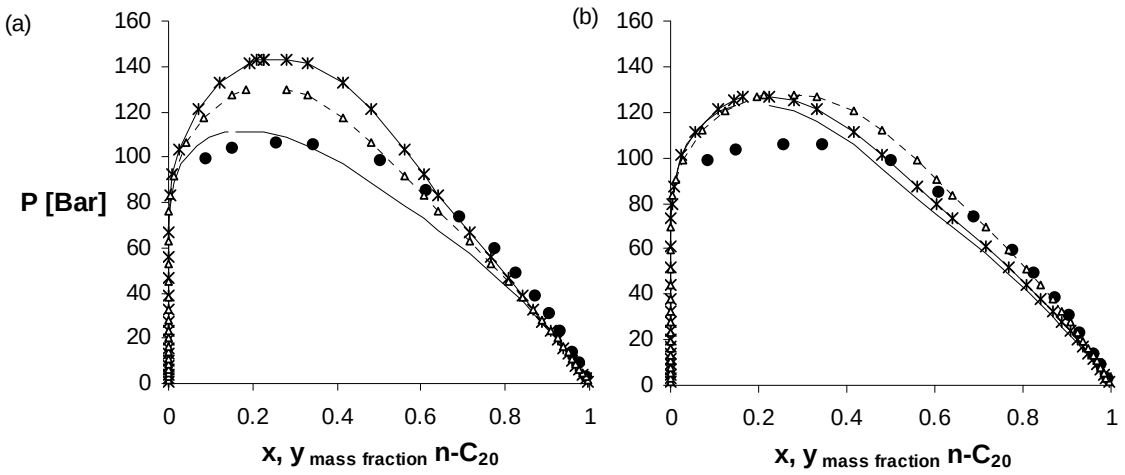

Figure 6.2 Ethane – n-Eicosane VLE at 340 K as represented by the (a) *simple-PHCT* and (b) *simple-PHCT-ltd* EOS. ● Experimental data [165], —— *CP* , —✳— VF and - -▵- - *2D* mixing rules.

On the other hand, by incorporating a volume fraction mixing rule for the molecular interaction energy, an improvement in the representation of the heavy phase (higher heavy component mass fraction) is obtained. As previously mentioned the volume fraction mixing rules are reminiscent of the mixing rules used in the activity coefficient models to represent the liquid phase. The observed improvement in the liquid phase representation of the *EOS* using a similar mixing rule, lends credence to this analogy. It appears as if at liquid-like densities the benefits of using theoretically correct mixing rules are outweighed by the benefits of accounting for the intermolecular interactions on an intuitively correct volume fraction rather than mole fraction basis.

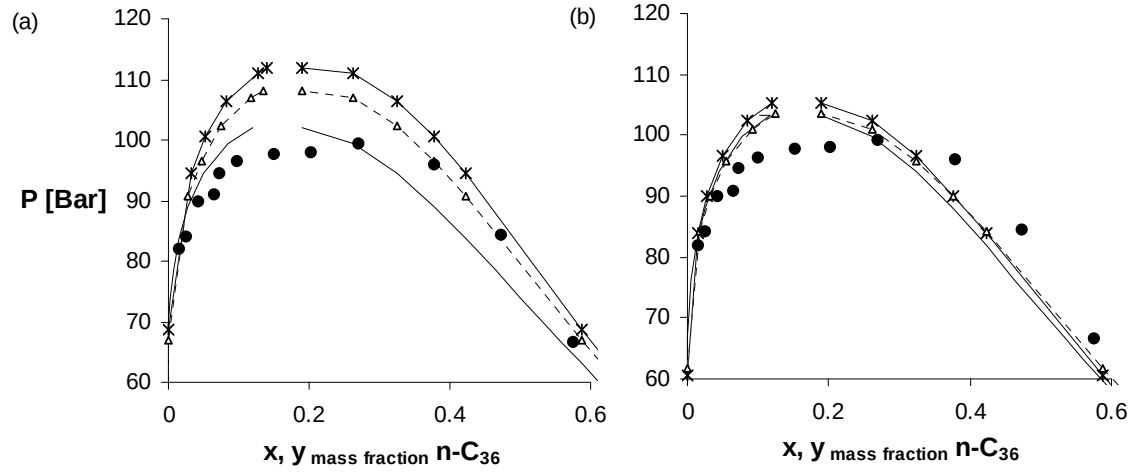

Figure 6.3 Propane – n-Hexatriacontane VLE at 340 K as represented by the (a) *simple-PHCT* and (b) *simple-PHCT-ltd* EOS. ● Experimental data [189] —— *CP* , —✳— VF and - -▵- - *2D* mixing rules.

Of the 6 equations investigated, the *simple-PHCT CP* and the *simple-PHCT-ltd* 2*D* models show the greatest potential to represent the binary phase equilibria of the asymmetric mixtures

of the n-alkane homologuous components. The *simple-PHCT CP* equation of state is able to correctly represent the light phase VLE behaviour and does not seriously over predict the mixture critical point, however it is less accurate in the heavy phase representation.

The *simple-PHCT-ltd* 2*D* equation by nature of its design is able to successfully incorporate both the correct second virial coefficient composition dependence limiting condition and the intuitive volume fraction interaction energy mixing rules. The benefits thereof can clearly be seen from Figure 6.1(b)-Figure 6.3(b), in that on the lighter phase side there is very little difference between using the *CP* and 2*D* mixing rules, whilst at the same time the model is also able to successfully represent the phase behaviour rich in heavy component. The superior behaviour of the *simple-PHCT-ltd* 2*D* equation to the *simple-PHCT-ltd VF* model in this region could possibly be attributed to the adherence of the second virial coefficient boundary condition.

All the models over predict the mixture critical point and as a result have a rather poor accuracy in the near-critical region. From the figures above it appears that an accurate critical point representation is accompanied by a poor performance in the heavier phase modelling and vice versa. (e.g. Figure 6.2(a) and Figure 6.3(a)) . It is however a commonly known fact that equations of state are generally unable to successfully represent the phase behaviour in the near-critical region and hence the poor predictive performance in this region should not be considered as a fatal flaw in the evaluation of the models.

It should be noted that binary mixtures of CO_2 and n-alkanes were not included in the evaluation of the specific mixing rules in this section. The generally poor predictive capabilities of all the models for CO_2 systems (see Figure 6.9) make the comparison between the marginal differences between different the mixing rules unfeasible. The ability of the two proposed models, the *simple-PHCT CP* and the *simple-PHCT-ltd* 2*D EOS,* to represent these systems as well as an extensive range of the n-alkane mixtures will be investigated in the following section.

6.5.2 Comparative study of the *simple-PHCT CP* and *simple-PHCT-ltd* 2*D* models

The ability of the *simple-PHCT CP* and *simple-PHCT-ltd* 2*D* mixture equations to represent a wide range of n-alkane – n-alkane and CO_2 – n-alkane binary mixtures will be investigated by comparing the performance of the two models applied both predictively and when fitted to the

experimental data. The temperature and pressure ranges of the various data sets used are listed in Table 6.4 and the various *EOS* molecular volume parameter ratios, as a measure of the mixture asymmetry, in Table 6.5. The experimental data sets were selected from the literature to enable the evaluation of the performance of the models over as wide as possible composition range. The proposed model binary interaction parameters were fitted to the experimental data and are listed in Table 6.6.

Figure 6.4 to Figure 6.7 are plots of the *VLE* data of the various binary systems investigated as represented by the *simple-PHCT CP* and *simple-PHCT-ltd* 2*D* models. From these plots it is apparent that the *simple-PHCT-ltd* 2*D* is much more successful than the *simple-PHCT CP* model in representing the binary systems predictively. As no such disparity in the ability of the models to represent the pure component properties was observed in Chapter 5 (the *simple-PHCT* model in fact even displayed a slightly smaller average vapour pressure error that the *simple-PHCT-ltd* model in section 5.4.4.b), the superior performance of the *simple-PHCT-ltd* 2*D EOS* may be attributed to the strength of the 2*D* mixing rules.

Table 6.5 Molecular size ratios of the binary mixture components.

Light Component (small)	Heavy Component (large)	$rv_{0\ large}/\ rv_{0\ heavy}$	
		Simple-PHCT	Simple-PHCTltd
CH_4	n-C_5H_{12}	2.75	2.62
CH_4	n-C_6H_{14}	3.10	2.94
CH_4	n-$C_{16}H_{34}$	8.42	7.80
C_2H_6	n-$C_{16}H_{34}$	5.64	5.98
C_2H_6	n-$C_{20}H_{42}$	5.64	5.98
C_2H_6	n-$C_{36}H_{74}$	11.75	12.63
n-C_5H_{12}	n-C_6H_{14}	8.88	9.61
n-C_6H_{14}	n-$C_{16}H_{34}$	1.13	1.13
n-C_6H_{14}	n-$C_{36}H_{74}$	2.71	2.65
CO_2	n-$C_{16}H_{34}$	5.73	5.51
CO_2	n-$C_{20}H_{42}$	9.09	8.60
CO_2	n-$C_{28}H_{38}$	11.14	10.48
CH_4	n-C_5H_{12}	17.24	16.07

Table 6.6 Fitted binary interaction parameters for the *simple-PHCT CP* and *simple-PHCT-ltd* 2*D EOS*.

Solute	Solvent	T [K]	Simple-PHCT CP l_{ij}	Simple-PHCT-ltd 2D l_{ij}	Simple-PHCT-ltd 2D (r_i=q_i) l_{ij}
CH_4	n-C_5H_{12}	377	0.025	0.020	0.006
CH_4	n-C_6H_{14}	373	0.013	0.001	-0.020
CH_4	n-$C_{16}H_{34}$	350	0.046	0.0004	-0.004
C_2H_6	n-$C_{16}H_{34}$	360	0.019	-0.004	-0.004
C_2H_6	n-$C_{20}H_{42}$	340	0.019	0.010	0.011
C_2H_6	n-$C_{36}H_{74}$	363	0.018	0.002	0.002
n-C_5H_{12}	n-C_6H_{14}	309	0.022	-0.0001	-0.0003
n-C_6H_{14}	n-$C_{16}H_{34}$	572	0.042	0.032	0.030
n-C_6H_{14}	n-$C_{36}H_{74}$	573	0.033	0.035	0.035
CO_2	n-$C_{16}H_{34}$	393	0.095	0.059	0.044
CO_2	n-$C_{20}H_{42}$	573	0.233	0.175	0.168
CO_2	n-$C_{28}H_{38}$	373	0.136	0.104	0.099

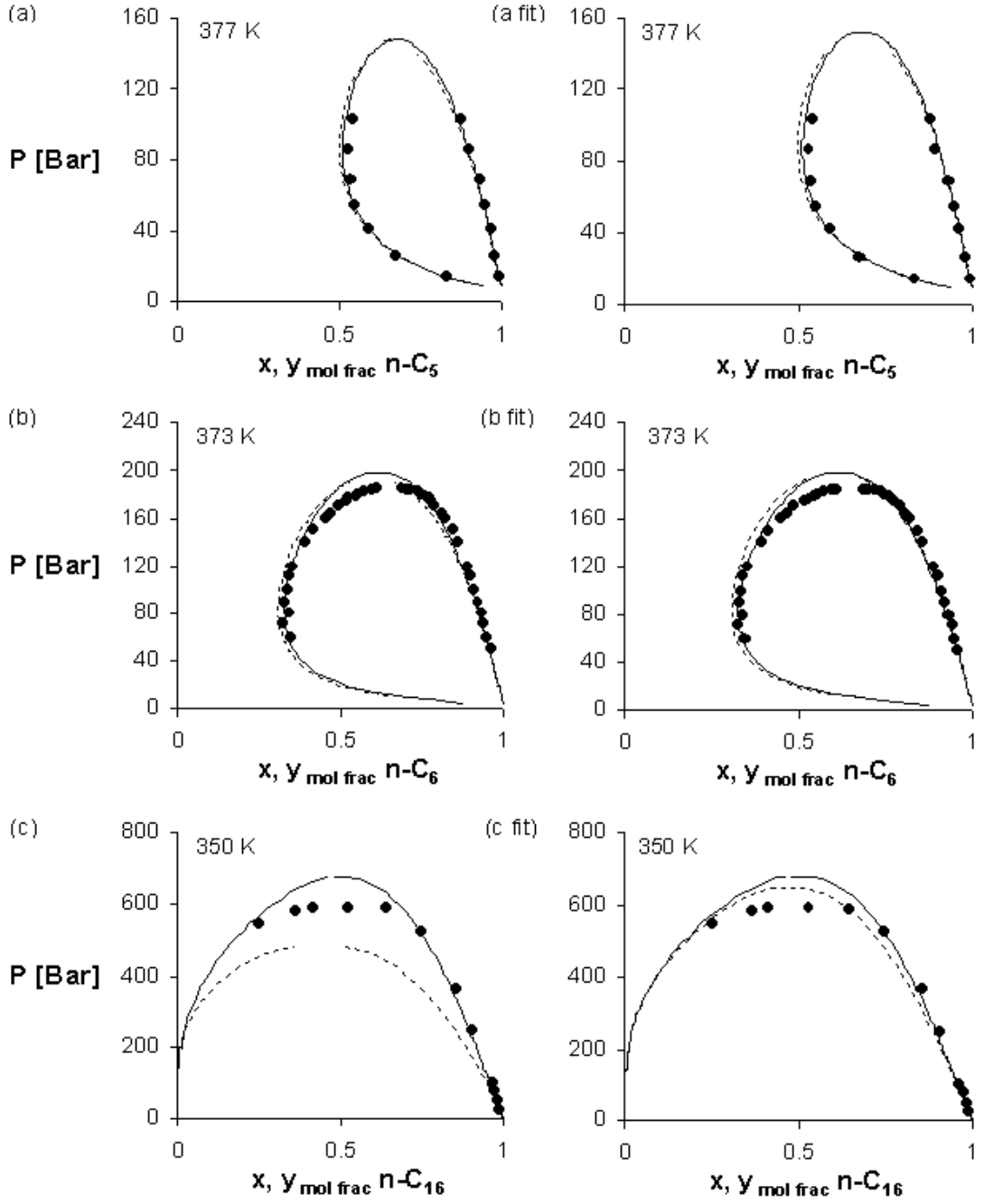

Figure 6.4 Methane – n-alkane binary VLE as represented by the -------- *simple-PHCT CP* and ——— *simple-PHCT-ltd* 2*D* models. (See Table 6.4 for the literature references of the ● experimental data, and Table 6.6 for the fitted binary interaction coefficient.)

From Figure 6.4 containing the plots of the methane binaries, it can be seen that the the *simple-PHCT-ltd* 2*D EOS* is able, without the use of interaction parameters, to represent the *VLE* data over the entire concentration range. When fitting the models to the data comparable results can be obtained for both models. The binary interaction parameters of the *simple-PHCT-ltd* 2*D* model are however much smaller than those of the *simple-PHCT CP* equation.

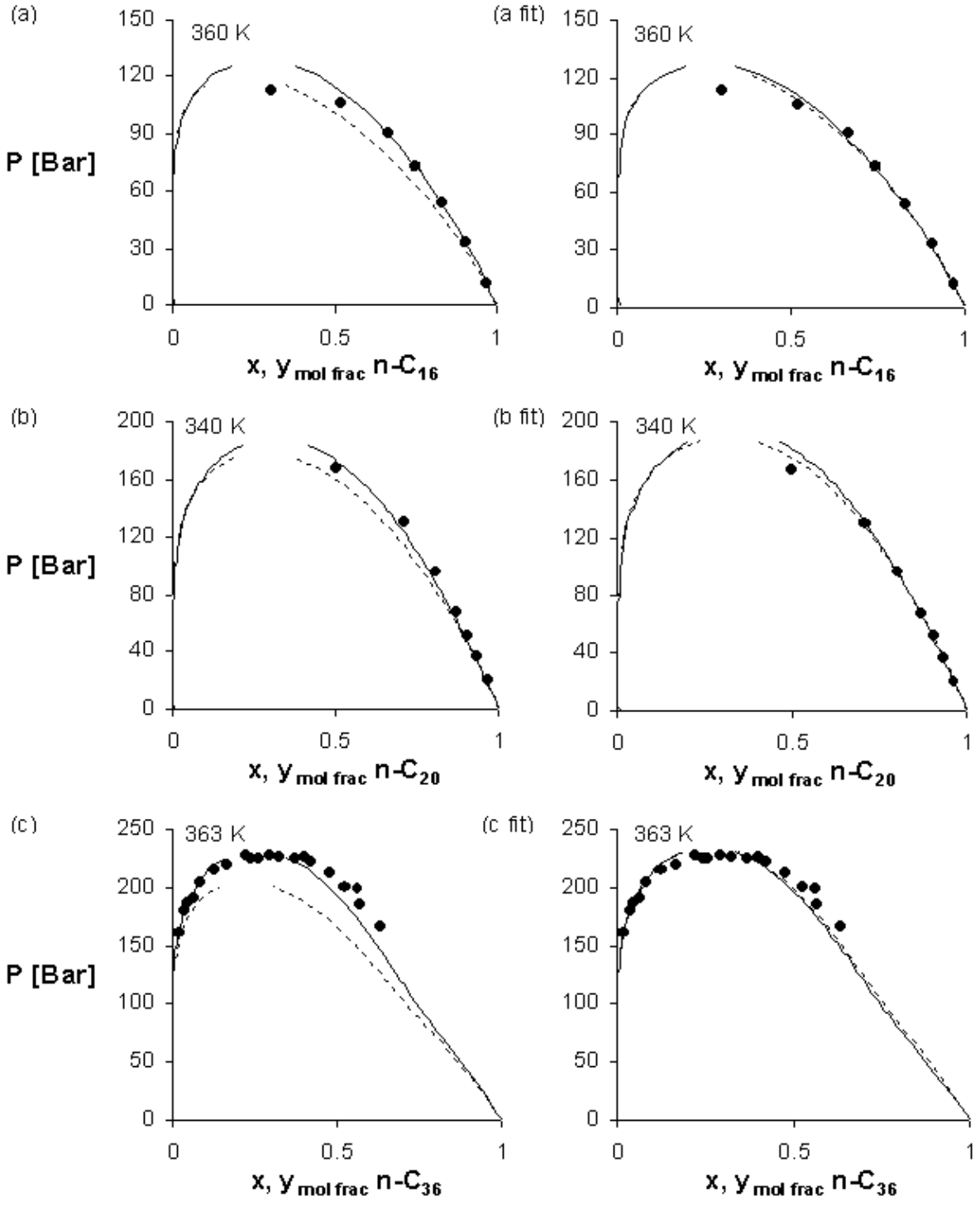

Figure 6.5 Ethane – n-alkane binary VLE as represented by the ..... *simple-PHCT CP* and ——— *simple-PHCT-ltd* 2*D* models. (See Table 6.4 for literature references of the ● experimental data, and Table 6.6 for the fitted binary interaction coefficient.)

For the ethane binary systems, shown in Figure 6.5, similar observations can be made on the predictive capability of the *simple-PHCT-ltd* 2*D* model and its subsequent small fitted binary interaction parameter. It is also encouraging to observe in Figure 6.5 (c) the success with which the near critical region of the ethane-n-hexatriacontane system can be represented.

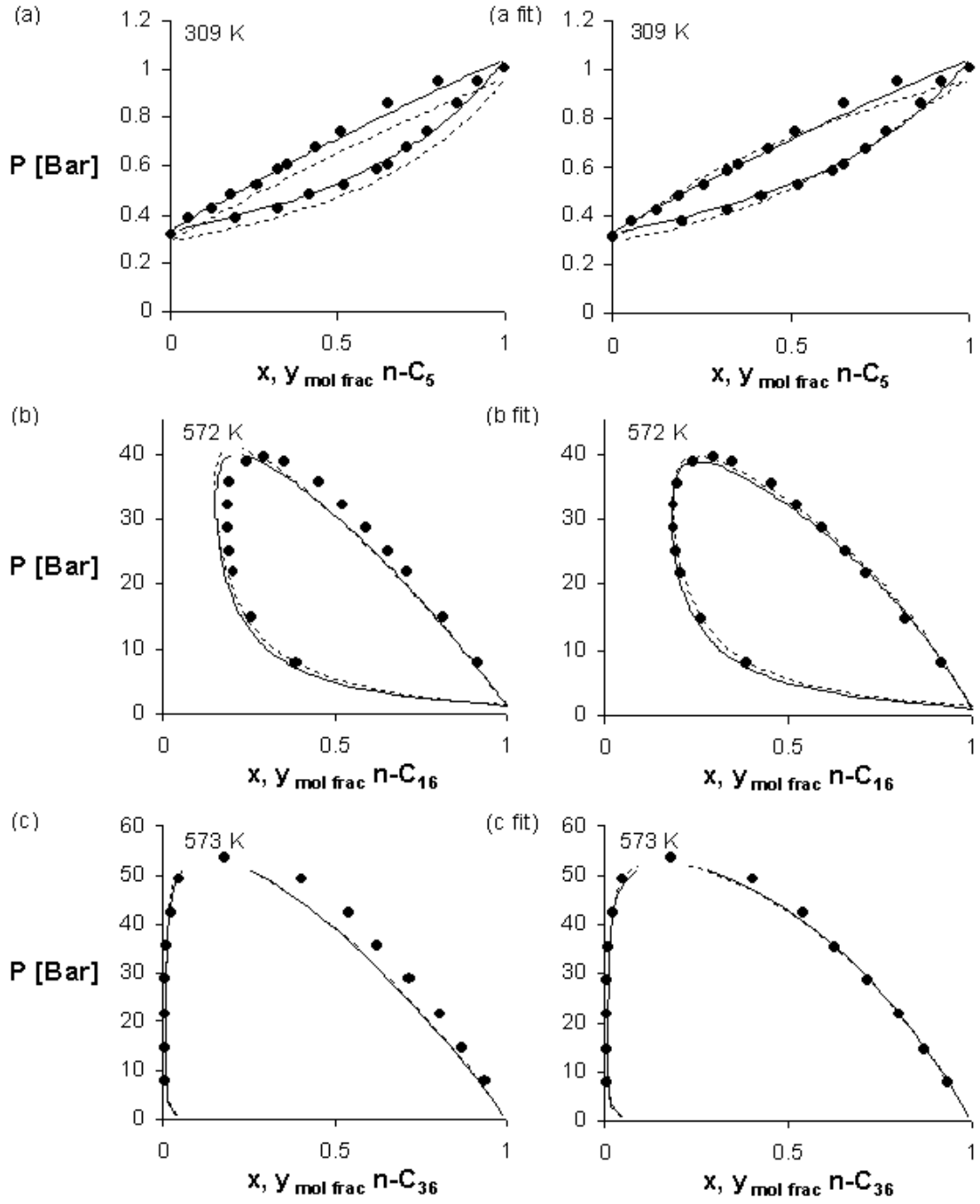

Figure 6.6 Hexane – n-alkane binary VLE as represented by the ..... *simple-PHCT CP* and ——— *simple-PHCT-ltd* 2*D* models. (See Table 6.4 for the literature references of the ● experimental data, and Table 6.6 for the fitted binary interaction coefficient.)

From Figure 6.6 it is apparent that with the exception of the n-hexane – n-pentane binary system, the two models give virtually indistinguishable results. The representation of the n-hexane – n-pentane binary system, as depicted in Figure 6.6 (a) and (a fit), is highly dependent on the accuracy with which the models can represent the pure component properties because of the very similar components and because the binary system is at a temperature below the critical temperature of the lighter components. The accuracy with which the two *EOS* are able

to represent the pure component vapour pressures greatly influences the overall binary *VLE* representation of the n-hexane – n-pentane binary system . This factor cannot be improved by the use of a binary interaction parameter. From Figure 6.6 it is apparent that the *simple-PHCT-ltd* model is able to represent the specific pure component vapour pressures more accurately than the unconstrained *simple-PHCT* equation.

The representation of carbon dioxide – n-alkane binaries is significantly more difficult than that of mixtures of species from the same homologous series. Furthermore the evaluation of the models is constrained by the limited availability of experimental data for these systems, as the VLE data over an entire concentration range are rarely reported in literature.

From Figure 6.7 it is apparent that even though the predictive representation of the CO_2 – n-alkane systems is still subject to large inaccuracies the *simple-PHCT-ltd* 2*D* model performs slightly better than the *simple-PHCT CP* equation in the modelling of the heavier phase saturated pressures. Furthermore by using a single binary interaction parameter both models were found to be able to represent these complex systems, and the *simple-PHCT-ltd* 2*D* model was found to generally require a smaller interaction parameter than the *simple-PHCT EOS* (Table 6.6) .

From the discussion above it is apparent that the *simple-PHCT-ltd* 2*D* model is more suited to represent the *VLE* data of the n-alkane and the CO_2 – alkane binary mixtures, being more predictive and hence requiring a smaller fitted interaction parameter than the *simple-PHCT CP* equation. This result is especially encouraging when considering the discussion on the computational speed of the modelling of multi-component thermodynamic properties in section 6.2.1.c. The *simple-PHCT CP* model requires a total of 3 *DSMR* and 2 *SSMR* whilst the *simple-PHCT-ltd* 2*D* model only needs 2 *DSMR* and 3 *SSMR* (see section 6.3.1). As discussed in section 6.2.1.c the calculation of a *DSMR* is much more costly than the calculation of a *SSMR* with the

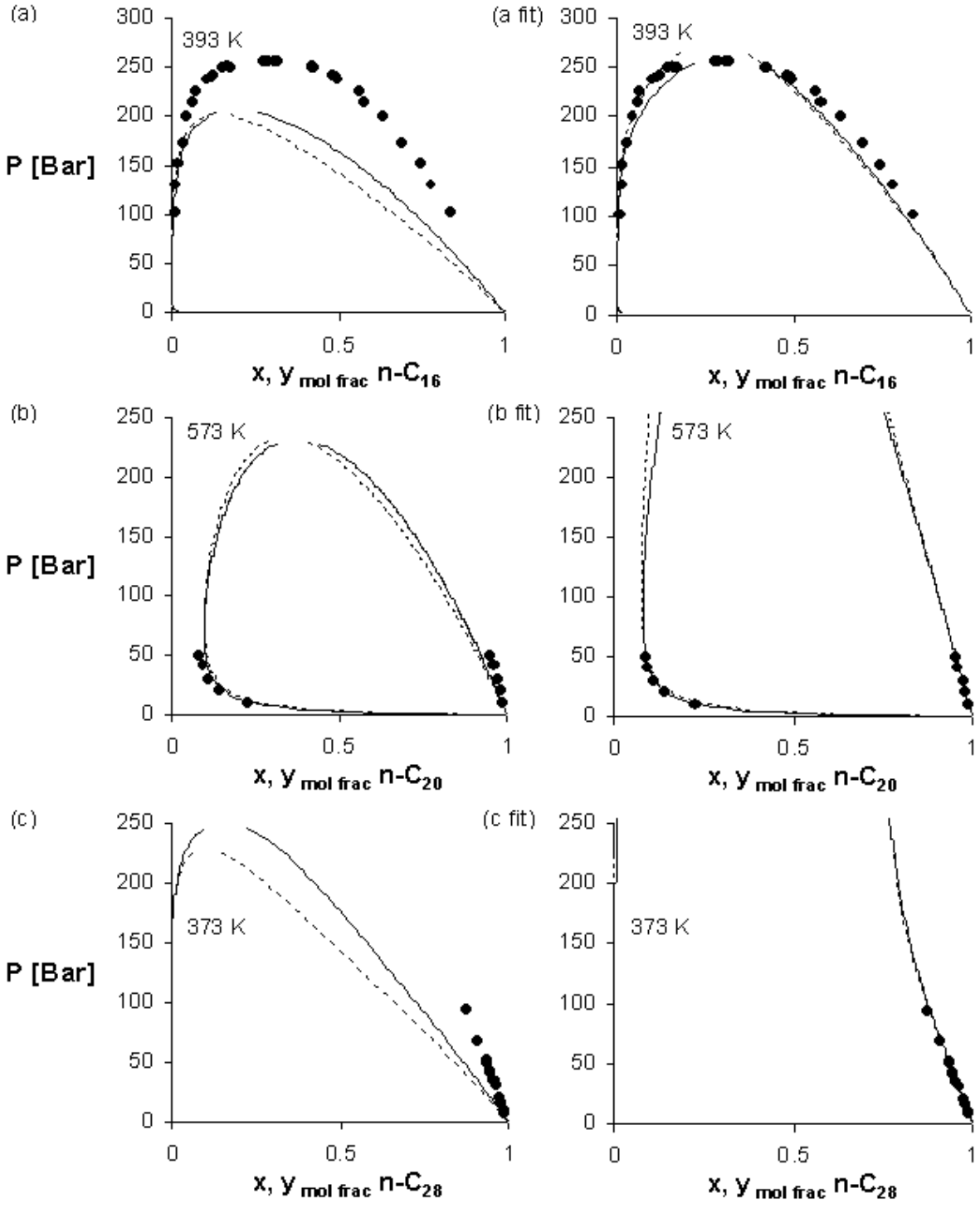

Figure 6.7 CO_2 – n-alkane binary VLE as represented by the ---------- *simple-PHCT CP* and ——— *simple-PHCT-ltd* 2*D* models. (See Table 6.4 for the literature references of the ● experimental data, and Table 6.6 for the fitted binary interaction coefficient.)

difference in computational speed of the two mixing rules will become more pronounced as the number of components in the fluid mixture increases. For a system of *n* components, using the *simple-PHCT-ltd* 2*D* model would therefore require $n^2 - n$ less calculations per iteration than if the *simple-PHCT CP* model had been used.

6.5.3 Definition of the v_{00} and ε'_0 parameters for the *simple-PHCT-ltd* 2*D* model

Up to this point in the investigation of the proposed equations of state only the first definition has been applied with the properties of the smallest component used as the universal constant values. Using the *simple-PHCT-ltd* 2*D* model the effect of using the alternate definitions of the terms v_{00} and ε'_0 was investigated.

As discussed in section 6.3.2.b the v_{00} and ε'_0 parameters can be assigned two different definitions. The first is to assign to them constant values characteristic of a segment particle. As discussed before, because of the mathematical structure of the mixing rules used in this investigation, the actual values of these constants will have no effect on the mixture properties. The second approach in defining the parameters is to set the q parameter equal to the segment number or chain length, r, instead of defining it as the molecular surface area. By setting r=1 for the smallest component in the fluid mixture and hence setting the 'segment volume' equal to the molecular volume of the smallest component, the ε'_0 parameter becomes the intermolecular interaction energy per molecular volume of the smallest component, which conceptually should facilitate the determination of fluid mixture properties of asymmetric systems. It was however found that the *simple-PHCT-ltd* 2*D* equation of state is fairly insensitive to definition of the v_{00} and ε'_0 parameters. This can be seen from the small difference in the fitted binary interaction parameters as listed in Table 6.6. With the exception of the methane and CO_2 binaries there is very little difference between the fitted interaction parameters. Figure 6.8 and Figure 6.9 are typical plots of the predictive representation of the methane – and CO_2 – n-alkane binary mixtures by the *simple-PHCT-ltd* 2*D* equation using the two different definitions for the v_{00} and ε'_0 parameters. When fitted to the experimental data or applied to the other n-alkane-n-alkane mixtures the two different methods produced virtually identical results. These figures are therefore not shown.

From Figure 6.8 and Figure 6.9 it seems that by setting r=q the mixture critical point as predicted by the equation of state is shifted to a higher pressure. This clarifies the increase observed in the fitted in the methane binary interaction coefficients compared to the decrease for the coefficients of the CO_2 binaries when the second definition is used to define the segment parameters (Table 6.6). As the *simple-PHCT-ltd* 2*D* already over predicts the mixture critical point using the original *EOS* form the error is increased by using the second definition and hence requires a larger interaction coefficient to compensate for it.

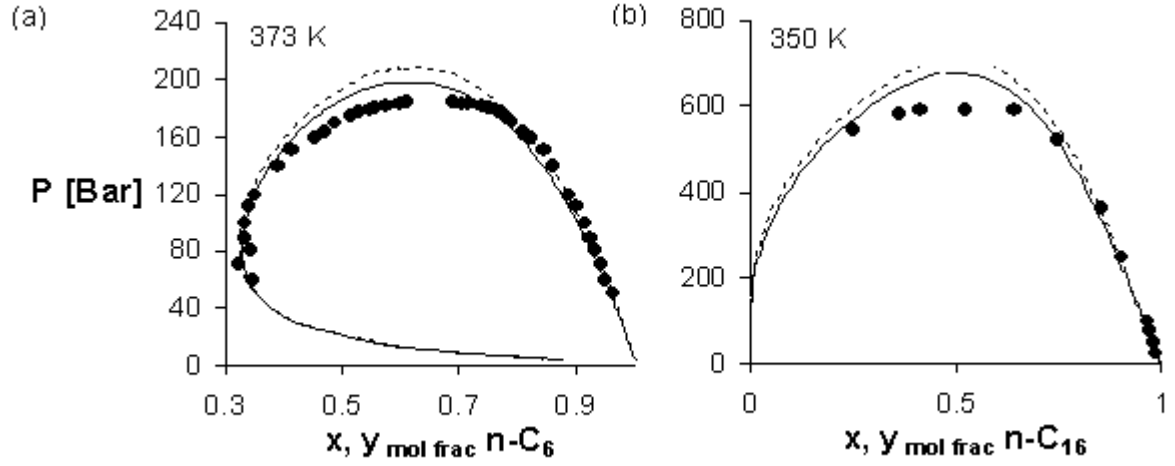

Figure 6.8 Methane – n-alkane binary VLE as represented by the *simple-PHCT-ltd* 2*D* model with l_{ij} = 0 and —— v_{oo} ε'_0 definition 1, and -------- v_{oo} ε'_0 definition 2.

On the other hand, because the *simple-PHCT-ltd* 2*D* severely under predicts the pressures of the *VLE* saturated boundary curves in the CO_2 systems, the second definition slightly reduces this error leading to a smaller interaction coefficient.

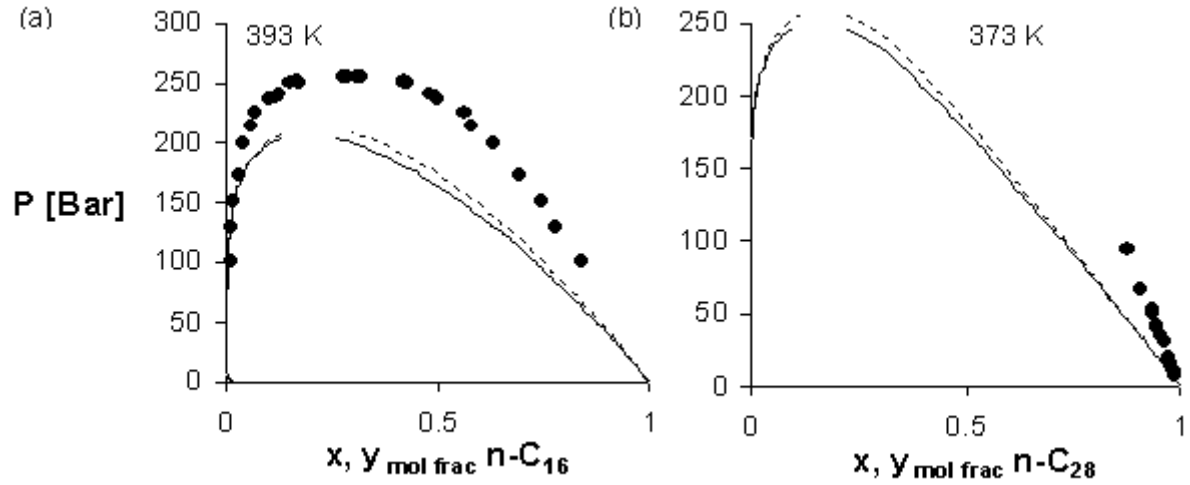

Figure 6.9 CO_2 – n-alkane binary VLE as represented by the *simple-PHCT-ltd* 2*D* model with l_{ij} = 0 and —— v_{oo} ε'_0 definition 1, and -------- v_{oo} ε'_0 definition 2.

The poor performance of the *simple-PHCT-ltd* 2*D* equation in representing the CO_2 – n-alkane systems can however not be solely attributed to an under-prediction of the mixture critical pressure, but should probably be attributed to the fact that all the intermolecular interactions have not completely been accounted for. Furthermore, as the original *simple-PHCT-ltd* 2*D* model is fairly predictive for the methane binary systems, it will require, if any, very small interaction coefficients whilst the CO_2 - n-alkane binaries would, even when setting $r=q$ (definition 2), require large interaction parameters. Using the second definition for the v_{00} and

ε'_0 would therefore in effect worsen the representation of the methane binary system, without having any significant benefit in the modelling of the CO_2 binaries.

From these observations it was therefore decided to continue using the original definition of the segment parameters with v_{00} and ε'_0 being set equal to the molecular values (rv_0 and $q\varepsilon'_0$) of the smallest component in the mixture.

6.5.4 Investigation into the temperature of the *simple-PHCT-ltd* 2*D EOS* interaction parameter

It is an important requirement of any practical equation of state that the binary interaction parameters be well behaved in order to facilitate the extrapolation to systems for which there is no experimental binary *VLE* data not available. In this section the binary interaction parameters of the *simple-PHCT-ltd* 2*D* model will be briefly investigated.

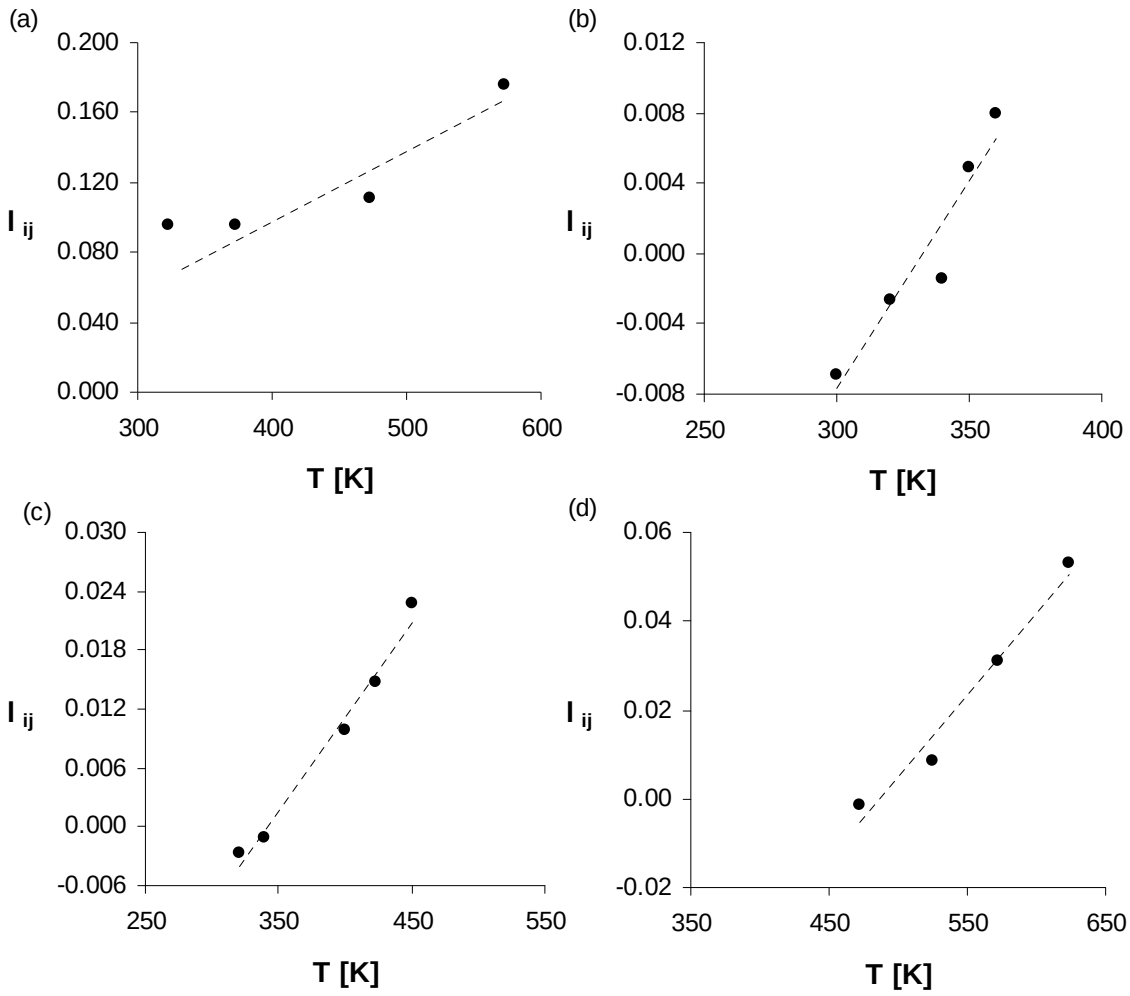

Figure 6.10 *simple-PHCT-ltd* 2*D* fitted binary interaction parameters as a function of temperature for the (a) CO_2 – n-$C_{20}H_{42}$, (b) CH_4 – n-$C_{16}H_{34}$ (c) C_2H_6 – n-$C_{20}H_{42}$ and (d) n-C_6H_{14} - n-$C_{16}H_{34}$ binary systems.

As can be seen from Figure 6.10 the binary interaction coefficients of the *simple-PHCT-ltd* 2*D EOS* are dependent on the system temperature. The temperature dependence appears to be a simple linear functionality with the interaction parameters however displaying a very small degree of scatter. Care should be taken when extrapolating these parameter values to temperatures outside the investigated range especially to conditions in close proximity to phase boundaries as the interaction parameters are expected to vary greatly in this region.

6.6 SUMMARY AND CONCLUSIONS

In this section the *simple-PHCT* and *simple-PHCT-ltd* equations of state were extended to fluid mixture systems. All the proposed mixing rules allow for the use of a single interaction parameter in the interaction energy combination rule. The mixing rules were evaluated according to performance, computational speed and simplicity and theoretical correctness.

Methane –, ethane – , hexane – and CO_2 – n-alkane binary *VLE* data over as wide a composition range as possible were used to test these mixing rules on systems with large size asymmetry and mixtures of unlike components.

It was found that violating the theoretically based quadratic compositional dependence of the virial coefficient decreases the performance of the equation of state modelling the light phase boundary line. On the other hand it was observed that by using a volume fraction mixing rule for the mixture interaction energy improved the performance of the model when applied to the heavier phase. It seems therefore that there is a trade off between the ability of the equation of state to model the two phases. The 2*D* mixing rule applied to the *simple-PHCT-ltd* incorporates both the correct second virial coefficient boundary condition and the volume fraction mixing rule and was found to be clearly superior to both the volume fraction and theoretically correct mixing rules.

It was furthermore found that the proposed equations of state are fairly insensitive to the definition of the 'segment' v_{00} and ε'_0 parameters. For the purposes of this study the mixture component with the smallest molecular volume will therefore be used to define the values for these parameters.

Based on the superior performance and simple structure of the mixing rules, requiring the calculation of 2 double summations and 3 single summations over the number of components in the mixture, the *simple-PHCT-ltd* 2*D* equation of state is found to be the most suitable model to represent the mixture *VLE,* with the fitted binary interaction parameters being generally small and well behaved with a linear temperature dependence very little scatter for varying system temperatures.

Chapter 7 ***The simple-PHCT-ltd Equation of State***

In the preceding chapters the development of the *simile-PHCT-ltd* equation of state has been outlined. This model has been specifically developed to satisfy the need for an accurate equation of state capable of representing chained systems whilst maintaining the computational and mathematical simplicity required for practical applications.

In this chapter the developed model be presented as a whole, the generalization of the model parameters for pure components will be discussed and the performance of the model will be evaluated against some of the more commonly applied equations of state, the *SRK, SAFT, PC-SAFT* and the *SPHCT* models.

7.1 OVERVIEW OF THE SIMPLE-PHCT-LTD EOS

Summarising the results of the preceding chapters, the proposed *simple-PHCT-ltd EOS* has the following form:

$$z = 1 + c\left(\frac{4\eta + b\eta^2 + e\eta^3}{1 - d\eta}\right) + c\left(\sum_n^3 \sum_m^3 mD_{nm}\left(\frac{\eta}{\tau}\right)^m \left(\frac{1}{T'^*}\right)^n\right) \qquad 7.1$$

where z is the *EOS* compressibility and

$$\begin{aligned} \eta &= r v_0 \tau \rho \\ T'^* &= \frac{ckT}{q\varepsilon'} \\ \tau &= \frac{\pi\sqrt{2}}{6} \end{aligned} \qquad 7.2$$

and

$$\begin{aligned} v_0 &= v_{00}\left(1 - 0.12\exp\left(-\frac{3\varepsilon'_0}{ckT}\right)\right) \\ \varepsilon' &= \varepsilon'_0\left(1 + \frac{\mu}{kT}\right) \end{aligned} \qquad 7.3$$

The model has three component specific parameters, the molecular volume, rv_{00}, the interaction energy, $q\varepsilon$', and the external degree of freedom parameter c. The parameter representing the temperature dependence of the interaction parameter, μ, for small molecules such as argon, nitrogen, methane and carbon dioxide is generally used as was determined by Chen and Kreglewski [42], and set to $\mu = 1$ for the n-alkane homologous series. The chain length parameter, r, and the interaction surface area parameter, q, are only found in their individual forms when the *EOS* is applied to fluid mixtures, and are then arbitrarily defined as being equal to the ratio of the specific molecular parameters of the component with the smallest molecular volume in the fluid mixture:

$$r_i = \frac{(rv_{00})_i}{(rv_{00})_{smallest\ \ component}}$$
$$q_i = \frac{(q\varepsilon')_i}{(q\varepsilon')_{smallest\ \ component}} \qquad 7.4$$

The universal parameters used in the hard sphere and perturbation double summation parameter matrix are listed in Table 7.1.

Table 7.1 Universal parameters for use in the *simple-PHCT-ltd EOS*

Simple-PHCT-ltd Universal Parameters			
Hard sphere term			
b	**e**		**d**
4.404	5.363		1.399
Perturbation Matrix			
D_{nm}	**m = 1**	**m = 2**	**m = 3**
n = 1	-8.11395	-4.12083	-4.94835
n = 2	0	12.4693	-6.2256
n = 3	0	-5.66021	4.85777

The following mixing rules were developed to enable the *simple-PHCT-ltd* equation to represent multi-component systems:

$$c_{mix} = \sum_{i=1}^{nc} x_i c_i \qquad 7.5$$

$$\left(rv_0\right)_{mix} = \sum_{i=1}^{nc} x_i \left(rv_0\right)_i$$

or

$$\eta_{mix} = \rho\tau \sum_{i=1}^{nc} x_i \left(rv_0\right)_i \qquad 7.6$$

and

$$\begin{aligned}\left(c\left(\frac{q\varepsilon'}{ck}\right)rv_0\right)_{mix} &= \sum_{i=1}^{nc}\sum_{j=i}^{nc} x_i x_j c_i \left(\frac{q_i\varepsilon'_{ij}}{c_i k}\right) r_j v_{0ij} \\ &= \sum_{i=1}^{nc}\sum_{j=i}^{nc} x_i x_j \left(\frac{q_i\varepsilon'_{ij}}{k}\right) r_j v_{0ij}\end{aligned} \qquad 7.7$$

$$\begin{aligned}\left(\frac{q\varepsilon'}{ckT}\right)_{mix} &= \sum_{i=1}^{nc}\sum_{j=1}^{nc} f_i f_j \left(\frac{q_i\varepsilon'_{ij}}{c_i k}\right) \\ &= \frac{\sum_{i=1}^{nc}\sum_{j=1}^{nc} x_i x_j r_i r_j v_{0i} v_{0j} \left(\frac{q_i\varepsilon'_{ij}}{c_i k}\right)}{\left(rv_0\right)^2_{mix}}\end{aligned} \qquad 7.8$$

The combination terms used in equations 7.7 and 7.8 allow for the use of one binary interaction parameter in model. The combination rules are defined as follows:

$$v_{0ij} = \left(\frac{v_{0i}^{1/3} + v_{0j}^{1/3}}{2}\right)^3 \qquad 7.9$$

and

$$\varepsilon'_{ij} = \sqrt{\varepsilon'_i \varepsilon'_j}\left(1 - l_{ij}\right) \qquad 7.10$$

In order to clarify the use of the mixing rules, equation 7.1 can be written in the following form, where equations 7.5 to 7.8 are used to determine the mixture properties:

$$\begin{aligned}z = 1 + c_{mix}&\left(\frac{4\eta_{mix} + b\eta_{mix}^{\ 2} + e\eta_{mix}^{\ 3}}{1 - d\eta_{mix}}\right) + \\ &\left(\frac{\rho D_{11}}{T}\left(c\left(\frac{q\varepsilon'}{ck}\right)rv_0\right)_{mix} + \sum_{n=2}^{3}\sum_{m=2}^{3} mD_{nm}\left(\frac{\eta_{mix}}{\tau}\right)^m \left(\frac{q\varepsilon'}{ckT}\right)^n_{mix}\right)\end{aligned} \qquad 7.11$$

Equations 7.1 to 7.10 comprise the entire *simple-PHCT-ltd* equation of state. No further equations or correlations are needed if the pure component parameters are already known. This is however not always the case, and, in order to facilitate the generalization of the model, correlations need to be developed in order to facilitate the estimation of these parameters. The generalization of the pure component parameters for the n-alkane homologous series will be presented in the next section.

Table 7.2 Simple-PHCT-ltd EOS pure component paramters

Simple-PHCT-ltd Fitted Parameters							
Component	**P [Bar]**	**T [K]**	**c**	**rv_{00} [1e6 m^3]**	**qε'/k [K]**	**μ/k [K]**	**Reference**
n-Alkanes							
Methane	0 - 1000	100 - 500	1	22.99	190.2	1	[130]
Ethane	0.97 - 600	150 – 620	1.23	32.59	348.9	1	[130]
Propane	0.06 - 450	182 – 620	1.48	42.01	477.4	1	[130]
n-Butane	0.06 – 400	216 – 580	1.72	51.18	607.0	1	[130]
n-Pentane	0.03 – 500	237 - 600	1.97	60.15	734.2	1	[130]
n-Hexane	0.01 – 370	244 – 600	2.22	67.69	861.6	1	[130]
n-Heptane	0.01 – 100	267 – 600	2.40	73.24	982.0	1	[130]
n-Octane	P sat.*	216 – 568	2.58	94.73	1072.4	1	[54]
n-Nonane	P sat.*	219 – 594	2.76	104.78	1182.2	1	[54]
n-Decane	P sat.*	243 – 617	2.93	114.16	1291.6	1	[54]
n-Undecane	P sat.*	247 – 639	3.23	122.43	1429.9	1	[54]
n-Dodecane	P sat.*	263 – 658	3.46	129.88	1553.1	1	[54]
n-Tridecane	P sat.*	267 – 675	3.71	139.94	1677.9	1	[54]
n-Tetradecane	P sat.*	279 – 693	3.94	147.52	1797.9	1	[54]
n-Pentadecane	P sat.*	283 – 708	4.07	158.18	1891.0	1	[54]
n-Hexadecane	P sat.*	291 – 723	4.40	164.33	2038.1	1	[54]
n-Heptadecane	P sat.*	295 – 736	4.56	173.66	2142.2	1	[54]
n-Octadecane	P sat.*	301 – 747	4.78	181.86	2254.9	1	[54]
n-Nonadecane	P sat.*	305 – 758	5.17	189.21	2419.0	1	[54]
n-Eicosane	P sat.*	309 – 768	5.34	195.95	2523.9	1	[54]
n-Octacosane	P sat.*	345 – 460	8.34	293.80	3757.9	1	[148, 168, 211]
n-Dotriacontane	P sat.*	350 – 460	9.67	335.12	4331.4	1	[148, 168, 211]

Simple-PHCT-ltd Fitted Parameters							
Component	**P [Bar]**	**T [K]**	**c**	**rv_{00} [1e6 m^3]**	**qε'/k [K]**	**μ/k [K]**	**Reference**
n-Hexatriacontane	P sat.*	355 – 460	10.99	373.05	4894.3	1	[148, 168, 211]
Other							
Argon	0.7 – 1000	84 – 700	1	17.35	150.9	0	[130]
Nitrogen	1 – 200	80 – 600	1	20.83	123.7	3	[130]
Carbon Dioxide	5 – 500	218 – 600	1.2	20.8	306	40	[130]
Carbon Monoxide	0 – 500	70 – 600	1	21.73	128	4.2	[130]
Hydrogen	13 – 500	80 – 360	0.806	13	26.06	1	[130]
i-butane	P sat.*	113 - 408	1.50	54.39	537.5	1	[54]
i-pentane	P sat.*	113 - 460	1.91	63.24	694.9	1	[54]
methylcyclopentane	P sat.*	130 - 532	1.66	66.59	747.8	1	[54]
cyclohexane	P sat.*	279 - 553	1.73	63.05	796.1	1	[54]
methylcyclohexane	P sat.*	146 - 572	1.86	76.07	852.1	1	[54]
benzene	P sat.*	278 - 562	1.71	52.75	805.4	1	[54]
toluene	P sat.*	178 - 591	1.88	63.62	894.2	1	[54]
m-xylene	P sat.*	225 - 617	2.12	74.51	1017.4	1	[54]
o-xylene	P sat.*	247 - 630	2.13	73.36	1040.7	1	[54]

*** Saturated Pressures in temperature range**

7.1.1 Pure component parameters and generalized correlations

The generalization of the pure component parameters of the various proposed chained equations have already been briefly discussed in section 5.4.4.d. With the final form of the equation of state now specified, correlations for the various pure component parameters can be developed. The pure component parameters fitted for the *simple-PHCT*-ltd equation of state are listed in Table 7.2.

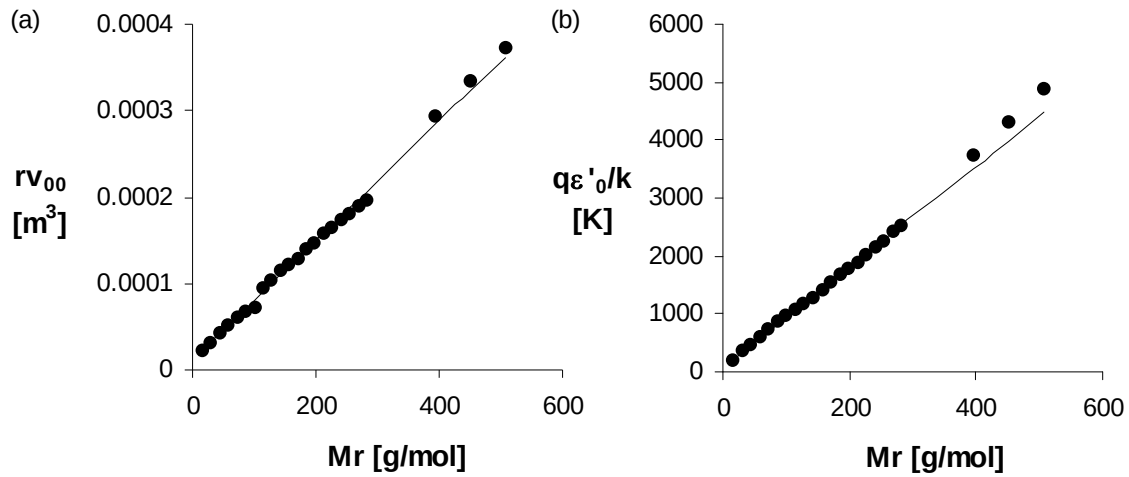

Figure 7.1 *Simple-PHCT-ltd EOS* n-alkane pure component parameters as a function of molecular weight. (a) rv_{00} and (b) $q\varepsilon'/k$ with ● the fitted parameters and —— the generalized correlation

As can be seen from Figure 7.1 and Figure 7.3 the *simple-PHCT-ltd EOS* parameters of the n-alkane homologous series display a simple relationship with the pure component molecular weight. (The slight deviation of the three heaviest components, n-octacosane, n-dotriacontane and n-hexatriacontane, from the regular behaviour can be attributed to the fact that the saturated properties of these components are available over a much smaller temperature range as can be seen in Table 7.2. These limited datasets could lead to an over-fitting of the *EOS* parameters in a specific region.) The simple linear relationship of the molecular volume and the interaction energy parameters with the component molecular weight is as expected as all the n-alkane species in the homologous series, with the exception of methane, only differ in the number of $-CH_2-$ segments. These segments should all contribute equally to the overall volume and interaction energy of the various components. This relationship between the molecular parameters and the $-CH_2-$ segment number is confirmed in Figure 7.2 which shows the reduced molecular volumes and intermolecular interaction energies plotted against the n-alkane molecular weight have to nearly identical slopes. This indicates that the energy and volume parameters are functions of the same characteristic parameter, and that this parameter varies linearly with the n-alkane molecular weight similarly to the manner in which the number of $-CH_2-$ segments in the homologous series varies. (The two molecular parameters in Figure 7.2 are scaled by the parameter values of n-hexatriacontane.)

In Figure 7.3 the n-alkane $q\varepsilon'/(ck)$ parameters are plotted against the component molecular weight. As discussed in section 5.4.4.d the $q\varepsilon'/(ck)$ parameter in effect represents the interaction energy contribution per external degree of freedom. From the figure it can be seen that as the molecular weight, and in effect the molecular length, reaches a certain value, the

interaction energy contribution stabilises at a specific value. The location of this point may be interpreted as the chain length where the CH_3 – end-effects cease to have a significant influence on the intra-molecular bond strengths and hence on the external degrees of freedom of motion. From this point on the addition of any more $–CH_2–$ segments will not change the *overall* 'rigidity' of the molecule and will only result in a proportional increase in the interaction energies and degrees of freedom of motion.

From the observed relationship with the n-alkane molecular weight, the following generalized pure parameter correlations were developed for n-alkanes:

$$rv_{00} = \left(0.6879Mr + 11.909\right) * 1e - 6 \qquad 7.12$$

$$\frac{q\varepsilon'}{k} = 8.6892 * Mr + 75.893 \qquad 7.13$$

$$\frac{q\varepsilon'}{ck} = 190.218 + \frac{\left(Mr - Mr_{methane}\right)}{Mr}\left[299.742 - 170.735\exp\left(-0.0143Mr\right)\right] \qquad 7.14$$

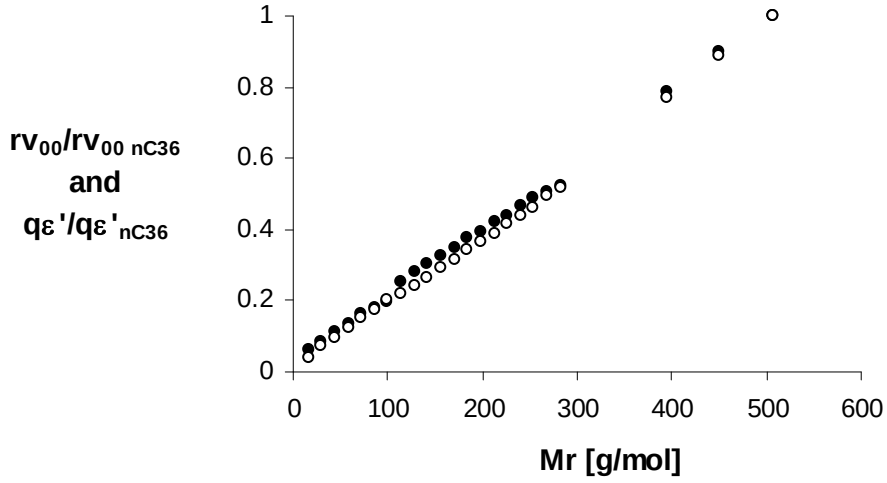

Figure 7.2 Scaled molecular volume and interaction energy parameter values as a function of n-alkane molecular weight. ● scaled rv_{00} and ○ scaled $q\varepsilon'/k$

Equation 7.14 incorporates the methane molecular weight into the correlation to ensure the correct *c* parameter for the smaller components. As discussed in section 7.1 above, the temperature dependence of the intermolecular interaction parameter is kept constant over the entire n-alkane homologous series, i.e. $\mu/k = 1$.

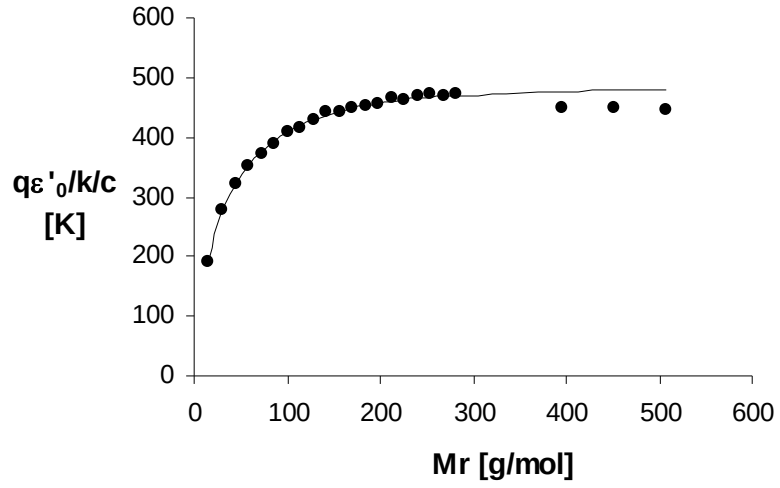

Figure 7.3 *Simple-PHCT-ltd EOS* n-alkane $q\varepsilon'/k/c$ value as a function of molecular weight, with ● the fitted parameters and —— the generalized correlation

The generalized correlations can be used to estimate *EOS* parameters for the modelling of thermodynamic properties of n-alkanes with molecular weights in the range 16 – 507 g/mol in the temperature range 310-540 K. Because equations 7.12 through to 7.14 are functions of molecular weight they can also be used to determine the *EOS* parameters of pseudo-components defined as having a molecular weight equal to the average weight of the n-alkane mixtures they are said to represent. The parameter behaviour appears to be well captured by the generalizations, facilitating the possible extrapolation of the correlations to temperatures and molecular weights outside the range in which they have been defined. Care should however always be taken when doing so and the calculated parameters subjected to critical evaluation.

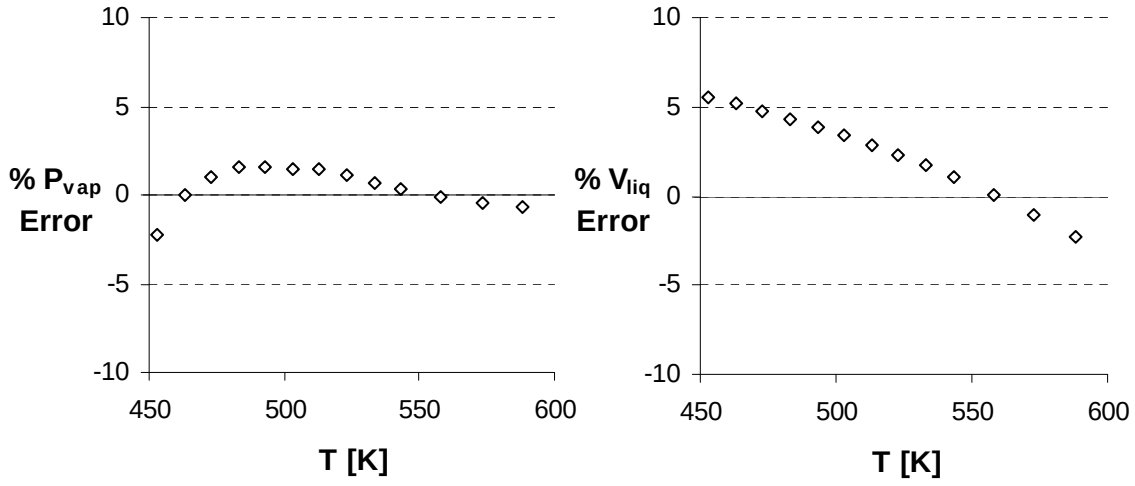

Figure 7.4 Error in vapour pressure estimation using the *simple-PHCT-ltd* EOS and equations 7.12 - 7.14. ◇ n-Tetradecane

Figure 7.4 is a plot of the errors in the saturated vapour pressure and liquid volume of n-tetracosane as reported by Morgan and Kobayashi [148] and determined using the *simple-PHCT-ltd* model with the generalized correlations. It should be noted that the *EOS* parameters of these components were not used in the development of the correlations. From Figure 7.4 it can be seen that by using equations 7.12 through 7.14 the n-tetracosane vapour pressures can be estimated to within 2.5 % and the liquid volume to 5% in the temperature range 450-600 K.

Unfortunately no reliable vapour pressure data of n-alkanes heavier than n-hexatriacontane is available in order to investigate the extrapolation of the developed correlations to higher molecular weight alkanes directly. The ability of the *simple-PHCT-ltd* model to represent the n-propane – n-$C_{60}H_{122}$ predictively (without the use of a binary interaction parameter) was therefore used as a measure of the success of the *EOS* parameter correlation extrapolation.

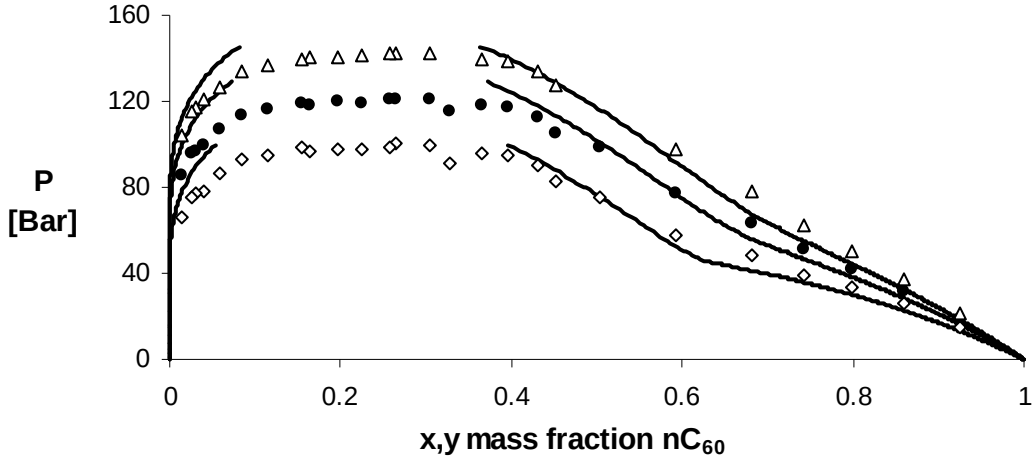

Figure 7.5 n-Propane – n- hexacontane binary *VLE* data at ○ 378 K, ● 393 K and △ 408 K as represented by the *simple-PHCT-ltd EOS* with l_{ij} = 0.

Figure 7.5 is a plot of the n-propane – hexacontane binary system at 378 and 408 K. The experimental data were obtained from the work by Schwarz and Nieuwoudt [189] and interpolated results of Peters et al. [166]. The *simple-PHCT-ltd EOS* is applied purely predictively, with the n-propane parameters as listed in Table 7.2 and using equations 7.12 to 7.14 to estimate the hexacontane parameters. As can be seen an excellent representation of the binary system can be obtained.

7.2 LITERATURE EQUATIONS OF STATE

The performance of the proposed *simple-PHCT-ltd* equation of state will be evaluated against some of the more commonly applied models in literature. As many of the important features of

these models have already been discussed in the preceding chapters the equations will only be presented here in brief, and the reader is referred to the original literature and the chapters 3 through 6 for a more in-depth discussion of the models.

7.2.1 Soave-Redlich-Kwong Equation of State

The Soave-Redlich-Kwong, *SRK*, *EOS* [196] is probably one of the most well known and commonly applied equations of state. It belongs to the family of cubic equations of state based on the original Van der Waals model. Although the model does not explicitly take the structure of the molecules into account it is known to be highly flexible through the use of fitted binary interaction parameters, furthermore its simple mathematical structure and cubic nature make the *SRK* exceptionally fast and highly favoured in practical calculations.

The *SRK* equation of state has the following mathematical form:

$$P = \frac{RT}{v-b} - \frac{a(T)}{v(v+b)} \qquad 7.15$$

$$a(T) = a_0 \alpha(T) \qquad 7.16$$

$$a_0 = 0.42748 \frac{(RT_c)^2}{P_c} \qquad 7.17$$

$$\alpha(T) = \left[1 + \left(0.48 + 1.574\omega - 0.176\omega^2\right)\left(1 - \sqrt{T/T_c}\right)\right]^2 \quad \text{for} \quad 0 < \omega < 0.5 \qquad 7.18$$

$$b = 0.08664 \frac{RT_c}{P_c} \qquad 7.19$$

To extend this equation to mixtures the mixture properties a_{mix} and b_{mix}, defined in equations 7.20 and 7.21, are used in equation 7.15.

$$\begin{aligned} a_{mix} &= \sum_{i=1}^{nc}\sum_{j=1}^{nc} x_i x_j a_{ij}(T) \\ b_{mix} &= \sum_{i=1}^{nc}\sum_{j=1}^{nc} x_i x_j b_{ij} \end{aligned} \qquad 7.20$$

with

$$a_{ij}(T) = (1 - l_{ij})\sqrt{a_i(T)a_j(T)}$$
$$b_{ij} = (1 - k_{ij})\frac{b_i + b_j}{2} \qquad 7.21$$

If $k_{ij} = 0$ b_{mix} reduces to a simple linear combination rule:

$$b_{mix} = \sum_{i=1}^{nc}\sum_{j=1}^{nc} x_i x_j b_{ij} \qquad 7.22$$

The component acentric factors, ω, and the critical temperature and pressure values, T_c and P_c, used in this study are listed in Table 7.3.

Table 7.3 Pure component critical properties used in the *SRK EOS*

Pure component properties							
	T_c [K]	P_c [bar]	ω		T_c [K]	P_c [bar]	ω
Methane	190.56	45.99	0.012	n-Nonadecane	758	12.10	0.852
Ethane	305.32	48.72	0.099	n-Eicosane	768	11.60	0.907
Propane	369.83	42.48	0.152	n-Octacosane	832	8.50	1.238
n-Butane	425.12	37.96	0.200	n-Dotriacontane	855	7.50	1.377
n-Pentane	469.70	33.70	0.252	n-Hexatriacontane	874	6.80	1.526
n-Hexane	507.60	30.25	0.301	Nitrogen	126.2	34	0.038
n-Heptane	540.20	27.40	0.349	Carbon Dioxide	304.21	73.83	0.224
n-Octane	568.70	24.90	0.400	Carbon Monoxide	132.92	34.99	0.0482
n-Nonane	594.6	22.9	0.443	Hydrogen	39.19	13.13	-0.216
n-Decane	617.70	21.10	0.492	i-butane	408.14	36.48	0.181
n-Undecane	639	19.50	0.530	i-pentane	460.43	33.81	0.227
n-Dodecane	658	18.20	0.576	methylcyclopentane	532.79	37.851	0.230
n-Tridecane	675	22.90	0.443	cyclohexane	553.58	40.73	0.210
n-Tetradecane	693	15.70	0.643	methylcyclohexane	572.19	34.71	0.235
n-Pentadecane	708	14.80	0.686	benzene	562.16	48.98	0.210
n-Hexadecane	721	14.19	0.744	toluene	591.8	41.06	0.232
n-Heptadecane	736	13.4	0.770	m-xylene	617.05	35.36	0.323
n-Octadecane	747	12.7	0.811	o-xylene	603.33	37.34	0.310

7.2.2 The Simplified Perturbed Hard Chain Equation

The Simplified Perturbed Hard Chain Theory [111], *SPHCT*, is based on the Perturbed Hard Chain Theory of Beret and Prausnitz [20] and Donohue and Prausnitz [60], but uses the simple local composition approximation of the perturbation term as developed by Lee et al. [126]. The *SPHCT* has been investigated by several authors [78, 169, 218] who have proposed various pure component parameter sets and generalized correlations. In order to evaluate all the theoretical models on the same basis all the *EOS* parameters used in this study were refitted to the same parameter sets used to obtain the *simple-PHCT-ltd* parameters. These values are listed in Table 7.4.

Similarly to the *simple-PHCT-ltd EOS*, the *SPHCT* has three component specific parameters, the closest packed molar volume, rv_0, the molecular interaction energy term, $q\varepsilon/k$, and the external degree of freedom parameter, c. This model however does not explicitly account for the temperature dependence of the London interaction energies and does not allow for the consideration of molecular softness. The *SPHCT EOS* for mixtures can be summarized as follows:

$$z = 1 + c_{mix} z_{mix}^{rep} - Z_m \frac{\left(crv_0 Y\right)_{mix}}{v + \left(crv_0 Y\right)_{mix} / c_{mix}} \qquad 7.23$$

with

$$z_{mix}^{rep} = \frac{4\eta_{mix} - 2\eta_{mix}^2}{\left(1 - \eta_{mix}\right)^3} \qquad 7.24$$

and

$$c_{mix} = \sum_{i=1}^{nc} x_i c_i \qquad 7.25$$

$$\eta_{mix} = \rho\tau \sum_{i=1}^{nc} x_i \left(rv_0\right)_i \qquad 7.26$$

Similarly to the *simple-PHCT-ltd* model the molecular volume and energy parameters are separated into a segment volume, v_{0i}, and number, r_i, and a surface area, q_i, and energy per surface area, ε', respectively, and these terms appear individually in the perturbation term mixing rule:

$$\left(crv_0 Y\right)_{mix} = \sum_{i=1}^{nc} \sum_{j=1}^{nc} x_i x_j c_i r_i v_{0ij} \left(\exp\left[\frac{q_i \varepsilon'_{ij}}{2 c_i kT} \right] - 1 \right) \qquad 7.27$$

The following combination rules are used in equation 7.27:

$$v_{0ij} = \left(\frac{v_{0i}^{1/3} + v_{0j}^{1/3}}{2} \right)^3 \qquad 7.28$$

and

$$\varepsilon'_{ij} = \sqrt{\varepsilon'_i \varepsilon'_j}\left(1 - l_{ij}\right) \qquad 7.29$$

The *SPHCT EOS* is used with the following parameters as proposed by Kim et al. [111] Z_m = 36, v_{0i} = 8.667e-6 m^3/mol and ε'/k = 62.5 K.

7.2.3 The Statistical Associating Fluid Theory

Statistical Associating Fluid Theory, *SAFT*, as discussed in section 5.2.2.b, takes the chainlike structure (and association) into account directly, and has been applied in a wide variety of equations of state. The most popular form of the equation however still remains the *SAFT EOS* as developed by Huang and Radosz [100, 101], and it is generally this version of the *SAFT* equation used in commercial simulation packages such as Pro/II [2] and Aspen Plus [1].

One of the most promising alternatives to the *SAFT EOS* of Huang and Radosz, from here on referred to as the original *SAFT* equation, is the Perturbed Chain Statistical Associating Fluid Theory, *PC-SAFT*, proposed by Gross and Sadowski [85, 86]. The novelty of this equation of state lies the incorporation of the entire hard–chain term in the perturbation approximation, and has already been discussed in section 5.3.1.b.

Both the *original-SAFT* and the *PC-SAFT* equations will be used in this chapter. As only weakly polar or non-polar systems are of interest in this study the association terms of both these models will be set to zero. The pure component parameters for the equations have been refitted on the dataset used to determine the *simple-PHCT-ltd EOS* parameters and are listed in Table 7.4.

7.2.3.a The Original-SAFT EOS

The *original-SAFT* equation of state has three pure component *EOS* parameters, the segment volume term, v_{00}, the chain length, r, and the segment interaction energy, u_0/k. The *original-SAFT EOS* for fluid mixtures can be expressed in terms of the residual specific Helmholtz energy, a^{resid}, through equation 7.30, where a^{resid} is defined as $a^{resid}(T,V,N) = a^{total}(T,V,N) - a^{ideal}(T,V,N)$.

$$\frac{a^{resid}}{RT} = \frac{a^{reference}}{RT} + \frac{a^{disp}}{RT} = \frac{a^{HS}}{RT} + \frac{a^{Chain}}{RT} + \frac{a^{disp}}{RT} \qquad 7.30$$

with

$$\frac{a^{HS}}{RT} = \frac{6}{\pi\rho}\left[\frac{(\xi_3)^2 + 3\xi_1\xi_2\xi_3 - 3\xi_1\xi_2(\xi_3)^3}{\xi_3(1-\xi_3)^2} - \left[\xi_0 - \frac{(\xi_2)^3}{(\xi_3)^2}\right]\ln(1-\xi_3)\right] \qquad 7.31$$

with ξ_k defined as:

$$\xi_k = \frac{\pi N_a}{6}\rho\sum_{i=1}^{nc} x_i r_i (d_{ii})^k \qquad 7.32$$

and d_{ii} is the temperature dependent segment diameter.

The mixture hard sphere radial distribution function for the like segments can be obtained from the following expression:

$$g_{ii}(d_{ii}) = \frac{1}{1-\xi_3} + \frac{2d_{ii}}{2}\frac{\xi_2}{(1-\xi_3)^2} + 2\left[\frac{d_{ii}}{2}\right]^2\frac{(\xi_2)^2}{(1-\xi_3)^3} \qquad 7.33$$

and is applied to obtain the mixture chain contribution as follows:

$$\frac{a^{chain}}{RT} = \sum_{i=1}^{nc} x_i(1-r_i)\ln(g_{ii}(d_{ii})) \qquad 7.34$$

The dispersion or perturbation contribution is determined using a double summation approximation of the form:

$$\frac{a^{disp}}{RT} = r_{mix}\sum_{n}\sum_{m} D_{nm}\left(\frac{\eta_{mix}}{\tau}\right)^m\left(\frac{\varepsilon}{kT}\right)^n_{mix} \qquad 7.35$$

The double summation is based on the Chen and Kreglewski perturbation approximation, and the matrix parameters are listed in Table 4.7. The mixture reduced density, η_{mix}, is equivalent to ξ_3 as defined in equation 7.32. The specific mixing rules for the other mixture terms in equation 7.35, have been discussed in section 6.1.4.b. In this study the Van der Waals one fluid averaging equation is used for the energy term, and a normal linear combination rule for the chain length:

$$\left(\frac{\varepsilon}{kT}\right)_{mix} = \frac{\sum_{i=1}^{nc}\sum_{j=1}^{nc} x_i x_j r_i r_j \left(\frac{\varepsilon_{ij}}{kT}\right) v_{0ij}}{\sum_{i=1}^{nc}\sum_{j=1}^{nc} x_i x_j r_i r_j v_{0ij}} \qquad 7.36$$

with the combination terms:

$$v_{0ij} = \left(\frac{v_{0i}^{1/3} + v_{0j}^{1/3}}{2}\right)^3 \qquad 7.37$$

and

$$\varepsilon'_{ij} = \sqrt{\varepsilon'_i \varepsilon'_j}\left(1 - l_{ij}\right) \qquad 7.38$$

and

$$r_{mix} = \sum_{i=1}^{nc} x_i r_i \qquad 7.39$$

Following Chen and Kreglewski [42] the *original-SAFT EOS* incorporates the temperature dependence of the non-central London interaction energies, through equation 7.40, with μ/k = 10 for most of components. (The exceptions to this approach are μ/k = 0 for argon, 3 for nitrogen, 1 for methane, 4.2 for CO and 40 for CO_2.)

$$\frac{\varepsilon_i}{kT} = \frac{\varepsilon_{0i}}{kT}\left(1 + \frac{\mu}{kT}\right) \qquad 7.40$$

The temperature dependence of the segment diameter is also taken into account through equations 7.41:

$$d_i = \sigma_i\left[1 - 0.12\exp\left[\frac{-3\varepsilon_{0i}}{kT}\right]\right]$$

or $$\qquad 7.41$$

$$v_{0i} = v_{00i}\left[1 - 0.12\exp\left[\frac{-3\varepsilon_{0i}}{kT}\right]\right]^3$$

7.2.3.b The PC-SAFT EOS

The *PC-SAFT* equation of state requires three component specific parameters, the chain length, r_i, the segment hard sphere diameter, σ_i, and the segment interaction energy ε/k. Similarly to the *original-SAFT* equation it incorporates the segment diameter temperature dependence through equation 7.41, but does however not take the temperature dependence of the interaction energy into account, i.e. $\varepsilon_{0i}/k = \varepsilon_i/k$.

Due to the fact that the entire hard chain term, and not only the hard sphere segments, is included in the perturbation approximation of the *PC-SAFT EOS* this model has a much more complicated structure than the *original-SAFT EOS*. The difference between the models is however only located in the perturbation term, and the hard sphere and chaining term expressions of the *PC-SAFT EOS* are identical to equations 7.30 through to 7.34.

The perturbation or dispersion Helmholtz energy of the *PC-PHCT EOS* is given by a second order perturbation expansion:

$$\frac{a^{disp}}{RT} = \frac{a_1}{RT} + \frac{a_2}{RT} \qquad 7.42$$

with

$$\frac{a_1}{RT} = -2\pi\rho\, I_1(\eta_{mix}, r_{mix}) \sum_{i=1}^{nc}\sum_{j=1}^{nc} x_i x_j r_i r_j \left(\frac{\varepsilon_{ij}}{kT}\right)\sigma_{ij}^3 \qquad 7.43$$

and

$$\frac{a_2}{RT} = -\pi\rho\, r_{mix} C(\eta_{mix}, r_{mix}) I_2(\eta_{mix}, r_{mix}) \sum_{i=1}^{nc}\sum_{j=1}^{nc} x_i x_j r_i r_j \left(\frac{\varepsilon_{ij}}{kT}\right)^2 \sigma_{ij}^3 \qquad 7.44$$

where

$$\begin{aligned} C(\eta, r) &= \left(1 + z^{HS} + \rho\frac{\partial z^{HS}}{\partial\rho}\right)^{-1} \\ &= \left(1 + r\frac{8\eta - 2\eta^2}{(1-\eta)^4} + (1-r)\frac{20\eta - 27\eta^2 + 12\eta^3 - 2\eta}{[(1-\eta)(2-\eta)]^2}\right)^{-1} \end{aligned} \qquad 7.45$$

and

$$I_1(\eta, r) = \sum_{i=1}^{6} a_i(r)\eta^i \qquad 7.46$$

$$I_2(\eta, r) = \sum_{i=1}^{6} b_i(r)\eta^i \qquad 7.47$$

The parameters in equations 7.46 and 7.47 are correlated as functions of the molecular chain length:

$$a_i(r) = a_{0i} + \frac{r-1}{r}a_{1i} + \frac{r-1}{r}\frac{r-2}{r}a_{2i} \qquad 7.48$$

and

$$b_i(r) = b_{0i} + \frac{r-1}{r}b_{1i} + \frac{r-1}{r}\frac{r-2}{r}b_{2i} \qquad 7.49$$

In total equations 7.46 to 7.49 require 42 parameter values. Gross and Sadowski [86] determined these parameters by fitting n-alkane vapour pressure and *P*-*v*-*T* data and used their results as universal constants in the model. The reader is referred to the original article by Gross and Sadowski [86] for these parameter values.

The r_{mix} and η_{mix} parameters are determined from equation 7.39 and equation 7.32 with $k = 3$. The combination rules for the interaction terms in equations 7.43 and 7.44 are:

$$\sigma_{ij} = \frac{\sigma_i + \sigma_j}{2} \qquad 7.50$$

and

$$\varepsilon'_{ij} = \sqrt{\varepsilon'_i \varepsilon'_j}\left(1 - l_{ij}\right) \qquad 7.51$$

7.3 COMPARISON BETWEEN THE MODELLING ABLITIES OF THE SIMPLE-PHCT-LTD EOS WITH EOS FROM LITERATURE

7.3.1.a Pure component representation

As mentioned above, in order to ensure a meaningful comparison between the various equations of state it is necessary to evaluate the performance of the models using parameter sets that have been fitted to the same pure component data, and for this reason the *PC-SAFT*, *SAFT* and the *SPHCT EOS* were refitted to the datasets listed in Table 7.2. The regressed parameter values of these models are listed in Table 7.4. The *SRK* equation of state parameters are related to the pure component critical properties through equations 7.17 and 7.19, and the temperature dependence of the attractive term, the *a* parameter, correlated to the pure component acentric factor. These *EOS* parameters do not need to be regressed from pure component *VLE* data. The relevant critical parameters and acentric factors used in this study are listed in Table 7.3.

Using the parameters in Table 7.2 through to Table 7.4, the performance of the performance of the various equations of state in the representation of the pure component saturated and supercritical phase behaviour can now be evaluated. Figure 7.6 and Figure 7.7 are plots of the relative errors in the pure component saturated pressures and fluid volumes as well as the supercritical fluid volumes of the smaller components up to hexane, as determined from the values predicted by the model equations.

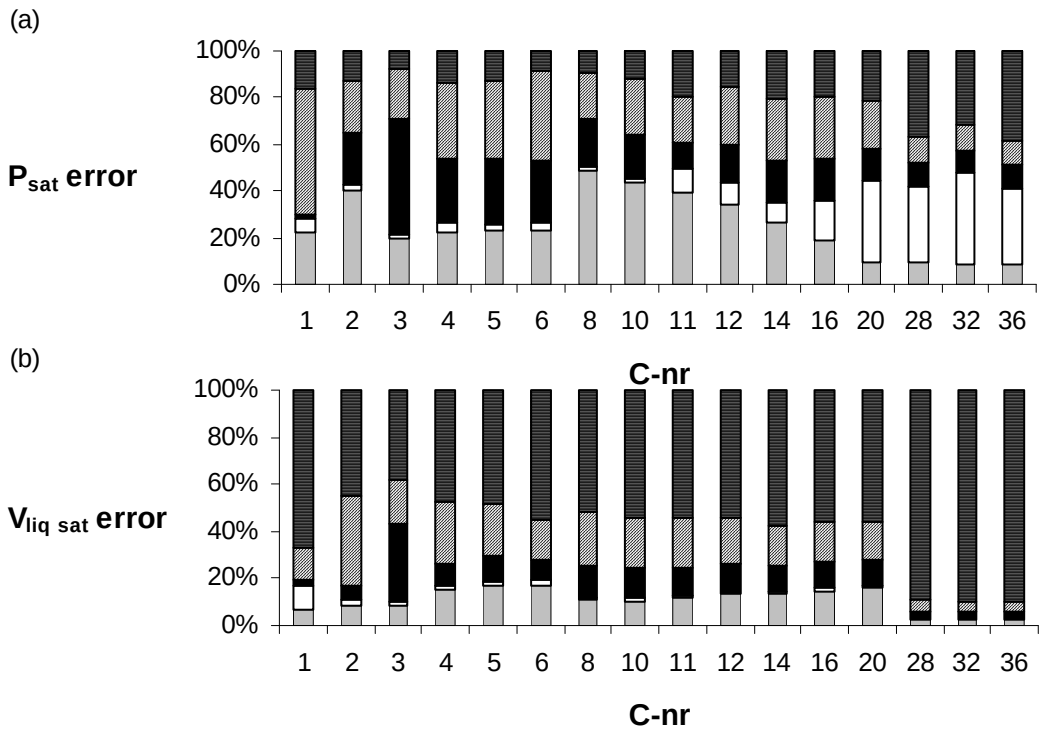

Figure 7.6 The relative errors of the *simple-PHCT-ltd,* *PC-SAFT,* *SAFT,* *SPHCT* and *SRK* equations in the representation of (a) the saturated vapour pressure and (b) the saturated liquid

Figure 7.6 (a) and (b) serves as a confirmation of the known failures of the *SRK EOS*, and most cubic equations of state in general, with large inaccuracies in the representation of the saturated fluid volumes and a decrease in the ability of the models to represent the fluid saturated vapour pressure as the molecular structure of the chemical species deviates from a simple sphere.

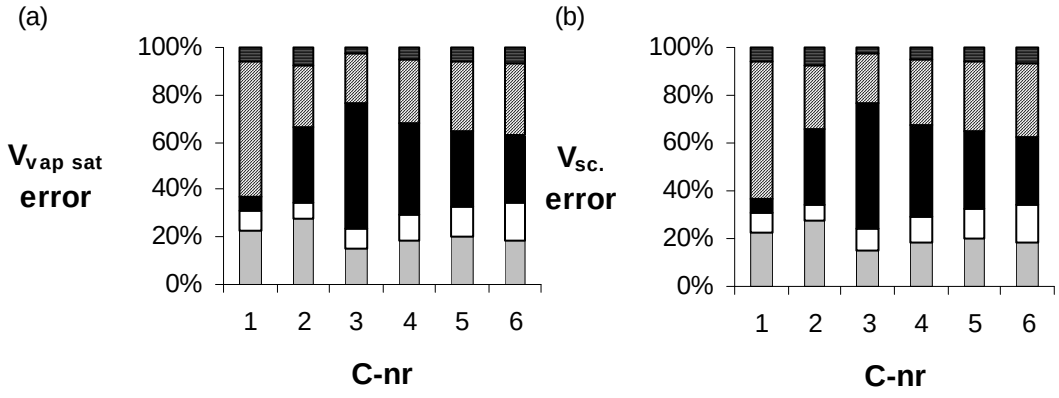

Figure 7.7 The relative errors of the *simple-PHCT-ltd,* *PC-SAFT,* *SAFT,* *SPHCT* and *SRK* equations in the representation of (c) the saturated vapour and (d) super critical fluid volumes of the light n-alkanes.

Table 7.4 Refitted EOS parameters of the PC-SAFT, SAFT and SPHCT models.

Refitted EOS Parameters									
	PC-SAFT			SAFT			SPHCT		
	r	σ [Å]	ε/k [K]	r	v_{00} [1e6 m^3]	ε/k [K]	c	rv_0 [1e6 m^3]	qε'/k [K]
Methane	1.00	3.70	150.02	1.00	21.55	190.06	1.00	18.19	81.75
Ethane	1.62	3.51	190.32	1.56	19.04	220.96	1.25	25.69	122.2
Propane	1.99	3.62	208.79	2.67	14.80	193.64	1.50	32.93	138.5
n-Butane	2.32	3.71	223.61	3.20	14.01	203.71	1.70	40.53	152.7
n-Pentane	2.70	3.75	230.91	4.08	12.21	200.01	1.92	47.79	162.3
n-Hexane	3.04	3.80	237.54	4.93	11.44	198.21	2.15	54.29	169.6
n-Heptane	3.32	3.85	245.04	5.69	10.99	199.78	2.32	60.42	178.0
n-Octane	3.81	3.84	242.96	6.04	12.70	204.84	2.23	78.23	192.3
n-Nonane	4.28	3.82	242.28	6.45	12.96	210.85	2.44	85.55	196.2
n-Decane	4.62	3.85	245.30	6.45	12.96	210.85	2.62	93.22	200.1
n-Undecane	5.11	3.83	243.89	7.39	12.44	206.47	2.93	100.44	199.4
n-Dodecane	5.45	3.85	245.98	8.04	12.16	207.79	3.16	107.99	201.0
n-Tridecane	5.85	3.86	246.54	9.57	11.92	205.93	3.28	116.06	205.6
n-Tetradecane	6.18	3.88	248.36	8.75	12.04	207.62	3.44	123.12	208.5
n-Pentadecane	6.44	3.91	251.20	10.11	12.59	215.40	3.55	131.83	212.4
n-Hexadecane	6.73	3.93	253.66	11.32	11.89	209.68	3.98	139.42	207.8
n-Heptadecane	7.01	3.95	255.87	11.37	12.33	216.11	3.95	145.64	215.2
n-Octadecane	7.56	3.92	252.73	11.98	12.31	216.09	4.14	153.40	216.0
n-Nonadecane	7.77	3.95	256.13	13.37	11.59	210.36	4.58	160.57	211.8
n-Eicosane	8.05	3.98	258.07	13.98	11.50	210.55	4.80	167.95	212.4
n-Octacosane	11.63	3.90	251.73	21.20	10.99	200.98	6.99	253.82	209.2
n-Dotriacontane	12.58	3.98	257.78	24.94	10.63	197.64	8.10	289.11	208.0
n-Hexatriacontane	14.82	3.91	250.49	28.52	10.32	195.37	9.25	320.88	206.4

Refitted EOS Parameters									
	PC-SAFT			SAFT			SPHCT		
	r	σ [Å]	ε/k [K]	r	v_{00} [1e6 m^3]	ε/k [K]	c	rv_0 [1e6 m^3]	qε'/k [K]
Nitrogen	1	3.59	99.69	1	19.55	123.48	1	16.88	54.54
Carbon Dioxide	2.38	2.62	158.74	1.51	12.88	205.48	1.77	14.22	108.6
Carbon Monoxide	1.41	3.17	87.90	1.23	15.67	111.13	1.13	16.29	54.78
Hydrogen	1	3.01	27.62	1	11.01	34.78	1	8.06	13.23
i-Butane	2.31	3.72	213.74	2.79	16.50	212.59	1.56	44.19	150.9
i-Pentane	2.49	3.85	234.65	3.44	15.57	214.19	1.60	53.65	171.2
Methylcyclopentan	2.72	3.77	258.87	3.75	14.56	236.86	1.67	55.08	194.5
Cyclohexane	2.70	3.75	268.64	4.59	11.06	218.60	1.68	51.65	200.5
methylcyclohexane	2.79	3.93	275.03	3.58	17.77	264.81	1.81	64.34	200.8
Benzene	2.48	3.63	286.58	3.59	12.26	256.26	1.60	43.12	209.4
Toluene	2.77	3.73	288.50	3.62	14.89	274.50	1.65	54.71	220.7
m-Xylene	3.11	3.78	288.05	5.05	12.23	239.11	1.83	63.07	223.8
o-Xylene	3.26	3.69	284.41	4.19	14.50	273.88	1.86	61.40	225.7

The superior ability of the *PC-SAFT EOS* is also clearly highlighted in Figure 7.6 and Figure 7.7. It should however be taken into consideration that the performance of the *PC-SAFT EOS* may be biased with regards to the representation of n-alkane saturated and *P-v-T* data as these systems were used to determine the universal constant model parameters applied in equations 7.46 to 7.49. (This is in contrast to the *simple-PHCT-ltd* and *SAFT* models where the *EOS* constants were determined from fitting argon thermodynamic data, and the *SPHCT* model that does not contain any fitted parameters.) The ability of the *PC-SAFT EOS* to represent the n-alkane vapour pressures does however seem to decrease with an increase in the molecular chain length. This could possibly be attributed to the fact that in the original article by Gross and Sadowiski [86] the n-alkane systems were only investigated up to n-eicosane. The higher molecular weight alkanes such as n-octacosane or n-hexatriacontane would therefore not have been used in the regression of the *EOS* universal constants.

With the exception of the vapour pressures of ethane and n-octane through to n-dodecane the *simple-PHCT-ltd EOS* is generally able to represent the thermodynamic properties of the n-alkanes to a similar extent or slightly better than the *SAFT* and *SPHCT* models.

Finally it can be said that when the pure component parameters listed in Table 7.2, Table 7.3 and Table 7.4, are used, because of the generally comparable accuracies of the various models in the representation pure component *VLE* data, no equation of state will be unfairly hampered by the poor pure component representation when evaluated against multi-component phase behaviour.

7.3.2 n-Alkane binary VLE representation.

The ability of the equations of state to represent the n-alkane binary *VLE* data can be seen as a measure of the ability of the model to represent mixtures of chainlike molecules with similar interaction energies as well as mixtures displaying large size asymmetry. The datasets used in this investigation are listed in table Table 7.5.

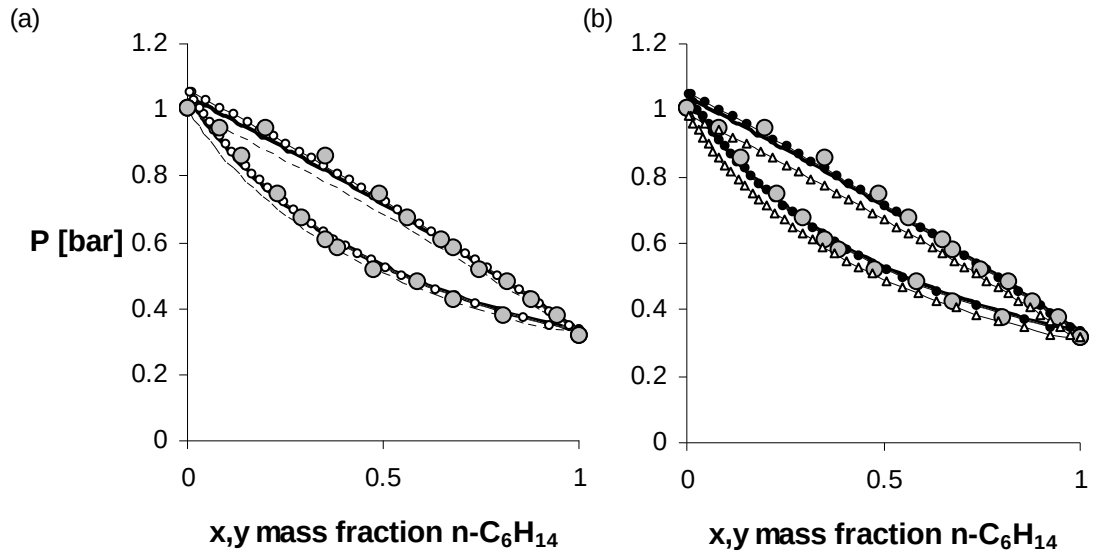

Figure 7.8 n-Pentane – n-hexane binary VLE at 309 K as represented by the ▬▬ *simple-PHCT-ltd*, ▬ ▬ *PC-SAFT*, ···○··· *SPHCT*, ···●··· *SAFT* and —△— *SRK EOS* and with ○ the data points

The *P-x-y* plots in Figure 7.8 and Figure 7.9 of the *VLE* of n-pentane – n-hexane and n-hexane – n-decane binary systems are representative of mixtures of chained systems with no significant size asymmetry. It can be seen that although the *PC-SAFT* and *SRK* models represent the correct n-hexane vapour pressure, these models slightly under-predict the bubble and dew point pressure lines especially at the lower heavy component compositions, whilst the *simple-PHCT-ltd*, the *SAFT* and the *SPHCT EOS* all predict more realistic saturated pressure curves over the majority of the composition range.

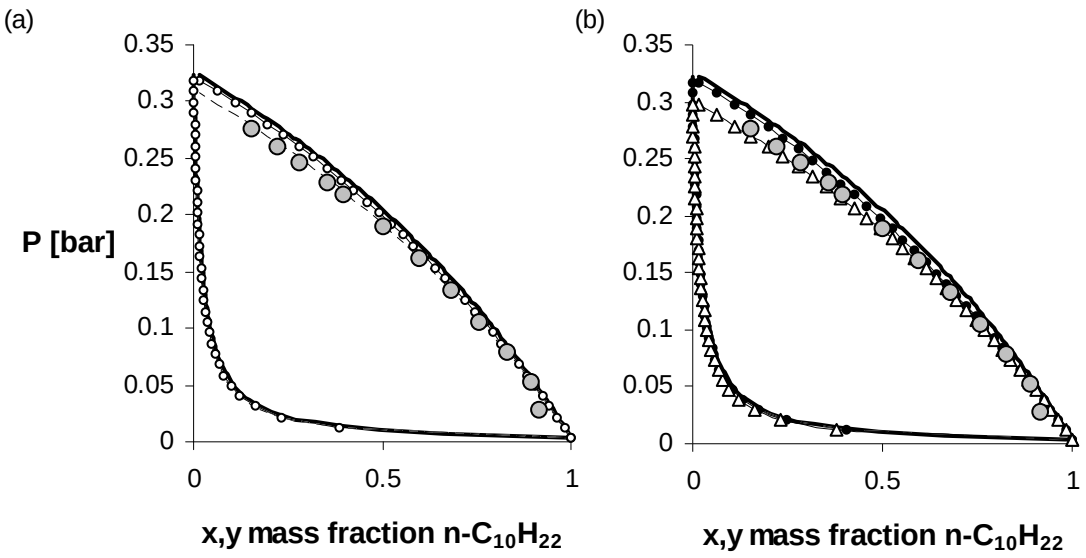

Figure 7.9 n-Hexane – n-decane binary VLE at 308 K as represented by the ——— *simple-PHCT-ltd,* - - - - - *PC-SAFT,* ·····○····· *SPHCT,* ·····●····· *SAFT* and —△— *SRK EOS* and with ○ the data points.

On the other hand *PC-SAFT* and *SRK* models appear to be more accurate in the representation of the n-hexane – n-decane binary system. It should however be taken into consideration that these two datasets were reported by different authors using different experimental techniques and will have differing degrees of accuracy. No conclusions on overall superior modelling performance of the investigated equations can therefore be drawn based purely on the small differences observed here. The plots however do serve to prove that the *simple-PHCT-ltd EOS* produces results that are comparable in accuracy to those of the *SAFT* and *SPHCT* models.

The representation of size asymmetric systems is depicted in Figure 7.10 and Figure 7.11. The datasets were specifically chosen to fall within the same temperature region to ensure that the effects observed are those of size asymmetry and not temperature. The ratios of the Van der Waals volumes as determined by Bondi [25] are used as a measure of the size asymmetry in the mixtures and are listed in Table 7.6.

Table 7.5 Binary VLE data used in this study

Comp. 1	Comp. 2	T Range [K]	P Range [bar]	x_2 mol frac.	Reference
n-pentane	n-hexane	309	3.2 - 10.6	0 - 1	[177]
n-hexane	n-decane	308	0.028 - 0.28	0.09 - 0.91	[84]
ethane	n-decane	378	3.9 -53.7	0.001 -0.9	[31, 172]
ethane	n-eicosane	340	0.33 - 10.6	0.009 - 0.91	[165]
methane	n-hexane	378	59.7 - 201	0.031 - 0.54	[139]
methane	n-dodecane	340	1 - 459	0.0001 - 0.9	[178]
methane	n-hexadecane	323	25 - 562	0.023 - 0.89	[83]
propane	n-tetratetracontane	408	87 - 115	0.001 - 0.08	[189]
propane	n-tertapentacontane	408	96 - 118	0.0008 - 0.046	[189]
propane	n-hexacontane	393 - 408	15 - 142	0.0007 - 0.39	[166, 189]
CO_2	n-decane	408	6.9 - 75.8	0.0014 - 0.93	[173]
CO_2	n-nonadecane	408	9.4 - 79.6	0.41 - 0.91	[70]
CO_2	n-octadecane	311	8.4 - 289.9	0.001 - 0.90	[77] [62]
H_2	n-hexane	278 - 478	34 – 690	0.23 – 0.97	[155]
CO	n-dodecane	344 - 411	6.9 - 87.5	0.85 - 0.98	[76]
H_2	n-dodecane	344 - 411	14 - 132	0.85 - 0.98	[76]
N_2	n-dodecane	344 - 411	12.1 - 95.5	0.85 - 0.98	[76]
CO	n-eicosane	373 - 573	10 - 50.6	0.98 - 0.8	[98]
H_2	n-eicosane	373 - 573	10 - 50.6	0.98 - 0.8	[98]
CO	n-octadecane	373 - 573	10 - 50.6	0.98 - 0.8	[98]
H_2	n-octadecane	373 - 573	10-50.6	0.98 - 0.8	[98]
CO	n-hexatriacontane	373 - 573	10 - 50.6	0.98 - 0.8	[98]
H_2	n-hexatriacontane	373 - 573	10-50.6	0.98-0.8	[98]

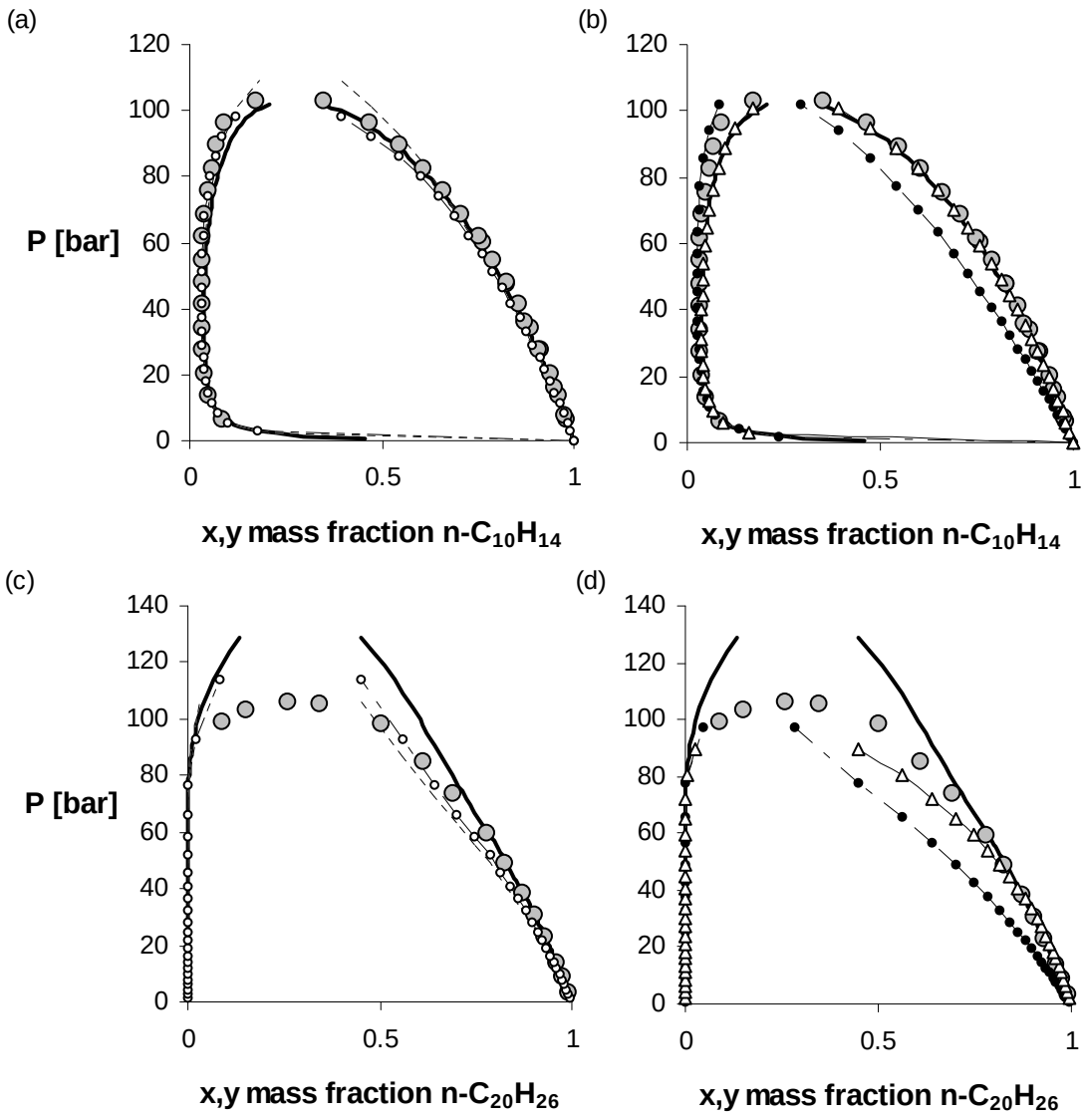

Figure 7.10 Ethane – n-alkane binary data. (a) and (b) n-decane (378 K), (c) and (d) n-eicosane (340 K) as represented by ▬▬ *simple-PHCT-ltd*, _____ *PC-SAFT*, ···○··· *SPHCT*, ···●··· *SAFT* and —△— *SRK EOS* and with ○ the data points

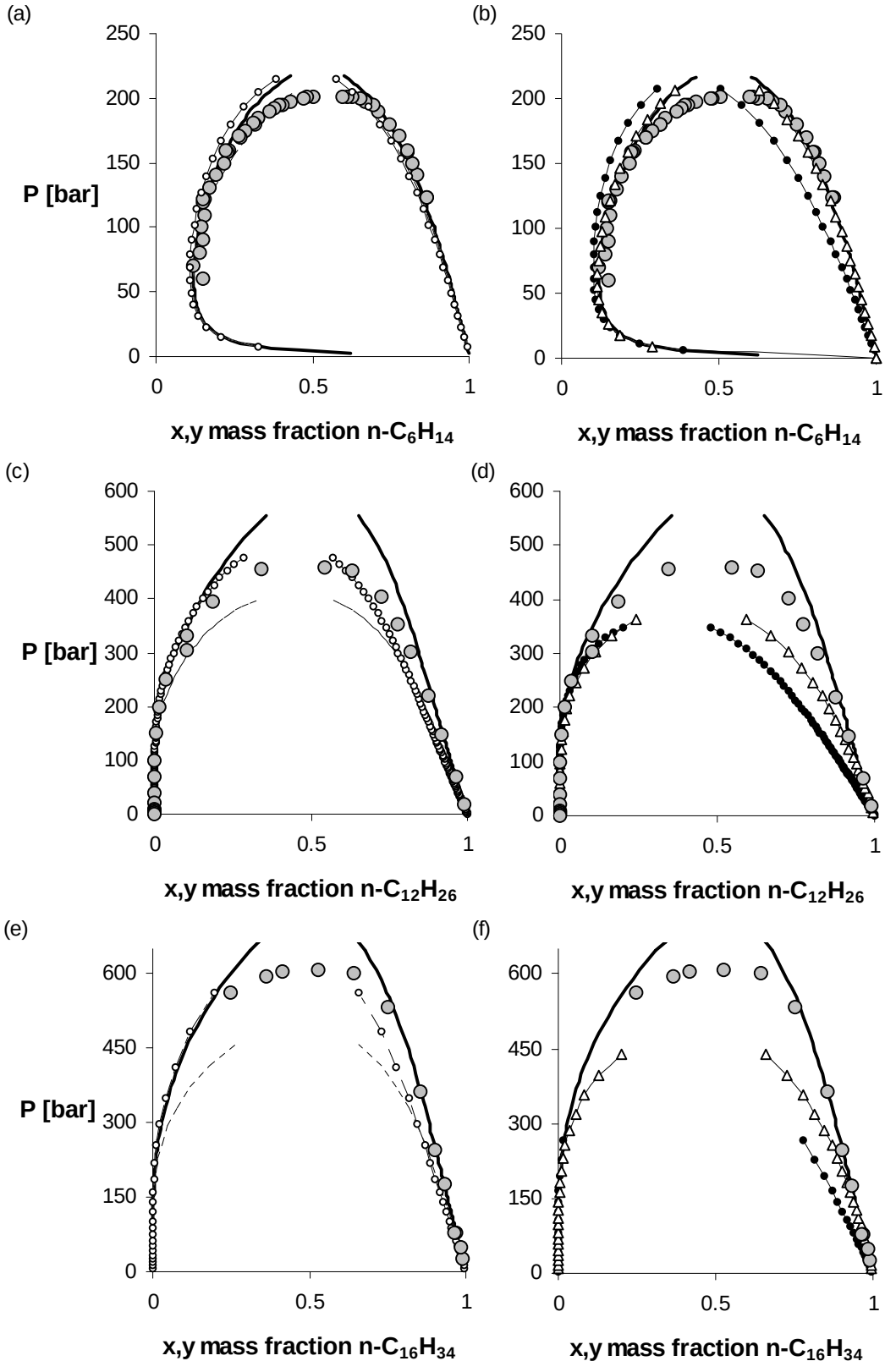

Figure 7.11 Methane – n-alkane binary data. (a) and (b) n-hexane (323 K), (c) and (d) n-dodecane (303 K), (e) and (f) n-hexadecane (340 K).as represented by ▬▬ *simple-PHCT-ltd*, - - - - - *PC-SAFT*, ···○··· *SPHCT*, ···●··· *SAFT* and —△— *SRK EOS* and with ○ the data points

Table 7.6 Bondi's Van der Waals volume ratios and the reduced temperatures of the n-alkane binary systems under investigation.

Size asymmetry of binary mixtures	
Second component	$V_{VDW\ large}/V_{VDW\ small}$
n-Pentane Binary Mixtures	
n-Hexane	1.18
n-Hexane Binary Mixtures	
n-Decane	1.60
Ethane Binary Mixtures	
n-Decane	3.99
n-Eicosane	7.74
Methane Binary Mixtures	
n-Hexane	3.99
n-Dodecane	7.57
n-Hexadecane	9.96
Propane Binary Mixtures	
n-Tetratetracosane	12.16
n-Tetrapentacosane	14.89

From Figure 7.10 (b) and Figure 7.11 (b) it is clear that the *SAFT* equation of state struggles to represent the systems with even a small degree of size asymmetry (the ethane – decane and methane – hexane mixtures both have V_{VDW} ratio's of 3.99). It is also apparent that the performance of the *SRK* equation of state also decreases as the degree of asymmetry in the increases (Figure 7.11 (b), (d) and (f).) This trend corresponds well with the decrease in the ability of the *SRK EOS* to represent pure chainlike components.

Although the *PC-SAFT EOS* fares much better than the *SAFT* equation in the representation of these systems, it does appear as if even this model struggles to represent systems with large asymmetry, with the model predicting a too narrow two phase envelope at higher system pressures. (See Figure 7.10 (c) and Figure 7.11 (c) and (e).) The *SPHCT EOS* does not display this type of behaviour to the same extent, and the *simple-PHCT-ltd EOS* generally provides very accurate results up to pressures close to the mixture critical pressure. These two models are based on the *Perturbed Hard Chain Theory* for chained systems, where as the *PC-SAFT* and *SAFT* equations are based on the *Statistical Associating Fluid Theory.* However, as there is no significant difference in the ability of the *SAFT* and the *SPHCT* and *simple-PHCT-ltd*

equations of state in describing pure chain-like systems and with the *PC-SAFT* being superior in the modelling homologous n-alkane series up to n-eicosane, the difference in the binary system representation cannot be directly attributed to the underlying theory on which these models are based. It should however be noted that both the *SPHCT* and the *simple-PHCT-ltd* equations have mixing rules that have a similar mathematical structure based on the mixing rules of Donohue and Prausnitz [60](equations 7.7 and 7.27) and adhere to the theoretical boundary condition of the quadratic composition dependence of the second virial coefficient, where as the mixing rules of the *SAFT* and *PC-SAFT* models have a different form and violate the boundary condition. As observed in section 6.5.1, the superior performance of a particular mixing rule however cannot be solely attributed to the incorporation of the correct virial coefficient boundary conditions and it appears as if the overall structure of the mixing rules proposed by Donohue and Prausnitz [60] are generally more suited to the representation of asymmetric systems than the mixing rules used in the *SAFT* and *PC-SAFT* models.

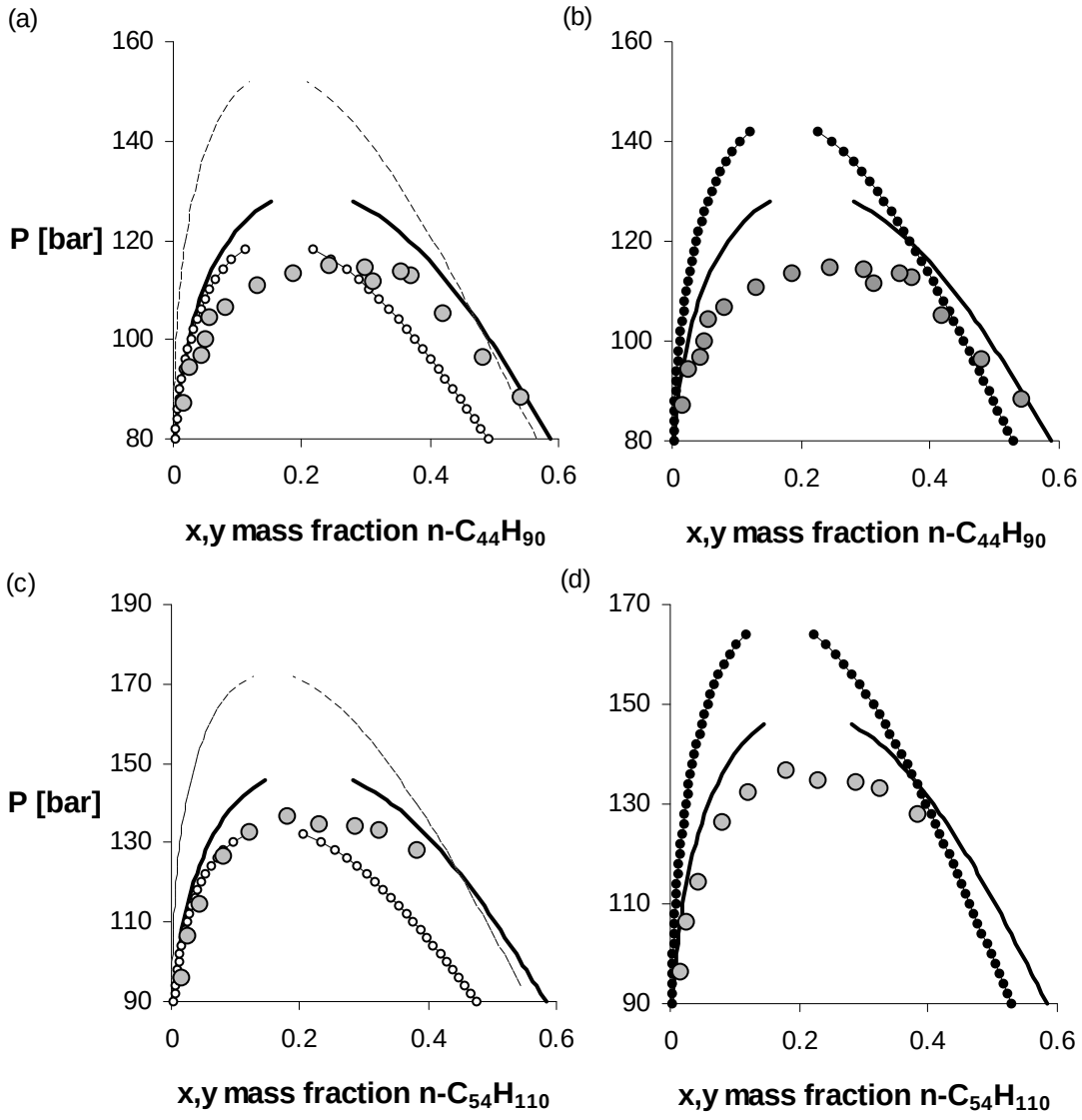

Figure 7.12 n-Propane – n-alkane binary data. (a) and (b) n-tetratetracontane (408 K), (c) and (d) n-tetrapentacontane (408 K) as represented by——— *simple-PHCT-ltd,* _____ *PC-SAFT,* ·····○····· *SPHCT* and ·····●····· *SAFT* with ○ the data points

Figure 7.12 is a plot of the representation of the highly asymmetric n-propane binary mixtures. The only data points available for these systems are in the high pressure near-critical region and due to a lack of pure component thermodynamic data the n-tetratetracontane and n-tetrapentacontane the *EOS* parameters for the various equations were determined by the extrapolation of the lower n-alkane parameter values. (See Appendix B.**)** There is a certain degree of uncertainty involved in the extrapolation of these parameter values, but as the various equations of state parameter values were regressed from the same data sets and similar methods were used to generalize the parameters, the equations can still be evaluated on an equal basis as each model has had access to the same information. From Figure 7.12 it appears as if the trends observed in Figure 7.10 and Figure 7.11 are continued in these systems, with

the slopes of the phase boundary lines predicted by the *PC-SAFT* and *SAFT* being greater than that of the *simple-PHCT-ltd* model, resulting in a narrower phase envelope. At these high system pressures and high degree of size asymmetry the performance of the *SPHCT* is significantly worse than what was previously observed. With the information available the exact cause of the poorer performance of this model cannot be determined.

It is however very encouraging to observe that that the proposed model still seems to display the correct trends in the representation of binary *VLE* data even at these extreme conditions.

7.3.3 VLE representation of binary mixtures of unlike components

The representation of binary mixtures of unlike components, or components not belonging to the same homologous series, is generally much more difficult than representing mixtures of similar components, as not only do the molecular structures of the components differ but also the nature of the intermolecular interactions exerted by the different chemical species. As the mixing rules for the *simple-PHCT-ltd EOS* were not explicitly developed for large differences in intermolecular potentials, it is vital to evaluate the ability of the model to represent such systems.

Figure 7.13 is a plot of the CO_2 – n-decane and CO_2 – n-nonadecane binary *VLE* data as represented by the various *EOS* under investigation. The models are used predictively, i.e. without the use of a binary interaction parameter, in order to observe the true effect of the mixing rules. It is clear that the mixing rules used by the *PC-SAFT* and *SAFT* models severely under predict the two phase region of CO_2 – n-alkane binary systems, whilst the *SPHCT* and the *simple-PHCT-ltd* models predict a phase boundary curve that has a more realistic shape. The *SRK* equation of state also fares fairly well in the representation of the CO_2 – n-decane system, but becomes less accurate as the system asymmetry and mixture critical pressure increases. This is especially apparent from Figure 7.14 which depicts the CO_2 – n-octacosane *VLE* behaviour. From Figure 7.14 (b) it can be seen that *SRK* equation of state is able to model the bubble point pressure curve at low pressures but severely under-predicts the mixture critical pressure of this system. This behaviour of the model is typical for all the highly asymmetric CO_2 – n-alkane binary systems. The *PC-SAFT*, *SAFT* and *simple-PHCT-ltd* models on the other hand tend towards comparatively higher mixture critical pressures, with the *simple-PHCT-ltd* continually predicting a more realistic two phase region.

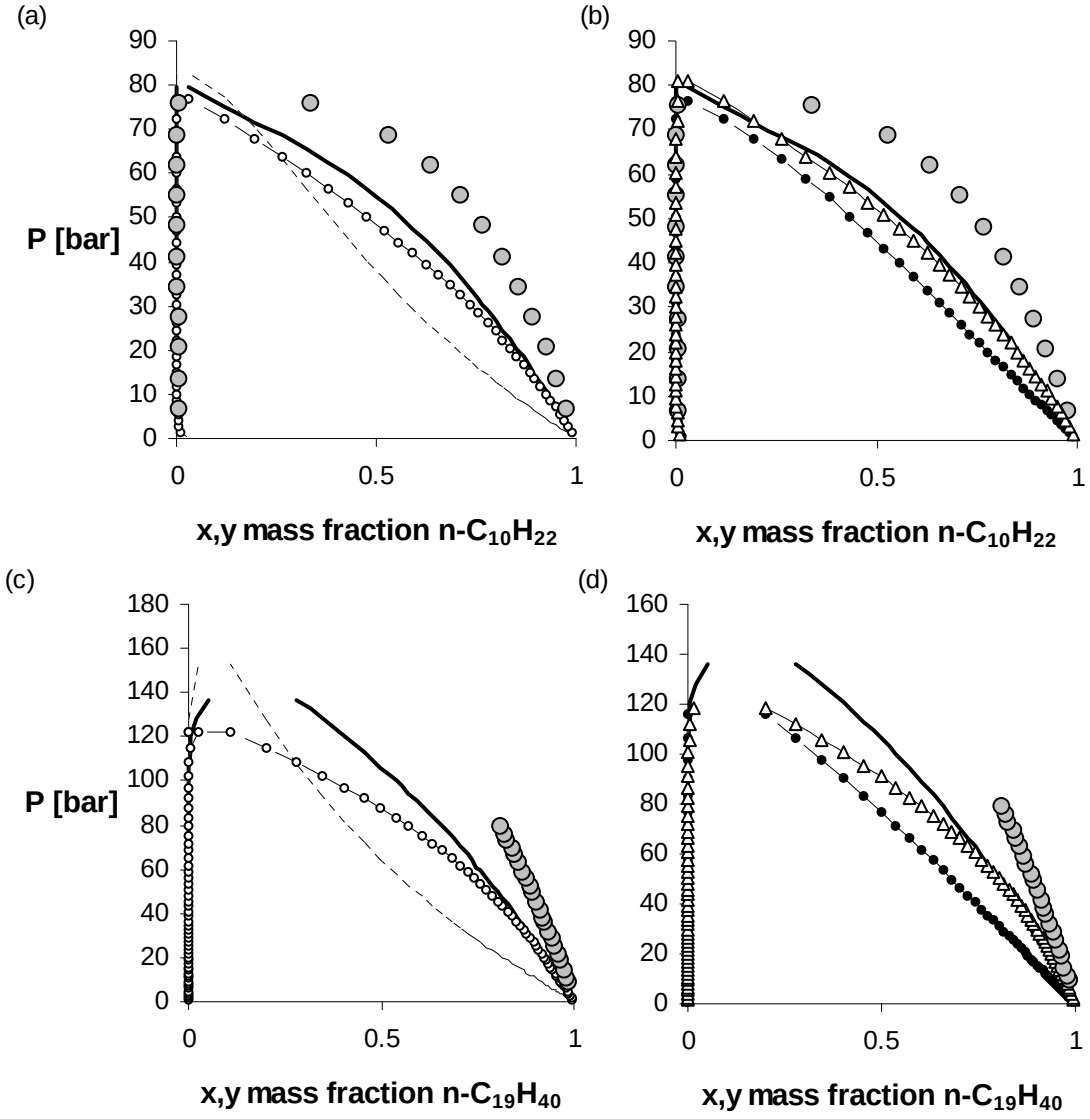

Figure 7.13 CO_2 – n-alkane binary data. (a) and (b) n-decane (311 K), (c) and (d) n-nonadecane (333 K) as represented by ——— *simple-PHCT-ltd*, _ _ _ _ _ *PC-SAFT*, ·····○····· *SPHCT*, ·····●····· *SAFT* and ——△—— *SRK EOS* and with ○ the data points.

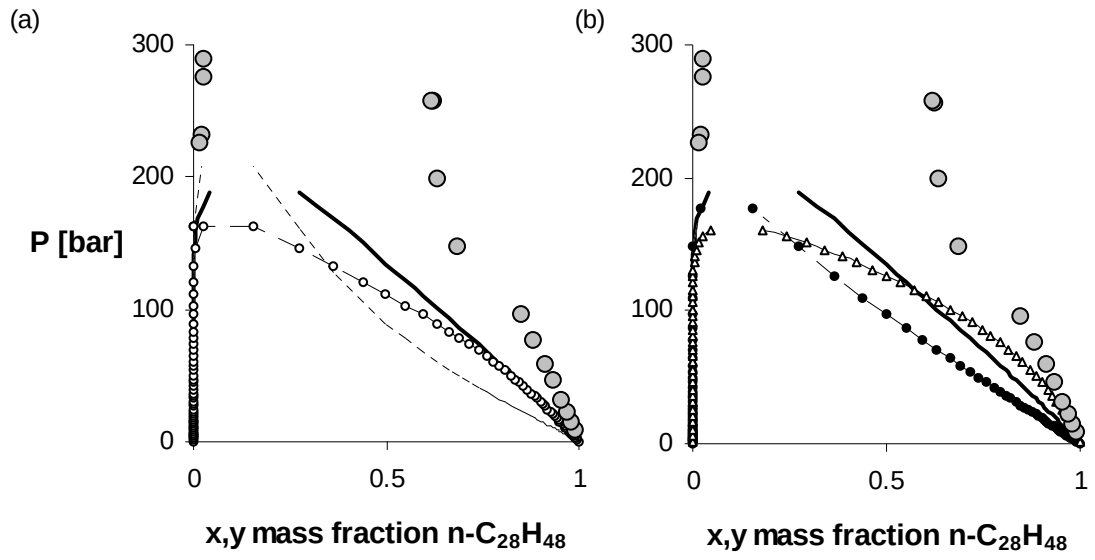

Figure 7.14 CO_2 – n-octacosane binary data (348 K) as represented by ▬▬ *simple-PHCT-ltd*, ⎯ ⎯ ⎯ *PC-SAFT*, ···○··· *SPHCT*, ···●··· *SAFT* and —△— *SRK EOS* and with ○ the data points.

Table 7.7 and Table 7.8 lists the percentage error in the saturated pressure representation of the bubble point curve of CO, H_2 and N_2 binary mixtures with n-alkanes. The binary data as determined by Huang [98] and Gau [76] are used in this evaluation. The binary data falls in the temperature range of 344 K – 573 K with the heavy n-alkane component molar fraction in the range of 0.85-0.99 in the liquid phase. The evaluation of the various equations of state in these tables therefore only covers a small composition range.

Table 7.7 % Pressure errors in the representation of the bubble point curve of binary mixtures of carbon monoxide, hydrogen and nitrogen with with n-docosane in the range temperature and composition range of 344 K – 411 K, 0.87 – 1 mol fraction n-docosane.

% Error in bubble point pressure of binary mixtures of unlike components												
	CO				**H_2**				**N_2**			
T [K]	**344**	**378**	**411**	**Ave.**	**344**	**378**	**411**	**Ave.**	**344**	**378**	**411**	**Ave.**
n-Docosane												
PC-SAFT	39.6	36.8	31.5	**36.0**	13.1	14.9	11.3	**13.1**	45.1	43.3	40.0	**42.8**
SAFT	43.7	42.4	38.8	**41.6**	26.0	27.5	24.4	**26.0**	57.4	55.2	52.0	**54.9**
SPHCT	37.5	34.2	29.3	**33.7**	12.1	11.2	7.2	**10.2**	55.3	51.8	48.0	**51.7**
SRK	19.3	16.3	11.0	**15.5**	24.5	25.5	22.4	**24.1**	29.7	26.1	22.1	**26.0**
Simple-PHCT-ltd	26.3	25.4	21.5	**24.4**	9.5	10.3	6.9	**8.9**	34.2	32.5	29.6	**32.1**

From these tables it is apparent that the *simple-PHCT-ltd EOS* is able to represent the binary mixtures to a similar degree as the generally applied chainlike models, the *SAFT* and the *SPHCT EOS*, with the accuracy of the models gradually decreasing as the size asymmetry of the mixtures increase. The *PC-SAFT* equation of state is generally able to represent the binary

systems with a much smaller error, but the superior performance of this model should continually be weighed against the mathematical complexity of the equation and its computational speed. (See Table 7.18).

From the results of the various binary systems it is furthermore apparent that the cubic *SRK* equation of state is consistently able to represent the binary systems with an accuracy that is similar or better that the best chained model. It should however be noted that the equations of state are evaluated over a very small compositional range and that no conclusions can be drawn on the performance of the model at higher system pressures and lower heavy component concentrations, as the performance of the *SRK EOS* may be significantly poorer at these conditions, as it has already been proven to be for the CO_2 – n-octacosane system plotted in Figure 7.14 (b).

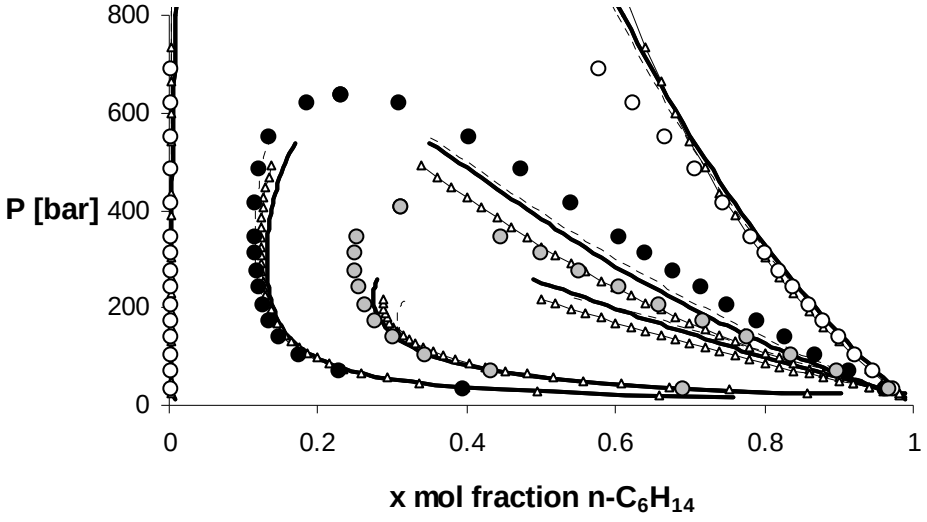

Figure 7.15 H_2 – n-Hexane binary VLE at ○ 277.3 K, ● 444.6 K and ○ 477.3 K as represented by the ▬▬ *simple-PHCT-ltd,* ⎯ ⎯ ⎯ *PC-SAFT* and —△— *SRK EOS.*

Figure 7.15 depicts the H_2 – n-hexane binary *VLE* behaviour over the entire composition range. Here it can be seen that the *simple-PHCT-ltd* and the *PC-SAFT* models are able to represent the system to a similar degree, but that at lower n-alkane concentrations and higher system temperatures the phase boundary line as predicted by the *SRK* model is significantly lower than the experimental values and those of the chainlike models.

Table 7.8 % Pressure errors in the representation of the bubble point curve of binary mixtures of carbon monoxide and hydrogen with n-eicosane, n-octacosane and n-hexatriacontane in the temperature and pressure range of 373 K – 573 K and 0-50 bar.

% Error in bubble point pressure of binary mixtures of unlike components								
	CO				H_2			
T [K]	**373**	**473**	**573**	**Ave.**	**373**	**473**	**573**	**Ave.**
	n-Eicosane							
PC-SAFT	42.5	30.3	22.9	**31.9**	19.8	9.3	8.1	**12.4**
SAFT	46.2	38.2	34.1	**39.5**	30.6	21.8	21.7	**24.7**
SPHCT	39.7	28.6	27.3	**31.9**	18.9	6.4	11.2	**12.2**
SRK	13.8	2.6	1.8	**6.1**	21.8	9.8	12.7	**14.8**
Simple-PHCT-ltd	29.8	21.2	23.1	**24.7**	16.3	5.4	13.5	**11.7**
	n-Octacosane							
PC-SAFT	38.7	30.3	25.6	**31.5**	10.5	13.0	9.8	**11.1**
SAFT	54.9	49.4	47.2	**50.5**	37.5	37.9	35.9	**37.1**
SPHCT	49.1	41.7	41.8	**44.2**	28.8	27.4	28.4	**28.2**
SRK	3.0	9.2	8.7	**7.0**	4.8	1.9	1.3	**2.7**
Simple-PHCT-ltd	46.9	41.8	44.5	**44.4**	33.2	33.7	37.5	**34.8**
	n-Hexatriacontane							
PC-SAFT	43.1	35.7	29.8	**36.2**	19.4	17.0	16.2	**17.5**
SAFT	60.0	55.2	52.4	**55.9**	44.2	41.6	42.1	**42.7**
SPHCT	54.8	48.3	47.4	**50.2**	38.9	33.6	36.5	**36.3**
SRK	5.7	19.9	21.7	**15.8**	3.0	9.2	8.7	**7.0**
Simple-PHCT-ltd	54.2	49.4	50.4	**51.3**	44.0	40.3	45.0	**43.1**

7.3.4 Multicomponent VLE representation

In the preceding sections the ability of the *simple-PHCT-ltd EOS* to resent the phase behaviour in binary systems has been investigated. The primary aim of the developed equation of state is however to represent real fluid systems in the reservoir fluids, gas condensate and Fischer-Tropsch process streams. These systems are multicomponent mixture consisting out of small molecules such as CO_2, H_2 and CO and a variety of hydrocarbon components. The ability of the proposed model to represent such systems is therefore of critical importance and will be investigated in the remainder of this section.

7.3.4.a CO_2 – Multicomponent Hydrocarbon Systems

Turek et al. [215] investigated the modelling of reservoir fluid systems through the use of a CO_2 – synthetic oil system. They determined the saturation pressures and densities for various CO_2 concentrations in the synthetic oil at 322 K and 338.7 K. In order to investigate the inherent capability of the various models to represent this system the saturated pressures and temperatures as predicted by the EOS without the use of binary interaction parameters are compared to the experimental values as determined by Turek et al. The synthetic oil is made up out of a mixture of n-alkanes with a maximum carbon number of 14. The composition of the synthetic oil is given in Table 7.9, and Table 7.10 and Table 7.11 list the errors in the values predicted by the equations of state.

Table 7.9 Synthetic oil composition as used by Turek et a. [215]

Component	Composition [mol %]
Methane	34.67
Ethane	3.13
Propane	3.96
n-Butane	5.95
n-Pentane	4.06
n-Hexane	3.06
n-Heptane	4.95
n-Octane	4.97
n-Decane	30.21
n-Tetradecane	5.04

The results in Table 7.10 and Table 7.11 were obtained by doing a bubble or dew point flash at the specified system temperature and compositions. Unless otherwise indicated the type of saturation pressure listed is a bubble point value. Where indicated the convergence criteria of the flash algorithm had to be reduced by up to an order of magnitude of 3 to obtain the results for the SAFT EOS. The errors in the saturated pressures and liquid densities are determined through equation 7.52. The average absolute errors values over the entire composition range are also listed in the tables in order to facilitate the comparison between the various models.

$$Error = \frac{Exp.\,Value - Predicted\ Value}{Exp.\,Value} * 100 \qquad 7.52$$

It is apparent from the results that the phase boundary lines as represented by the various models do not follow the same trends as observed experimentally, with only the *simple-PHCT-ltd* and *SRK* models predicting the experimentally observed dew point behaviour at 339K and 97 % overall CO_2 molar concentration. The *simple-PHCT-ltd EOS* is however still able to predict the saturated pressures of the CO_2 – synthetic oil systems much more accurately than any of other models investigated. This superior performance of the proposed equation of state can be attributed to the fact that, as found in section 7.3.3, the *simple-PHCT-ltd EOS* is able to predict the CO_2 – n-alkane binary systems more accurately than the other equation of state.

Besides the superior performance in the saturated pressure representation, the *simple-PHCT-ltd* model is also highly successful in representing the saturated liquid densities of the system. It is closely followed by the *SPHCT EOS* with the second smallest average error values, whilst the *PC-SAFT EOS* displays large average errors in the predicted saturated liquid densities. The performance of the *PC-SAFT EOS* deteriorates as the CO_2 concentration in the fluid mixture increases, with the model displaying very small errors for the system with no CO_2 content and large errors at high CO_2 concentrations. The small errors at low CO_2 concentrations correspond well with the high accuracy in pure n-alkane fluid volume representation by the *PC-SAFT EOS* observed in Figure 7.6 (b). The poor liquid density performance of the *PC-SAFT* model could therefore possibly be attributed to the poor representation of the liquid volume behaviour of pure CO_2. The average absolute error in the saturated CO_2 liquid volume over the temperature range of 216 K – 302 K as determined by the *simple-PHCT-ltd*, the *PC-SAFT EOS* using the parameters fitted in this study as well as the original parameters determined by Gross and Sadowski [86] are 0.71%, 2.93 % and 2.09% respectively. In order to investigate whether the refitted CO_2 parameters are the cause of the poor performance of the *PC-SAFT* model, the error values in the predicted saturated pressure and density values were determined using the original *PC-SAFT* CO_2 parameters as determined by Gross and Sadowski [86].

Table 7.10 Errors in the predicted saturated pressure values for the CO_2 – synthetic oil mixtures as determined by the various equations of state.

% Error in Sat. Pressure of CO_2 – Synthetic Oil system					
%Psat Error at T = 322.0 K					
CO_2 in Mixture [mol %]	Simple-PHCT-Ltd	PC-SAFT	SAFT	SPHCT	SRK
0.0	2.8	13.2	40.7	17.9	11.8
19.9	14.4	24.2	43.5	26.6	22.2
39.7	20.1	28.6	42.0	31.1	26.4
49.7	21.0	28.1	39.3[1]	31.5	26.3
59.7	20.4	25.5	35.1	30.4	24.4
69.8	18.4	20.3	29.1	27.4	20.7
74.8	16.7	16.5	25.3	25.1	18.1
79.9	14.6	11.9	21.1[1]	22.0	14.9
84.9	11.8	6.2	16.3[1]	18.0	11.0
89.9	8.2	-0.2	11.1[1]	1.8	6.4
93.4 (dew point)	5.3	-4.4	7.7[1]	9.2	3.3
95.0 (dew point)	4.2	-6.0	6.4	7.6	2.2
96.7 (dew point)	2.1	-8.2	one phase	one phase	one phase
Ave. Abs. Error	**12.3**	**14.9**	**28.5**	**26.4**	**15.6**
%Psat Error at T = 338.7 K					
CO_2 in Mixture [mol %]	Simple-PHCT-Ltd	PC-SAFT	SAFT	SPHCT	SRK
0	3.2	12.1	38.5[1]	16.2	10.0
20.2	13.8	23.2	41.1	24.2	20.2
40.4	19.3	27.5	39.6[1]	28.7	24.5
60.4	18.5	22.9	32.0	27.4	21.9
80.2	13.1	7.6	18.4[1]	19.9	13.5
85.3	10.4	0.6	13.4[1]	15.9	9.9
87.3 (dew point)	9.1	-2.5	11.2[1]	14.1	8.4
90.3 (dew point)	7.3	-7.2	8.0[1]	11.2	6.3
95.2 (dew point)	3.6 (dew point)	one phase	one phase	one phase	3.2 (dew point)
Ave. Abs. Error	**10.9**	**13.0**	**25.3**	**19.7**	**13.1**

[1] **Reduced convergence criteria**

Table 7.11 Errors in the predicted saturated liquid densities of the CO_2 – synthetic oil mixtures as determined by the various equations of state.

% Error in Sat. liquid densities of CO_2 – Synthetic Oil system					
% Density Error at T = 322.0 K					
CO_2 in Mixture [mol %]	Simple-PHCT-Ltd	PC-SAFT	SAFT	SPHCT	SRK
0.0	-2.9	1.4	-2.1	-8.3	16.2
19.9	-2.8	-1.4	-3.0	-6.8	15.6
39.7	-2.4	-5.1	-3.9[1]	-5.1	15.0
49.7	-2.1	-7.4	-4.5	-4.2	14.7
59.7	-2.0	-10.7	-5.6	-3.7	14.1
69.8	-2.4	-15.4	-7.5	-3.9	13.0
74.8	-2.5	-18.1	-8.6	-4.1	12.5
79.9	-2.9	-21.7	-10.4[1]	-4.9	11.7
84.9	-3.7	-26.1	-12.8[1]	-6.3	10.6
89.9	-6.8	-34.0	-18.6[1]	-13.6	7.8
93.4	-12.0	-44.0	-27.3[1]	-17.9	3.7
95.0	-14.2	-48.7	-32.1	-21.7	2.2
96.7	-15.8	-53.6	one phase	one phase	one phase
Ave. Abs. Error	**5.6**	**22.1**	**10.5**	**7.7**	**11.4**
% Density Error at T = 338.7 K					
CO_2 in Mixture [mol %]	Simple-PHCT-Ltd	PC-SAFT	SAFT	SPHCT	SRK
0	-4.0	0.0	-2.8[1]	-8.3	14.9
20.2	-3.1	-2.4	-3.1[1]	-6.0	15.0
40.4	-2.2	-6.1	-3.8	-3.7	14.8
60.4	-2.6	-13.6	-6.9	-3.2	13.2
80.2	-3.3	-26.7	-13.0[1]	-4.6	10.8
85.3	-4.8	-33.3	-17.2[1]	-7.0	9.0
87.3	-5.1	-36.0	-18.9[1]	-7.9	8.6
90.3	-5.5	-40.6	-22.1[1]	-9.7	7.9
95.2	-18.1	one phase	one phase	one phase	-6.8
Ave. Abs. Error	**5.4**	**19.9**	**11.0**	**6.3**	**11.2**

[1] **Reduced convergence criteria**

These results are listed in Table 7.12. It can be seen that the saturated pressure values are fairly insensitive to the CO_2 parameter set used, whilst using the original CO_2 do in fact lead to a reduction in the errors in the saturated liquid density representation. The overall trends are however still maintained and the *simple-PHCT-ltd EOS* is still more accurate than the *PC-SAFT* model.

Table 7.12 Errors in the predicted saturated pressures and liquid densities of the CO_2 – synthetic oil mixtures using the *PC-SAFT EOS* with the CO_2 parameters as determined by Gross and Sadowski [86].

% Error values using the PC-SAFT EOS with original CO2 Parameters					
T = 322.0 K			T = 338.7 K		
CO_2 in Mixture [mol %]	% Pressure Error	% Liquid Density Error	CO_2 in Mixture [mol %]	% Pressure Error	% Liquid Density Error
0.0	13.2	1.4	0	12.1	0.0
19.9	24.5	-0.7	20.2	23.4	-1.6
39.7	29.0	-3.4	40.4	27.8	-4.1
49.7	28.6	-5.1	60.4	23.8	-9.3
59.7	26.2	-7.7	80.2	10.6	-17.0
69.8	21.5	-11.4	85.3	4.8	-20.5
74.8	16.3	-14.9	87.3	2.2	-21.8
79.9	12.0	-16.9	90.3	-1.5	-23.9
84.9	7.0	-18.2	95.2	one phase	one phase
89.9	2.4	-22.0			
93.4	-4.4	-44.0			
95.0	-1.1	-38.9			
96.7	-2.9	-42.7			
Ave. Abs. Error	**14.5**	**17.5**	**Ave. Abs. Error**	**13.3**	**12.3**

7.3.4.b VLE of a typical gas condensate

Ng et al. [154] investigated the phase behaviour of a typical gas condensate and determined the VLE data for the 36 component system at 311 K and a variety of pressures, and their results were used as a further case study for the predictive capability of the *simple-PHCT-ltd*, *PC-SAFT*, *SAFT*, *SPHCT* and the *SRK* models. The overall composition of the fluid system is listed in Table 7.14. In modelling the system the C6+ components were treated as primarily consisting out of n-alkanes with an equivalent carbon number and were modelled using pure n-alkanes *EOS* parameter values.

Figure 7.16 depicts the saturated liquid and vapour densities of the system, with the errors in the model predictions, calculated with equation 7.52, summarised in Table 7.13. From these results it is apparent that the *simple-PHCT-ltd*, *PC-SAFT* and the *SPHCT* models are able to represent the saturated vapour densities to similar degree of accuracy, with the largest errors found at the highest system pressure, near the mixture critical point. In this region it appears as if the *SPHCT* is slightly less accurate than the other two models. Furthermore although the *SPHCT EOS* appears to be successful in representing the liquid phase densities at high system pressures, on the whole, the model appears to predict an incorrect saturated liquid density trend. The same can be said for the *PC-SAFT EOS* where the slope of the saturated liquid density line is too large and the model under-predicts the liquid densities at lower system pressures.

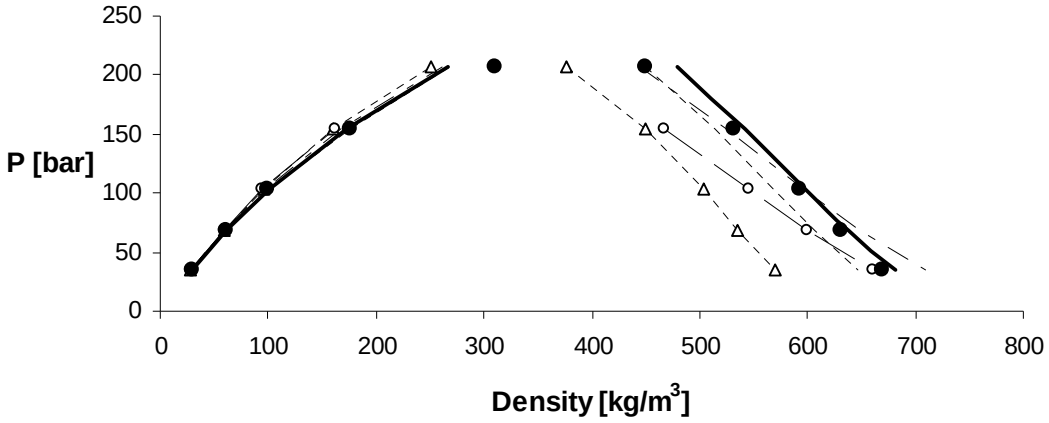

Figure 7.16 Experimental saturated liquid and vapour densities of a gas condensate ● as represented by the ——— *simple-PHCT-ltd,* _ _ _ _ _ *PC-SAFT,* —◇— *SAFT,* _ . _ . _ . *SPHCT* and - - △ - - *SRK EOS.*

The inability of cubic equations of state to represent saturated liquid volumes or densities again becomes apparent in these results, whilst the *SAFT EOS* also severely under predicts the saturated liquid densities. The *SAFT EOS* also fails to predict the liquid-vapour equilibria at 206.8 bar as this is higher than the mixture critical pressure predicted by the model.

Table 7.13 Errors in the saturated liquid and volume densities of a gas condensate as determined by the *simple-PHCT-ltd, PC-SAFT, SAFT, SPHCT* and the *SRK* equations of state.

% Errors in Saturated Densities of a Typical Gas Condensate at 311 K						
Liquid Densities						
Pressure [bar]	**34.5**	**68.9**	**103.4**	**155.1**	**206.8**	**Abs. Ave. Error**
PC-SAFT	3.3	3.9	4.1	3.3	0.2	**3.0**
SAFT	1.3	5.0	7.9	12.2	*	**6.6**
SPHCT	-6.0	-2.9	-0.6	1.4	1.1	**2.4**
SRK	14.9	15.1	15.2	15.4	16.4	**15.4**
Simple-PHCT-ltd	-1.9	-1.0	-0.9	-1.9	-6.7	**2.5**
Vapour Densities						
Pressure [bar]	**34.5**	**68.9**	**103.4**	**155.1**	**206.8**	**Abs. Ave. Error**
PC-SAFT	1.6	-1.1	-2.5	-0.4	13.4	**3.8**
SAFT	3.3	2.6	3.9	7.8	*	**4.4**
SPHCT	2.5	1.1	1.4	4.8	15.5	**5.1**
SRK	2.4	1.6	3.1	8.9	19.1	**7.0**
Simple-PHCT-ltd	0.7	-1.7	-1.9	1.8	14.0	**4.0**

*** Not converged**

From the results discussed above it appears as if the *simple-PHCT-ltd*, the *SPHCT* and the *PC-SAFT* equations of state are the most successful in the representation of the gas condensate system. The *K* values of the specific components (vapour phase mole fraction / liquid phase mole fraction) as determined by these three models are plotted against the system pressure in Figure 7.17. (The *K* values for the C6+ compounds were determined by combining the molar fractions of all the compounds between it and the next lower carbon-number n-alkane, e.g. the C7 *K* values include n-heptane, cyclohexane, benzene and methylcyclopentane.)

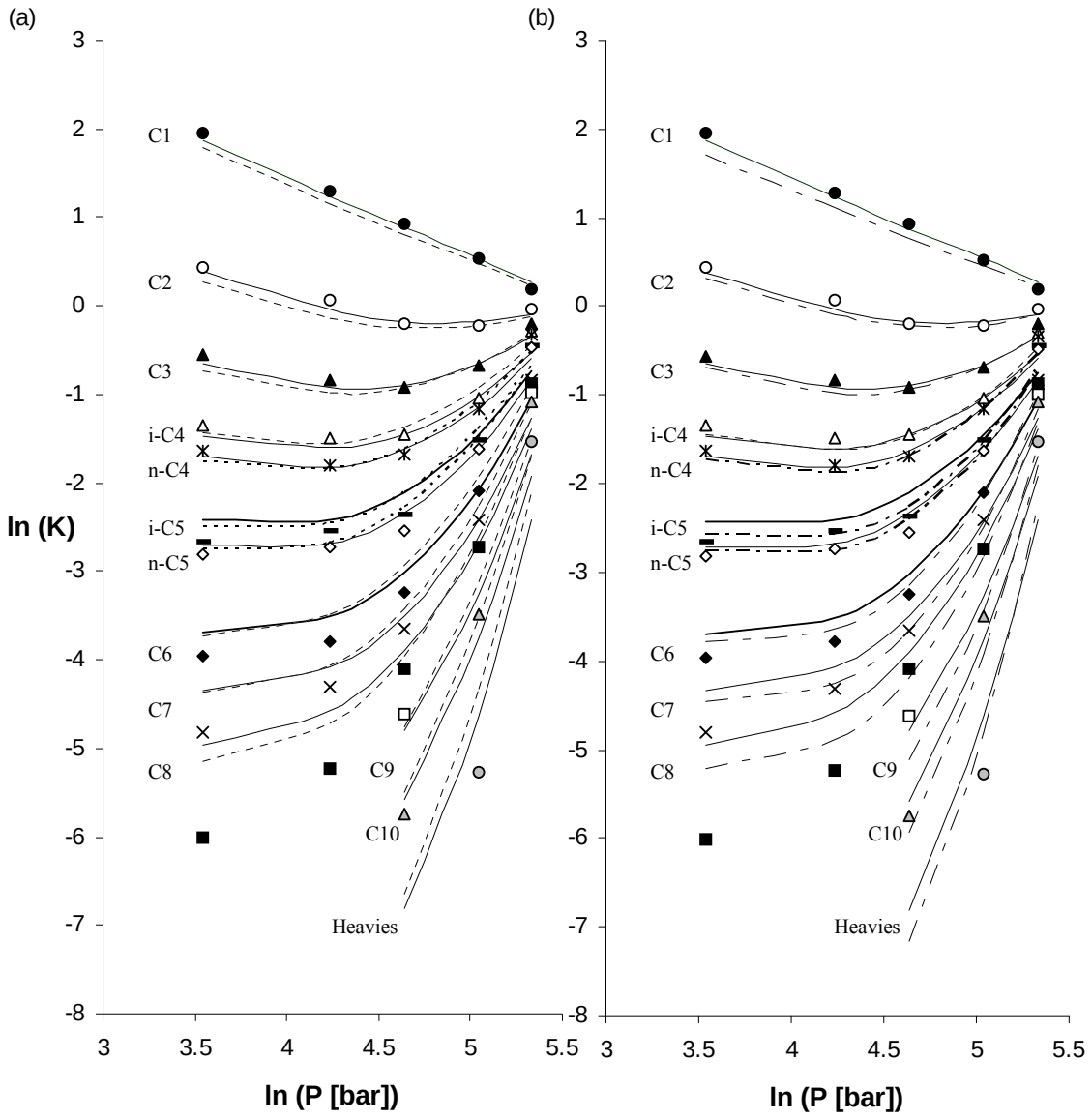

Figure 7.17 Gas condensate K values at 310.98 K as modelled by the ▬▬ *simple-PHCT-ltd EOS* and the (a) ‗‗‗‗‗ *PC-SAFT* and (b) ‗·‗·‗·‗ *SPHCT* models. With ● methane, ○ ethane, ▲ propane, △ iso-butane, ✳ n-butane, ▬ iso-pentane, ◇ n-pentane, ◆ C6, × C7, ■ C8, □ C9, △ C10, ○ heavies

From the figure it is apparent that the *simple-PHCT-ltd EOS* is highly successful in representing the lighter compounds that are present in the highest concentration in the fluid mixture and have the greatest volatility, whilst all of the models struggle to represent the heavier compound *K* values. Because of the low heavy component vapour fractions (and the resultant exceptionally small *K*-values) the accuracy of the experimental data will be less than that of the components present in greater concentrations in both phases. Furthermore the very small molar fractions of these components could possibly lead to truncation errors during the simulation process. The poor performance of the various models in representing these components should therefore not be seen as a fatal flaw, as the experimental and calculated results are less reliable.

Table 7.14 Gas condensate composition as used by Ng. et al. [154].

Gas Condensate Composition			
Component	**Mol %**	**Component**	**Mol %**
Methane	73.8425	C10	0.6041
Ethane	7.2998	C11	0.3384
Propane	4.6031	C12	0.1726
i-Butane	0.9098	C13	0.1217
n-Butane	1.8082	C14	0.0690
i-Pentane	0.8626	C15	0.0310
n-Pentane	0.9655	C16	0.0236
C6	1.4289	C17	0.0164
Methylcyclopentane	0.3652	C18	0.0104
Benzene	0.0449	C19	0.0059
Cyclohexane	0.6811	C20	0.0034
C7	1.5889	C21	0.0014
Methylcyclohexane	1.1746	C22	0.0009
Toluene	0.3926	C23	0.0007
C8	1.4322	C24	0.0006
m-Xylene	0.3559	C25	0.0005
o-Xylene	0.0881	C26	0.0004
C9	0.7549	C27	0.0003

From the results in Figure 7.17 (b) it can be seen that mathematically *simple-PHCT-ltd EOS* and the complex *PC-SAFT* model produce very similar results for the various components, with the *simple-PHCT-ltd EOS* being slightly more accurate than the literature model. The *SPHCT EOS* on the other hand produces results that differ markedly from those of the *PC-SAFT* and *simple-PHCT-ltd EOS* (Figure 7.17 (b)) with larger errors in the *K*-values of the lighter components, and generally more accurate results for the heavier components. As already discussed above the accurate representation of the lighter components should be seen as much more significant in the evaluation of the performance of the models, and as a result it can be concluded that the *simple-PHCT-ltd EOS* is generally more suited to model this system.

7.4 COMPUTATIONAL SPEED

One of the primary aims of this study was to develop an equation of state that has a mathematically simple structure to facilitate the computation of the phase behaviour of complex fluid mixtures during practical calculations, as the complex nature of many of the theoretical equations of state still prove prohibitive in their general application. In this section the computational speed of the *simple-PHCT-ltd EOS* will be compared to literature models discussed in section 7.2.

7.4.1 Computational Technique

Ideally in any flash calculation the component specific fugacity coefficient is determined by obtaining the analytical compositional derivative of the overall fluid fugacity expression:

$$\ln \hat{\phi}_i^{\alpha} = \frac{\partial}{\partial n_i}\left[n \ln \phi^{\alpha}\right]\Big|_{T,P,n_j} \qquad 7.53$$

However because of the complex compositional dependence of the *PC-SAFT EOS* the determination of the analytical solution of the component specific fugacity coefficient is highly involved. It was therefore decided to obtain the derivative numerically through an expression similar to equation 7.54. (See section 8.2 for a detailed discussion on the determination of the numerical derivative.)

$$\ln \hat{\phi}_i^{\alpha} = \frac{(1+dx_i)\ln \phi^{\alpha}_{+dn_i}(T,P) - (1-dx_i)\ln \phi^{\alpha}_{-dn_i}(T,P)}{2dx_i} \qquad 7.54$$

In order to evaluate the various models on the same basis, unless mentioned otherwise, the numerical derivative was used to obtain $\hat{\phi}_i^{\alpha}$ for all the models.

Furthermore, all the models, with the exception of the *SRK EOS*, have a density dependence greater than 4, and hence the fluid density or volume roots need to be determined through numerical techniques. (See section 8.1 for a discussion on the root finding procedures.) Since one of the major strengths of the cubic equations of state is in fact the ability to determine the volume roots analytically, a standard method was use to solve the roots of the *SRK EOS* algebraically. This allowed the true power of the *SRK EOS* to be studied.

Identical computational algorithms and convergence criteria were used for all the models. In order not to penalise any model unnecessarily, wherever possible, the evaluation of the mixing rules for all the *EOS* parameters of a particular model were done in the same summation loops. No additional optimisation of the computer code was done for any of the models. The only exception to this is in the evaluation of the segment volume combination rule of the *simplePHCTltd*, *SPHCT* and *SAFT* models (equations 7.9, 7.28 and 7.50 respectively). The manner in which a power function where the exponent is not an integer, is evaluated in most programming languages is through the evaluation of an exponential and logarithmic function in an operation similar to equation 7.55, whilst when the exponent value is a whole number, the function is simply evaluated through a series of multiplications.

$$base^{exponent} = \exp\left[exponent * \ln\left(base\right)\right] \qquad 7.55$$

The determination of an exponential or logarithmic function on a computer is generally much slower than that of a simple multiplication function. To avoid having to evaluate these slower functions repeatedly, the relevant segment volume parameters of these models were all converted to segment diameters before the actual flash iterations. The segment volume combination term could therefore be determined according to the equivalent but much faster function:

$$v_{ij} = \left(\frac{d_i + d_j}{2}\right)^3 \qquad 7.56$$

Where d_i represents the temperature dependent segment diameter.

The pure component size parameter of *PC-SAFT EOS* is already defined as a segment diameter, and hence the evaluation of the volume combination term is already in the optimised form. (See equations 7.43, 7.44 and 7.50). By using equation 7.56 in the other models all the equations of state can therefore be evaluated on the same basis.

7.4.2 System properties and evaluation technique

The various models were evaluated on an Intel ® Pentium ® 4, 3.00 GHz computer with 1.98 Gb of RAM using a Borland Delphi Open Source program GpProfile 1.3.3 to determine the speed of the calculations.

The models were evaluated according to three criteria, the speed of convergence the *P-T* flash algorithm, the total time required for a flash calculation using a specific vapour to feed molar ratio, *B*, estimate such as 0.5, and finally the time required to calculate the fugacity coefficient ratio, *K*, at the specific liquid and vapour compositions at which the flash algorithm had converged for that specific model.

The computational times are taken as the average time determined over 10 flash or *K* value calculations.

7.4.3 Evaluation of the computational speed of the equations of state

Three datasets with an increasing number of components were used in the investigation of the computational speed of the various models, a simple binary mixture of n-ethane – n–decane at 378 K and 41.4 bar, a 12 component mixture of consisting out of CO_2, N_2 and a mixture of n-alkanes as studied by Turek et al. [215] at 322 K and 69.15 bar (see Table 7.15 for overall composition of the system) and the 36 component gas condensate system listed in Table 7.14 at 310.95 K and 34.5 bar.

Table 7.15 Synthetic oil composition as used by Turek et a. [215]

Component	Composition [mol %]
Nitrogen	0.456
Carbon Dioxide	69.52
Methane	10.13
Ethane	0.851
Propane	1.195
n-Butane	1.798
n-Pentane	1.305
n-Hexane	0.966
n-Heptane	1.482
n-Octane	1.505
n-Decane	9.196
n-Tetradecane	1.596

Initially the number of flash iteration steps required for the various *EOS* to converge to an answer of the P-T flash of the given systems was determined. The results are reported for different initial estimates of the vapour to feed molar ratio, *B*, and serve as an indication of the

ease with which the specific models can converge for the particular systems. Table 7.16 lists the number of iterations required if an initial estimate of 0.1, 0.5 and 0.9 were used for the *B* value, it also contains the number of iterations required if the final *B* value to which the particular model had converged was used as the initial estimate. These final *B* values are listed in Table 7.17.

Table 7.16 The number of P-T flash iterations required for the various models in evaluating a binary, 12 and 36 component system.

Number of iteration steps required in the P-T flash calculations															
	Binary system					**12 component system**					**36 component system**				
B estimate	**0.1**	**Final**	**0.5**	**0.9**	**Ave.**	**0.1**	**Final**	**0.5**	**0.9**	**Ave.**	**0.1**	**0.5**	**Final**	**0.9**	**Ave.**
PC-SAFT	6	5	5	6	**6**	27	33	36	45	**35**	11	11	9	10	**9**
SAFT	13	14	14	15	**14**	15	10	13	32	**18**	10	8	8	8	**8**
SPHCT	9	8	8	9	**9**	30	45	31	13	**30**	10	9	8	9	**9**
SRK	12	12	12	12	**12**	22	45	19	16	**26**	12	11	10	11	**10**
Simple-PHCT-ltd	11	10	10	10	**10**	20	13	15	24	**18**	12	11	10	11	**10**

From Table 7.16 it appears as if the rate of convergence of the various models in the flash calculations is unrelated to the number of components the mixture, but rather dependent on the complexity of the system, as the 12 component system, the only system containing CO_2 and N_2, generally requires more iterative steps than either the binary or 36 component systems, consisting entirely out of hydrocarbons.

Furthermore it can be seen that for the CO_2 containing system, the models convergence show a marked dependency on the initial estimates used in the flash algorithm, with the *SPHCT* and the *SRK* models displaying the greatest variation in the number of iterative steps. The *simple-PHCT-ltd* and *SAFT* equations appear to be the least affected by the change in character of the test system, with both models displaying only a slight dependence on the initial *B* value estimates, and requiring only a small increase in the average number of iterative steps in the flash algorithm when compared to the number of iterations needed for the pure hydrocarbon mixtures.

Table 7.17 The vapour to feed ratios of the various models converged to during the P-T Flash calculations

B values converged to in the P-T flash calculations			
	Binary system	**12 component system**	**36 component system**
PC-SAFT	0.4298	0.2117	0.8324
SAFT	0.3170	0.2111	0.8155
SPHCT	0.4326	0.2820	0.8301
SRK	0.4590	0.3645	0.8343
Simple-PHCT-ltd	0.4495	0.4070	0.8389

The rate of convergence alone however does not control the rate of the flash calculations, and other factors such as the determination of the volume or compressibility roots, the calculation of the mixture parameters and the specific mathematical structure of the models all contribute to the computational time of the models. Table 7.18 lists the average time required for each model for a *PT* flash calculation using $B = 0.5$ as an initial estimate.

Table 7.18 Time required for a single P-T flash calculation using B=0.5 as an initial estimate, in absolute and relative % values.

Average Time for a P-T Flash Calculation						
	Binary system		**12 component system**		**36 component system**	
	Time [s]	**Relative**	**Time [s]**	**Relative**	**Time [s]**	**Relative**
PC-SAFT	0.0052	15.8%	0.4097	52.7%	1.0418	37.0%
SAFT	0.0238	72.4%	0.2326	29.9%	0.9395	33.4%
SPHCT	0.0009	2.8%	0.0861	11.1%	0.3452	12.3%
SRK	0.0004	1.3%	0.0127	1.6%	0.1508	5.4%
Simple-PHCT-Ltd	0.0026	7.8%	0.0371	4.8%	0.3356	11.9%

As expected is the *SRK EOS* with its simple mixing rules and mathematical structure is clearly much faster than any of the other models. The effect of the complex structure of the *SAFT* and *PC-SAFT* models is also clearly visible, with both models being significantly slower than the *SRK*, *SPHCT* and the *simple-PHCT-ltd EOS*. The *SAFT EOS* appears to be significantly slower than the more complex *PC-SAFT EOS* in representing a simple binary system. This may in part be attributed to the larger number of iterative steps required for the flash calculation to converge when using the *SAFT* model (see Table 7.16). The overall computational time of the *SAFT EOS* is however also greatly influenced by the time spent finding the liquid and volume roots of the model as is apparent from Figure 7.18, a plot of the time spent finding the liquid and vapour volume roots of the various equations of state.

The results for this figure were obtained at the converged conditions of the specific model and using an identical root finding algorithm in all instances. Table 7.19 lists the total number of iterations required to determine the volume roots at these conditions. From these values the reason behind the long computational times of the *SAFT EOS* becomes apparent as the combinatorial effect of the difficulty experienced in the convergence of the root finding algorithm and the overall complex structure of the model.

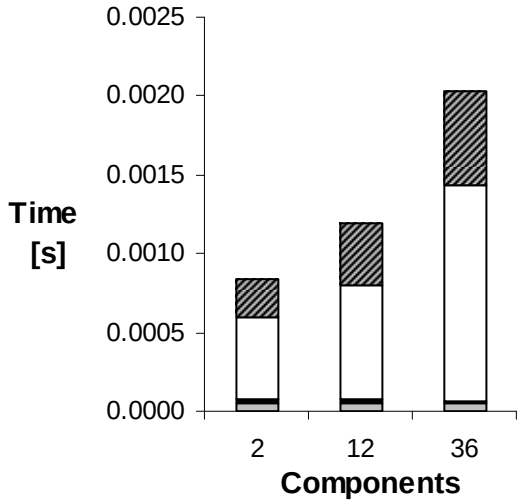

Figure 7.18 Time spent solving the liquid and vapour volume roots at the converged conditions. ■ *PC-SAFT,* □ *SAFT,* ■ *SPHCT,* □ *simple-PHCT-ltd.*

The *SPHCT EOS* requires almost the same number of iterative steps in determining the volume roots as the *SAFT EOS*, but as the structure of the *SPHCT* is much simpler the overall computational time of this model is not affected as dramatically. Furthermore it is clear that although the mathematical structure of the perturbation term of the *SAFT EOS* is a simple polynomial function in density (as a result of the application of the double summation perturbation approximation of Chen and Kreglewski [42]), it is less suited to the determination of the volume roots through a simple Newton-Raphson search technique than the complex density dependent form of the second perturbation approximation used in the *PC-SAFT* model. (See Section 8.1.1.b).

Although the perturbation approximation term of the *simple-PHCT-ltd EOS* is also a double summation approximation, it is clear from the results in Figure 7.18 and Table 7.19 that this simplified form of the perturbation approximation does not suffer from the same limitations discussed above, and that the volume roots can readily be obtained.

Table 7.19 Total number of iterations in the liquid and vapour volume root search at P-T flash converged compositions.

Total number of iterations in liquid and vapour volume root search			
	Binary system	**12 component system**	**36 component system**
PC-SAFT	52	336	864
SAFT	136	816	2376
SPHCT	132	816	2304
Simple-PHCT-Ltd	76	504	1368

From the results of the flash calculations (Table 7.18) it can be seen that whilst the *simple-PHCT-ltd EOS* is slightly slower than the *SPHCT* model for systems with a small number of components, the *P-T* flash calculations with the *simple-PHCT-ltd EOS* are faster for the more complicated mixtures (containing n-alkanes and CO_2) and mixtures with a larger number of components. These results are confirmed in Table 7.20 which lists the average computational time for a single *K* value, or the component specific vapour and liquid fugacity coefficient, at the phase compositions to which the models have converged.

Table 7.20 Time required for a K ratio calculation (vapour and liquid component specific fugacity coefficient ratio) at the P-T flash conversion conditions in absolute and relative % values.

Average Time for the calculation of a single K value						
	Binary system		**12 component system**		**36 component system**	
	Time [s]	**Relative**	**Time [s]**	**Relative**	**Time [s]**	**Relative**
PC-SAFT	0.00104	33.4%	0.01092	31.0%	0.08779	29.9%
SAFT	0.00171	54.7%	0.01918	54.5%	0.12709	43.3%
SPHCT	0.00010	3.3%	0.00205	5.8%	0.03865	13.2%
SRK	0.00004	1.2%	0.00058	1.7%	0.01176	4.0%
Simple-PHCT-Ltd	0.00023	7.4%	0.00246	7.0%	0.02831	9.6%

From the results above, if a choice had to be made based purely on the computational speed of the various models, the *SPHCT*, *simple-PHCT-ltd* and *SRK* models would clearly be favoured. These results are however based on the numerical derivation of the mixture fugacity coefficient. Table 7.21 lists the computational times required for a *K* value calculation using analytical derivation of the fugacity coefficients of these models.

Table 7.21 Time required for a K ratio calculation (vapour and liquid component specific fugacity coefficient ratio) at the P-T flash conversion conditions using the analytical derivative of the fugacity coefficient

Average Time for the analytical calculation of a single K value			
	Binary system	**12 component system**	**36 component system**
	Time [s]	**Time [s]**	**Time [s]**
SPHCT	0.00003	0.00019	0.00134
SRK	0.00001	0.00007	0.00044
Simple-PHCT-Ltd	0.00006	0.00018	0.00088

The effect of determining the compositional derivatives analytically is clearly visible with an overall improvement of between 70 – 97 % in the computational speed of the various models. However the comparative behaviour of the models are still the same and the observations made based on the models in their numerical form are still relevant, with the cubic *SRK EOS* being the fastest model overall and the *simple-PHCT-ltd EOS* whilst being slower than other models when modelling small systems, outperforming the *SPHCT EOS* when applied to mixtures with a large number of components. The effect of an increasing number of components in the fluid mixture is depicted in Figure 7.19. From this plot it is clear that the rate of increase in the computational time with an increasing number of components in the fluid mixture is much greater for the *SPHCT EOS* than for the *simple-PHCT-ltd* equation of state. The higher rate of increase for the *SPHCT EOS* can be attributed to the exponential function used in the perturbation term of the model (see sections 4.3.5.c). As mentioned before the evaluation of an exponential function on a computer is much slower than normal addition or multiplication functions. As the number of components in the fluid mixture increases the effect of these functions will become greater as the number of times they need to be evaluated increases at a rate of N^2, where N represents the number of components in the system. As the perturbation term of the *simple-PHCT-ltd EOS* is a simple polynomial function that can be evaluated purely through simple multiplication, the effect of an increase in the number of times it needs to be evaluated will not be as large.

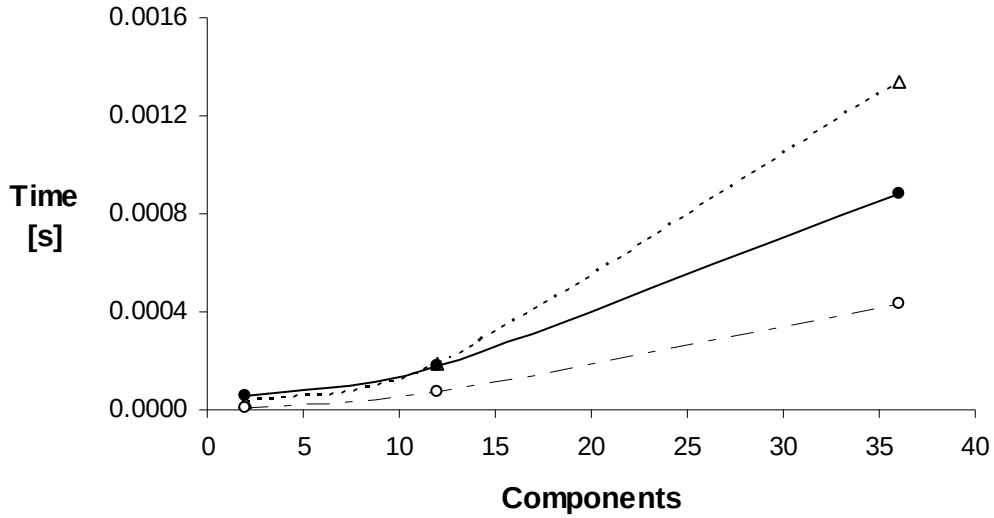

Figure 7.19 Increase in the computational time of a K value calculation with an increase in the number of components in the fluid mixture. —●— *simple-PHCT-ltd,* - - ▲ - - *SPHCT,* - ·○· - *SRK*

When the number of components in the fluid mixture are small the more simple mathematical structure of the *SPHCT* equation will dominate over the effect of the exponential functions, and the slightly more complex *simple-PHCT-ltd* equation of state will be slower. However at these conditions although the speed of the *simple-PHCT-ltd* model may be slower than that of the *SPHCT EOS*, the difference between the models is in the order of magnitude of 40 microseconds, and will not have any practical significance.

7.5 SUMMARY AND CONCLUSIONS

The new equation of state has been developed with the aim to represent systems containing large n-alkanes or hydrocarbons generally. The representation of these systems are problematic for several reasons: firstly, the limited availability of relevant binary *VLE* data from which binary interaction parameters can be regressed for many of the systems of interest requires that the models should be able to represent these systems largely predictively; secondly the nature of the mixture systems, the large degree of asymmetry between the components, and differing chemical natures of the components, are very taxing on the mixing rules of the models. Finally the proposed methods or routes through which the chainlike structure and suitable mixing rules can be incorporated into a model often lead to mathematically complex equations with very slow computational times making them impractical for general applications. The aim of this study was therefore to develop an equation of state that could satisfactorily address these factors.

In this chapter the proposed *simple-PHCT-ltd EOS* has been presented in its final form along with the fitted pure component parameters of the relevant components investigated in this work. It has also been shown that the pure component parameters of the n-alkane homologous series can be readily generalized, and that the developed correlations can be successfully used to estimate the parameters of components within the molecular weight range of 18 – 506 g/mol. Although the extrapolation of these correlations to higher molecular weights should be done with care, using the extrapolated parameter values to model the binary *VLE* data containing n-alkanes with very high molecular weights (619 – 844 g/mol) has lead to very satisfactory results.

The n-alkane homologous series was used as the base case for a chainlike non-polar system. In the modelling of the pure component *VLE* and supercritical *P-v-T* behaviour of these components, it has been shown that the proposed model is able to represent these systems to a similar degree of accuracy than the generally applied *SAFT* and *SPHCT* models for chained systems.

When applied to binary mixtures of the n-alkanes the *simple-PHCT-ltd EOS* again proved to be able to successfully represent these systems. One of the major difficulties in modelling mixtures containing large chainlike molecules is that there is generally a large degree of size asymmetry in the fluid mixture that needs to be taken into account through the *EOS* parameter mixing rules. The *simple-PHCT-ltd EOS* was shown to be able to represent these difficult systems successfully over a wide range of system pressures, with the model generally outperforming the traditional equations.

The proposed model was also tested against mixtures containing differing species, using the n-alkanes as the chainlike component, and CO_2, CO, H_2 and N_2 as the secondary species. The *simple-PHCT-ltd* model was found to represent the mixtures of n-alkanes with CO_2 much more successfully than any of the other models, predicting a more realistic phase envelope. Over the limited range the data available for the mixtures with the other components the *simple-PHCT-ltd EOS* was again found to represent the data to a similar degree of accuracy as the *SAFT* and *SPHCT* models.

The ability of the model, or more specifically the newly developed mixing rules, to be extended to multi-component mixtures was also evaluated. An 11 component mixture consisting out of CO_2 and n-alkane species up to n-tetradecane, and a 36 component system

containing a mixture of hydrocarbon species were used as representative systems for possible applications of the model. The new equation of state was found to be highly successful in predicting the saturated pressures and liquid densities of these systems as well as the *K* values of the major components in the 36 component system.

Thus having proven the capability of the new model to represent the desired systems successfully the final requirement was to investigate the actual computational speed of the model. It was shown that the rate of convergence of the *simple-PHCT-ltd EOS* over a simple *P-T* flash for binary, 12 and 36 component mixtures is comparable to the models found in the literature, and is generally insensitive to the initial estimates in the flash algorithm. Furthermore it was shown that although the model is quintic in volume and the fluid volume roots need to be obtained numerically, the structure of the model is such that it converges much more successfully to the desired roots than either the *SAFT* or the *SPCHT EOS*. Finally it was shown that although the *simple-PHCT-ltd EOS* is initially slower than the *SPHCT EOS* when modelling binary systems, the rate of increase in the computational time required for an increasing number of components in the fluid mixture is much lower for the new model.

From the results in this section it can therefore be said that the *simple-PHCT-ltd EOS* will be the method of choice for the modelling of chained systems large enough for the computational time to become prohibitive.

Chapter 8 ***Computational techniques and algorithms***

In this chapter the various computational algorithms and numerical techniques used throughout this study will be discussed and some general problems in the determination of the fluid phase equilibria will be addressed.

All of the thermodynamic calculations and parameter regressions in this study were done using software developed in-house, specifically for this purpose. Several non-traditional routes were followed in the determination some of the thermodynamic properties to overcome various problems associated with computational accuracy and the flexibility.

8.1 SOLVING THE FLUID VOLUME ROOTS OF AN EOS

For any given equation of state, at the specified temperature and pressure conditions, there will be, depending thermodynamic state of the system and the structure of the model, one or more fluid volumes or densities that satisfy the equation of state. Of these fluid volumes, the value that result in a minimum in the Gibbs free energy, will indicate a thermodynamically stable state of the system. For a pure component system at the saturated conditions below the critical point, two such volume roots can be determined, with generally the smallest fluid volume being that of the thermodynamically stable saturated liquid phase and the largest that of the saturated vapour phase. At conditions not on the phase boundary line only one real volume root exit will exist.The same can be said for multi-component systems, where on the phase boundary line, if multiple roots are found the largest root is the saturated vapour volume or conversely the smallest root the saturated liquid volume.

In this section the computational techniques used and the possible problems in the determination of the fluid volumes will be discussed.

8.1.1 Mathematical and computational algorithms for the calculation of the fluid volumes.

As mentioned before, one of the strengths of a cubic equation of state is the fact that the solutions for the fluid volume roots of the model can be obtained analytically. Whilst it is still possible to obtain the solution of a quartic equation analytically following Ferrari's method of

the general quartic equation [114] by solving a series of cubic and quadratic equations, the roots of the equations with a greater order in volume need to be obtained numerically.

The following computational procedures and algorithms were used in the solution of the volume roots.

8.1.1.a Solving the cubic roots

The solution of the roots of a cubic equation is readily available and generally published in text books on mathematical and numerical techniques [114, 171]. It will therefore only be discussed in brief, and only the real solutions of the equation will be considered, as complex volume roots (as well as negative roots) have no physical meaning in the current application.

For a general cubic equation of the form:

$$x^3 + ax^2 + bx + c = 0 \qquad 8.1$$

the following expressions can be written:

$$Q = \frac{a^2 - 3b}{9} \qquad 8.2$$

and

$$R = \frac{2a^3 - 9ab + 27c}{54} \qquad 8.3$$

If Q and R are real, and $R^2 \leq Q^3$ then the equation has 3 three real roots.

By defining θ as:

$$\theta = \arccos\left(\frac{R}{\sqrt{Q^3}}\right) \qquad 8.4$$

the solutions for the roots can be obtained:

$$x_1 = -2\sqrt{Q}\cos\left(\frac{\theta}{3}\right) - \frac{a}{3}$$
$$x_2 = -2\sqrt{Q}\cos\left(\frac{\theta + 2\pi}{3}\right) - \frac{a}{3} \qquad 8.5$$
$$x_3 = -2\sqrt{Q}\cos\left(\frac{\theta - 2\pi}{3}\right) - \frac{a}{3}$$

The second possibility, where $R^2 > Q^3$ results in only one real root, which can be determined by defining A and B as:

$$A = -sign(R)\left[|R| + \sqrt{R^2 - Q^3}\right]^{1/3} \qquad 8.6$$

and

$$B = \begin{cases} \dfrac{Q}{A} & A \neq 0 \\ 0 & A = 0 \end{cases} \qquad 8.7$$

and using the following relation:

$$x_1 = (A + B) - \frac{a}{3} \qquad 8.8$$

8.1.1.b Numerical solution for the fluid volume roots

Besides the *SRK EOS*, all of the models used in this study require a numerical solution of the *EOS* volume roots, with the proposed *simple-PHCT-ltd EOS* being quintic in volume and the literature models *SAFT*, *PC-SAFT* and *SPHCT EOS* all displaying even higher order dependencies on the fluid volume. In order to facilitate the comparison between the computational times required by the various models, the same algorithm and convergence criteria were used for all of the models.

The fluid volume roots were determined by a simple Newton-Raphson search algorithm:

$$z_{new} = z_{old} + f(z_{old}) \Big/ \left(\frac{df(z_{old})}{dx}\right) \qquad 8.9$$

where $f(z)$ is the difference between the compressibility expression of the equation of state (e.q. equation 7.1) and the value z_{old}:

$$f(z) = z_{EOS} - z_{old} \qquad 8.10$$

The convergence of the Newton-Raphson technique is dependent on the quality of the initial estimates used in the algorithm. In the modelling of the *fluid mixtures* a compressibility of 1 is used as the initial estimate for the vapour phase volume determination whilst the compressibility value at fluid densities 0.1% smaller than the maximum density for which the *EOS* will have real finite solutions is used in the liquid volume determination. This initial estimate for the liquid volume was chosen as such to eliminate the possibility that any small valid roots are missed by selecting a too large starting value for the fluid volume or compressibility. (See section 8.1.2.b) The *SAFT*, *PC-SAFT* and *SPHCT* equations are all based on the *Carnahan Starling* expression for the hard sphere volume and the initial estimates for the compressibilities of the fluid volumes of these models would therefore be the compressibility at 99.9% of the closest packed density or :

$$z_{estimate} = 1.001 * \frac{P}{RT} \tau \, rv_{0m} \qquad 8.11$$

where $\tau = \pi * 2^{1/2}/6$, and $rv_{0\,m}$ is the mixture closest packed volume of the molecular species in the system.

The hard sphere term of the *simple-PHCT-ltd EOS* differs from that of the *Carnahan Starling* expression (equation 3.20), with the coefficient of the reduced density term in the denominator larger than 1. The *simple-PHCT-ltd EOS* therefore has a smaller maximum density that can be obtained before the model has a discontinuity where the denominator approaches zero. The initial estimate of the liquid compressibility factor of the *simple-PHCT-ltd EOS* is therefore:

$$z_{estimate} = 1.001 * d \frac{P}{RT} \tau \, rv_{0m} \qquad 8.12$$

Where d is defined as a universal constant for the model and is equal to 1.399. (See Table 7.1)

Using the initial estimates, equation 8.9 is evaluated repeatedly until the change in the compressibility value is smaller than the convergence criteria set for the equations.

No attempt has been made to optimise the fluid volume search algorithm, and it would be possible to improve the convergence of the method by using better estimates for the initial liquid volume, as can be seen from Figure 8.1 a plot of the relative time spent solving the liquid and vapour volume roots. However as the same method was used for all the models all of the non-cubic equations of state are evaluated on the same basis, and the conclusions regarding the computational times remain relevant.

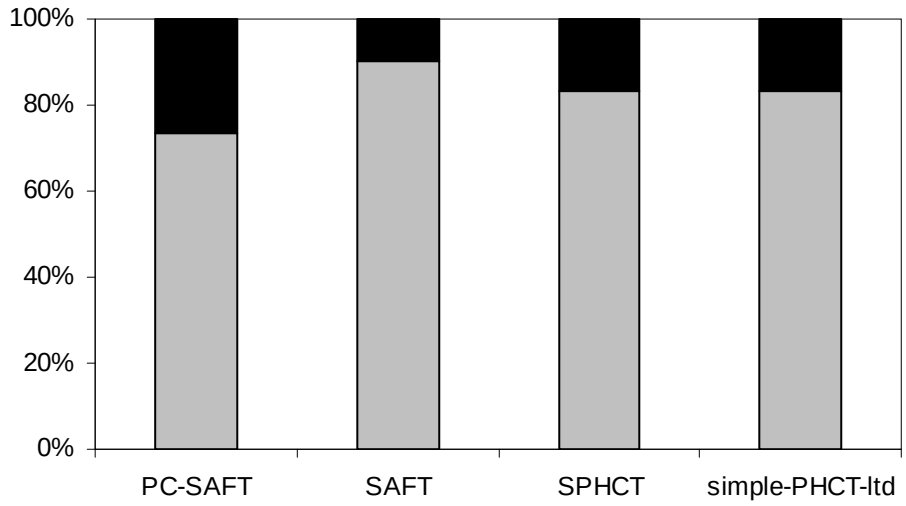

Figure 8.1 Relative time spent in the determination of a liquid and vapour volumes during a P-T flash calculation of a 36 component system as classified in chapter 7. With □ liquid volume and ■ vapour volume calculations.

8.1.2 Computational aspects regarding the determination of fluid volume roots

Two different types of problems were experienced in the determination of the fluid volumes in this study. The first is attributable to the rounding errors during the computation of the saturated fluid volumes of low vapour pressure components, and the second to the actual structure of the *SAFT EOS.*

Both these problems and how they were addressed are discussed below.

8.1.2.a Rounding errors in analytical solution of volume roots of low vapour pressure components

Because of the manner in which data is managed in computers, real numbers cannot be stored to an infinite precision, and the accuracy to which the number can be represented is dependent on the word-length, or the number of computer memory bits, used to store the information. Furthermore, arithmetic in real numbers on computers can never be exact because of the way

the computation is executed and the evaluation of expressions involving numbers of vastly differing magnitudes will generally be accompanied by a loss in accuracy because of the rounding off of the numbers [171]. This problem will especially be aggravated when calculations such as the subtraction or division of two real numbers of vastly differing magnitudes are evaluated. Although the loss in accuracy can never be entirely eliminated in computer calculations, there are ways, such as avoiding the subtraction of numbers with a large difference in size, through which the effect of the rounding error can be minimised.

During the course of this investigation the effect of the rounding errors was especially noticed in the determination of the saturated volume roots of the low vapour pressure n-alkanes when analytical methods were used to solve the exceptionally small liquid volumes of these components. These observations can be clarified by the following example:

The saturated vapour pressure of n-hexatriacontane at 360 K is 7.463e-06 Pa, and the coefficients of the compressibility function of the *SRK EOS* at these conditions expressed in the form of equation 8.1 are in the order of magnitude of $a \approx -1$, $b \approx 1e-10$ and $c \approx -1e-22$. Upon closer inspection of the analytical solution of the cubic equation it is apparent that the evaluation of several functions that involve the addition and subtraction of parameters differing up to 1e-12 in size is required. (See equation 8.3.) As mentioned before, such calculations greatly contribute to the rounding error as the smaller parameters will effectively be seen as equal to zero and will not be taken into consideration in the arithmetic procedure. This rounding error leads to the determination of inaccurate fluid volume roots and results in the failure of the equation of state to converge. This behaviour is clearly visible in Figure 8.2 (a), where the *SRK EOS* fails to converge at conditions below 0.001 Pa.

This problem with the determination of the analytical solution of the roots of a cubic equation of state has been previously reported by Zhi and Lee [250]. They found that the problem with the rounding errors may be avoided by using the numerical Newton-Raphson technique to obtain the fluid volume roots. However, although using equation 8.9 (the Newton-Raphson search algorithm) eliminates the need to subtract parameters of differing magnitudes and hence minimises the rounding errors, having to resort to this numerical approach negates one of the greatest strengths of the family of cubic equations of state.

Several alternate methods of avoiding or minimising the rounding errors whilst still solving the liquid analytically were investigated. Extending the precision to which the various model

parameters are stored from using a double wordlenght, or 8 bits, to an extended format which uses up to 10 bits and a specially defined format of 16 bits, was found to alleviate the problem to a certain extent. However this approach in effect simply shifts the problem to lower system temperatures and does not offer a feasible sustainable solution over the entire vapour pressure range. A entirely different approach was therefore needed to solve the fluid volume roots of the pure component properties.

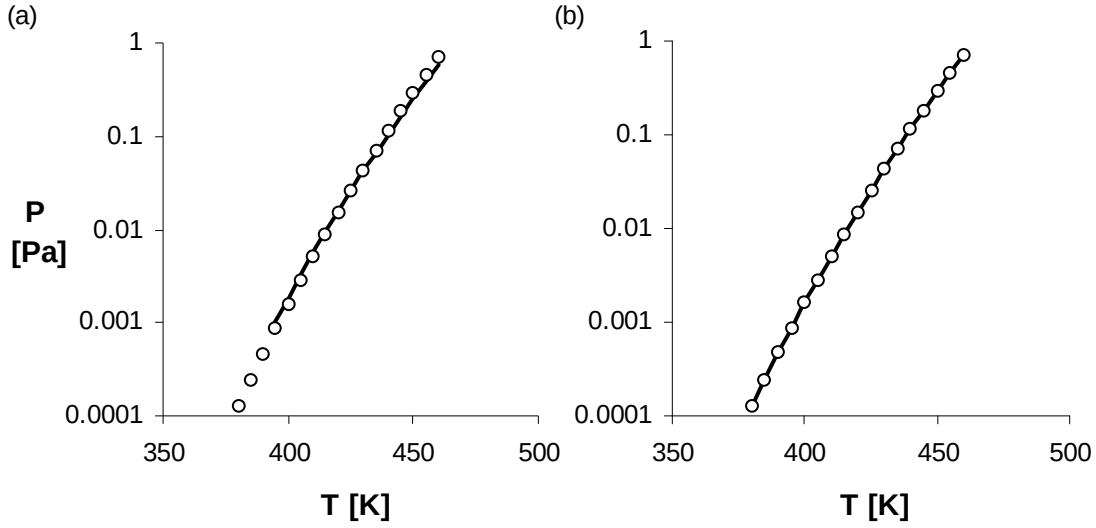

Figure 8.2 Improved convergence of the *SRK EOS* (——) in the representation of the n-hexatriacontane saturated vapour pressure data ○, with (a) using the standard compressibility solution algorithm, and (b) finding the saturated liquid density and saturated vapour compressibility roots.

It was found that the effect of the rounding errors is fairly insignificant on the model performance if the actual determined parameter is comparatively large as in the case of the calculation of a vapour phase compressibility value. This parameter is generally is quite close to 1 and if it is inaccurate in the 12^{th} decimal, as a result of the rounding errors, the error would have a fairly small effect on the accuracy of the calculations further on. The liquid phase compressibility of an n-alkane such as n-hexatriacontane can on the other hand be as small as 2e-12 at low temperatures and it is immediately apparent that an inaccuracy in the 12^{th} decimal of this value will have a significant effect on the solution of the saturated liquid volume. This problem can however be avoided by determining the liquid volume root not through the solution of the volume or compressibility expression of the equation of state but rather by solving equation 8.1 written in a cubic density form as the saturated liquid density value is a very large value and a rounding error of 1e-12 will be negligible.

The solution algorithm of the fluid volumes of cubic equations therefore requires the determination of two different roots: for the calculation of the saturated vapour volume, the

largest value satisfying the compressibility expression of the equation of state, and also the saturated liquid density, the largest root of the equation of state in its density form from which the liquid volume can be determined.

This approach successfully deals with the effect of the rounding errors whilst maintaining the computational speed of the cubic equation of state. The improvement in the convergence of the equation of state at the lower saturated temperatures of n-alkanes is clearly discernable in Figure 8.2 (a) and (b).

8.1.2.b The multiple volume roots of the SAFT equation of state

During the course of this study it was found that it was in fact possible for the compressibility expression of the *SAFT* equation of state to have more than three positive volume roots at certain conditions for both methane and argon systems.

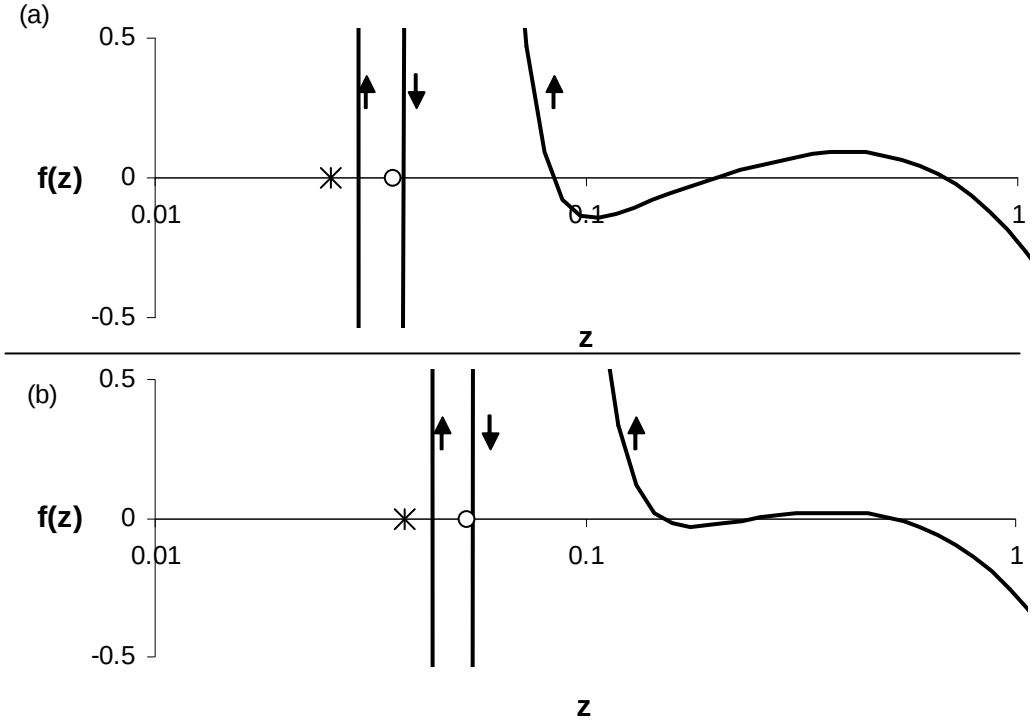

Figure 8.3 Plot of the compressibility function (equation 8.10) of the *SAFT EOS* at saturated conditions for (a) Argon at 133.7 K and (b) Methane at 183.8 K determined using the pure component parameters as determined by Huang and Radosz [100]. ⁎ Indicates the minimum z value allowable for the equation and ○ $1.399*z_{min}$, the minimum value for the *simple-PHCT-ltd EOS*

This phenomenon is depicted in Figure 8.3(a) and (b) as graphical representations of equation 8.10 evaluated at the saturated conditions for argon and methane at 133.7 K and 183.8 K respectively. (Due to a problem of scale the entire extent of the function cannot be shown, and

the plots only focus on the relevant areas around the zero or root values of the equation.) At these saturated conditions the equation of state is expected to have three real positive roots with the smallest and largest roots being those of the saturated liquid and vapour volumes, however 5 possible roots can be discerned on the graphs.

Koak et al. [115] have achieved similar results for methane and found that the *SAFT EOS* could have 5 positive real roots with the two additional positive roots found at densities greater than the theoretical closest packed density.

Although it could be argued that the additional densities as reported by Koak et al. [115] are physically unreasonable, because they are at densities greater than those that are physically realisable, the behaviour reported in this current study has however a much more serious consequence because all 5 roots can be found within the physically realisable range. (The * in Figure 8.3 (a) and (b) and Figure 8.5 indicates the limiting compressibility value or closet packed density of the *SAFT EOS.*) The choice of the correct liquid volume root becomes very complicated as the third root in fact leads to the correct model performance, and corresponds to the correct liquid compressibilities as determined by other models, whilst the traditional criterion for the selection of the volume root is the smallest root that would result in a negative slope in the pressure-volume relationship.

The problem of the multiple volume roots is furthermore not only limited to the saturated conditions, as it has also been found that the *SAFT EOS* has three volume roots in the supercritical phase region of both the argon and methane systems where theoretically there should only be one root. (See Figure 8.4)

The observations on the methane and argon systems were made using the original pure component parameters as determined by Huang and Radosz [100]. However the same behaviour can be discerned when the *EOS* parameters are refitted to the data used in this work, indicating that the problem is rooted in the structure of the model and not to the regressed pure component parameters.

Furthermore, it can be said that the problem is not unique to the statistical associating theory directly but rather stems from the work of Chen and Kreglewski [42] and the *BACK* equation of state on which the *SAFT EOS* is based, as this multiple root phenomenon can be observed for spherical components for which the chain term is equal to zero. The source of the problem could therefore lie in either the hard sphere compressibility or perturbation terms. However as

no such behaviour was not observed over the entire range of methane and argon data for either the *SPHCT* or the *PC-SAFT* models, both of which utilise the same hard sphere term as the *SAFT EOS*, the problem seems to stem from the double summation perturbation term.

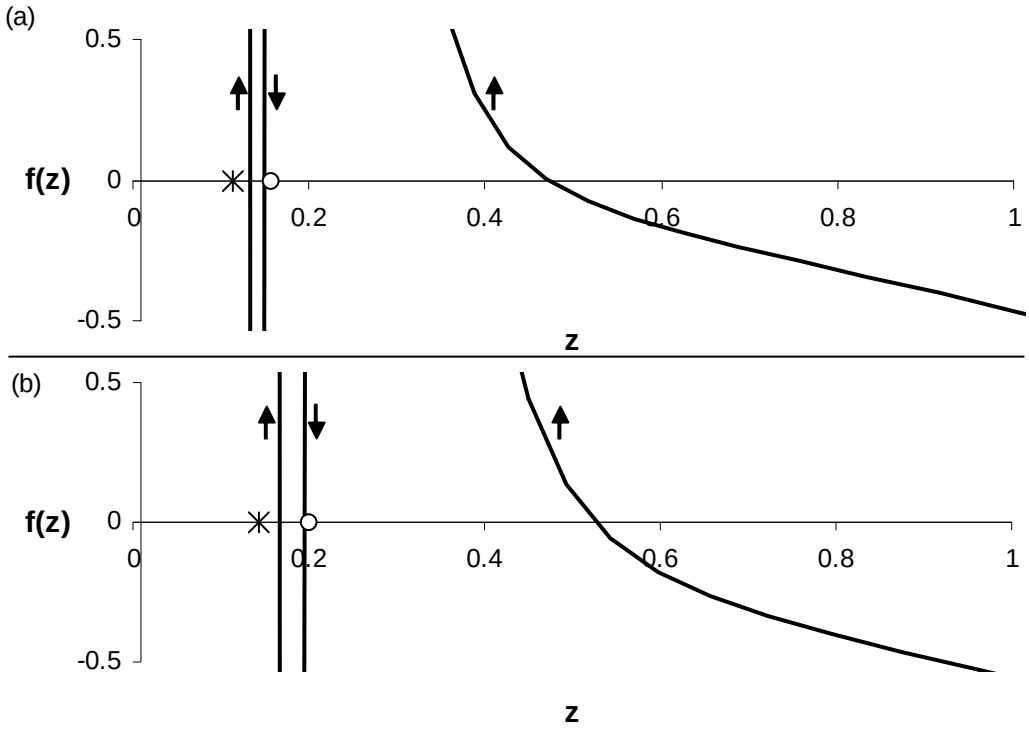

Figure 8.4 Plot of the compressibility function (equation 8.10) of the *SAFT EOS* at the supercritical conditions for (a) Argon at 170 K and 135 bar and (b) Methane at 210 K and 160 bar determined using the pure component parameters as determined by Huang and Radosz [100]. ✳ Indicates the minimum z value allowable for the equation and ○ 1.399*z_{min}, the minimum value for the *simple-PHCT-ltd EOS*

As the refitting of the pure component parameters did not alleviate the problem, the incorrect behaviour of the *SAFT EOS* cannot be overcome without changing the underlying structure of the equation of state. For this reason it was therefore decided to ensure the correct behaviour of the equation artificially by enforcing the selection of the correct liquid and supercritical compressibilities in the computer code. In the supercritical and one phase regions the root finding algorithm is therefore structured to always select the largest compressibility root. For the *VLE* calculations the total number of roots of the equation at the specific conditions is first determined, and if the roots total more than 3, the largest compressibility root is taken as that of the vapour phase and the third largest as the liquid phase compressibility.

(The importance of selecting a suitable initial value for the liquid volume calculations become apparent from Figure 8.3 and Figure 8.4, as not all of the compressibility roots may have been detected had a larger initial value, such as the minimum compressibility value of the *simple-PHCT-ltd EOS*, been used.)

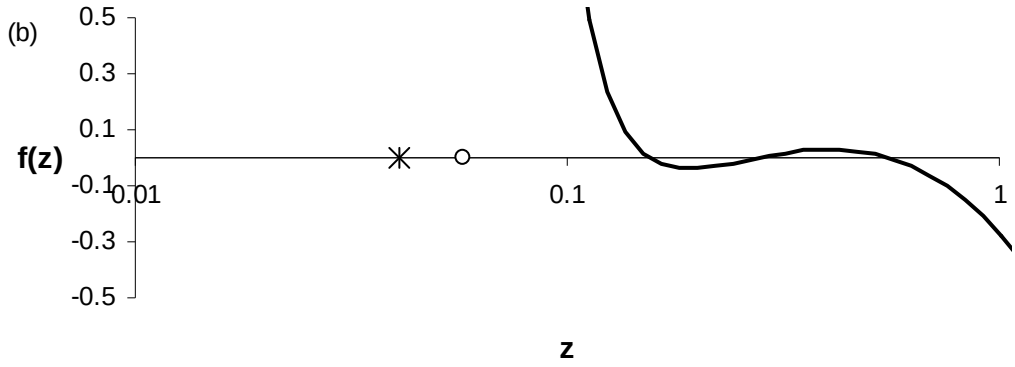

Figure 8.5 Plot of the compressibility function (equation 8.10) of the *simple-PHCT-ltd EOS* at saturated conditions for Methane at 183.8 K ✳ Indicates the minimum z value allowable for the Carnahan-Starling type equations of state and ○ the minimum z value for the *simple-PHCT-ltd EOS*

As can be seen from Figure 8.5, the compressibility function of saturated methane at 183.3 K, the *simple-PHCT-ltd EOS*, although it also utilises a double summation perturbation approximation, does not have the superfluous fluid volume roots as have been observed at the same conditions for the *SAFT EOS.* The *simple-PHCT-ltd EOS* has been tested for multiple roots over a wide range of conditions for the methane and argon systems, between 0-1000 bar and 100 – 500 K for methane and 0 – 1000 bar and 100 – 700 K for argon, and no anomalous fluid volume behaviour was observed. Furthermore, no such behaviour was observed for any of the other systems studied during the course of this work. It therefore appears as if the smaller, constrained perturbation matrix does not suffer from the same deficiencies as the Chen and Kreglewski term.

8.2 THE COMPONENT SPECIFIC FUGACITY COEFFICCIENT

The evaluation of a component specific fugacity coefficient in a particular phase, $\hat{\phi}_i^{\alpha}$, can often be, depending on the structure of the model and the complexity of the mixing rules used, very involved, as it requires the calculation of the compositional derivative of the overall mixture fugacity coefficient:

$$\ln \hat{\phi}_i^{\alpha} = \frac{\partial}{\partial n_i}\left[n \ln \phi^{\alpha}\right]\Big|_{T,P,n_j} \qquad 8.13$$

Throughout the course of this study very many different equations with a variety of mixing rules were evaluated. In order to facilitate programmable flexibility and enable the rapid evaluation of the proposed models, instead of rigorously obtaining the derivative analytically,

numerical techniques were used to determine the component specific fugacity coefficient. However, in doing this, great care had to be taken not to introduce unnecessary errors into the functional value due to rounding and truncation effects.

Following Price et al. [171] the symmetric from of the definition of the derivative function was used in this study:

$$f'(a)_{numerical} = \frac{\partial f(a)}{\partial a} = \frac{f(a+h) - f(a-h)}{2h} \qquad 8.14$$

Secondly to minimise the possibility of introducing any rounding errors due to the fact that not all real numbers can be saved accurately in computer memory, the interval size h was selected to be free from rounding errors by defining it in the following manner in the computer code [171] :

$$\begin{aligned} temp &= a + h \\ h &= temp - a \end{aligned} \qquad 8.15$$

Applying equation 8.14 to equation 8.13 leads to the following expression for the fugacity coefficient:

$$\ln \hat{\phi}_i^{\alpha} = \frac{(n+dn_i)\ln \phi^{\alpha}(T,P,n+dn_i) - (n-dn_i)\ln \phi^{\alpha}(T,P,n-dn_i)}{2dn_i} \qquad 8.16$$

where n is the original total number of moles in the mixture and dn_i the amount with which component i is changed, i.e. the interval size. However as the fugacity coefficient ϕ^{α} is a function of the mol fractions, x_j, and not the total mol numbers, n_j, of the various components it is more convenient to define equation 8.16 in terms of mole fractions with the interval size defined as $dx_i = dn_i/n$:

$$\ln \hat{\phi}_i^{\alpha} = \frac{(1+dx_i)\ln \phi^{\alpha}_{+dn_i}(T,P) - (1-dx_i)\ln \phi^{\alpha}_{-dn_i}(T,P)}{2dx_i} \qquad 8.17$$

It is important to bear in mind that as the number of moles of one of the components present in the fluid mixture change it will affect the mole fractions of all the components in the fluid mixture. The fugacity coefficient functions $\ln \phi^{\alpha}_{\pm dni}(T, P)$ should therefore be evaluated at the mole fractions defined equation 8.18:

$$1 = \sum_{j=i}^{nc} x_j^{\pm dn_i} = \sum_{j=1}^{nv} \begin{cases} \dfrac{x_i \pm dx_i}{1 \pm dx_i} & j = i \\ \dfrac{x_j}{1 \pm dx_i} & j \neq i \end{cases} \qquad 8.18$$

Equations 8.17 and 8.18 along with an interval size of dx_i = 1e-4*x_i were used to obtain the numerical derivatives of the various models in this study.

This technique has been evaluated by comparing the results obtained, using both the numerical and analytical derivatives of the fugacity coefficients of the *SRK* and the proposed *simple-PHCT-ltd* equations of state modelling the n-pentane – n-hexane and methane – n-tetracosane systems at 308 K and 374 K respectively. The comparisons were done by executing a series of bubble flash calculations to generate the phase boundary curve over the entire composition range and comparing the results obtained for the saturated pressure and vapour phase composition at a specific liquid phase composition, as well as the liquid and vapour phase densities and compressibilities at those conditions. The percentage deviation between the results obtained through the analytical and numerical techniques are then determined through equation 8.19:

$$\%\,dev. = \frac{Property_{analytical} - Property_{numerical}}{Property_{analytical}} * 100 \qquad 8.19$$

For both of the systems investigated, the numerical and analytical techniques resulted in the exact same values for the saturated pressure and vapour phase composition over the entire composition range. The observed deviations for the other properties are depicted in Figure 8.6 and Figure 8.7.

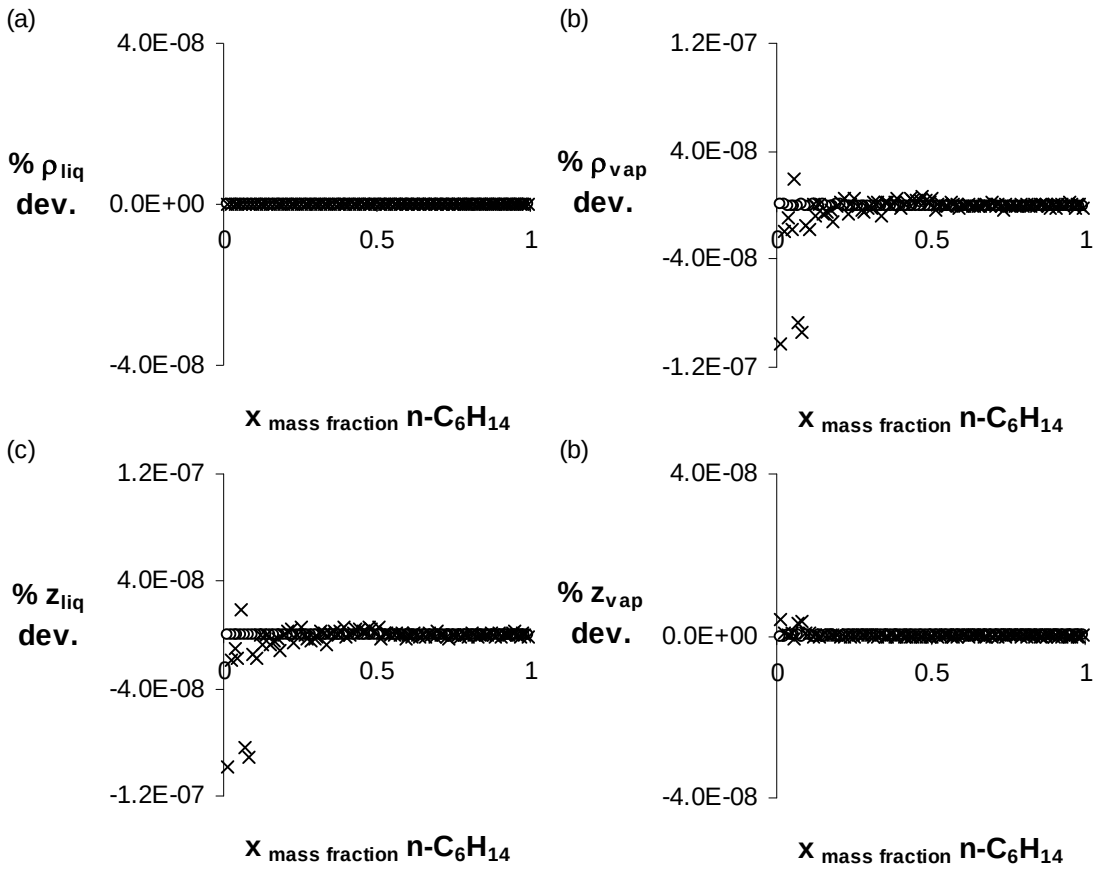

Figure 8.6 Percentage deviation between the results obtained for the n-pentane – n-hexane binary mixture at 308 K using the analytical and numerical compositional derivatives of the fugacity coefficients of the *SRK* and *simple-PHCT-ltd EOS*.

As can be seen from these figures the difference between using the numerical or analytical techniques is almost negligible with the percentage deviation in the predicted value of *any* property never larger than 6e-7 percent. The larger deviations observed for the methane – n-tetracosane system may be attributed to two factors. Firstly the vapour phase mole fraction of n-tetracosane at low pressures (or equivalently high n-tetracosane liquid phase mole fractions) is very low and these small values will be very sensitive towards any rounding errors in the calculations resulting in the difference in the values predicted by the two methods. Secondly, the methane – n-tetracosane binary system approaches the mixture critical region at the lower n-tetracosane liquid phase concentrations of Figure 8.7. This region is notoriously difficult to model, with most of the equations of state struggling to converge in this region. The gradual increase in the difference between the two approaches could indicate that the two methods may have a slightly different convergence in this region. The differences between the two methods, however, still remain small enough to justify the use of the numerical derivative in the computational procedure.

Finally, it should be stressed that the determination of the component specific fugacity coefficient through a numerical derivative is done purely to facilitate the evaluation of a vast number of different models and mixing rules. As the numerical derivative requires the repeated evaluation of the *EOS* mixing rules, this method will be computationally much slower than the analytical route when applied to a multi-component system. In practical applications the analytical derivative of the model should always be used.

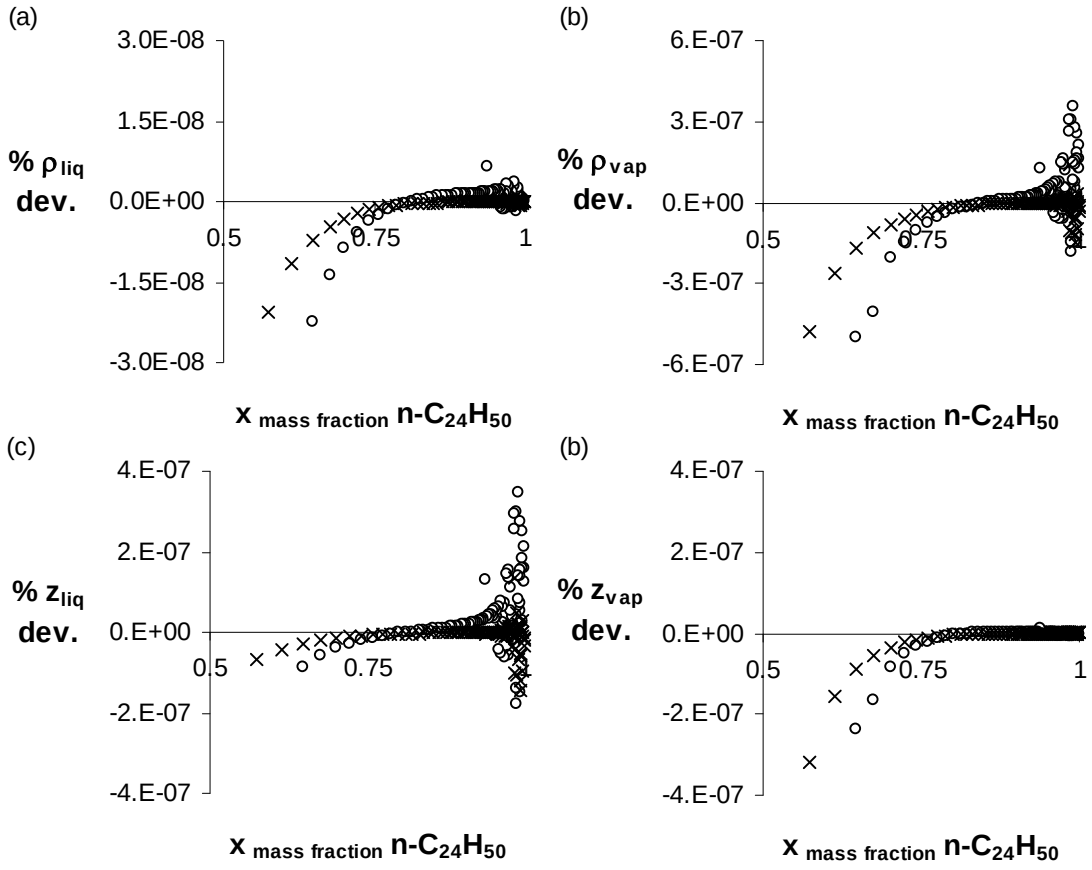

Figure 8.7 Percentage deviation between the results obtained for the methane – n-tetracosane binary mixture at 374 K using the analytical and numerical compositional derivatives of the fugacity coefficients of the *SRK* and *simple-PHCT-ltd EOS*.

8.3 PARAMETER REGRESSION

Throughout the course of this investigation into the optimisation of the chain-like equation on state, parameter regression had to be done on a regular basis to determine amongst others the optimum parameters for use in the double summation perturbation approximation, the various component specific equation of state parameters and, in the modelling of fluid mixtures, the various binary interaction parameters.

The parameter regression was generally done by minimising an error function that is dependent on more than one type of thermodynamic property. In doing so the optimal representation of more than one property, the possibility that the fitted parameter values are merely the result of forcing a function of a certain mathematical structure to give a specific result will be minimised and the regressed parameters will be relevant to the actual the thermodynamic model.

In the regression of the parameters for the various perturbation matrices in Chapter 4 information on the pure component second virial coefficient, the saturated vapour pressures, and fluid volumes in both the saturated and supercritical phases were used, whilst the fitting of the pure component *EOS* parameters for the heavy n-alkanes required the minimisation of the errors in the saturated vapour pressures and the liquid volumes. The regression of the parameters for the lighter compounds also included the vapour phase and supercritical fluid volumes. The regression of the binary interaction parameters was done by minimising the errors in the liquid and vapour phase compositions. (The only exception to using this approach in the regression was in the determination of the binary interaction parameters of systems where only information on the composition of one fluid phase was available. The binary interaction parameters regressed in these instances should be applied with caution.)

It is generally known that most parameter regression techniques require reasonable first estimates of the parameters to ensure the rapid and successful convergence to the optimum parameter set. Furthermore, care has to be taken to ensure that during the non-linear parameter regression the optimisation method used does in fact converge to a global and not just a local minimum condition as it has been shown that such behaviour can have a serious impact on the performance of a thermodynamic model [80]. In the case of the regression of the pure component parameters, because the various model parameters have a physical connotation, such as the molecular closest packed volume as an example, it is possible to provide reasonable initial estimates for these parameter values, however in the case of the regression of the parameters for the perturbation approximation there are no guidelines for the initial parameter estimates.

In order to overcome the problem of initial estimates and the convergence to local minima the parameter regression in this study was done using a combination of two data regression techniques namely particle swarm optimisation, *PSO*, and the Levenberg-Marquardt least squares algorithm.

The particle swarm optimisation was originally developed by Kennedy and Eberhardt [110] to simulate the movement found in flocks of birds and fish schools. It is based on the concept of a population of particles randomly distributed and moving about in the search space. The movement of each particle is governed by the knowledge of its own optimum position achieved in the past and that achieved by the entire swarm as well as a certain degree of randomness and inertia. It has been found that the *PSO* technique is capable to rapidly converge to the global optimum of very complicated and large search spaces, and found to be an ideal precursor for a more traditional gradient search technique [63].

The Levenberg-Marquard method, *LM*, has been proposed as a suitable compromise between the initial rapid converging steepest decent and local linear approximating Taylor series methods [138], and has become the standard of non-linear least squares routines [171].

The parameter regression procedure used in this study is outlined in Figure 8.8. A suitable search space is first defined by selecting realistic upper and lower bounds for the various parameters to be regressed. The number of parameters to be used in the *PSO* can then be defined, as well as the number of movements or iteration steps each parameter can execute in the optimisation. If the nature of the parameters to be regressed is unknown a very large search space with a large number of particles and steps can be defined, whilst for better defined parameters such as the component specific *EOS* parameters, the search space, number of particles and iterative steps can be much smaller. After the *PSO* iterations have converged to an optimum parameter-set, these parameter values are then used as the initial values in the Levenberg-Marquardt optimisation. In this manner the entire search space is evaluated and good initial estimates in the vicinity of the global optimum is used to initiate the gradient search, this will ensure the rapid convergence of the *LM* algorithm and minimise the risk of the method converging to a local minimum value.

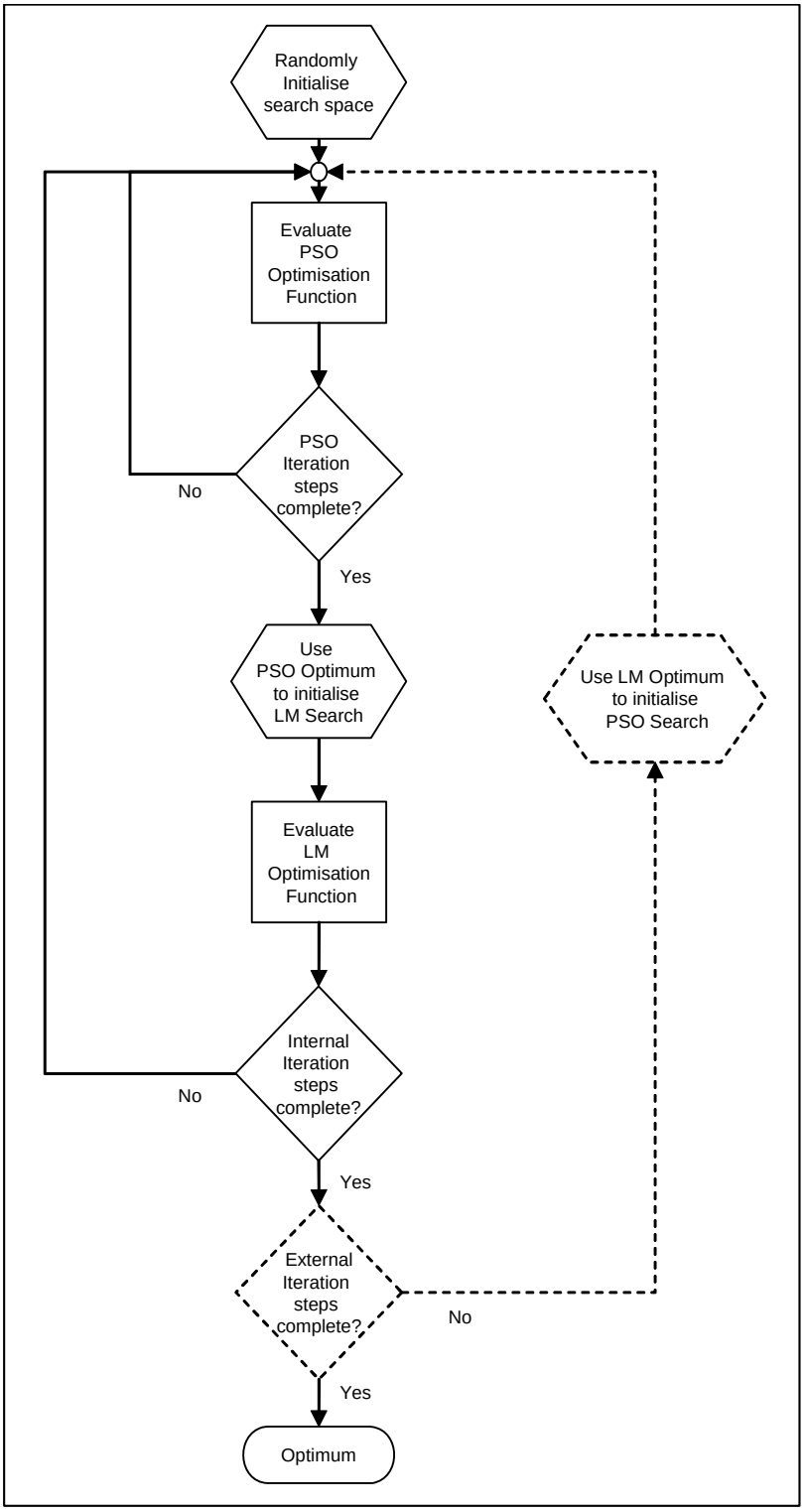

Figure 8.8 Block flow diagram of the parameter regression algorithm

As the *PSO* method does contain a measure of randomness in the parameter distribution and movement, it is preferable to repeat the search algorithm several times to ensure that the optimum values have indeed been obtained. In this internal iteration loop the *PSO* parameters are randomly initialised at the start of each iteration loop and the result of each *LM*

optimisation is stored. Once the internal iterations have been completed the optimum *LM* regression result is selected and applied further down stream.

If the initial *PSO* search space is poorly defined, i.e. a very large search space with the parameters to be regressed allowed to vary over a large range, it is often necessary to include a second iterative loop (indicated by the dashed lines in Figure 8.8). In this loop the optimum results obtained from the internal iterations are used to seed the parameters in the *PSO* procedure, i.e. the information about the location of the optimum parameters found in the internal loop is used in the swarming algorithm. This focuses the search for the optimum parameters in a region where it is most likely to be found.

8.4 SUMMARY AND CONCLUSIONS

In this chapter some background information has been given on the numerical procedures followed throughout this study in the determination of the *EOS* volume roots, component fugacity coefficients and parameter regression.

Computational algorithms have been provided to overcome the problems associated with determining the volume roots of a cubic equation of state analytically when modelling substances with very low vapour pressures.

It has also been shown that the double summation perturbation approximation developed by Chen and Kreglewski and applied in the *SAFT EOS* can, at certain conditions, predict up to 5 fluid volume roots for a pure component, which would when applying the standard criteria of selecting the liquid volume root, would lead to incorrect results. It has also been shown that the newly developed *simple-PHCT-ltd EOS* with a constrained 3x3 perturbation matrix does not seem to suffer from the same problematic behaviour .

By comparing the results obtained in the determination of the binary *VLE* of two model systems, it has been concluded that it is possible, in order to facilitate the rapid evaluation of a wide variety of equations of state, to determine the component specific fugacity coefficient of a model numerically without seriously compromising the accuracy of the results.

Chapter 9 **Conclusion**

When looking at the open literature, it is clear that there are thousands of equations of state in existence today, each claiming to be more suitable or accurate in certain applications than others. However, even though there is such a large amount of models available, there are still several systems and conditions that are difficult to model effectively. This study has been focused on addressing the problems associated with modelling one of these systems: mixtures of simple non-polar spherical and chain-like components.

The equations of state typically used to model these systems are numerically complex (high order in density) and computationally intensive, resulting in long computational times which are limiting when using the models in everyday practical thermodynamic simulations. When developing a successful equation of state a suitable compromise between model accuracy, mathematical complexity and computational speed needs to be found. Many of the accepted literature models have been developed as improvements and expansions on existing equations, building onto the underlying structure of the older equation of state, with each expansion focussing on improving on individual aspects of the model, rather than focussing on the performance of the entire equation as a whole. In this study, such an approach, of optimising the overall performance of the model, was followed. This was accomplished by re-evaluating the theoretical approach behind the derivation of equations of state and ensuring that each step in the derivation adheres to the model requirements, of accuracy, simplicity and computational speed. The various steps in the development of the equation of state have been summarised in Figure 9.1.

From an evaluation of the statistical mechanical theory, it was found that the perturbation approach would be the most suited to the development of a practical equation of state. The perturbation approach requires expressions for a hard sphere reference term, representing the repulsive interactions of the molecular particles, an intermolecular potential model to enable the incorporation of molecular softness into the model, and a term representing the perturbation expansion on the hard sphere reference model.

In this study a new hard sphere equation of state has been proposed. This new equation provides a suitable compromise between the model performance, i.t.o. the representation of the hard sphere virial coefficients and simulated compressibilities, as well as mathematical

structure. (The new model has a denominator which is first order in density as apposed to the generally applied Carnahan-Starling, *CS*, hard sphere term with a denominator that is third order in density.)

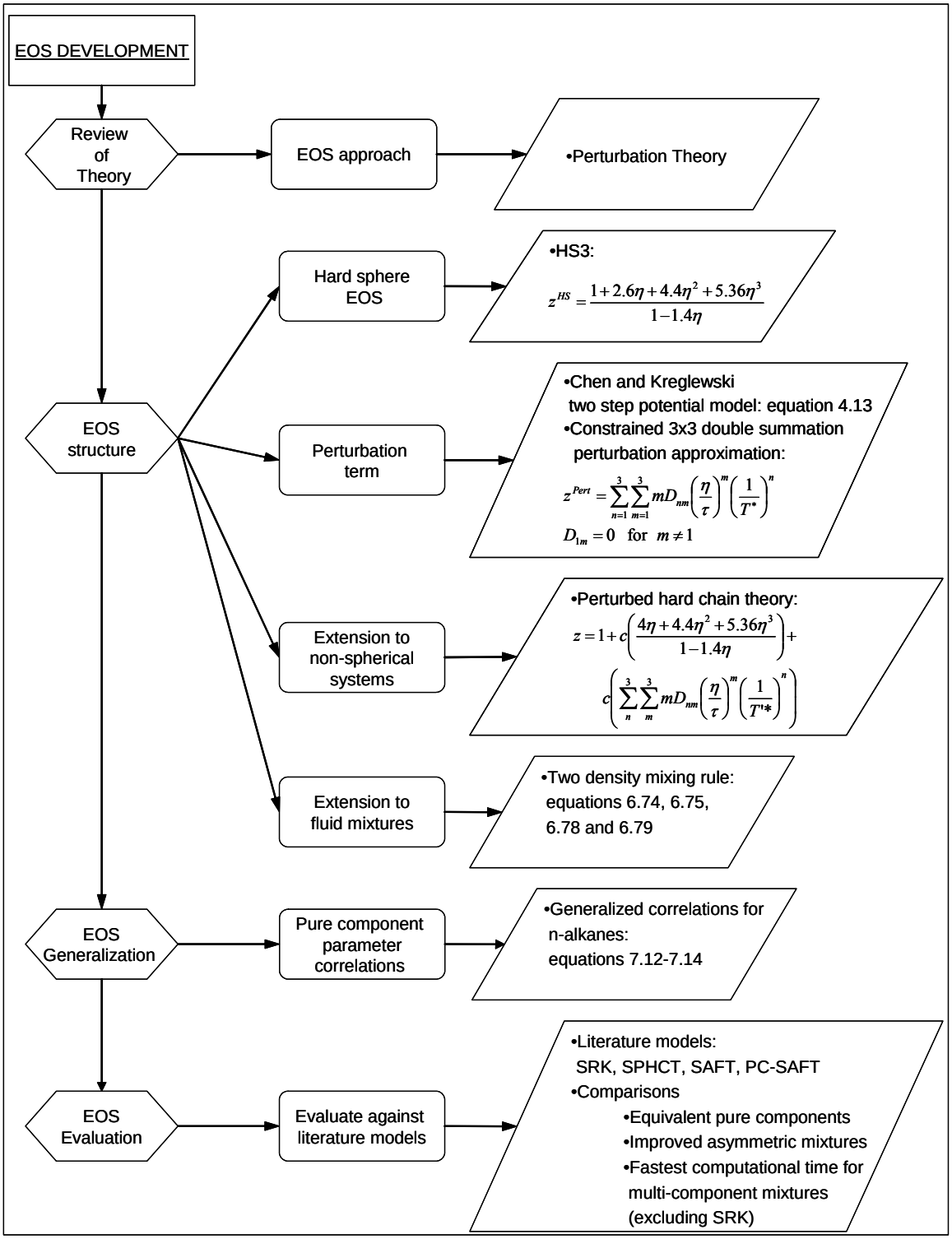

Figure 9.1 Flow diagram of logical progression in the development of the EOS in this study

In the newly developed model the molecular softness is taken into account through the Barker-Henderson approach by defining an effective segment diameter that is a function of the system temperature through the intermolecular potential energy. The two-step potential as developed by Chen and Kreglewski is used as the potential model in the new equation.

A 3x3 double summation term has been developed to represent the perturbation expansion of the hard sphere equation. The perturbation approximation is therefore third order in $1/T$ and density. The perturbation matrix parameters have been fitted to Argon second virial coefficient and *P-v-T* data and are used as constants for all components. In a novel approach to simplify the equation of state mixing rules whilst ensuring that the correct second virial coefficient composition dependence is maintained, the parameters in the perturbation matrix have been constrained in such a manner that the contribution of the perturbation term to the *EOS* second virial coefficient expansion is first order in $1/T$ only.

Several methods of extending an equation of state for spherical components to chain-like systems have been evaluated. It has been found that the *Perturbed Hard Chain Theory*, when applied to the constrained form of the newly developed equation of state (the hard sphere and perturbation terms), resulted in the most successful overall representation of the saturated and supercritical *P-v-T* behaviour of the n-alkane homologous series. Applying the *Perturbed Hard Chain Theory* to the new equation results in a model that has a 5^{th} order density dependence.

A 2*D* mixing rule has been developed for the new equation of state. Using this mixing rule in the model enables the equation to adhere to the correct second virial coefficient boundary condition at low densities whilst, in an approach similar to the solution theory, having volume fraction weighted mixture properties at high densities

The *EOS* pure component parameters regressed for the n-alkane homologous series have been shown to display a regular behaviour with the component molecular weight, leading to the development of simple generalized correlations from which the pure component parameters may be estimated. The correlations have been proven to give satisfactorily results when used within the specified molecular weight range (smaller than hexatriacontane), and although the correlations should be used with care when extrapolating to higher molecular weights, satisfactory results have even been obtained when estimating the properties of mixtures containing hexacontane.

The performance of the new model has been evaluated against several equations of state that are commonly used to represent similar systems. The literature models used in the comparison are the *SRK*, *SPHCT*, *SAFT* and *PC-SAFT* equations. The new equation has been shown to be capable of representing the pure component systems to a similar degree of accuracy as the literature models and to equal or improve on the predictive ability of these models when representing fluid mixtures consisting out of chainlike or size and energetic asymmetric components. The new model has also been proven to be significantly faster than the *SAFT* and *PC-SAFT* equations when representing fluid mixtures, and because of its simple mathematical structure is ideally suited to representing large multi-component fluid mixtures.

The new model has been shown to have overcome some of the anomalous behaviour associated with the more complex equations. A novel technique to determine the fluid volume roots of low vapour pressure has also been devised, overcoming the problem of rounding and truncation errors associated with computer calculations. This has been achieved by solving the density rather than the volume root for the liquid phase of the heavy component. Lastly by coupling a random search algorithm, the *Particle Swarm Optimisation*, with the Levenberg-Marquardt parameter regression technique, the problem of local minima has been addressed successfully.

Bibliography

1. *Aspen Plus*, Aspen Technology, Inc., 1981-2003

2. *Pro/II*, Simulation Sciences Inc., 1994-2001

3. Y. Adachi and H. Sugie, *A new mixing rule - modified conventional mixing rule.* Fluid Phase Equilibria, 1986. **28**: p. 103-118.

4. H. Adidharma and M. Radosz, *Prototype of an Engineering Equation of State for Heterosegmented Polymers.* Industrial and Engineering Chemistry Research, 1998. **37**: p. 4453-4462.

5. H. Adidharma and M. Radosz, *Square-well SAFT equation of state for homopolymeric and heteropolymeric fluids.* Fluid Phase Equilibria, 1999. **158-160**: p. 165-174.

6. H. Adidharma and M. Radosz, *A study of square-well statistical associating fluid theory approximations.* Fluid Phase Equilibria, 1999. **161**: p. 1-20.

7. B. J. Alder, W. G. Hoover, and D. A. Young, *Studies in Molecular Dynamics. V. High-Density Equation of State and Entropy of Hard Disks and Spheres.* Journal of Chemical Physics, 1968. **49**(8): p. 3688-3698.

8. B. J. Alder and T. E. Wainwright, *Studies in Molecular Dynamics. II. Behaviour of a Small Number of Elastic Spheres.* Journal of Chemical Physics, 1960. **33**(5): p. 1439-1451.

9. B. J. Alder, D. A. Young, and M. A. Mark, *Studies in Molecular Dynamics. X. Corrections to the Augmented van der Waals Theory for the Square Well Fluid.* Journal of Chemical Physics, 1972. **56**(6): p. 3013-3029.

10. A. Anderko, *Equation-of-State Methods for the Modelling of Phase Equilibria.* Fluid Phase Equilibria, 1990. **61**: p. 145-225.

11. S. Angus and B. Armstrong, eds. *International Thermodynamic Tables of the Fluid State. Argon, 1971*. 1972, Butterworth & Co. (Publishers) Ltd.: London.

12. M. Banaszak, C.-K. Chen, and M. Radosz, *Copolymer SAFT Equation of State. Thermodynamic Perturbation Theory Extended to Heterobonded Chains.* Macromolecules, 1996. **29**: p. 6481-6486.

13. M. Banaszak, Y. C. Chiew, R. O'Lenick, and M. Radosz, *Thermodynamic perturbation theory: Lennard-Jones chains.* Journal of Chemical Physics, 1994. **100**(5): p. 3803-3807.

14. M. Banaszak, Y. C. Chiew, and M. Radosz, *Thermodynamic perturbation theory: Sticky chains and square-well chains.* Physical Review E, 1993. **48**(5): p. 3760-3765.

15. J. A. Barker and D. Henderson, *Perturbation Theory and Equation of State for Fluids. II A successful Theory of Liquids.* The Journal of Chemical Physics, 1967. **47**(11): p. 4714-4721.

16. J. A. Barker and D. Henderson, *Perturbation Theory and Equation of State for Fluids: The Square-Well Potential.* The Journal of Chemical Physics, 1967. **47**(8): p. 2856-2861.

17. J. A. Barker and D. Henderson, *Theories of Liquids.* Annual review of physical chemistry, 1972. **32**: p. 439-484.

18. J. A. Barker and D. Henderson, *What is "liquid"? Understanding the states of matter.* Reviews of Modern Physics, 1976. **48**(4): p. 587-671.

19. M. Baus and J. L. Colot, *Thermodynamics and structure of a fluid of hard rods, disks, spheres, or hyperspheres from rescaled virial expansions.* Physical Review A, 1987. **36**(8): p. 3912-3925.

20. S. Beret and J. M. Prausnitz, *Perturbed Hard-Chain Theory: An Equation of State for Fluids Containing Small or Large Molecules.* AIChE Journal, 1975. **21**(6): p. 1123-1132.

21. F. J. Blas and L. F. Vega, *Prediction of Binary and Ternary Diagrams using the Statistical Associating Fluid Theory (SAFT) Equation of State.* Industrial and Engineering Chemistry Research, 1998. **37**: p. 660-674.

22. C. P. Bokis and M. D. Donohue, *A Closed-Form Equation of State for Lennard-Jones Molecules Based on Perturbation Theory.* Journal of Physical Chemistry, 1995. **99**: p. 12655-12660.

23. C. P. Bokis, M. D. Donohue, and C. K. Hall, *Local Composition Model for Square-Well Chains Using the Generalised Flory Dimer Theory.* Journal of Physical Chemistry, 1992. **96**: p. 11004-11009.

24. L. Boltzmann, *Verslag Gewone Vergadering Afdeling Natuurkunde Koninklike Nederlandse Akademie Wetenskap.*. 1899. p. 484.

25. A. Bondi, *Van der Waals Volumes and Radii.* Journal of Physical Chemistry, 1964. **68**(3): p. 441-451.

26. T. Boublík and B. C.-Y. Lu, *Mixing rules for the BACK equation of state.* Collection Czechoslovak Chemical Communications, 1987. **52**: p. 29-44.

27. T. Boublík and I. Nezbeda, *Equation of State for Hard Dumbbells.* Chemical Physics Letters, 1977. **46**(2): p. 315-316.

28. T. Boublík and I. Nezbeda, *P-V-T behaviour of hard body fluids. Theory and Experiment.* Collection Czechoslovak Chemical Communications, 1986. **59**(11): p. 2301-2432.

29. F. Brandani, S. Brandani, and V. Brandani, *The Wong-Sandler mixing rules and EOS which are thermodynamically consistent at infinite pressure.* Chemical Engineering Science, 1998. **53**(4): p. 853-856.

30. S. Brandani and V. Brandani, *On the inapplicability of mixing rules based on the infinite pressure reference state for equations of state which use the hard-sphere repulsive term.* Fluid Phase Equilibria, 1996. **121**: p. 179-184.

31. B. A. Bufkin, R. L. Robinson, Jr., S. S. Estrera, and K. D. Luks, *Solubility of Ethane in n-Decane at Pressures to 8.2 Mpa and Temperatures from 278 to 411 K.* Journal of Chemical and Engineering Data, 1986. **31**: p. 421-423.

32. N. F. Carnahan and K. E. Starling, *Equation of State of Nonattracting Rigid Spheres.* Journal of Chemical Physics, 1969. **51**(2): p. 635-636.

33. N. F. Carnahan and K. E. Starling, *Boublik's Application of the CST Rigid-Sphere Equation.* Journal of Chemical Physics, 1970. **53**: p. 472-473.

34. N. F. Carnahan and K. E. Starling, *Intermolecular Repulsions and the Equation of State for Fluids.* AIChE Journal, 1972. **18**(6): p. 1184-1189.

35. J. Chang and S. I. Sandler, *A completely analytic perturbation theory for the square-well fluid of variable width.* Molecular Physics, 1994. **81**(3): p. 745-765.

36. J. Chang and S. I. Sandler, *An equation of state for the hard chain fluid: theory and Monte Carlo simulation.* Chemical Engineering Science, 1994. **49**: p. 2777-2791.

37. J. Chang and S. I. Sandler, *A real function representation for the structure of the hard-sphere fluid.* Molecular Physics, 1994. **81**(3): p. 735-744.

38. W. G. Chapman, K. E. Gubbins, G. Jackson, and M. Radosz, *SAFT: Equation-of-State Solution Model for Associating Fluids.* Fluid Phase Equilibria, 1989. **52**: p. 31-38.

39. W. G. Chapman, K. E. Gubbins, G. Jackson, and M. Radosz, *New Reference Equation of State for Associating Liquids.* Industrial and Engineering Chemistry Research, 1990. **29**: p. 1709-1721.

40. C.-K. Chen, M. Banaszak, and M. Radosz, *Statistical Associating Fluid Theory Equations of State with Lennard-Jones Reference applied to Pure and Binary n-Alkane Systems.* Journal of Physical Chemistry B, 1998. **102**: p. 2427-2431.

41. J. Chen and J.-g. Mi, *Equation of state extended from SAFT with improved results for non-polar fluids across the critical point.* Fluid Phase Equilibria, 2001. **186**: p. 165-184.

42. S. S. Chen and A. Kreglewski, *Applications of the Augmented van der Waals Theory of Fluids. I. Pure Fluids.* Berichte de Bunsen-Gesellschaft, 1977. **81**(10): p. 1048-1053.

43. C. H. Chien, R. A. Greenkorn, and K. C. Chao, *Chain-of-Rotators Equation of State.* AIChE Journal, 1983. **29**(4): p. 560-571.

44. Y. C. Chiew, *Percus-Yevick integral equation theory for athermal hard-sphere chains. I. Equations of State.* Molecular Physics, 1990. **70**: p. 129-143.

45. Y. C. Chiew, *Percus-Yevick integral equation theory for athermal hard-sphere chains. II. Average intermolecular correlation functions.* Molecular Physics, 1991. **73**(2): p. 359-373.

46. L. Chunxi, L. Yigui, and L. Jiufang, *Investigation and improvement of equations of state for Lennard-Jones fluid.* Fluid Phase Equilibria, 1997. **127**: p. 71-81.

47. G. Ciocca, I. Nagata, and V. Brandani, *Density dependence of the external degrees of freedom: application to a simplified version of the perturbed hard chain theory.* Fluid Phase Equilibria, 1987. **41**: p. 59-80.

48. R. L. Cotterman and J. M. Prausnitz, *Molecular Termodynamica for Fluids at Low and High Densities. Part II: Phase Equilibria for Mixtures Containing Components with Large Differences in Molecular Size or Potential Energy.* AIChE Journal, 1986. **32**(11): p. 1799-1812.

49. R. L. Cotterman, B. J. Schwarz, and J. M. Prausnitz, *Molecular Thermodynamics for fluids at Low and High Densities. Part I: Pure Fluids Containing Small or Large Molecules.* AIChE Journal, 1986. **32**(11): p. 1787-1797.

50. P. Coutsikos, N. S. Kalospiros, and D. P. Tassios, *Capabilities and limitations of the Wong-Sandler mixing rules.* Fluid Phase Equilibria, 1995. **108**: p. 59-78.

51. F. Cuadros and W. Ahumada, *Accurate analytical expressions of thermodynamic properties of supercritical Lennard-Jones fluids.* Thermochimica Acta, 1997. **297**: p. 109-116.

52. F. Cuadros, A. Mulero, and W. Ahumada, *An extensive study of the Helmholtz free energy of Lennard-Jones fluids using the WCA theory.* Thermochimica Acta, 1996. **277**: p. 85-105.

53. S. Dahl and M. L. Michelsen, *High-Pressure Vapor-Liquid Equilibrium a UNIFAC-Based Equation of State.* AIChE Journal, 1990. **36**(12): p. 1829-1839.

54. T. E. Daubert, R. P. Danner, H. M. Sibul, and C. C. Stebbins, *DIPPR Data Compilation of Pure Compound Properties, Project 801 Sponsor Release.* 1993, New York: Design Institute for Physical Property Data, AIChE.

55. R. De Goede, C. J. Peters, H. J. Van der Kooi, and R. N. Lichtenthaler, *Phase Equilibria in Binary Mixtures of Ethane and Hexadecane.* Fluid Phase Equilibria, 1989. **50**: p. 305-314.

56. J. J. De Pablo, M. Bonnin, and J. M. Prausnitz, *Vapor-liquid equilibria for polyatomic fluids from site-site computer simulations: pure hydrocarbons and binary mixtures containing methane.* Fluid Phase Equilibria, 1992. **73**: p. 187-210.

57. L. E. S. De Souza and D. Ben-Amotz, *Optimized perturbed hard sphere expressions for the structure and thermodynamics of Lennard-Jones fluids.* Molecular Physics, 1993. **78**: p. 137-149.

58. R. Dickman and C. K. Hall, *Equation of state for chain molecules: Continuous-space analog of Flory theory.* Journal of Chemical Physics, 1986. **85**(7): p. 4108-4115.

59. R. Dickman and C. K. Hall, *High density Monte Carlo simulations of chain molecules: Bulk equation of state and density profile near walls.* Journal of Chemical Physics, 1988. **89**(5): p. 3168-3174.

60. M. D. Donohue and J. M. Prausnitz, *Perturbed Hard Chain Theory for Fluid Mixtures: Thermodynamic Properties for Mixtures in Natural Gas and Petroleum Technology.* AIChE Journal, 1978. **25**(5): p. 849-860.

61. M. Du Rand and I. Nieuwoudt, *Measurement of Phase Equilibria of Supercritical Ethane and Paraffins.* Journal of Supercritical Fluids., 2001. **21**: p. 181-193.

62. M. Du Rand and I. Nieuwoudt, *Measurement of Phase Equilibria of Supercritical Carbon Dioxide and Paraffins.* Journal of Supercritical Fluids., 2002. **22**: p. 185-199.

63. M. Du Rand and I. Nieuwoudt. *Modelling of the Fractionation of Paraffins with Supercritical Fluids.* in *4th International Symposium on High Pressure Process Technology and Chemical Engineering.* 2002. Venice, Italy: AIDIC.

64. J. H. Dymond and E. B. Smith, *The Virial Coefficients of Pure Gases and Mixtures. A Critical Compilation.*. 1980, Oxford University Press: New York.

65. I. G. Economou, *Statistical Association Fluid Theory: A Successful Model for the Calculation of Thermodynamic and Phase Equilibrium Properties of Complex Fluid Mixtures.* Industrial and Engineering Chemistry Research, 2002. **41**: p. 953-962.

66. J. R. Elliot, Jr., S. J. Suresh, and M. D. Donohue, *A Simple Equation of State for Nonspherical and Associating Molecules.* Industrial and Engineering Chemistry Research, 1990. **29**: p. 1476-1485.

67. J. J. Erpenbeck and W. W. Wood, *Molecular Dynamics Calculations of the Hard-Sphere Equation of State.* Journal of Statistical Physics, 1984. **35**(3/4): p. 321-340.

68. G. N. Escobedo-Alvarado and S. I. Sandler, *Study of EOS-G^{ex} Mixing Rules for Liquid-Liquid Equilibria.* AIChE Journal, 1998. **44**(5): p. 1178-1187.

69. H. Eyring and J. Hirschfleder, *The Theory of the Liquid State.* Journal of Physical Chemistry, 1937. **41**: p. 249-256.

70. D. J. Fall, J. L. Fall, and K. D. Luks, *Liquid-Liquid-Vapor Immiscibility Limits in Carbon Dioxide + n-Paraffin Mixtures.* Journal of Chemical and Engineering Data, 1985. **30**: p. 82-88.

71. W. Feng, H. Wen, Z. Xu, and W. Wang, *Comparison of Perturbed Hard-Sphere-Chain Theory with Statistical Associating Fluid Theory for Square-Well Fluids.* Industrial and Engineering Chemistry Research, 2000. **39**: p. 2559-2567

72. P. J. Flory, *Thermodynamics of High Polymer Solutions.* Journal of Chemical Physics, 1941. **9**: p. 660-661.

73. H. Frisch and J. L. Lebowitz, *The Equilibrium Theory of Classical Fluids.* 1964, New York: W.A. Benjamin.

74. Y.-H. Fu and S. I. Sandler, *A Simplified SAFT Equation of State for Associating Compounds and Mixtures.* Industrial and Engineering Chemistry Research, 1995. **34**: p. 1897-1909.

75. J. Gao and J. H. Weiner, *Contribution of covalent bond force to pressure in polymer melts.* Journal of Chemical Physics, 1989. **91**(5): p. 3168-3173.

76. W. Gao, *High pressure solubility measurements for selected asymmetric mixtures and equation-of-state development.*, Doctoral Thesis, Faculty of the Graduate College, Oklahoma State University, 1999.

77. K. A. M. Gasem and R. L. Robinson, Jr., *Solublities of Carbon Dioxide in Heavy Normal Paraffins (C_{20}-C_{44}) at Pressures to 9.6 Mpa and Temperatures from 323 to 423 K.* Journal of Chemical and Engineering Data, 1985. **30**: p. 53-56.

78. K. A. M. Gasem and R. L. Robinson, Jr., *Evaluation of the simplified perturbed hard chain theory (SPHCT) for prediction of phase behaviour of n-parrafins and mixtures of n-paraffins with ethane.* Fluid Phase Equilibria, 1990. **58**: p. 13-33.

79. R. P. H. Gasser and W. G. Richards, *An Introduction to Statistical Thermodynamics.* 1995, New Jersey: World Scientific Publishing Co. Pte. Ltd.

80. C.-Y. Gau, J. F. Brennecke, and M. A. Stadtherr, *Reliable nonlinear parameter estimation in VLE modelling.* Fluid Phase Equilibria, 2000. **168**: p. 1-18.

81. D. Ghonasgi and W. G. Chapman, *A new equation of state for hard chain molecules.* Journal of Chemical Physics, 1994. **100**(9): p. 6633-6639.

82. A. Gil-Villegas, A. Galindo, P. J. Whitehead, S. J. Mills, G. Jackson, and A. N. Burgess, *Statistical associating fluid theory for chain molecules with attractive potentials of variable range.* Journal of Chemical Physics, 1997. **106**(10): p. 4168-4186.

83. M. Glaser, C. J. Peters, H. J. Van der Kooi, and R. N. Lichtenthaler, *Phase Equilibria of (Methane + n-Hexadecane) and (p, V_m, T) of n-Hexadecane.* Journal of Chemical Thermodynamics, 1985. **17**: p. 803-815.

84. J. Gmehling, U. Onken, and B. Kolbe, *Vapor-Liquid Equilibrium Data Collection. Aliphatic Hydrocarbons. (Supplement 1)*. Dechema Chemistry Data Series, ed. D. Behrens and R. Eckermann. Vol. I, Part 6c. 1982.

85. J. Gross and G. Sadowski, *Application of perturbation theory to a hard-chain reference fluid: an equation of state for square-well chains.* Fluid Phase Equilibria, 2000. **168**: p. 183-199.

86. J. Gross and G. Sadowski, *Perturbed-Chain SAFT: An Equation of State Based on a Perturbation Theory for Chain Molecules.* Industrial and Engineering Chemistry Research, 2001. **40**: p. 1244-1260.

87. E. A. Guggenheim, *Variations on van der Waals' equation of state for high densities.* Molecular Physics, 1965. **9**: p. 199-200.

88. H. S. Gulati and C. K. Hall, *Fluids and fluid mixtures containing square-well diatomics: Equations of state and canonical molecular dynamics simulation.* Journal of Chemical Physics, 1997. **107**(10): p. 3930-3946.

89. H. Happel, Annalen der Physik, 1906. **21**: p. 342.

90. R. A. Heidemann and S. L. Kokal, *Combined excess free energy models and equations of state.* Fluid Phase Equilibria, 1990. **56**: p. 17-37.

91. D. Henderson, *Perturbation theory for a mixture of hard spheres and square-well molecules.* Journal of Chemical Physics, 1974. **61**(3): p. 926-931.

92. T. L. Hill, *Statistical Mechanics.* 1956, New York: McGraw-Hill.

93. T. L. Hill, *An Introduction to Statistical Thermodynamics.* 1960, Reading: Addison-Wesley Publishing Company, Inc.

94. T. Hino and J. M. Prausnitz, *A perturbed hard-sphere-chain equation of state for normal fluids and polymers using the square-well potential of variable width.* Fluid Phase Equilibria, 1997. **138**: p. 105-130.

95. K. G. Honnell and C. K. Hall, *A new equation of state for athermal chains.* Journal of Chemical Physics, 1989. **90**(3): p. 1841-1855.

96. Y. Hu, H. Liu, and J. M. Prausnitz, *Equation of state for fluids containing chainlike molecules.* Journal of Chemical Physics, 1996. **104**(1): p. 396-404.

97. Y. Hu, D. Lüdecke, and J. M. Prausnitz, *Molecular thermodynamics of fluid mixtures containing molecules differing in size and potential energy.* Fluid Phase Equilibria, 1984. **17**: p. 217-241.

98. S. H. Huang, *Synthesis gas solubility in Fisher-Tropsch slurry.* Doctoral Thesis Prudue University: Prudue. 1987

99. S. H. Huang, H. M. Lin, and K. C. Chao, *Solubility of Carbon Dioxide, Methane, and Ethane in n-Eicosane.* Journal of Chemical and Engineering Data, 1988. **33**: p. 145-147.

100. S. H. Huang and M. Radosz, *Equation of State for Small, Large, Polydisperse, and Associating Molecules.* Industrial and Engineering Chemistry Research, 1990. **29**: p. 2284-2294.

101. S. H. Huang and M. Radosz, *Equation of State for Small, Large, Polydisperse, and Associating Molecules: Extension to Fluid Mixtures.* Industrial and Engineering Chemistry Research, 1991. **30**: p. 1994-2005.

102. M. L. Huggins, *Solutions for Long Chain Compounds.* Journal of Chemical Physics, 1941. **9**: p. 440.

103. M.-J. Huron and J. Vidal, *New Mixing Rules in Simple Equations of State for Representing Vapour-Liquid Equilibria of Strongly Non-Ideal Mixtures.* Fluid Phase Equilibria, 1979. **3**: p. 255-271.

104. E. L. Janse van Rensburg, *Virial coefficients for hard discs and hard spheres.* Journal of Physics. A : Mathematical and General, 1993. **26**: p. 4805-4818.

105. J. K. Johnson and K. E. Gubbins, *Phase Equilibria for Associating Lennard-Jones Fluids from Theory and Simulation.* Molecular Physics, 1992. **77**: p. 1033-1053.

106. J. K. Johnson, J. A. Zollweg, and K. E. Gubbins, *The Lennard-Jones equation of state revisited.* Molecular Physics, 1993. **78**(3): p. 591-618.

107. P. C. Joyce and M. C. Thies, *Vapor-Liquid Equilibria for the Hexane + Hexadecane and Hexane + 1-Hexadecanol Systems at Elevated Temperatures and Pressures.* Journal of Chemical and Engineering Data, 1998. **43**: p. 819-822.

108. H. K. Kamerlingh Onnes, *The equation of state of gases and liquids as a power series.* Archives Néelandaises, 1901. **6**: p. 874-888.

109. S. Kemény, I. Frakas, and A. Deák, *EOS mixing rules and the quadratic concentration dependence of the second virial coefficient.* Fluid Phase Equilibria, 1997. **128**: p. 131-135.

110. J. Kennedy and R. C. Eberhart. *Particle swarm optimization.* in *IEEE International conference on Nueral Networks.* 1995. Piscataway, N.J.: IEEE.

111. C.-H. Kim, P. Vimalchand, M. D. Donohue, and S. I. Sandler, *Local Composition Model for Chainlike Molecules: A New Simplified Version of the Perturbed Hard Chain Theory.* AIChE Journal, 1986. **32**(10): p. 1726-1734.

112. I. H. Kim and Y. C. Bae, *Equations of state for hard spheres and hard-sphere chains.* Fluid Phase Equilibria, 2000. **167**: p. 187-206.

113. I. H. Kim and Y. C. Bae, *Phase Equilibria of fluid mixtures using a modified perturbed hard-sphere-chain equation of state.* Fluid Phase Equilibria, 2000. **168**: p. 201-216.

114. R. B. King, *Beyond the Quartic Equation.* 1996, Boston: Birkhäuser.

115. N. Koak, T. W. De Loos, and R. A. Heidemann, *Effect of the Power Series Dispersion Term on the Pressure-Volume Behaviour of Statistical Associating Fluid Theory.* Industrial and Engineering Chemistry Research, 1999. **38**: p. 1718-1722.

116. J. Kolafa and I. Nezbeda, *The Lennard-Jones fluid: An accurate analytic and theoretically-based equation of state.* Fluid Phase Equilibria, 1994. **100**: p. 1-35.

117. T. Kraska and K. E. Gubbins, *Phase Equilibria Calculations with a Modified SAFT Equaiton of State. 1. Pure Alkanes, Alkanols, and Water.* Industrial and Engineering Chemistry Research, 1996. **35**: p. 4727-4737.

118. K. W. Kratky, *A new graph expansion of virial coefficients.* Journal of Statistical Physics, 1982. **27**(3): p. 533-551.

119. K. W. Kratky, *Overlap graph representation of B/sub 6/ and B/sub 7/.* Journal of Statistical Physics, 1982. **29**(1): p. 129-138.

120. A. Kreglewski, *Equilibrium properties of fluids and fluid mixtures.* 1984: Texas A&M Universtiy press, Collage Station.

121. A. Kreglewski and R. C. Wilhoit, *Thermodynamic properties of systems with specific interactions calculated from the hard-sphere equation of state. II. Binary systems of electron donors and acceptors.* Journal of Physical Chemistry, 1975. **79**(5): p 449-454

122. J. G. Kirkwood, *Statistical Mechanics of Fluid Mixtures.* The Journal of Chemical Physics, 1935. **3**: p. 300.

123. W. L. Kubic, Jr., *A Quartic Hard Chain Equation of State for Normal Fluids.* Fluid Phase Equilibria, 1986. **31**: p. 35-56.

124. J. L. Lebowitz, *Exact Solution of Generalized Percus-Yevic Equation for a Mixture of Hard Spheres.* Physical Review, 1964. **133**: p. A895.

125. J. L. Lebowitz and J. S. Rowlinson, *Thermodynamic Properties of Mixtures of Hard Spheres.* Journal of Chemical Physics, 1964. **41**: p. 133-138.

126. K.-H. Lee, M. Lombardo, and S. I. Sandler, *The generalized Van der Waals partition function. II. Application to the square-well fluid.* Fluid Phase Equilibria, 1985. **21**: p. 177-196.

127. K.-H. Lee and S. I. Sandler, *The generalized Van der Waals partition function. IV. Local composition models for mixtures of unequal-size molecules.* Fluid Phase Equilibria, 1987. **34**: p. 113-147.

128. K.-H. Lee, S. I. Sandler, and N. C. Patel, *The generalized Van der Waals partition function. III. Local composition models for a mixture of equal size square-well molecules.* Fluid Phase Equilibria, 1986. **25**: p. 31-49.

129. R. J. Lee and K.-C. Chao, *Local Composition Embedded Eqautions of State for Strongly Nonideal Fluid Mixtures.* Industrial and Engineering Chemistry Research, 1989. **28**: p. 1251-1261.

130. E. W. Lemmon, M. O. McLinden, and D. G. Friend, *Thermophysical Properties of Fluid Systems*, in *NIST Chemistry WebBook, NIST Standard Reference Database Number 69*, P.J. Linstrom and W.G. Mallard, Editors. 2003, National Institute of Standards and Technology: Gaithersburg MD, (http://webbook.nist.gov).

131. P. Li, X.-Y. Zheng, and J.-F. Lin, *Liquid volumetric behavior and phase equilibrium calculations by a hard-sphere three-parameter equation of state.* Fluid Phase Equilibria, 1991. **67**: p. 173-195.

132. H. M. Lin, H. Kim, T. M. Guo, and K. C. Chao, *Cubic Chain-of-Rotators Equation of state and VLE Calculations.* Fluid Phase Equilibria, 1983. **13**: p. 143-152.

133. H. Liu and Y. Hu, *Molecular thermodynamic theory for polymer systems Part II. Equation of state for chain fluids.* Fluid Phase Equilibria, 1996. **122**: p. 75-97.

134. F. London, *The General Theory of Molecular Forces.* Transactions of the Faraday Society., 1936. **33**: p. 8-26.

135. M. J. Maeso, J. R. Solana, J. Amorós, and E. Villar, *Equations of state for hard spheres fluid in the metastable fluid region.* Journal of Chemical Physics, 1991. **94**(1): p. 551-555.

136. A. Malijevsky and J. Veverka, *New equations of state for pure and binary hard-sphere fluids.* Physical Chemistry Chemical Physics., 1999. **1**: p. 4267-4270.

137. G. A. Mansoori, N. F. Carnahan, K. E. Starling, and T. W. Leiland, Jr., *Equilibrium Thermodynamic Properties of the Mixture of Hard Spheres.* Journal of Chemical Physics, 1971. **54**(4): p. 1523-1525.

138. D. W. Marquardt, *An algorithm for least squares estimation of non-linear parameters.* Journal of the Society for Industrial and Applied Mathematics., 1963. **11**: p. 431-441.

139. P. h. Marteau, *Experimental determination of the phase behavior of binary mixtures: methane-hexane and methane-benzene.* Fluid Phase Equilibria, 1997. **129**: p. 285-305.

140. P. M. Mathias and T. W. Copeman, *Extension of the Peng-Robinson equation of state to complex mixtures: Evaluation of the various forms of the local composition concept.* Fluid Phase Equilibria, 1983. **13**: p. 91-108.

141. P. M. Mathias, H. C. Klotz, and J. M. Prausnitz, *Equation-of-State mixing rules for multicomponent mixtures: the problem of invariance.* Fluid Phase Equilibria, 1991. **67**: p. 31-44.

142. D. A. McQuarrie, *Statistical Mechanics.* 2000, Sausalito: University Science Books.

143. M. L. Michelsen, *A Method for incorporating excess Gibbs energy models in equations of state.* Fluid Phase Equilibria, 1990. **60**: p. 47-58.

144. M. L. Michelsen and R. A. Heidemann, *Some Properties of Equation of State Mixing Rules Derived from Excess Gibbs Energy Expressions.* Industrial and Engineering Chemistry Research, 1996. **35**: p. 278-287.

145. M. L. Michelsen and H. Kistenmacher, *On composition-dependent interaction coefficients.* Fluid Phase Equilibria, 1990. **58**: p. 229-230.

146. J. Mollerup, *A note on excess Gibbs energy models, equations of state and the local compostion concept.* Fluid Phase Equilibria, 1981. **7**: p. 121-138.

147. J. Mollerup, *A note on the derivation of mixing rules from excess Gibbs free energy models.* Fluid Phase Equilibria, 1986. **25**: p. 323-327.

148. D. L. Morgan and R. Kobayashi, *Direct vapor pressure measurements of ten n-alkanes in the C10-C28 range.* Fluid Phase Equilibria, 1994. **97**: p. 211-242.

149. W. O. Morris, P. Vimalchand, and M. D. Donohue, *The perturbed-soft-chain theory: An equation of state based on the Lennard-Jones potential.* Fluid Phase Equilibria, 1987. **32**: p. 103-115

150. A. Mulero, C. Galán, and F. Cuadros, *Equations of state for hard spheres. A review of accuracy and applications.* Physical Chemistry Chemical Physics., 2001. **3**: p. 4991-4999.

151. E. A. Müller and K. E. Gubbins, *An Equation of state for water from a simplified intermolecular potential.* Industrial and Engineering Chemistry Research, 1995. **94**: p. 3662-3673.

152. E. A. Müller and K. E. Gubbins, *Molecular-Based Equations of State for Associating Fluids: A Review of SAFT and Related Approaches.* Industrial and Engineering Chemistry Research, 2001. **40**: p. 2193-2211.

153. I. Nezbeda, *On dispersion force correction terms in perturbed equations of state.* Fluid Phase Equilibria, 2001. **180**: p. 175-181.

154. H.-J. Ng, C.-J. Chen, and D. B. Robinson, *Vapor Liquid Equilibrium and Condensing Curves in the Vicinity of the Critical Point for a Typical Gas Condensate.*, Report nr.: RR-96, Gas Processors Association, 1986

155. W. B. Nichols, H. H. Reamer, and B. H. Sage, *Volumetric and phase behavior in the hydrogen - n-hexane system.* AIChE Journal, 1957. **3**(2): p. 262-267.

156. J. J. Nicolas, K. E. Gubbins, W. B. Streett, and D. J. Tildesley, *Equation of state for the Lennard-Jones fluid.* Molecular Physics, 1979. **37**(5): p. 1429-1454.

157. B. R. A. Nijboer and L. Van Hove, *Radial Distribution Function of a Gas of Hard Spheres and the Superposition Approximation.* Physical Review, 1952. **85**: p. 777-783.

158. H. Orbey, C. P. Bokis, and C.-C. Chen, *Polymer-Solvent Vapor-Liquid Equilibrium: Equations of State versus Activity Coefficient Models.* Industrial and Engineering Chemistry Research, 1998. **37**: p. 1567-1573.

159. H. Orbey and S. I. Sandler, *Reformulation of the Wong-Sandler mixing rule for cubic equations of state.* AIChE Journal, 1995. **41**: p. 683-690.

160. N. Orbey and S. I. Sandler, *Vapor-Liquid Equilibrium of Polymer Solutions Using a Cubic Equation of State.* AIChE Journal, 1994. **40**(7): p. 1203-1209.

161. L. S. Ornstein and F. Zernike, *Accidental deviations of density and opalescence at the critical point of a single substance.* Proc. K. Ned. Akad. Wet.., 1914. **17**: p. 793-806.

162. N. C. Patel and A. S. Teja, *A New Cubic Equation of State for Fluids and Fluid Mixtures.* Chemical Engineering Science, 1982. **37**(3): p. 463-473.

163. D. Y. Peng and D. B. Robinson, *A new two constant equation of state.* Industrial and Engineering Fundamentals., 1976. **15**: p. 59-64.

164. I. B. Petche and P. G. Debenedetti, *Influence of Solute-Solven Asymmetry upon the Behaviour of Dilute Supercritical Mixtures.* Journal of Physical Chemistry, 1991. **95**: p. 386-399.

165. C. J. Peters and J. L. De Roo, *Measurements and Calculations of Phase Equilibria of Binary Mixtures of Ethane+Eicosane. Part I: Vapour + Liquid Equilibria.* Fluid Phase Equilibria, 1987. **34**: p. 287-308.

166. C. J. Peters, J. L. De Roo, and J. De Swaan Arons, *Phase equilibria in binary mixtures of propane and hexacontane.* Fluid Phase Equilibria, 1993. **85**: p. 301-312.

167. O. Pfohl and G. Brunner, *2. Use of BACK To Modify SAFT in Order To Enable Density and Phase Equilibrium Calculations Connected to Gas-Extraction Processes.* Industrial and Engineering Chemistry Research, 1998. **37**: p. 2966-2976.

168. V. Piacente, D. Fontana, and P. Scardala, *Enthalpies of Vaporization of a Homologous Series of n-Alkanes Determined from Vapor Pressure Measurements.* Journal of Chemical and Engineering Data, 1994. **39**: p. 231-237.

169. L. Ponce-Ramirez, C. Lira-Galeana, and C. Tapia-Medina, *Application of the SPHCT model to the prediction of phase equilibria in CO_2-hydrocarbon systems.* Fluid Phase Equilibria, 1991. **70**: p. 1-18.

170. J. M. Prausnitz, R. N. Lichtenthaler, and E. G. d. Azevedo, *Molecular Thermodynamics of Fluid-Phase Equilibria.* Third Edition ed. Prentice Hall International Series in the Physical and Chemical Engineering Sciences., ed. N.R. Amundson. 1999, Upper Saddle River: Prentice Hall PTR.

171. W. H. Press, S. A. Teukolsky, W. T. Vetterling, and B. P. Flannery, *Numerical Recipes in C. The Art of Scientific Computing.* Second Edition ed. 1997, Cambridge: Cambridge University Press.

172. H. H. Reamer and B. H. Sage, *Phase Equilibria in Hydrocarbon Systems. Volumetric and Phase Behavior of the Ethane-n-Decane System.* Journal of Chemical and Engineering Data, 1962. **7**(2): p. 161-168.

173. H. H. Reamer and B. H. Sage, *Phase Equilibria in Hydrocarbon Systems. Volumetric and Phase behavior of the n-Decane-CO_2 System.* Journal of Chemical and Engineering Data, 1963. **8**(4): p. 508-513.

174. F. H. Ree and W. G. Hoover, *Fifth and Sixth Virial Coefficients for Hard Spheres and Disks.* Journal of Chemical Physics, 1964. **40**(4): p. 939-950.

175. F. H. Ree and W. G. Hoover, *Seventh Virial Coefficients for Hard Spheres and Disks.* Journal of Chemical Physics, 1967. **46**(11): p. 4181-4197.

176. H. Reiss, H. L. Frisch, and J. L. Lebowitz, *Statistical Mechanics of Rigid Spheres.* Journal of Chemical Physics, 1959. **31**(2): p. 369-380.

177. P. Rice and A. El-Nikheli, *Isothermal vapour-liquid equilibrium data for the systems n-pentane with n-hexane, n-octane and n-decane.* Fluid Phase Equilibria, 1995. **107**: p. 257-267.

178. M. P. W. M. Rijkers, V. B. Manduro, C. J. Peters, and J. De Swaan Arons, *Measurement on the phase behavior of binary mixtures for modelling the condensation behavior of natural gas.* Fluid Phase Equilibria, 1992. **72**: p. 309-324.

179. J. S. Rowlinson, *Liquids and Liquid Mixtures.* 1969, London: Butterworth & Co. (Publishers) Ltd.

180. G. Sadowski, *A square-well based equaiton of state taking into account the connectivity in chain molecules.* Fluid Phase Equilibria, 1997. **149**: p. 75-89.

181. R. J. Sadus, *Equations of State for Hard-Sphere Chains.* Journal of Physical Chemistry, 1995. **99**: p. 12363-12366.

182. R. J. Sadus, *Simple Equation of State for Hard-Sphere Chains.* AIChE Journal, 1999. **45**(11): p. 2454-2457.

183. I. C. Sanchez, *Virial coefficients and close-packing of hard spheres and disks.* Journal of Chemical Physics, 1994. **101**(8): p. 7003-7006.

184. S. I. Sandler, *The Generalized Van Der Waals Partition Function. I. Basic Theory.* Fluid Phase Equilibria, 1985. **19**: p. 233-257.

185. S. I. Sandler, *Models for Thermodynamic and Phase Equilibria Calculations.*, ed. S.I. Sandler. 1994, New York: Marcel Dekker, Inc.

186. J. Schwartzentruber, F. Galivel-Solastiouk, and H. Renon, *Representation of the Vapor-Liquid Equilibrium of the Ternary System Carbon-Dioxide-Propane-Methanol and Its Binaries with a Cubic Equation of State: A New Mixing Rule.* Fluid Phase Equilibria, 1987. **38**: p. 217-226.

187. J. Schwartzentruber and H. Renon, *Extension of UNIFAC to high pressures and temperatures by the use of a cubic equation of state.* I.E.C. Research, 1989. **28**: p. 1049-1055.

188. J. Schwartzentruber and H. Renon, *Equations of state: how to reconcile flexible mixing rules, the virial coefficient constraint and the "Michelsen-Kistenmacher syndrome" for mylticomponent systems.* Fluid Phase Equilibria, 1991. **67**: p. 99-110.

189. C. Schwarz and I. Nieuwoudt, *Phase equilibrium of propane and alkanes part II:hexatriacontane through hexacontane.* Fluid Phase Equilibria, 2003. **27**: p. 145-156.

190. J. V. Sengers, R. F. Kayser, C. J. Peters, and J. H.J. White, *Equations of State for Fluids and Fluid Mixtures. Part 1.* Experimental Thermodynamics., ed. J.V. Sengers, R.F. Kayser, C.J. Peters, and J. H.J. White. Vol. Volume V. 2000, Amsterdam: Elsevier.

191. J. V. Sengers, R. F. Kayser, C. J. Peters, and J. H.J. White, *Equations of State for Fluids and Fluid Mixtures. Part 2.* Experimental Thermodynamics., ed. J.V. Sengers, R.F. Kayser, C.J. Peters, and J. H.J. White. Vol. Volume V. 2000, Amsterdam: Elsevier.

192. V. M. Shah, P. R. Bienkowski, and H. D. Cochran, *Generalized Quartic Equation of State for pure Nonpolar Fluids.* AIChE Journal, 1994. **40**(1): p. 152-159.

193. R. D. Shaver, R. L. Robinson, Jr., and K. A. M. Gasem, *Modified SPHCT equation of state for improved predictions of equilibrium properties of pure fluids.* Fluid Phase Equilibria, 1995. **112**: p. 223-248.

194. B. Smit, *Phase diagrams of Lennard-Jones fluids.* Journal of Chemical Physics, 1992. **96**(11): p. 8639-8640.

195. W. R. Smith, D. Henderson, and J. A. Barker, *Approximate evaluation of the second-order term in the perturbation theory of fluids.* Journal of Chemical Physics, 1970. **53**(2): p. 508-515.

196. G. Soave, *Equilibrium constants for the modified Redlich-Kwong equation of state.* Chemical Engineering Science, 1972. **27**: p. 1197-1203.

197. G. S. Soave, A. B. Bertucco, and M. Sponchiado, *Avoiding the Use of Critical Constants in Cubic Equations of State.* AIChE Journal, 1995. **41**(8): p. 1964-1971.

198. Y. Song, S. M. Lambert, and J. M. Prausnitz, *Equations of State for mixtures of Hard-Sphere Chains Including Copolymers.* Macromolecules, 1994. **27**: p. 441-448.

199. Y. Song, S. M. Lambert, and J. M. Prausnitz, *Liquid-liquid phase diagrams for binary polymer solutions from a perturbed hard-sphere-chain equation of state.* Chemical Engineering Science, 1994. **49**(17): p. 2765-2775.

200. Y. Song, S. M. Lambert, and J. M. Prausnitz, *A Perturbed Hard-Sphere-Chain Equation of State for Normal Fluids and Polymers.* Industrial and Engineering Chemistry Research, 1994. **33**: p. 1047-1057.

201. Y. Song and E. A. Mason, *Statistical-mechanical theory of a new analytical equation of state.* Journal of Chemical Physics, 1989. **91**(12): p. 7840-7853.

202. M. Spee and G. M. Schneider, *Fluid Phase Equilibrium Studies on Binary and Ternary Mixtures of Carbon Dioxide with Hexadecane, 1-Dodecanol, 1,8-Octanediol and Dotriacontane at 393.2 K and Pressures up to 100 MPa.* Fluid Phase Equilibria, 1991. **65**: p. 263-274.

203. R. J. Speedy, *Pressure of the metastable hard-sphere fluid.* Journal of Physics. Condensed Matter : An Institute of Physics Journal, 1997. **9**: p. 8591-8599.

204. W. B. Streett and D. J. Tildesley, *Fluids of hard-core triatomic molecules. Computer simulations of polyatomic molecules. Part 4.-Monte Carlo simulations of hard-core triatomics.* Faraday Discussions of the Chemical Society, 1978. **66**: p. 27-38.

205. R. Stryjek and J. H. Vera, *An improved Peng-Robinson equation of state for accurate vapor-liquid equilibrium calculations.* The Canadian Journal of Chemical Engineering, 1986. **64**: p. 334-340.

206. R. Stryjek and J. H. Vera, *PRSV2: a cubic equation of state for accurate vapor-liquid equilibrium calculations.* The Canadian Journal of Chemical Engineering, 1986. **64**: p. 860-826.

207. R. Stryjek and J. H. Vera, *Vapor-liquid equilibria for hydrochloric acid and solutions with the PRSV equation of state.* Fluid Phase Equilibria, 1986. **25**: p. 279-290.

208. S. P. Tan, H. Adidharma, and M. Radosz, *Weeks-Chandler-Andersen Model for Solid-Liquid Equilibria in Lennard-Jones Systems.* Journal of Physical Chemistry B, 2002. **106**: p. 7878-7881.

209. E. Thiele, *Equation of State for Hard Spheres.* Journal of Chemical Physics, 1963. **39**(2): p. 474-479.

210. M. Thiesen, *Untersuchungen über die Zustandsgleichung.* Annual review of physical chemistry, 1885. **24**: p. 467-474.

211. F. Tobler, *Correlation of the Density of the Liquid Phase of Pure n-Alkanes with Temperature and Vapor Pressure.* Industrial and Engineering Chemistry Research, 1998. **37**: p. 2565-2570.

212. J. Tobochnik and P. M. Chapin, *Monte Carlo simulation of hard spheres near random closest packing using spherical boundary conditions.* Journal of Chemical Physics, 1988. **88**(9): p. 5824-5829.

213. K. Tochigi, S. Kurita, and T. Matsumoto, *Prediction of PVT and VLE in polymer solutions using a cubic-perturbed equation of state.* Fluid Phase Equilibria, 1999. **158-160**: p. 313-320.

214. R. J. Topliss, D. Dimitrelis, and J. M. Prausnitz, *Computational Aspects of Non-Cubic Equations of State for Phase Equilibrium Calculations. Effect of Density Dependent Mixing Rules.* Computational Chemical Engineering., 1988. **12**(5): p. 482-489.

215. E. A. Turek, R. S. Metcalfe, L. Yarborough, and R. L. Robinson, Jr., *Phase Equilibria in CO_2 - Multicomponent Hydrocarbon Systems: Experimental Data and an Improved Prediction Technique.* Society of Petroleum Engineers Journal., 1984. **24**: p. 308-324.

216. C. H. Twu, L. L. Lee, and K. E. Starling, *Improved analytical representation of argon thermodynamic behaviour.* Fluid Phase Equilibria, 1980. **4**: p. 35-44.

217. J. D. Van der Waals, *De Continuiteit van den Gas- en Vloeistoftoestand.* Doctoral Thesis, Leiden University: Leiden, 1873.

218. A. Van Pelt, C. J. Peters, and J. De Swaan Arons, *Application of the Simplified-Perturbed-Hard-Chain Theory for pure components near the critical point.* Fluid Phase Equilibria, 1992. **74**: p. 67-83.

219. J. H. Vera and J. M. Prausnitz, *Interpretative Review. Generalized van der Waals Theory for Dense Fluids.* The Chemical Engineering Journal, 1972. **3**: p. 1-13.

220. L. Verlet, *Computer "Experiments" on Classical Fluids. II Equilibrium Correlation Functions.* Physical Review, 1968. **165**(1): p. 201-214.

221. L. Verlet and J.-J. Weis, *Equilibrium Theory of Simple Liquids.* Physical Review A, 1972. **5**(2): p. 939-952.

222. P. Vimalchand and M. D. Donohue, *Comparison of Equations of State for Chain Molecules.* Journal of Physical Chemistry, 1989. **93**: p. 4355-4360.

223. P. Vimalchand, A. Thomas, I. G. Economou, and M. D. Donohue, *Effect of Hard-Sphere Structure of Pure-Component Equation of State Calculations.* Fluid Phase Equilibria, 1992. **73**(1-2): p. 39-55.

224. N. Von Solms, M. L. Michelsen, and G. M. Kontogeorgis, *Computational and Physical Performance of a Modified PC-SAFT Equation of State for Highly Asymmetric and Associating Mixtures.* Industrial and Engineering Chemistry Research, 2003. **42**: p. 1098-1105.

225. J. M. Walsh and K. E. Gubbins, *A Modified Thermodynamic Perturbation Theory Equation for Molecules with Fused Hard Sphere Cores.* Journal of Physical Chemistry, 1990. **94**: p. 5115-5120.

226. L.-S. Wang and T. M. Guo, *A Cubic Simplified Perturbed Hard-Chain Equation of State for Fluids with Chainlike Molecules.* The Canadian Journal of Chemical Engineering, 1993. **71**: p. 591-604.

227. W. Wang, M. K. Khoshkbarhci, and J. H. Vera, *A new volume dependence for the equations of state of hard spheres.* Fluid Phase Equilibria, 1996. **115**: p. 25-38.

228. J. D. Weeks, D. Chandler, and H. C. Andersen, *Role of Repulsive Forces in Determining the Equilibrium Structure of Simple Liquids.* The Journal of Chemical Physics, 1971. **54**(12): p. 5237-5247.

229. Y. S. Wei and R. J. Sadus, *Equations of State for the Calculation of Fluid-Phase Equilibria.* AIChE Journal, 2000. **47**(1): p. 169-196.

230. M. S. Wertheim, *Exact Solution of the Percus-Yevick Integral Equation for Hard Spheres.* Physical Review Letters, 1963. **10**(8): p. 321-323.

231. M. S. Wertheim, *Fluids with Highly directional Attractive Forces. I. Statistical Thermodynamics.* Journal of Statistical Physics, 1984. **35**: p. 19-34.

232. M. S. Wertheim, *Fluids with Highly directional Attractive Forces. II. Thermodynamic Perturbation Theory and Integral Equations.* J. Stat. Phys., 1984. **35**: p. 35-47.

233. M. S. Wertheim, *Fluids of Dimerizing Hard Spheres, and Fluid Mixtures of Hard Spheres and Dispheres.* J. Chem. Phys., 1986. **85**: p. 2929-2936.

234. M. S. Wertheim, *Fluids with Highly directional Attractive Forces. III. Multiple Attraction Sites.* Journal of Statistical Physics, 1986. **42**: p. 459-476.

235. M. S. Wertheim, *Fluids with Highly directional Attractive Forces. IV. Equilibrium Polymerization.* Journal of Statistical Physics, 1986. **42**: p. 477-492.

236. M. S. Wertheim, *Thermodynamic Perturbation Theory of Polymerization.* Journal of Chemical Physics, 1987. **87**: p. 7323-7331.

237. W. B. Whiting and J. M. Prausnitz, *Equations of state for strongly nonideal fluid mixtures: Application of local compositions toward density-dependent mixing rules.* Fluid Phase Equilibria, 1982. **9**: p. 119-147.

238. D. S. H. Wong, H. Orbey, and S. I. Sandler, *Equation of State Mixing Rule for Nonideal Mixtures Using Available Activity Coefficient Model Parameters and That Allows Extrapolation over Large Ranges of Temperature and Pressure.* Industrial and Engineering Chemistry Research, 1992. **31**: p. 2033-2039.

239. D. S. H. Wong and S. I. Sandler, *A Theoretically Correct Mixing Rule for Cubic Equations of State.* AIChE Journal, 1992. **38**(5): p. 671-680.

240. L. V. Woodcock, *Hard-Sphere Fluid Equation of State.* Journal of the Chemical Society Faraday Transactions 2, 1976. **72**: p. 731-730.

241. T. Yang, G.-J. Chen, W. Yan, and T.-M. Guo, *Extension of the Wong-Sandler mixing rule to the three-parameter Patel-Teja equation of state: Application up to the near-critical region.* Chemical Engineering Journal, 1997. **67**: p. 27-36.

242. L. V. Yelash and T. Kraska, *A generic equation of state for the hard-sphere fluid incorporating the high density limit.* Physical Chemistry Chemical Physics, 2001. **2001**(3): p. 3114-3118.

243. L. V. Yelash, T. Kraska, and U. K. Deiters, *Closed-loop critical curves in simple hard-sphere van der Waals-fluid models consistent with the packing fraction limit.* Journal of Chemical Physics, 1999. **110**(6): p. 3079-3084.

244. M. S. Yeom, J. Chang, and H. Kim, *A new equation of state for the hard-sphere chain fluid based on the thermodynamic perturbation theory and the multidensity integral equation.* Fluid Phase Equilibria, 2000. **173**: p. 177-187.

245. A. Yethiraj and C. K. Hall, *Local structure of fluids containing chain-like molecules: Polymer reference interaction site model with Yukawa closure.* Journal of Chemical Physics, 1990. **93**: p. 5315-5321.

246. A. Yethiraj and C. K. Hall, *Generalized Flory Equations of state for square-well chains.* Journal of Chemical Physics, 1991. **95**(11): p. 8498-8506.

247. A. Yethiraj and C. K. Hall, *Monte Carlo simulations and integral equation theory for microscopic correlations in polymeric fluids.* Journal of Chemical Physics, 1992. **96**: p. 797-807.

248. B.-J. Zhang, *Cakcualting thermodynamic properties from perturbation theory I. An analytic representation of square-well potential hard-sphere perturbation theory.* Fluid Phase Equilibria, 1999. **154**: p. 1-10.

249. B.-J. Zhang, S. Liang, and Y. Lu, *Calculating the thermodynamic properties from perturbation theory II. An analytic representation for the square-well chain fluid.* Fluid Phase Equilibria, 2001. **180**: p. 183-194.

250. Y. Zhi and H. Lee, *Fallibility of analytic roots of cubic equations of state in low temperature regions.* Fluid Phase Equilibria, 2002. **201**: p. 287-294.

251. R. W. Zwanzig, *High-Temperature Equation of State by a Perturbation Method. I. Nonpolar Gases.* Journal of Chemical Physics, 1954. **22**(8): p. 1420-1426.

Appendix A Perturbation Term Parameter Regression

In chapter 3, various configurations for the perturbation approximation term, including the double summation perturbation approximation, have been investigated. The perturbation matrix parameters used in the double summation approximations were determined from the argon thermodynamic data, and will be presented in this section.

A.1 REGRESSION OF THE ARGON EOS PARAMETERS FOR THE HS3CK, HS3SW AND HS3LJ EOS MODELS

The *HS3SW*, *HS3CK* and *HS3LJ* models were originally evaluated based on their performance using a 6x4 perturbation matrix. The perturbation expression is given by equation A.1.

$$\frac{A^{pert}}{NkT} = \sum_{n}\sum_{m} D_{nm}\left(\frac{\eta}{\tau}\right)^{m}(T^{*})^{n} \qquad \text{A.1}$$

where D_{nm} represents the perturbation parameters, n = 4, representing the degree of density dependence and m = 6 the perturbation order of the model.

Three different versions of the *HS3LJ* equations were investigated, the first where the pure component parameters are allowed to vary freely in the fit *HS2LJ-LJ*, the second where the mean well depth of the Lennard-Jones potential function is constrained to be equal to the critical temperature of the system used to regress the parameter values (argon) resulting in the *HS3LJ-Mean* parameter set, and lastly the parameters regressed for the *HS3LJ-Real* equation, where the pure component maximum well depth of the *Lennard-Jones* potential function is set equal to the critical temperature of the dataset used in the regression (argon).

The argon pure component parameters as well as the D_{n1} parameters were regressed from the argon second virial coefficient data [64]. The *EOS* parameters are listed in tables 4.14 and 4.15 and the perturbation parameters in table A.1.

Table A.1 The perturbation matrix parameter values regressed from the argon second virial coefficient data

D_{n1} parameters				
	D_{11}	D_{21}	D_{31}	D_{41}
HS3CK	-8.754	3.080	-3.476	0.651
HS3SW	-6.118	-5.389	1.007	-0.346
HS3LJ-LJ	-9.892	-2.955	1.064	-1.417
HS3LJ-mean	-0.875	-0.128	0.009	-0.0005
HS3LJ-real	-7.222	-2.151	0.691	-0.505

The entire remaining perturbation matrix parameters were regressed from the argon *P-v-T* data. The perturbation matrices for the *HS*3*CK*, *HS*3*LJ-LJ* and *HS*3*LJ-real* models are listed in table A.2. (The development of the *HS*3*SW* and *HS*3*LJ-mean* equations was not extended up to this phase.)

Table A.2 The double summation perturbation approximation parameters as regressed for a 4x6 matrix for the *HS*3*CK, HS*3*LJ-LJ, HS*3*LJ -mean* and *HS*3*LJ -Real* models

	HS3CK $D_{n\,m}$				HS3LJ-LJ $D_{n\,m}$				HS3LJ-Real D_n			
m	**n = 1**	**n = 2**	**n = 3**	**n = 4**	**n = 1**	**n = 2**	**n = 3**	**n = 4**	**n = 1**	**n = 2**	**n = 3**	**n = 4**
1	-8.754	3.080	-3.476	0.651	-9.892	-2.955	1.064	-1.417	-7.222	-2.151	0.691	-0.505
2	-2.707	3.880	0.183	0.610	-1.597	8.143	-3.457	3.022	-1.477	7.776	-4.838	1.393
3	2.465	-3.905	1.283	2.001	-1.605	3.597	0.414	11.683	-3.768	3.051	-0.988	9.528
4	-13.747	-2.949	25.291	-21.245	-12.717	-0.856	-20.105	-8.723	-9.442	4.120	-15.849	-8.437
5	-8.212	-20.250	3.181	8.004	5.531	-37.824	-26.181	-7.373	9.577	-22.422	-17.609	-6.427
6	100.238	-67.906	-4.117	18.145	78.448	30.600	50.463	1.640	56.052	32.596	44.670	-0.498

The HS3CK parameter matrix was further used in the regression of the methane, N_2 and CO_2 parameters during the investigation of the effect for the inclusion of the temperature dependent non-central London energies. The relevant EOS parameters are listed in Table A.3.

Table A.3 The HS3CK 4x6 EOS parameters for Methane, N_2 and CO_2 with and without the temperature dependent interaction energies.

Pure component EOS parameters for the HS3CK 4x6 Matrix			
Component	**v_{00} [1e6m^3/mol]**	**ε/k [K]**	**μ/k [K]**
Methane	20.85	190.50	1
Methane	20.81	191.76	0
N_2	18.74	123.95	3
N_2	18.66	127.80	0
CO_2	20.13	275.12	40
CO_2	20.54	317.01	0

A.2 THE OPTIMISATION OF THE PERTURBATION MATRIX

Various simplifications of the perturbation matrices have also been investigated for the *HS*3*CK*, *HS*3*LJ-LC* and *HS*3*LJ-LJ* models. The matrix parameters for 4x2, 4x3, 3x3 and 3x2 matrix configurations have been determined for all three models. See Table A.4:

Table A.4 The simplified double summation perturbation matrices as regressed for the *HS*3*CK, HS*3*LJ-LJ, HS*3*LJ -mean* and *HS*3*LJ -Real* models

HS3CK $D_{n\,m}$				HS3LJ-LJ $D_{n\,m}$				HS3LJ-Real $D_{n\,m}$			
m n = 1	**n = 2**	**n = 3**	**n = 4**	**n = 1**	**n = 2**	**n = 3**	**n = 4**	**n = 1**	**n = 2**	**n = 3**	**n = 4**
1 -8.754	3.080	-3.476	0.651	-9.892	-2.955	1.064	-1.417	-7.222	-2.151	0.691	-0.505
2 -4.385	7.720	-3.267	0.990	-0.981	6.685	-4.239	3.240	-2.795	8.872	-5.471	1.950
HS3CK $D_{n\,m}$				**HS3LJ-LJ $D_{n\,m}$**				**HS3LJ-Real $D_{n\,m}$**			
m n = 1	**n = 2**	**n = 3**	**n = 4**	**n = 1**	**n = 2**	**n = 3**	**n = 4**	**n = 1**	**n = 2**	**n = 3**	**n = 4**
1 -8.754	3.080	-3.476	0.651	-9.892	-2.955	1.064	-1.417	-7.222	-2.151	0.691	-0.505
2 -7.903	7.787	7.788	-4.828	-6.260	12.531	10.371	-9.144	-4.643	5.439	7.298	-4.040
3 16.646	-30.773	4.107	4.859	11.385	-27.746	-8.882	18.480	18.082	-34.120	7.477	3.793
HS3CK $D_{n\,m}$				**HS3LJ-LJ $D_{n\,m}$**				**HS3LJ-Real $D_{n\,m}$**			
m n = 1	**n = 2**	**n = 3**	**n = 4**	**n = 1**	**n = 2**	**n = 3**	**n = 4**	**n = 1**	**n = 2**	**n = 3**	**n = 4**
1 -7.829	0.066	-1.048	0	-11.653	-1.169	-2.705	0	-7.494	-0.964	-0.695	0
2 -3.707	8.509	-1.350	0	-2.254	12.462	-0.620	0	2.966	-1.960	3.127	0
3 3.848	-15.370	6.426	0	-1.764	-16.360	10.729	0	-8.044	5.619	-2.555	0
HS3CK $D_{n\,m}$				**HS3LJ-LJ $D_{n\,m}$**				**HS3LJ-Real $D_{n\,m}$**			
m n = 1	**n = 2**	**n = 3**	**n = 4**	**n = 1**	**n = 2**	**n = 3**	**n = 4**	**n = 1**	**n = 2**	**n = 3**	**n = 4**
1 -6.990	-2.574	0	0	-12.237	-7.104	0	0	-6.935	-2.724	0	0
2 0.598	4.873	0	0	-1.855	17.806	0	0	0.176	5.303	0	0
3 -7.104	0.839	0	0	-5.037	-7.438	0	0	-5.821	0.075	0	0

The pure component specific EOS parameters regressed for argon and methane using these perturbation matrices are listed in Table A.5:

Table A.5 Pure component parameters as regressed for argon and methane for the various simplifications of the double summation perturbation matrices.

EOS parameters for the various perturbation matrices investigated in section 4.4.3.b									
	Argon			Methane			Methane (T>130 K)		
	v_{00} [1e6m^3/mol]	ε/k [K]	μ/k [K]	v_{00} [1e6m^3/mol]	ε/k [K]	μ/k [K]	v_{00} [1e6m^3/mol]	ε/k [K]	μ/k [K]
HS3CK 4x3	14.94	150.86	0	19.87	190.60	1	19.83	190.67	1
HS3CK 4x2	14.94	150.86	0	17.91	193.87	1	17.71	194.18	1
HS3CK 3x3	15.09	150.86	0	19.71	192.65	1	19.47	192.98	1
HS3CK 2x3	14.29	150.86	0	18.78	191.56	1	18.50	192.60	1
HS3LJ-LJ 4x3	15.65	112.58	0	20.61	143.00	1	20.43	143.19	1
HS3LJ-LJ 4x2	15.65	112.58	0	18.57	144.78	1	18.41	144.96	1
HS3LJ-LJ 3x3	16.12	99.14	0	21.02	126.51	1	20.69	126.77	1
HS3LJ-LJ 2x3	15.44	87.12	0	20.18	110.68	1	19.95	111.16	1
HS3LJ-Real 4x3	15.70	150.86	0	20.82	189.72	1	20.82	189.72	1
HS3LJ- Real 4x2	15.70	150.86	0	18.26	193.57	1	18.05	193.91	1
HS3LJ- Real 3x3	14.98	150.86	0	19.47	191.32	1	19.23	191.68	1
HS3LJ- Real 2x3	13.80	150.86	0	18.04	190.54	1	17.85	191.50	

As a final permutation a constrained 3x3 perturbation matrix for the *HS3CK* equation of state was investigated. The regressed parameter values of this matrix are listed in Table A.6.

Table A.6 The constrained perturbation matrix of the HS3CK-ltd EOS

HS3CK-ltd $D_{n\,m}$			
m	**n = 1**	**n = 2**	**n = 3**
1	-8.11395	0	0
2	-4.120830	12.4693	-5.66021
3	-4.948350	-6.2256	4.85777

A.3 THE INVESTIGATION INTO THE EFFECT OF THE TEMPERATURE DEPENDENT LONDON ENERGIES IN THE LLS MODEL

The following pure component parameters, listed in Table A.7, were regressed for the HS3LLS EOS for the temperature dependent and independent attractive energies of methane, N_2 and CO_2 as used applied in section 4.4.3.c:

Table A.7 The EOS pure component parameters for methane, N_2 and CO_2 in the HS3LLS EOS with Z_m=36.

Pure component EOS parameters for the HS3LLS EOS			
Component	**v_{00} [1e6m^3/mol]**	**ε/k [K]**	**μ/k [K]**
Methane	18.40	81.32	1
Methane	18.34	81.91	0
N_2	16.88	53.05	3
N_2	16.80	54.75	0
CO_2	17.76	118.03	40
CO_2	17.95	136.40	0

Appendix B Generalized correlations for the refitted SAFT, PC-SAFT and SPHCT pure component parameters

In order to facilitate the direct comparison between the developed *simple-PCHT-ltd EOS* and the equations found in literature, it is important to use pure component parameter values regressed form the same datasets. The newly regressed parameter values are listed in Table 7.4.

It is however also to developed generalized correlations for these parameter values, to facilitate the estimation of the parameters for components for which no pure component datasets are available. The generalised correlations for the estimation of the n-alkane pure component parameters of the *SAFT*, *PC-SAFT* and *SPHCT* models are presented in this section. Where possible the structure of the generalized correlations, as reported in the original articles on the models, were used and only the model coefficients were refitted to the new pure component parameter datasets.

B.1 GENERALIZATION OF THE SAFT EOS PARAMETERS

The generalised correlations for the *SAFT EOS* developed in this study are as follows:

$$m = 0.059Mr + 0.0532 \qquad \text{B.1}$$

$$mv_0 = 0.6308Mr + 11.889 \qquad [1e6m^3] \qquad \text{B.2}$$

$$\varepsilon / k = 209.999 - 25.808\exp\left[-0.0161Mr\right] \qquad [K] \qquad \text{B.3}$$

with *Mr* the pure component molecular weight in g/mol.

These correlations have the same structure as reported used in the original article by Huang and Radosz [100].

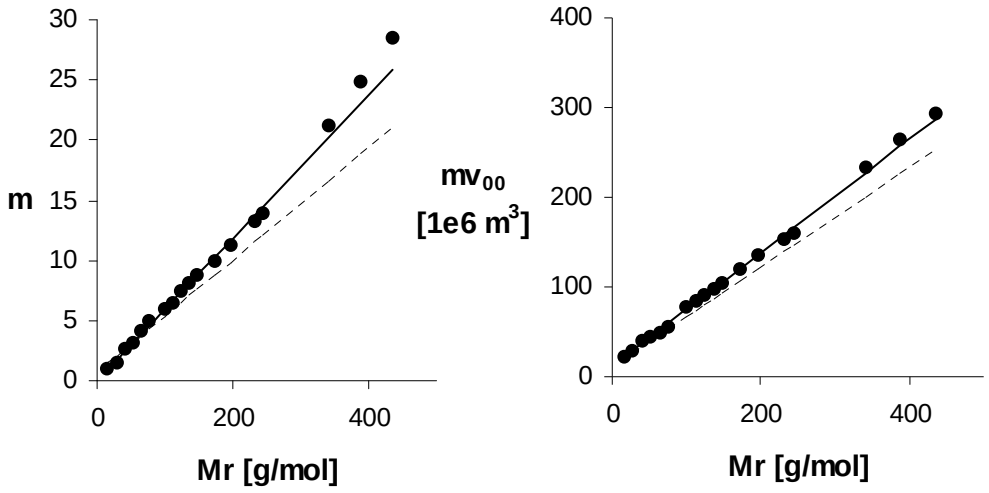

Figure B.1 Generalized correlations for the *SAFT* n-alkane m and v_{00} parameters, with • the regressed parameters used in this study and the —— new and _____ original correlations.

The new correlations are plotted in Figures B.1 and B.2 along with the regressed parameter values and the original correlations. A considerable amount of scatter can be seen in the ε/k parameter values (Figure B.2), with the n-octacosane, n-dotriacontane and n-hexatriacontane parameter values showing large deviations from the expected trends as extrapolated from the lighter component parameter values and predicted by the original correlations. As has been discussed in section 7.1 this may be attributed to the smaller datasets used to fit these parameters. There is however a good agreement between the new and original correlations at these higher molecular weights, improving the confidence in the extrapolation of the new correlation for the energy parameters.

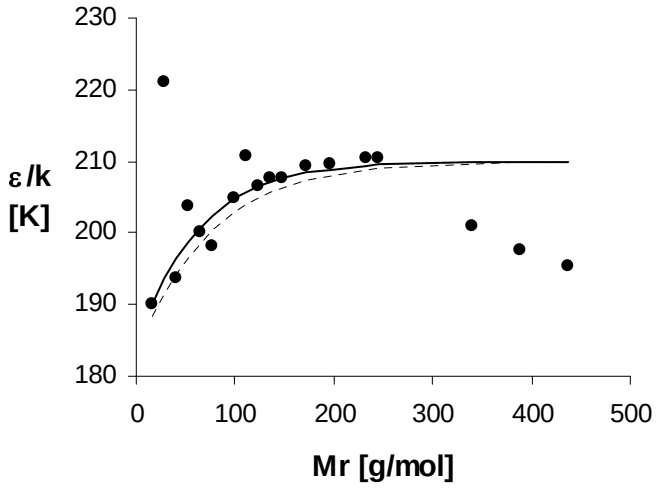

Figure B.2 Generalized correlations for the *SAFT* n-alkane ε/k parameters, with • the regressed parameters used in this study and the —— new and _____ original correlations.

B.2 GENERALIZATION OF THE PC-SAFT EOS PARAMETERS

The generalization of the *PC-SAFT EOS* parameters for n-alkanes, was done in a manner similar to that discussed above, by simply fitting new coefficient values of the existing correlations [86] for the equation of state. The new correlations are:

$$m = Mr\left(0.06233 - 0.01893\frac{Mr - Mr_{CH_4}}{Mr} - 0.01339\frac{Mr - Mr_{CH_4}}{Mr}\frac{Mr - 2Mr_{CH_4}}{Mr}\right) \qquad \text{B.4}$$

$$\sigma = 3.702 - 0.264\frac{Mr - Mr_{CH_4}}{Mr} - 0.6048\frac{Mr - Mr_{CH_4}}{Mr}\frac{Mr - 2Mr_{CH_4}}{Mr} \qquad \left[\overset{\circ}{A}\right] \qquad \text{B.5}$$

$$\varepsilon / k = 150.019 + 96.618\frac{Mr - Mr_{CH_4}}{Mr} + 17.209\frac{Mr - Mr_{CH_4}}{Mr}\frac{Mr - 2Mr_{CH_4}}{Mr} \qquad [K] \qquad \text{B.6}$$

with Mr the pure component molecular weight in g/mol, and Mr_{CH4} the molecular weight of methane, 16.043 g/mol.

Figures B.3 and B.4 are plots of the new and original correlations against the n-alkane molecular weights. It can be seen that there is a good agreement between the new correlations and the regressed parameter values.

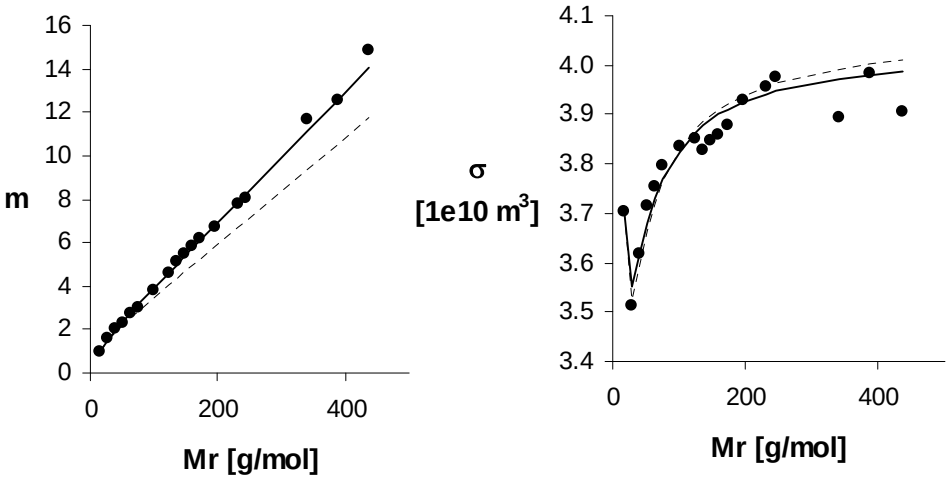

Figure B.3 Generalized correlations for the *PC-SAFT* n-alkane m and v_{00} parameters, with • the regressed parameters used in this study and the —— new and _____ original correlations.

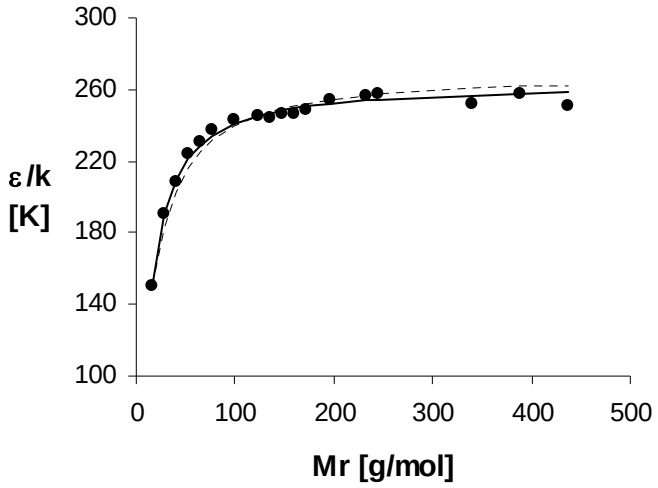

Figure B.4 Generalized correlations for the *PC-SAFT* n-alkane *ε/k* parameters, with • the regressed parameters used in this study and the —— new and _____ original correlations.

B.3 GENERALIZATION OF THE SPHCT EOS PARAMETERS

In the original work by Kim et al. [111], although the authors did discuss the regular behaviour of the *EOS* parameters with the n-alkane carbon number, no generalised correlations had been suggested for the *SPHCT*. Gasem and Robinson later developed such correlations specifically for the n-alkane systems, but these were developed in terms of the pure component carbon number. It was decided for the sake of consistency in this work, to generalize the newly regressed parameters in terms of the n-alkane molecular weight. The generalized correlations for the *SPHCT EOS* used in this study are listed in equations B.7, B.8 and B.9:

$$c = 0.01602Mr + 0.85761 \qquad \text{B.7}$$

$$rv_0 = 0.7238Mr + 3.005 \qquad [1e6m^3] \qquad \text{B.8}$$

$$q\varepsilon'/k = \frac{\left(Mr - Mr_{methane}\right)}{Mr}\left[226.037 - 123.79\exp\left(-0798Mr\right)\right] \qquad [K] \qquad \text{B.9}$$

with Mr in g/mol, and Mr_{CH4} the molecular weight of methane, 16.043 g/mol.

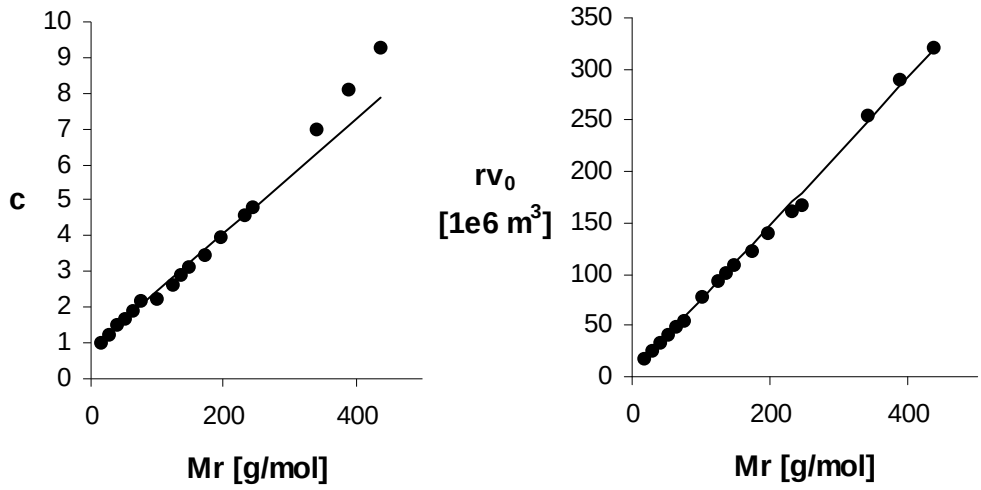

Figure B.5 Generalized correlations for the *SPHCT* n-alkane c and rv_0 parameters, with • the regressed parameters used in this study and the —— new generalized correlation.

As can be seen form Figure B.5 the molecular volume and external degrees display a simple linear relationship with the n-alkane molecular weight and can be accurately represented by equations B.7 and B.8, with only the *c* parameters of the heavy n-octacosane, n-dotriacontane and n-hexatriacontane parameters deviating from this trend. (See section B.1 for a discussion on the heavy n-alkane parameters.)

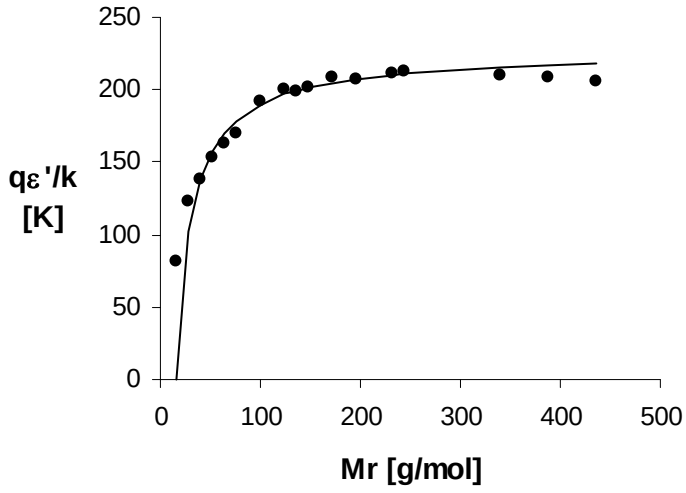

Figure B.6 Generalized correlations for the *SPHCT* n-alkane *qε'/k* parameters, with • the regressed parameters used in this study and the —— new generalized correlation

It is apparent from equation B.9 that this correlation will predict an incorrect *qε'/k* value of zero for methane, however as can be seen from Figure B.6 this correlation provides an excellent estimate of the higher n-alkane (from n-propane) parameter values. As the regressed parameter values for methane and ethane are already available there is no need to use the

correlation to estimate the parameter values of the lighter n-alkanes, and hence will not affect the performance of the model.

Nomenclature

Symbol	Definition	Units	Value
a (Chapter 2)	Van der Waals Attractive Term	Jm^3/mol^2	
a	Specific Helmholtz energy	J/mol	
A	Helmholtz Free Energy	J	
b	$4*b_0$	m^3/mol	
b'	$4*b'_0$	m^3/molecule	
B_I	i^{th} virial coefficient (molar based)	m^3/mol	
B'_I	i^{th} virial coefficient	m^3/molecule	
b_0	Hard-sphere volume per mole	m^3/mol	
b'_0	Hard-sphere volume per molecule	m^3/molecule	
b^{VDW}	Van der Waals volume term $(4*N\pi\sigma^3/6)$	m^3	
c	Degrees of freedom of motion per molecule		
c'	Degrees of freedom of motion per segment		
c(r)	Direct correlation function		
d_B	Effective hard sphere diameter	m^3/mol	
d_{BH}	BH effective hard sphere diameter	m^3/mol	
d_{CWA}	CWA effective hard sphere diameter	m^3/mol	
E	Internal Energy	J	
f(r)	Meyer function		
G	Gibbs Free Energy	J	
H	Enthalpy	J	
h (Chapter 2)	Planck's constant		
h	Chen and Kreglewski step height		

Symbol	Definition	Units	Value
h(r)	Total correlation function		
k	Boltzmann Constant	$J.K^{-1}$	1.38065e-23
K	Equilibrium ratio (y_i/x_i)		
K^{HS}	Isothermal hard sphere compressibility		
L	Dumbbell geometric ratio		
l	Distance between two segment centres in a dumbbell		
m	Chain length		
N	Number of Molecules		
n	Mole Number	mol	
N_A	Avegadro's constant	molecules/mole	6.022 e 23
N_c	Coordination number		
N_i (Chapter 2)	Most probable number of molecules in an energy state/level i		
P	Pressure	Pa	
$p(N_0,N_1,\ldots)$	Probability function in grand canonical ensemble		
P_c	Critical Pressure	Pa	
p_I	Degeneracy		
q	Partition function		
Q	Canonical Partition Function		
r	Distance vector		
r	Distance or length	m	
r	Chain length		
R	Universal Gas Constant	J/mol/K	8.3144
S	Entropy	J/K	

Symbol	Definition	Units	Value
T	Temperature	K	
T*	Reduced temperature kT/ε		
T_c	Critical Temperature	K	
T_r	Reduced Temperature (T/T_c)		
U	Interaction or Potential energy	J	
v	Specific Volume	m^3/mol	
V	Volume	m^3	
V_f	Free volume	m^3	
V_σ	Excluded volume	m^3	
v_0	Specific close packed volume	m^3/mol	
V_0	Close packed volume $N\sigma^3/\sqrt{2}$	m^3	
v_{00}	Temperature independent closest packed volume.	m^3/mol	
x	Reduced intermolecular distance (r/σ)		
x_I	Mole fraction of species i		
z	Compressibility		
Z_{config}	Configurational Integral	m^3	
α	Non-sphericity parameter		
α^{VDW}	Van der Waals Mean-Field attractive term.		
β	1/(kT)	J	
ε	Attractive well depth		
γ	Activity coefficient model	J	

Symbol	Definition	Units	Value
ϕ	Reduced perturbation energy		
ϕ^{α}	Fugacity coefficient of phase α of the fluid mixture		
$\hat{\phi}_i^{\alpha}$	Fugacity coefficient of species i in phase α of the fluid mixture		
η	Reduced Density or Packing fraction $N(\pi/6)\sigma^3/V$ or $Nr(\pi/6)\sigma^3/V$		
φ	Mean potential function	J	
λ	Attractive well width parameter		
Λ	De Broglie wavelength	m	
μ (Chapter 2)	Chemical Potential	J/K	
μ	Chen and Kreglewski energy correction	J/K	
ρ	Density (N/V)	Molecules/m^3	
ρ^*	Reduced density $\rho\sigma^3$		
ρ_{mol}	Molar density	Mol/m^3	
σ	Hard Sphere diameter	m/molecule	
τ	$\pi\sqrt{2}/6 \approx 0.74048$		
ξ	V_0/V		
ξ (Chapter 2)	Coupling parameter		
ζ	Intermolecular distance in mean-value theory		
Ξ	Grand Canonical Partition Function		

Subscripts

f	Freezing point
m	Melting point

Symbol	Definition	Units	Value
rcp	Random fluid close packed limit		
cp	Close packed limit		

Superscript

E	Excess property